Inhibitory superagonistic antibodies as novel therapeutics



Robert Friedrich Donat
Wadham College

Supervisors: Simon J. Davis, Richard J. Cornall

Thesis submitted for the degree of Doctor of Philosophy
Hilary Term 2023

Acknowledgements

Firstly, I would like to thank my supervisors Simon Davis and Richard Cornall for their support and guidance over the years. I have greatly enjoyed being a member of both your labs and your encouragement has kept me going.

I would like to thank the past and present members of the Davis and Cornall labs. In the Davis lab, Heather and Chris for taking me in and showing me the ropes and Mai for sharing her helpful tips and tricks around the lab and how to get the most protein possible out of any transfection. Oliver and Mafalda for your never-ending willingness to help with everything and anything. And of course, the Davis lab DPhil students who I shared the lab with Martin, Matt, Caitlin, Joao and Ed thanks for continually inviting me to lunch even if I didn't often join and making the lab feel like home.

Over in CCMP, I would like to thank Tanya for her colony management and generally keeping everything running smoothly and keeping the biscuit tin supplied. Mukta for helping me with flow cytometry analysis. Rose and Aneesha for all their help with mice (#7), histology, flow cytometry and always being willing to help. Jenny for having the same glove size as me and letting me bring her two boxes of gloves knowing full well that I would "borrow" at least half of them and Jianwei for his help and staying later than I thought things would take.

Thank you to Jack, Pramila and Lisa for showing me the Expi expression system and letting me use your incubator and being wonderful company during the lockdowns.

To my Mum and Dad thank you for your encouragement, love and support. I wouldn't be where I am without you. To my friends Rory and Caoimhin thank you for listening to my woes and keeping me entertained (egg). Thank you Lucija for being my companion through both our undergraduate degrees in Edinburgh and now our DPhils in Oxford.

Last but not least, to Vicky. I cannot describe how much you have helped and supported me, you have been amazing. I appreciate you putting up with the odd hours I sometimes kept and for being with me through the highs and the lows. Thank you.

COVID-19 Statement

Due to the outbreak of SARS-CoV-2 the experimental work for this thesis was heavily disrupted. During the university building closures from March to June 2020 I worked in the lab of Alain Townsend purifying and characterising anti-SARS-CoV-2 antibodies and publications from this time are in cited in appendix 7.2. From June 2020 until the end of 2021 after university buildings were re-opened, a limit on the number of people permitted in our lab required a reduction in the number of hours spent in the lab by roughly half over this time period.

Declaration of work done in collaboration with others

This thesis contains some work done in collaboration with others. Where this is the case it has been specified in the text.

Table of Contents

Abstract *13*

Abbreviations *15*

Chapter 1 Introduction *18*

1.1 Immunoreceptors **19**

1.2 Models of immunoreceptor receptor triggering **21**

1.2.1 Aggregation 21

1.2.2 Conformational change and mechanotransduction 22

1.2.3 The kinetic-segregation model 23

1.3 Mechanism of immunoreceptor antibody agonist signalling **26**

1.3.1 Extension of the mechanisms of immunoreceptor antibody agonism 29

1.4 Cytokine receptor signalling **30**

1.4.1 Receptor protein tyrosine phosphatases in cytokine signalling 33

1.5 Association of inhibitory receptors with autoimmunity **36**

1.6 Receptors explored in this thesis **38**

1.6.1 PD-1 38

1.6.2 BTLA 40

1.6.3 TIGIT 43

1.6.4 IL-10R 45

1.7 Bispecific antibodies **48**

1.7.1 Murine Bispecific Antibodies 51

1.8 Work leading up to this thesis **52**

1.9 Aims of thesis **55**

Chapter 2 Material and Methods *58*

2.1 Molecular Cloning **58**

2.1.1 Design of IL-10Rα mutants 59

2.1.2 Bispecific antibody design 59

2.1.3 IL-10R design 60

2.2 Cell culture **60**

2.2.1 HEK293T 60

2.2.2 CHO-K1 61

2.2.3 ExpiCHO-S 61

2.2.4 Expi293F 61

2.2.5 B-cell hybidromas 61

2.2.6 EL4 cells 62

2.2.7 Primary murine cells 62

2.2.8 Stable transfection of CHO-K1 cells 62

2.2.9 Transduction of HEK293T cells 63

2.2.10 Transient transfection of HEK293T cells 64

2.2.11 Transient transfection of ExpiCHOs and Expi294 64

2.3 Protein Purification **65**

2.3.1 Nickel-purification ... 65
2.3.2 C-tag purification ... 66
2.3.3 Protein-G purification ... 66
2.3.4 Controlled Fab arm exchange ... 67
2.3.5 Protein concentration and buffer exchange ... 67
2.3.6 Size-exclusion chromotography ... 67
2.3.7 Protein concentration quantification ... 68
2.3.8 Polyacrylamide-gel electrophoresis ... 68
2.3.9 Western Blot ... 69
2.3.10 Endotoxin testing ... 69
2.3.11 Biotinylation ... 70

2.4 Surface Plasmon Resonance ... 70

2.5 Flow Cytometry ... 72
2.5.1 Fluorescent antibody conjugation ... 72
2.5.2 Epitope mapping of anti-IL-10Rα antibodies by flow cytometry ... 72
2.5.3 *Ex vivo* flow cytometry ... 73
2.5.4 Phospho-FLOW and intracellular staining ... 73
2.5.5 mOVA-EL4 binding assay ... 73
2.5.6 Legendplex ... 73
2.5.6 Antibodies for flow cytometry ... 74

2.6 Histology ... 75
2.6.1 Tissue fixation and sectioning ... 75
2.6.2 H&E staining ... 75
2.6.3 Immunohistochemistry ... 76

2.7 *Ex vivo* IL-10 signalling assay ... 76

2.8 Animal work ... 77
2.8.1 Genotyping of transgenic mice ... 77
2.8.2 RIPmOVA model ... 79
2.8.3 hIL-10Rα mouse model ... 80
2.8.4 MC38 tumour model ... 80
2.8.5 Immunisation, construction and isolation of nanobodies ... 81

Chapter 3 Murine bispecific creation and characterisation ... 83

3.1 Introduction ... 83

3.2 Production of murine bispecific antibodies ... 84

3.3 Assessing antibody bispecificity using surface plasmon resonance-based assays ... 89
3.3.1 Surface Plasmon Resonance ... 89
3.3.2 Sandwich SPR assay ... 90
3.3.3 Rmax comparison SPR assay ... 93
3.3.3 Bispecificity of the 286*2C1 (Labrijn) antibody ... 94
3.3.4 Bispecificity of 286*2C1 (Wang) ... 100

3.4 Further bispecific-antibody production ... 102
3.4.1 Anti-IL-10 receptor bispecific antibody production ... 102
3.4.2 Other anti-hBTLA*anti-OVA bispecific antibody production ... 104

3.5 Western blot analysis of bispecific antibodies ... 108

3.6 SPR analysis of further bispecific antibodies ... 112
3.6.1 Anti-IL-10 receptor bispecific antibody bispecificity ... 112

3.6.2 Other anti-hBTLA*anti-OVA bispecific antibody bispecificity 115
3.7 Endotoxin testing of bispecific antibodies 116
3.8 Discussion 118
Chapter 4 Effects of inhibitory immunoreceptor agonists in the OT-I RIP-mOVA diabetes mouse model 123
4.1 OT-I RIP-mOVA diabetes model pilot study 125
4.2 Anti-mOVA antibody selection 129
4.3 hBTLA, hPD-1 and hTIGIT agonists in the OT-I RIP-mOVA mouse model 133
4.4 OT-I T-cell expansion *in vivo* in the presence of Cl.19 and 286 138
4.5 Effects of other anti-hPD-1 antibodies in the OT-I RIP-mOVA model 141
4.6 Effects of anti-hPD-1 antibodies in a MC38 tumour model. 144
4.7 Conclusion 146
Chapter 5 Bispecific agonism of the interleukin-10 receptor 150
5.1 Introduction 150
5.2 Characterisation of anti-hIL-10Rα antibodies 150
5.2.1 Affinity 151
5.2.2 Epitope mapping 151
5.3 Characterisation of anti-hIL-10Rβ antibodies 154
5.4 Characterisation of anti-mIL-10Rβ nanobodies 157
5.4.1 Affinity 159
5.4.2 Domain mapping 160
5.5 *Ex vivo* IL-10 signalling assays 165
5.5.1 IL-10 signalling in hIL10Rα peritoneal exudate cells 165
5.5.2 Antibody agonism of the IL-10R 166
5.5.3 Antibody blockade of the IL-10R 168
5.6 Bispecific anti-IL-10R *in vivo* 171
5.6.1 hIL10Rα mouse phenotype 171
5.6.2 Anti-IL-10R bispecific antibody tolerability in hIL10Rα mice 172
5.7 Discussion 177
Chapter 6 Discussion 181
6.1 Fc-receptor independent BTLA agonism 182
6.2 PD-1 agonism exacerbated OT-I T cell driven diabetes 185
6.3 Ligand vs antibody-based approaches for checkpoint agonism 190
6.4 Lessons learned from bispecific antibody IL-10R agonism 192
6.5 Closing remarks 197
Chapter 7 Appendix 200
7.1 hIL10Ra mouse generation 200

8.2 Publications relating to SARS-CoV-2 201

Chapter 8 References 204

List of Figure

Figure 1.1. Proposed mechanisms of immunoreceptor triggering. 26

Figure 1.2. Kinetic-segregation model-based explanation for immunoreceptor agonist antibody signalling. 28

Figure 1.3. PD-1 ligand interactions and signalling. 39

Figure 1.4. BTLA ligand interactions and signalling. 41

Figure 1.5. TIGIT-ligand interactions and signalling. 44

Figure 1.6. IL-10R formation and signalling. 46

Figure 1.7. Principle of murine bispecific antibody generation by controlled Fab-arm exchange. 53

Figure 1.8. Principle of murine bispecific generation by electrostatic steering. 54

Figure 3.1. Purification of the parental 2C1 and 286 (Labrijn) antibodies. 85

Figure 3.2. Production of the bispecific 286*2C1 (Labrijn) antibody. 87

Figure 3.3. Size exclusion chromatography of the bispecific 286*2C1 (Wang) antibody. 88

Figure 3.4. Affinity purification of the bispecific 286*2C1 (Labrijn) antibody. 90

Figure 3.5. SPR approaches for assessing bispecificity. 91

Figure 3.6. Assessment of 286*2C1 bispecific binding capacity (Labrijn). 98

Figure 3.7. Varying reduction conditions of the parental (Labrijn) antibodies. 99

Figure 3.8. Assessment of the 286*2C1 (Wang) bispecific binding capacity. 103

Figure 3.9. Purification of anti-IL-10 bispecific antibodies. 105

Figure 3.10. Purification of 286*Nb82. 106

Figure 3.11. Purification of bispecific antibodies with a 286scFv-arm 106

Figure 3.12. Western blots of bispecific antibodies used in animal experiments using anti-kappa, anti-His and anti-C-tag detection antibodies. 110

Figure 3.13. SPR analysis of anti-IL-10R bispecific antibodies. 113

Figure 3.14. Sandwich SPR of anti-IL-10R bispecific antibodies. 115

Figure 3.15. SPR analysis of hBTLA/OVA bispecific antibodies. 117

Figure 3.16 Endotoxin quantification of bispecific antibodies used in animal experiments. 119

Figure 4.1. Model of autoimmune diabetes in RIP-mOVA mice by transfer of OT-I $CD8^+$ T-cells. 126

Figure 4.2. Exemplar histology sections of RIP-mOVA islet of Langerhans infiltrate scoring. 127

Figure 4.3. Assessment of RIP-mOVA and WT mice after OT-I T-cell transfer. 128

Figure 4.4. Comparison of RIP-mOVA and WT pancreas histology sections with and without OT-I transfer. 130

Figure 4.5. Antibody and nanobody binding of mOVA. 132

Figure 4.6. Antibody treatment of OT-I RIP-mOVA diabetes mice. 136

Figure 4.7. $V\alpha2^+$ T-cell flow cytometry analysis of OT-I RIP-mOVA diabetes mice after antibody treatment. 137

Figure 4.8. *In vivo* comparison of humanised and murine OT-I T-cell expansion in RIP-mOVA mice. 139

Figure 4.9. Analysis of *in vivo* comparison of humanised and native OT-I T-cell expansion in RIP-mOVA mice after four days. 140

Figure 4.10. The effect of anti-hPD-1 antibodies in an autoimmune diabetes model using humanised OT-I T-cells. 143

Figure 4.11. The effect of anti-hPD-1 antibodies in an MC38 tumour mouse model. 145

Figure 5.1. SPR analysis of anti-hIL-10Rα antibodies binding to hIL-10Rα. 152

Figure 5.2. Epitope mapping of anti-hIL-10Rα antibodies. 155

Figure 5.3. SPR analysis of anti-mIL-10Rβ antibodies binding to mIL-10Rβ. 158

Figure 5.4. Production of the mIL-10Rβ extracellular domain. 159

Figure 5.5. Anti-mIL-10Rβ nanobody production. 160

Figure 5.6. Anti-mIL-10Rβ nanobody kinetic analysis. 161

Figure 5.7. Chimaeric human/murine IL-10Rβ production. 163

Figure 5.8. Screen of anti-mIL-10Rβ nanobody binding to chimaeric and wild-type mIL-10Rβ. 164

Figure 5.9. Ability of IL-10 to agonise peritoneal exudate cells from hIL10Rα mice. 167

Figure 5.10. Ability of IL-10 antibodies to stimulate hIL10Rα peritoneal exudate cells. 169

Figure 5.11. Ability of anti-IL-10 antibodies to block hIL-10 signalling in hIL10Rα PECs. 170

Figure 5.12. Humanised IL10Rα mouse phenotype comparison. 172

Figure 5.13. Anti-IL-10R bispecific antibody tolerability study. 174

Figure 5.14. Serum cytokines in homozygous hIL10Rα mice seven days post anti-IL-10R bispecific antibody treatment and untreated heterozygous hIL10Rα mice. 175

Figure 5.15. MHC II expression on mixed macrophage/monocyte populations of hIL10Rα mice treated with anti-IL-10R bispecific antibodies. 176

Figure. 6.1. Possible non-signalling conformations of the anti-IL10R bispecific antibody IL-10R complex. 193

Abstract

Immune cells express many different receptors capable of modulating their behaviour, with inhibitory immunoreceptors being especially important for maintaining immune tolerance by suppressing autoreactivity. Therapeutic antibodies capable of inducing inhibitory immunoreceptor signalling could, in principle, be useful tools for the treatment of autoimmune diseases. The mechanistic basis of signalling by so-called "superagonist" antibodies reactive with immunoreceptor family receptors are becoming increasingly well understood, with the simultaneous binding of a membrane proximal epitope on the immunoreceptor, and Fc receptor engagement, both appearing to be critical requirements. We sought to examine whether the superagonistic activity of an inhibitory antibody against hBTLA could be directed to specific tissues, by making it engage a tissue cell surface antigen in lieu of the Fc receptor *in vivo*. For this, murine bispecific antibodies were generated, and the approach showed early promise, although further experiments are needed to confirm and extend the initial findings. It is also unknown whether the requirements of immunoreceptor superagonists apply to other receptor families such as the cytokine receptors. To investigate this, we sought to generate murine bispecific IL-10R agonist antibodies capable of dimerising IL-10Rα and IL-10Rβ. However, none of the anti-IL-10R bispecific antibodies exhibited agonistic activity *in vitro* or *in vivo,* indicating that merely co-localising the two receptor chains is insufficient to trigger signalling and that there are likely to be additional strict geometric requirements for signalling. Both sets of experiments relied on the generation of murine bispecific antibodies and two different methods described in the literature were tried. Only one of these was found to produce high quality bispecific antibody. Finally, this thesis describes the use of new surface plasmon resonance (SPR)-based techniques for assessing the functional bispecificity of such molecules. Both a sandwich SPR-based assay and an Rmax comparison SPR-based assay were each

developed, with the two complementary approaches producing similar results. Overall, the thesis strengthens the idea that there is considerable scope for generating a large variety of potentially useful therapeutic agonists.

Abbreviations

ADCC	Antibody-dependent cellular cytotoxicity
AMPK	5' adenosine monophosphate-activated protein kinase
APC	Antigen presenting cell
BCR	B-cell receptor
BiTE	Bispecific T-cell engager
BTLA	B- and T- lymphocyte attenuator
CAR	Chimeric antigen receptor
cFAE	Controlled Fab arm exchange
CH1, CH2 or CH3	Heavy chain C domain 1, 2, or 3
CRD1	Cysteine rich domain 1
CRO	Contract research organisation
cryo-EM	Cryo-electron microscopy
CTLA-4	Cytotoxic T-lymphocyte-associated protein 4
DC	Dendritic cell
EAE	Experimental autoimmune encephalomyelitis
ELISA	Enzyme-linked immunosorbent assay
Fab	Fragment antigen binding
FERM	Four-point-one, ezrin, radixin, moesin
GMCSF	Granulocyte-macrophage colony-stimulating factor
GPCR	G protein-coupled receptor
GVHD	Graft-versus-host disease
H	Antibody hinge region
HC	Antibody heavy chain
HVEM	Herpesvirus entry mediator
IBD	Inflammatory bowel disease
IFN	Interferon
IL	Interleukin
IMAC	Immobilized metal affinity chromatography
IRAEs	Immune related adverse events
ITAM	Immunoreceptor tyrosine-based activation motif
ITIM	Immunoreceptor tyrosine-based inhibitory motif
ITSM	Immunoreceptor tyrosine-based switch motif
JAK	Janus kinase
LC	Antibody light chain
MCP-1	Monocyte chemoattractant protein-1
MHC	Major histocompatibility complex
MS	Multiple sclerosis
NK cell	Natural killer cell
OVA	Ovalbumin
PBMC	A peripheral blood mononuclear cell
PD-1	Programmed cell death protein 1

PD-L1	Programmed death-ligand 1
PD-L2	Programmed death-ligand 2
PECs	Peritoneal exudate cells
PI3K	Phosphoinositide 3-kinases
pMHC	Peptide-MHC
PVR	Poliovirus receptor
PVRL2	Poliovirus receptor-related protein 2
RIP	Rat insulin promoter
RMSD	Root-mean-square-distance
RPTP	Receptor protein tyrosine phosphatase
SAP	SLAM-associated protein
scFv	Single-chain variable fragment
SDS-PAGE	Sodium dodecyl sulfate–polyacrylamide gel electrophoresis
SH2	Src Homology 2
SHIP-1	SH-2 containing inositol 5' polyphosphatase
SLAM	Signalling lymphocyte activation molecule
SPR	Surface plasmon resonance
STAT	Signal transducer and activator of transcription
TCR	T-cell receptor
Tfh	T follicular helper cell
Th	T helper cell
TIGIT	T cell immunoreceptor with Ig and ITIM domains
TNF	Tumour necrosis factor
Treg	Regulatory T-cell
TYK2	Non-receptor tyrosine-protein kinase (member of the JAK family)
VH	Variable domain of the heavy chain
VL	Variable domain of the light chain

Chapter 1

Chapter 1 Introduction

The reactivity of the immune system is tightly controlled to avoid self-harm. Approximately 5% of the world's population suffer from autoimmune diseases, which are caused by a loss of self-tolerance and responses to autoantigens (1,2). However, the immune system must be responsive to harmful pathogens and suppress tumour development. To maintain this balance the immune system has developed central tolerance, which comprises a series of checkpoints during cell development to eliminate or tolerise auto-reactive cells. Additionally, in the periphery, immune cells express many receptors capable of producing either stimulatory or inhibitory signals, which are integrated to determine whether the cells should react and the strength of this activation.

T cells are believed to require three signals for activation *in vivo*. The first signal results from antigen recognition by T-cell receptors (TCRs). Signal one results in the upregulation of cell activation genes, changes in cell adhesion receptors and cytoskeletal rearrangements (3). However, TCR stimulation alone is not sufficient for full T-cell activation and instead induces an unresponsive state known as anergy. A second co-stimulatory signal is required from co-stimulatory receptors, such as CD28, to amplify downstream signalling by the TCR (4). Co-stimulatory ligands are expressed by antigen presenting cells (APCs) and provide context about the surrounding environment and whether activation is warranted. APCs can also present the ligands of co-inhibitory receptors on T cells and negatively regulate T-cell responses through inhibitory receptor signalling, which diminishes TCR signalling. Thirdly, cytokine receptors on T cells bind small soluble cytokines of different types that further shape their response. For example, IL-12 polarises T-cell development towards a Th1 phenotype, whereas IL-4 drives Th2 cell development (5). Immune cells therefore interact with their environment through a variety of receptors expressed on their surface which, by binding extracellular ligands, convey environmental cues to the cell via signalling. The

receptors that determine immune cell behaviour fall into different families, and include immunoreceptors, cytokine receptors, G-protein-coupled receptors, ligand gated ion channels, TNF receptors and receptor tyrosine kinases (6).

1.1 Immunoreceptors

The family of immunoreceptors includes many of the key receptors present on immune cells, comprising both stimulatory and inhibitory receptors such as the TCR, B-cell receptor (BCR), CD28, programmed cell death protein 1 (PD-1) and B and T lymphocyte attenuator protein (BTLA) (6). The family comprises approximately one hundred immunoreceptors that share several key characteristics (7). They tend to have relatively small (< 10 nm) extracellular domains and bind similarly-sized membrane-bound ligands on other cells. Their intracellular domains carry various combinations of three conserved tyrosine motifs known as immunoreceptor tyrosine-based activation, inhibitory or switch motifs (ITAM, ITIM and ITSM domains). The immunoreceptors have been referred to as non-catalytic tyrosine receptors, as they lack kinase activity or constitutive association with kinases and are nevertheless dependent on tyrosine phosphorylation (7). These common characteristics suggest that the immunoreceptors may share a common triggering mechanism whereby the information that extracellular ligand binding has occurred is transmitted into the cell (7).

The conserved tyrosine motifs in the intracellular domains of immunoreceptors are phosphorylated by extrinsic Src-family kinases, such as Lck, and dephosphorylated by receptor protein tyrosine phosphatases (RPTPs), especially CD45. Upon their phosphorylation, the ITIM, ITAM and ITSM motifs recruit proteins containing Src-homology-2 (SH2) domains responsible for transducing their downstream signalling effects. These motifs all vary slightly in their sequences and recruit distinct downstream mediators with different functions. The ITAM sequence is Yxx(L/I)x6-8Yxx(L/I) and phosphorylation

results in the recruitment, especially, of Syk-family kinases, which phosphorylate substrates in a signalling cascade ultimately leading to cellular activation (8). The ITIM sequence is (S/I/V/L)xYxx(I/V/L) and upon phosphorylation this motif most notably recruits the SH2 domain-containing phosphatases 1 (SHP-1) and 2 (SHP-2). SHP-1 and SHP-2 dephosphorylate ITAMs and the signalling proteins downstream of ITAMs, in this way inhibiting signalling (9). Additionally, ITIMs can also recruit SH2 domain-containing inositol phosphatase 1 (SHIP-1) which counteracts phosphoinositide 3-kinase (PI3K), a mediator of cellular activation. The ITSM sequence is TxYxx(I/V), and the phosphorylation of this motif can have either an inhibitory or stimulatory effect depending on the cellular context (10). ITSMs can recruit phosphatases and, like ITIMs, inhibit activation. However, ITSM motifs can also recruit signalling lymphocyte activation molecule (SLAM)-associated protein (SAP) family adapters, which can recruit Src-family kinases and other stimulatory molecules, explaining the cellular context-dependent signalling effects of these motifs.

Whereas a fraction of the Lck kinase expressed in T cells is associated with the co-receptors, CD4 and CD8, both Src-family kinases and RPTPs otherwise freely diffuse in the cell membrane and are not constitutively associated with immunoreceptors. Free diffusion of kinases and phosphatases enables them to constantly add or remove phosphate groups on the receptors bearing tyrosine motifs that they encounter (11). This suggests that there is a balance established between kinase and phosphatase activity that, in resting cells, favours the phosphatases, and that changes in this balance could lead to receptor signalling. The observation that pervanadate, a phosphatase inhibitor, was able to cause T-cell receptor signalling supports this idea (12). Similarly, the artificial recruitment of CD45 into the proximity of PD-1, an inhibitory immunoreceptor, increased PD-1 dephosphorylation and inhibited its ability to suppress T-cell activation, suggesting that this is a general phenomenon (13).

1.2 Models of immunoreceptor receptor triggering

Different mechanistic models have been proposed to explain how ligand binding by immunoreceptors results in signalling, mostly based on attempts at understanding TCR triggering (7,14,15). The proposed models can be seen as reflecting the important principle that altering the balance between kinase and phosphatase activity, either by increasing kinase concentration or activity locally, or by excluding RPTPs, could all lead to net receptor phosphorylation. The models are not necessarily mutually exclusive and include triggering mechanisms depending on aggregation, conformational change, mechanotransduction and phosphatase segregation. These will be discussed here in the context of what is known about TCR triggering, but due to the shared characteristics of immunoreceptors referred to above, the explanations may be more or less applicable to the family more broadly.

1.2.1 Aggregation

Aggregation is one mechanism by which receptors can be triggered. In one scenario Src-family kinases are associated with the cytoplasmic tails of receptors and upon ligand induced receptor dimerisation or oligomerisation the associated kinases are brought into proximity such that they trans-phosphorylate each other's intracellular signalling motifs resulting in signalling (Fig. 1.1A) (7). The suggestion that immunoreceptor signalling could occur in this manner is based on other receptor families relying on phosphorylation of intracellular kinases, such as receptor tyrosine kinases and cytokine receptors, which are well known to be triggered upon ligand induced dimerization (16,17). It is supported by observations that CD28 and TCR can both be triggered by antibody crosslinking, as widely utilised in *in vitro* T-cell activation assays (18). However, the mechanism according to which TCRs would dimerise *in vivo* is not clear as TCR, like most immunoreceptors, have monovalent ligands. One possibility is that the observed TCR clustering in T-cell/APC contacts would produce

sufficient local proximity to initiate signalling and indeed it has been shown that the greater the amount of TCR clustering the stronger the signalling (19). This observation is also compatible with other models of TCR triggering.

1.2.2 Conformational change and mechanotransduction

Some receptors change conformation upon ligand binding, such as ligand-gated ion channels or G protein-coupled receptors (GPCRs) (20,21). In the case of ion channels, this conformational change opens a pore permitting ions to travel through the membrane, whereas for the GPCRs, the receptors become able to interact with downstream mediators of signalling, i.e., G proteins. A common feature of ligand gated ion channels and GPCRs is that they have multi-pass transmembrane domains which may potentiate the ability to transmit allosteric conformational changes through the membrane, which most immunoreceptors lack. The TCR is a special case insofar as it comprises a bundle of eight transmembrane domains, but the expectation is that this is more to do with complex assembly and stabilization (22). Nonetheless, conformational change has been proposed as a mechanism of TCR triggering. One proposal is that the signalling motifs of the TCR are inaccessible at rest but that conformational change upon ligand binding makes them accessible to kinases (Fig. 1.1B) (23). It has been previously proposed that the TCRα constant domain undergoes some conformational change upon ligand binding (24). However, recent cryo-electron microscopy (cryo-EM) studies of the unbound TCR and TCR bound to a high affinity peptide-MHC molecule (pMHC) offer little support for the notion that conformational change is part of the signalling mechanism for the TCR. The structures only differed in the root-mean-square-distance (RMSD) between their Cα atoms, a measure of the average deviation between two superimposed structures, by 1.2Å (25,26). This change is likely too small to constitute a significant conformational change. The previously

mentioned TCR α-chain 'conformational change' had an RMSD of only 0.5Å. The ligand-bound TCR structure was solved using a high affinity TCR/pMHC complex, possibly reducing the flexibility of the TCR in question. However, it seems likely that a weaker ligand would shift between the position found in the bound and unbound states, which are very similar, rather than adopt a third new conformation. Additionally, the cryo-EM studies did not support TCR oligomerisation by conformational changes of the extracellular domains of the TCR upon ligand binding, because the surface of the TCR did not change and create new putative interaction sites. (25,26).

The cryo-EM studies cannot be used to infer information about the possibility of signalling by mechanotransduction, however. In this model, according to one suggestion, receptors act as mechanosensors, with forces pulling on the receptor freeing the cytoplasmic tails from association with the membrane enabling their phosphorylation by kinases (Fig. 1.1C) (23,27). Evidence for this has been found in studies observing T-cell signalling upon applying ~50 pN of traction forces to cell-bound TCRs (28). Another study found that TCR-imposed forces on T cells interacting with ligand on fluid-phase supported lipid bilayers, which are mimics of the cell membrane, were 30-fold smaller than the forces used in the initial studies but still caused T-cell triggering (29). However, it is unclear how mechanotransduction or conformational change would account for the observation that TCR triggering can occur in a ligand-independent manner on supported lipid bilayers (30).

1.2.3 The kinetic-segregation model

The previously discussed mechanisms of signalling relied on increasing the local concentration of kinases or increasing the availability of signalling motifs to the kinases. The kinetic-segregation model proposes that it is the local removal of inhibitory RPTPs that 'takes the brakes off' and allows kinase activity to predominate and for signalling to occur

(Fig. 1.1D) (31). In this model, receptor-ligand interaction holds the receptor-ligand complex in a close contact between the ligand-presenting cell and the receptor-expressing cell. The close contact depth, set by similarly sized adhesion molecules (e.g. CD2 and CD58), matches the receptor-ligand length, i.e., ~15 nm for the TCR-pMHC interaction (32). This would explain the consistent, small size of immunoreceptors. RPTPs, e.g., CD45 and CD148, have large rigid extracellular domains which limit their entry into the close-contact region (33–35). Conversely Src-family kinases attached to the inner leaflet of the membrane, do not have extracellular domains and can freely diffuse into the contact area and phosphorylate receptor signalling motifs to initiate signalling (30). It has been suggested that Lck associates with the CD4 and CD8 co-receptors on T cells, but even in this case the extracellular domains of CD4 and CD8 are smaller than 15 nm and would freely enter a close contact (36,37).

In support of the RPTP exclusion theory, truncation of the CD45 extracellular domain was found to prevent TCR triggering (35). Additionally, experiments widening the gap between opposing cells by increasing the length of the peptide-MHC complex found that TCR triggering was reduced and that CD45 segregation was decreased (38,39). Additional support for the kinetic-segregation model can be found in studies that show TCR triggering in absence of a ligand by forming large close-contacts with supported lipid bilayers excluding CD45 (30). Further, Chen *et al.* observed that TCR bound to peptide-MHC would only stimulate T cells minimally in solution, but that on encountering an apposing supported lipid bilayer, whereupon the diffusion of the TCR was slowed, strong signalling was observed (40). Additionally, peptide-MHC tethered to an apposing membrane induced a greater amount of triggering than observed with untethered peptide-MHC (41). It was noted that the diffusion rate of untethered peptide-MHC-TCR complexes in close-contact areas was reduced by ~80% in comparison to unbound TCR. This supports the suggestion that

TCR dwell time within the contact area, segregated from CD45, is an important contributor to triggering (41). The 'dwell time' explanation would also account for the ligand-independent triggering observed by Chang *et al.* on bilayers with which very large contact areas were formed (30).

Observations supporting the role of CD45 exclusion for signalling by immunoreceptors beyond the TCR have been made in FcεRI signalling, and for signalling in NK cells and CAR T-cells. CD45 exclusion from close contacts formed by FcεRI ligand interactions was observed to be sufficient to trigger signalling (42). Conversely, truncated CD45 was found to inhibit FcεRI signalling. NK cell activation relies on the net effect of stimulatory and inhibitory receptors, which also form close contacts ~15 nm in depth. Extending the ligand of the stimulatory receptor NKG2D from the membrane was found to prevent NKG2D signalling despite receptor-ligand binding (7,43). CAR T-cells express a receptor comprised of an extracellular antibody variable domain fused to the ITAM-containing intracellular domain of CD3, allowing the artificial immunoreceptor to target cytotoxic activity towards particular antigens. CAR T-cells have been found to be increasingly less effective at killing target cells as the height of the extracellular domain is increased (44,45). Additionally, CAR T-cells that recognize epitopes that lie more membrane-proximally are more effectively triggered (46–48). These findings demonstrate that the kinetic-segregation model might apply to other immunoreceptors including inhibitory receptors such as PD-1, BTLA and T cell immunoreceptor with Ig and ITIM domain (TIGIT).

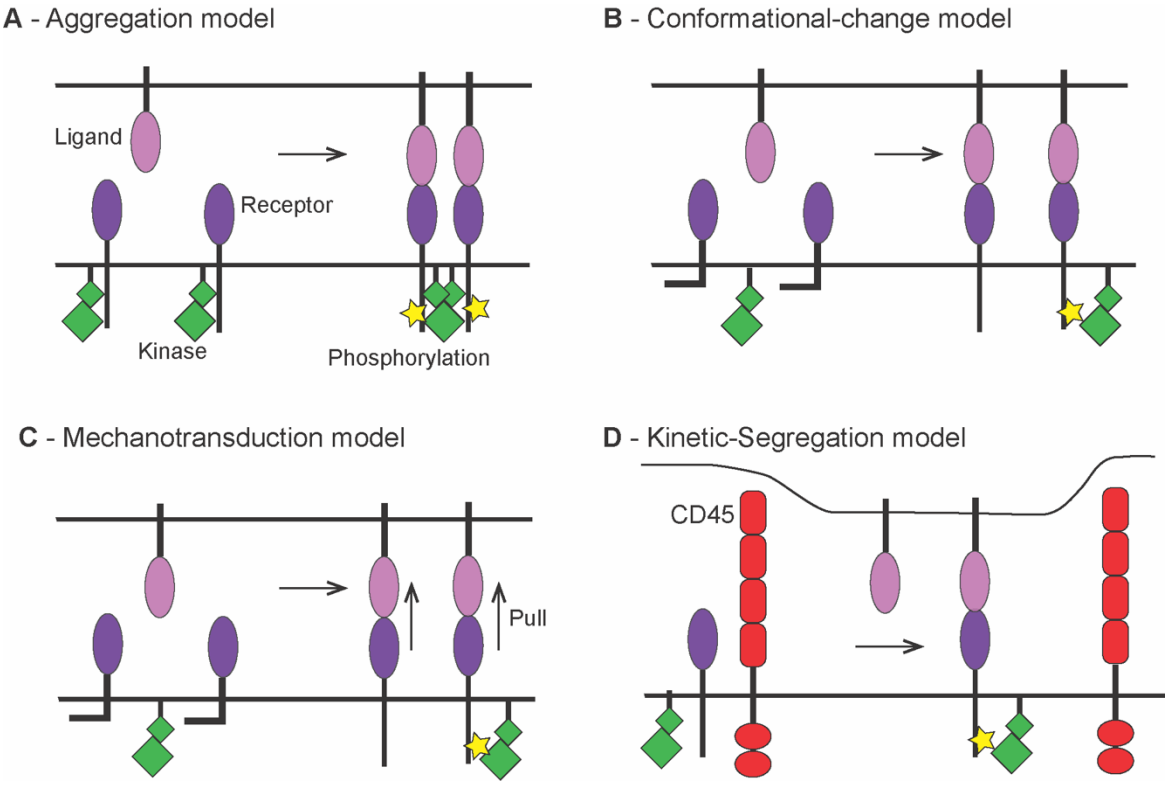


Figure 1.1. Proposed mechanisms of immunoreceptor triggering. (A) Receptors are aggregated on ligand binding which causes receptor phosphorylation. (B) Conformational changes upon ligand binding make signalling motifs accessible for phosphorylation. (C) Ligand binding exerts a pulling force on the receptor which releases the cytoplasmic tails from the membrane making signalling motifs accessible for phosphorylation. (D) Local exclusion of large RPTPs, such as CD45, allows kinase activity to predominate resulting in net phosphorylation.

1.3 Mechanism of immunoreceptor antibody agonist signalling

The signalling models described above focused mainly on explaining ligand-receptor interactions and how these lead to signalling. However, many of the same principles likely apply to antibody agonists that artificially agonise immunoreceptors. Antibodies that trigger immunoreceptors are often used to activate and induce T-cell proliferation *in vitro*. Immobilising agonist antibodies on a surface increases their potency (49). One explanation for this observation is that antibodies binding such surfaces, but also Fc receptors on apposing cells, generate close contacts that exclude RPTPs leading to signalling. Alternatively, agonist antibody immobilisation could lead to greater receptor aggregation.

An infamous immunoreceptor agonist is an anti-CD28 antibody called TGN1412. In 2006 this antibody was trialled in six healthy human volunteers with disastrous consequences. TGN1412 was thought to inhibit immune responses through activation of regulatory T-cells and therefore be a promising therapeutic. However, all of the volunteers receiving the antibody experienced 'cytokine storms' with TGN1412 activating effector T-cells in the absence of cognate peptide-MHC (50).

CD28 agonists can be divided into two types: conventional agonists, which are capable of delivering co-stimulatory signals, but are not mitogenic by themselves; and superagonists, that are capable of activating and initiating the proliferation of T cells in the absence of direct TCR stimulation (51). Comparative structural studies of the two types of CD28 agonists revealed that superagonists had membrane-proximal epitopes, whereas conventional agonists had more membrane-distal epitopes (52,53). Another key finding regarding the CD28 superagonists was that their agonistic activity was dependent on the presence of Fc receptor expressing cells (54–56). At sufficient expression levels, all human FcγRs other than FcγRI have been found to trigger the superagonistic activity of TGN1412 (56). It is unknown why FcγRI was unable to support CD28 superagonism. However, FcγRI differs from the other FcRs structurally. It has one additional immunoglobulin superfamily domain inserted between the transmembrane domain and the Fc binding site, suggesting that antibody complexes formed using FcγRI would be less compact than those with other FcRs. These observations are consistent with the suggestion by Davis *et al.* that antibody superagonism can be explained by an extension of the kinetic-segregation model (31). Davis *et al.* proposed that by binding a membrane proximal epitope on CD28 and to an Fc receptor on an opposing cell, superagonists would generate a more-shallow close contact between the two cells and thereby exclude RPTPs more effectively than their non-superagonistic counterparts (Fig. 1.2) (31).

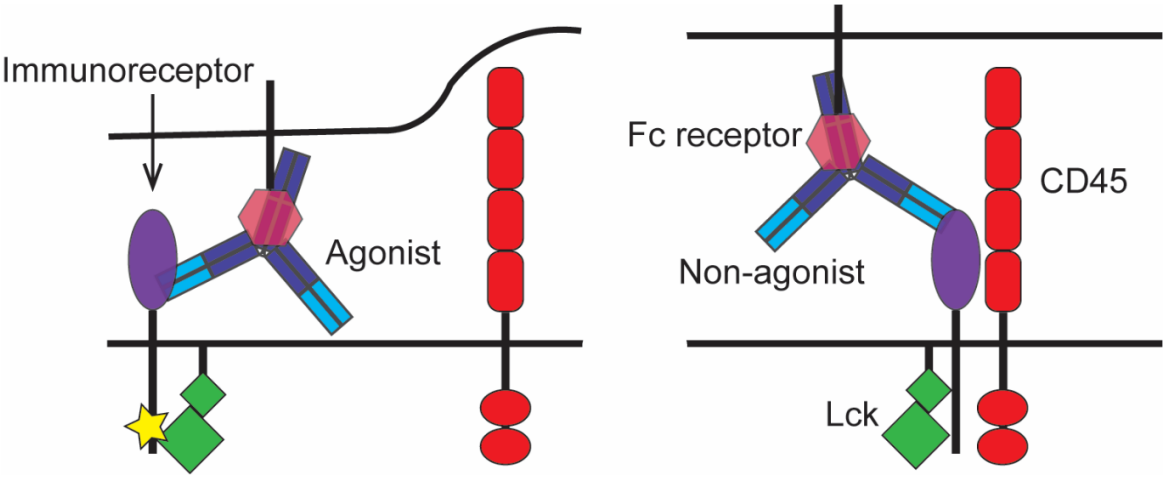


Figure 1.2. Kinetic-segregation model-based explanation for immunoreceptor agonist antibody signalling. *Left panel*: an agonist antibody (*blue)* creating a close contact by binding a membrane proximal epitope on an immunoreceptor (*purple*) on one cell and Fc receptor (*pink*) on an apposing cell. This small gap excludes large RPTPs (*red)* and allows unopposed receptor phosphorylation (*star*) by kinases (*green*). *Right panel*: a non-agonistic antibody (*blue*) which binds to a membrane distal epitope on an immunoreceptor creating a large intercellular gap that less efficiently excludes RPTPs (*red)*, allows access for phosphatases, thereby preventing or weakening signalling.

Lippert *et al.* analysed the steric requirements of a rat CD28 superagonistic antibody JJ316 (manuscript submitted). They found that the superagonistic activity of JJ316 was lost upon increasing the length of the JJ316/CD28 complex, either by extending the JJ316 antibody or CD28. Analysis of CD45 exclusion in this setting established a positive correlation between CD45 exclusion and antibody signalling activity. As seen with the TCR and FcεRI, a truncated form of CD45 also inhibited the activity of JJ316. Interestingly, a truncated form of CD148 was found to inhibit even more potently. RPTP exclusion therefore appears to play an important role in antibody mediated agonism of stimulatory immunoreceptors.

The study of inhibitory immunoreceptor agonists has mostly focused on their cellular effects rather than the mechanisms underlying their signalling activity (57). Lippert *et al.* analysed the agonistic activity of three anti-PD1 antibodies whose epitopes ranged from membrane proximal to membrane distal (manuscript submitted). They observed that agonism was Fc receptor dependent as seen with CD28 agonists (53–55). Further, they found that anti-PD-1 agonist-mediated T-cell inhibition decreased with increasing epitope distance from the

membrane. Lastly, as in the case of the CD28 agonist JJ316, Lippert *et al.* found that increases in CD45 exclusion correlated with increases in anti-PD-1 agonist activity.

A recent study by Suzuki *et al*. characterised a series of 81 anti-PD-1 antibodies and also found a clear distinction in the epitope locations of agonist versus non-agonist antibodies (58); the agonists bound a range of membrane-proximal epitopes. Interestingly, Suzuki *et al.* also demonstrated that antibody agonism of PD-1 could be achieved without binding PD-1 directly (58). They showed this by introducing a membrane-proximal or membrane-distal FLAG tag into PD-1 and by using an anti-FLAG antibody to initiate signalling, observing that binding the membrane-proximal tag produced the most signalling. Additionally, they found that agonism was dependent on the immobilisation of PD-1 antibodies on a surface or the presence of Fc-receptor expressing cells (58).

The observations made for CD28 superagonist antibodies also apply to PD-1 agonist antibodies. They are dependent on binding membrane proximal epitopes and are Fc receptor dependent. Further, increased potency of antibody agonism correlates with greater CD45 exclusion from close contacts. These commonalities suggest a unifying mechanism by which antibody agonism of immunoreceptors occurs and are consistent with the model of antibody agonism proposed by Lippert *et al.* (manuscript submitted).

1.3.1 Extension of the mechanisms of immunoreceptor antibody agonism

With evidence mounting that RPTP exclusion is important in immunoreceptor agonism, the question arises of whether RPTP exclusion can be leveraged in the agonism of other receptor families. RPTPs are known to be highly non-specific, are often ubiquitously expressed and their phosphatase activity is not constrained to immunoreceptor signalling motifs (59). The criteria for sensitivity to RPTP exclusion-induced agonism of a given receptor therefore may depend on only three factors: (1) the receptor relies on tyrosine phosphorylation for

signalling; (2) the receptor is small enough to fit into close contacts capable of excluding RPTPs; and (3) the receptor is expressed on cells expressing RPTPs.

Cytokine receptors meet all three criteria and their activation with antibody agonists has potential uses both as therapeutics and research tools (60,61). Cytokine receptors rely on the phosphorylation of intracellular tyrosine residues for signalling (62). Even large cytokine receptors such as the shared receptor chain gp130, which has six extracellular domains with an estimated elongated height from the membrane of ~115 Å, would not be excluded from the ~15 nm intercellular gap known to exclude RPTPs (63). Cytokine receptors are also known to be susceptible to inhibition by tyrosine phosphatases (62).

However, there are key differences between cytokine receptor and immunoreceptor triggering, which indicate that *in vivo* phosphatase exclusion is not the mechanism used by cytokine receptors to initiate signalling. For example, cytokines are typically soluble and dimeric, and it is difficult to imagine how they would generate a close contact with an opposing cell. Instead, the mechanism by which they trigger is suggested to be aggregation, i.e., oligomerization.

1.4 Cytokine receptor signalling

Cytokine receptors are composed of two or more single-pass transmembrane proteins, which can be homomeric or heteromeric. The intracellular domains of cytokine receptor chains are constitutively bound to one of four members of the Janus kinase (JAK) family, with different receptor chains associating with different JAKs (Table 1.1). JAKs all comprise a four-point-one, ezrin, radixin, moesin (FERM) domain, Src homology 2 domain, pseudokinase domain and tyrosine kinase domain. The receptors therefore possess pseudo-intrinsic kinase activity and behave like receptors with intrinsic kinase activity. They will be referred to as having intrinsic kinase activity for the purposes of this thesis to differentiate them from

Table 1.1: Immune related type I and II cytokine receptor families and associated Jaks

Cytokine Receptor Family	Associated JAKs	Receptor binding cytokines
Type I common γ chain cytokines	JAK1, JAK3	IL-2, IL-4, IL-7, IL-9, IL-15, IL-21
Type I common β chain cytokines	JAK2	IL-3, IL-5, GM-CSF
Type I gp130 cytokines	JAK1, JAK2, TYK2	IL-6, IL-27
Type I dimeric cytokines	JAK2, TYK2	IL-12, IL-23, IL-27, IL-35
Type I hormone-like cytokines	JAK2	G-CSF
Type II IFN family cytokines	JAK1, TYK2	IFNα, IFNβ, IFNγ, IL-28, IL-29
Type II IL-10 family cytokines	JAK1, JAK2, TYK2	IL-10, IL-19, IL-20, IL-22

immunoreceptors which lack intrinsic or pseudo-intrinsic kinase activity. Expressed alone, the JAK tyrosine kinase domain is active (64). However, the pseudokinase domain is autoinhibitory and by interacting with the tyrosine kinase domain it sequesters the active domain (65,66).

The mechanism by which cytokine receptors were thought to trigger has evolved over time. Initially it was believed that cytokine receptors triggered upon ligand mediated dimerisation (67). Later findings suggested that cytokine receptors formed dimers in the unliganded state and so conformational changes were proposed to underpin the triggering mechanism (68). However, it is unclear how conformational changes would release JAK tyrosine kinase domains from autoinhibition. With the advent of super-resolution microscopy and development of novel approaches to image low density single molecules on cell membranes it has recently been emphatically shown that the thrombopoietin receptor, Epo receptor and GH receptor are randomly distributed monomers at rest (69). Further, a strong correlation between increasing receptor dimerisation and receptor activation was noted (69), with only a low level of intrinsic dimerization being responsible for tonic signalling.

Using cryo-EM the structure of an active murine JAK1-IFNλR1 complex has been solved (70,71). In the active dimer, JAK1 pseudokinase domains were found to bind one another and the JAK tyrosine kinase domains adopted positions in which they were closely apposed and their active sites were oriented towards one another, indicating how trans-phosphorylation of the JAK activation loops, needed for full JAK activity, and phosphorylation of tyrosine signalling motifs in the receptor intracellular domains could occur (70,71). In the active state the tyrosine kinase domains had been released from binding to the pseudokinase domain seen in the inactive TYK2 kinase tandem structure (65). Glassman *et al.* proposed a mechanism of signalling in which pseudokinase domain binding of the tyrosine kinase domain is in flux and changes from its inactive closed conformation to a partially active open conformation (71). Upon ligand binding, and receptor dimerisation, the pseudokinase domains bind one another in trans and the tyrosine kinase domains are freed from their autoinhibition. The tyrosine kinase domains subsequently trans-phosphorylate each other and fully activated JAKs then phosphorylate the tyrosine residues of the receptor's intracellular domains, which in turn recruit signal transducer and activator of transcription proteins (STATs).

There are seven STATs (STAT1-4, STAT5A, STAT5B and STAT6) which bind to phosphorylated tyrosines of different cytokine receptors via their SH2 domain (72). Upon recruitment these STATs are themselves phosphorylated by JAKs, leading to the formation of pSTAT dimers. In their dimeric form pSTATs can act as transcription factors and translocate into the nucleus where they perform their effector functions (73). Between the seven STATs and four different JAKs, JAK-STAT signalling is capable of transmitting signals from ~40 distinct cytokine receptors (73).

1.4.1 Receptor protein tyrosine phosphatases in cytokine signalling

JAK-STAT signalling is negatively regulated by a variety of mediators which target different parts of the signalling pathway. For example, STAT-induced suppressors of cytokine signalling (SOCS) act directly on the receptor chains by binding to phosphorylated tyrosines present on activated cytokine receptors, blocking STAT recruitment (74). SOCS can also bind directly to JAKs preventing their activity (74,75). Phosphatases including the RPTP CD45 have also been shown to regulate cytokine signalling, suggesting that their exclusion could potentiate signalling (76).

The ability of CD45 to dephosphorylate JAKs was first observed in both murine and human cells lacking CD45 activity (77). CD45 was able to dephosphorylate JAK2 in a dose-dependent manner in murine bone marrow derived mast cells *in vitro* and mast cell proliferation was found to increase in the absence of CD45 (77). Additionally, CD45-deficient human T-cells produced more potent IFNα signalling *in vivo*, demonstrating that CD45 has an inhibitory effect on cytokine signalling outcomes (77). CD45 has also been found to reduce IL-4 induced class switch recombination in B cells by dephosphorylating JAK1 and JAK3 (78). Collectively, these findings suggest that CD45 has a physiological role in modulating cytokine signalling.

The most direct evidence that CD45 negatively regulates JAK-STAT signalling and that segregation of the RPTP from a cytokine receptor is agonistic was obtained by Kojima *et al.*, who developed reporter HEK293T cells expressing IL-4Rα and IL-13Rα1, which together form the IL-13R, alongside the downstream signaling mediator STAT6 (79). Introduction of CD45 into this system inhibited IL-13R signalling in a dose dependent manner and, using a membrane bound IL-13R "ligand", Kojima *et al.* showed that CD45 exclusion alleviated this inhibition (79). Further, truncation of CD45 prevented its exclusion and inhibition was restored (79). Interestingly, an extracellularly truncated IL-4Rα which

would generate a closer contact, was found to strengthen signalling, perhaps due to increased CD45 exclusion (79). These findings indicate that CD45 exclusion alone was sufficient to potentiate signalling. The authors noted that triggering was dimerisation independent under conditions in which IL-4Rα was held in the close contact but IL-13Rα1 diffused freely. However, given the crystallographic findings outlined above and the weak affinity between receptors and their associated JAKs it seems likely that brief interactions between IL-4Rα and IL-13Rα1 occurred and that this was sufficient for signalling in areas of CD45 exclusion (69). It therefore seems more likely that cytokine RPTP exclusion can potentiate signalling triggered by receptor dimerisation rather than initiating triggering in the absence of dimerisation. The role of close contact formation and RPTP exclusion *in vivo* is unclear. Creation of cytokine/antibody complexes or cytokine/Fc fusion proteins that could generate close contacts may offer some insight.

The activity of IL-2 is known to be increased by the formation of IL-2 anti-IL-2 antibody complexes *in vivo* (80). The mechanism of these effects is not fully understood but it is possible that they rely on the creation of pseudo membrane-bound IL-2 via Fc receptor interactions. However, IL-2/anti-IL-2 treated mice lacking expression of FcγRs showed that the increase in IL-2 potency was largely FcγR independent (81), whereas deleting neonatal FcRn reduced IL-2/anti-IL-2 activity significantly (81). The effect might therefore be due to the increased half-life of the cytokine/anti-cytokine antibody complexes, mediated by FcRn, compared to soluble cytokines. In 2022, Van Dyke *et al.* showed that an immunocytokine created by fusing IL-2 to the N-terminus of an antibody light chain induced regulatory T-cell (Treg) expansion, without engaging Fc receptors *in vivo* (82). However, no investigation was made into the underlying mechanism of this effect.

To extend the half-lives of cytokines *in vivo*, cytokine-Fc fusions have been generated. If the cytokines are fused to the antibody hinge-CH2-CH3 domains these constructs could

create more efficient RPTP exclusion in the presence of an Fc receptor than cytokine/anti-cytokine antibody complexes, if this was important. In a comparative study of recombinant IL-10 vs an IL-10Fc fusion protein it was found that the ability to suppress IFNγ production of PHA stimulated peripheral blood mononuclear cells (PBMC) *in vitro* was higher for IL-10Fc compared to IL-10 alone (83). However, IL-10 is much smaller than IL-10Fc and so has a higher relative concentration at EC_{50} for concentrations in ng/mL. Thus, IL-10-Fc is likely far more potent than IL-10. Both IL-10 and IL-10Fc have the same valency as IL-10 forms a noncovalent homodimer and IL-10Fc is dimerised by Fc-Fc interactions. This increased activity could be explained sterically: recruitment of the second IL-10R to associate with a dimer may be less hindered in the IL-10Fc than for IL-10. Alternatively, as Fc receptors are expressed on PBMCs, IL-10Fc could create close contacts excluding RPTPs. ADCC appears less likely as IL-10Fc was found to be non-cytolytic (84). An IL-2 immunocytokine in which IL-2 was fused to the C-terminus of the light chains of an intact antibody, increased its biological activity in the presence of antigen expressing beads (85). The authors hypothesised that this was due to increasing IL-2 accessibility by constraining the receptor arms (85). However, the beads interacting with the cells could create very close contacts due to the small distance between light chain C-terminus and antibody variable domains, which could produce phosphatase exclusion and hence, enhanced activation of the IL-2R.

It is very challenging to draw meaningful conclusions about the role of tyrosine receptor phosphatase exclusion from studies of cytokine antibody complexes or cytokine-Fc fusion proteins due to the different, not mutually exclusive, factors which can account for their activities versus cytokines alone. However, CD45 can directly inhibit JAK activity *in vivo* and its exclusion *in vitro* was shown to potentiate and possibly initiate signalling cytokine

receptor signalling. As such, an agonist antibody against cytokine receptors capable of RPTP exclusion may be more potent than an antibody unable to do so.

1.5 Association of inhibitory receptors with autoimmunity

Inhibitory immunoreceptors, including CTLA-4, BTLA, PD-1 or TIGIT as well as the IL-10 cytokine receptor, have been associated with autoimmune diseases, both in humans and in animal models, indicating the vital roles they play in maintaining self-tolerance. Among those, CTLA-4 is the only inhibitory immunoreceptor known to have monogenic germline heterozygous mutations causing immune dysregulation with multi-organ lymphocyte infiltration (86). CTLA-$4^{-/-}$ mice mirror this phenotype, exhibiting prominent lymphocyte proliferation and immune-mediated multi-organ tissue destruction (87). Susceptibility to various autoimmune diseases has also been linked to polymorphisms in *PDCD1*, the gene encoding PD-1. For example, susceptibility to ankylosing spondylitis, rheumatoid arthritis and type 1 diabetes were all linked to *PDCD1* polymorphisms in a 2015 meta-analysis (88). A group of rheumatoid patients expressing anti-PD-L1 antibodies were identified and a correlation between disease severity and the presence of anti-PD-L1 antibodies was observed (89). In line with this are studies showing that PDCD$1^{-/-}$ mice develop different autoimmune disorders depending on the strain; C57BL/6 developed a lupus-like disease whereas BALB/c developed autoimmune cardiomyopathy (90,91).

Rheumatoid arthritis has also been linked to BTLA polymorphisms (92,93). For example, a single nucleotide polymorphism (SNP), 590C, in BTLA was found to mediate susceptibility to rheumatoid arthritis, and patients possessing the 590C allele developed disease earlier in life (93). Additionally, the 590C SNP expressed in human T-cells was found to increase their response to stimulation (93). BTLA expression on $CD4^+$ T-cells from systemic lupus erythematosus (SLE) patients was found to be decreased and the cells were less responsive

to BTLA-mediated inhibition (94). Similar to PDCD1$^{-/-}$ mice, BTLA$^{-/-}$ mouse models develop multi-organ inflammatory infiltrates and hepatitis-like disease (95). In contrast to PD-1 and BTLA, TIGIT deficiency in mice has not been linked to spontaneous autoimmune disease. However, it can increase susceptibility to disease in experimental autoimmune encephalomyelitis (EAE), an animal model of multiple sclerosis (MS), and T-cell hyperproliferation upon challenge (96). Further, the suppressive function of human Tregs from relapsing-remitting MS patients was found to be restored using a TIGIT agonist antibody (97). The link between inhibitory immunoreceptor dysfunction and autoimmunity is reviewed by Deng *et al.* (98), Ning *et al.* (99) and Yue et al. (100) for PD-1, BTLA and TIGIT respectively.

Defects in inhibitory cytokine signalling are also linked to autoimmune disorders. IL-10 deficiency is strongly linked to the development of inflammatory bowel disease (IBD) in humans and mice, a link first made in a study of IL-10 deficient mice which developed spontaneous colitis, in 1993 (101). Moreover, it has been shown that loss-of-function mutations in *IL10RA* and *IL10RB* genes in humans abolish the transmission of IL-10 signalling and are linked to the development of severe IBD, usually within the first three months of life (102–105). The connection between autoimmune diseases and IL-10 is well recognised and has also been reviewed (106).

Inhibitory immunoreceptors have also, of course, been linked to tumorigenesis. Immunodeficiencies are known to increase the risk of cancer (107). The immune system exerts a selective pressure on cancer cells resulting in the development of 'so-called' immune evasion strategies by the tumours. Recognition of this has led to the development of therapies which seek to heighten immune system activity. For example, IL-2 therapy was approved for metastatic renal cell carcinoma and metastatic melanoma in 1992 and 1998, respectively (108). More recently, immune checkpoint inhibitors reactive with CTLA-4 and

PD-1 have been developed and approved for use (109,110). These checkpoint inhibitors block inhibitory immunoreceptor signalling and lower the threshold for T-cell activation. However, some patients develop autoimmune side effects known as immune related adverse events (IRAEs) which usually cease upon termination of treatment (111). Collectively, the association of inhibitory receptors with autoimmunity and the occurrence of IRAEs in the course of checkpoint blockade treatment raises the question of whether inhibitory receptor agonism could be used in the treatment of autoimmune diseases. The potential of this approach has been gaining more attention recently, particularly for immunoreceptors (57,112).

1.6 Receptors explored in this thesis

1.6.1 PD-1

Programmed cell death protein 1 (PD-1 or CD279) is an immunoglobulin superfamily protein with a single IgV-like domain, a single-pass transmembrane region and a cytoplasmic tail with an ITIM and ITSM (113). It is expressed on $CD4^+$ and $CD8^+$ T-cells, B cells, NK cells, NKT cells, monocytes and dendritic cells (DCs) in the periphery (114). PD-1 is upregulated upon T-cell activation and in exhausted T-cells (115,116). There are two PD-1 ligands, PD-L1 (CD279 or B7-H1) and PD-L2 (CD273 or B7-DC) (Fig. 1.3) (113).

Upon ligand binding, PD-1's intracellular signalling motifs are phosphorylated and recruit the protein phosphatase SHP-2 to the cell membrane (117,118). At the membrane, SHP-2 dephosphorylates the ITAMs of stimulatory receptors, such as CD28, and other downstream mediators of signalling (113,119). PD-1 signalling has been found to support Treg development and stability (120,121). Moreover, T follicular helper (Tfh) cells, which

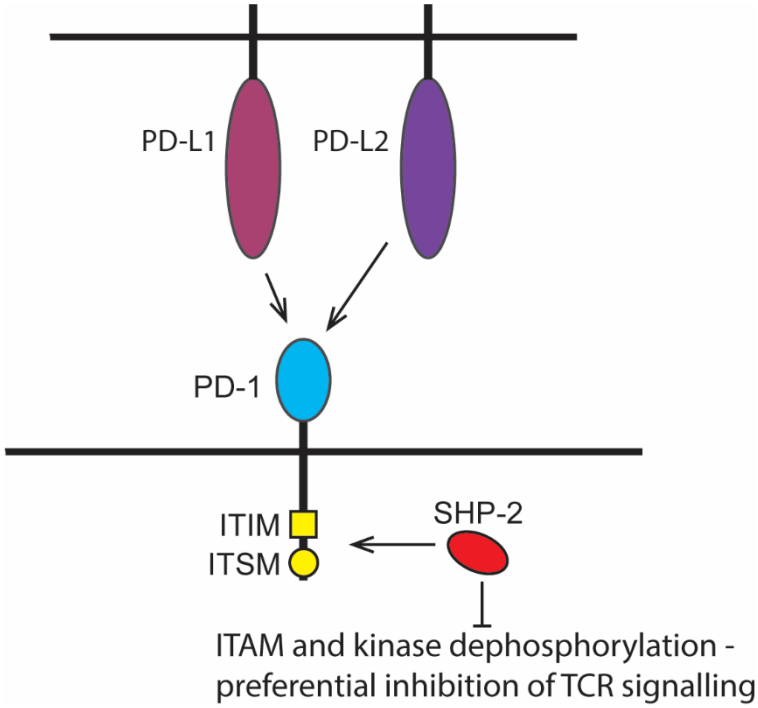


Figure 1.3. PD-1 ligand interactions and signalling.

promote B-cell antibody production, express very high levels of PD-1, which may be due to the intensity of antigen exposure within germinal centres (122). It has also been proposed that PD-1 supports Tfh cell function directly (122–124).

A handful of PD-1 agonists have been tested for their immunomodulatory ability. A PD-L1 fusion to mIgG2α Fc (mutated to prevent FcγR1 and C1q interaction) was found to ameliorate disease in mouse models of colitis and arthritis by dampening T-cell responses (125–127). Another PD-1 agonist comprising a *de novo* designed anti-PD1 trimer was found to reduce T-cell activation in response to plate-bound anti-CD3 stimulus (128). In addition, a fusion protein between an autoantigen-reactive TCR and PD-L1 was created which bound target cells expressing auto-antigen and inhibited auto-reactive human T-cell activation by delivering PD-1 signalling in trans (129). Agonistic anti-PD-1 antibodies have also shown promise in reducing airway hyperreactivity and inflammation (130). However, depletion of PD-1-expressing effector cells can also regulate airway hyperreactivity suggesting that immunosuppression by anti-PD1 antibodies may be independent of their agonistic effects

on signalling (131). This also applies to "agonists" against other inhibitory receptors bearing Fc domains and is often not considered. Suzuki *et al.* demonstrated that their PD-1 antibody was a bona fide agonist which caused PD-1 phosphorylation and induced PD-1 signalling, and this antibody suppressed graft versus host disease and T-cell transfer colitis *in vivo* (58). They also intentionally used a mIgG1 backbone for their agonist which is a poor mediator of ADCC (58).

1.6.2 BTLA

B- and T-lymphocyte attenuator (BTLA or CD272) is an immunoglobulin superfamily protein that consists of a single IgV-like extracellular domain, a single pass transmembrane domain and a cytoplasmic tail with an ITIM, an ITSM and two Grb2 binding domains (mice only have one Grb2 binding domain) (132). BTLA is predominantly expressed on B and T cells but has also been found on monocytes and DCs (133). Naïve T-cells constitutively express BTLA, which upregulates rapidly upon T-cell activation followed by a reduction in expression to a lower level than on naïve T-cells (134). Murine Th1 and anergic T-cells retain high BTLA expression (135).

BTLA has one known human ligand, herpes virus entry mediator (HVEM) (Fig. 1.4) (136). Intriguingly, HVEM itself is a stimulatory receptor and binds several other proteins, i.e., LIGHT, CD160 and LTα, which in turn also bind other proteins (137,138). BTLA and CD160 compete for binding to HVEM as they both bind its cysteine rich domain 1 (CRD1) (139). LIGHT and LTα bind CRD3 and CRD2 of HVEM, respectively (140). It is therefore possible that HVEM could form the core of a tetrameric complex (138). BTLA has been found to bind HVEM in trans as well as in cis when the two proteins are co-expressed on the same cell (141). The BTLA/HVEM cis interaction has been shown to prevent stimulatory HVEM signalling by its other ligands in trans, whereas inhibitory BTLA signalling from

trans interactions is unimpaired (111), indicating that inhibitory signalling outcompetes the stimulatory function of HVEM. Upon phosphorylation of the tyrosine signalling motifs in BTLA's cytoplasmic tail it preferentially recruits the more potent phosphatase SHP-1, but also recruits SHP-2, which strongly regulates TCR and CD28 signalling (117,143). BTLA therefore appears to inhibit T-cell responses via the recruitment of phosphatases to the cell surface and by inhibiting HVEM stimulatory signalling. Additionally, the Grb2 binding domains of BTLA have been suggested to produce a pro-survival signal by recruiting PI3K and Akt (144,145).

BTLA deficient T-cells were found to be hyperresponsive and proliferate more readily in response to antigen stimulation (132,146). Additionally, BTLA blockade, compared to PD-1 blockade, better enhanced the responsiveness of exhausted human T cells (147). Conversely, T cells stimulated with a BTLA agonist antibody were less responsive to anti-CD3 stimulation in terms of decreased proliferation and production of IFNγ (148). A similar

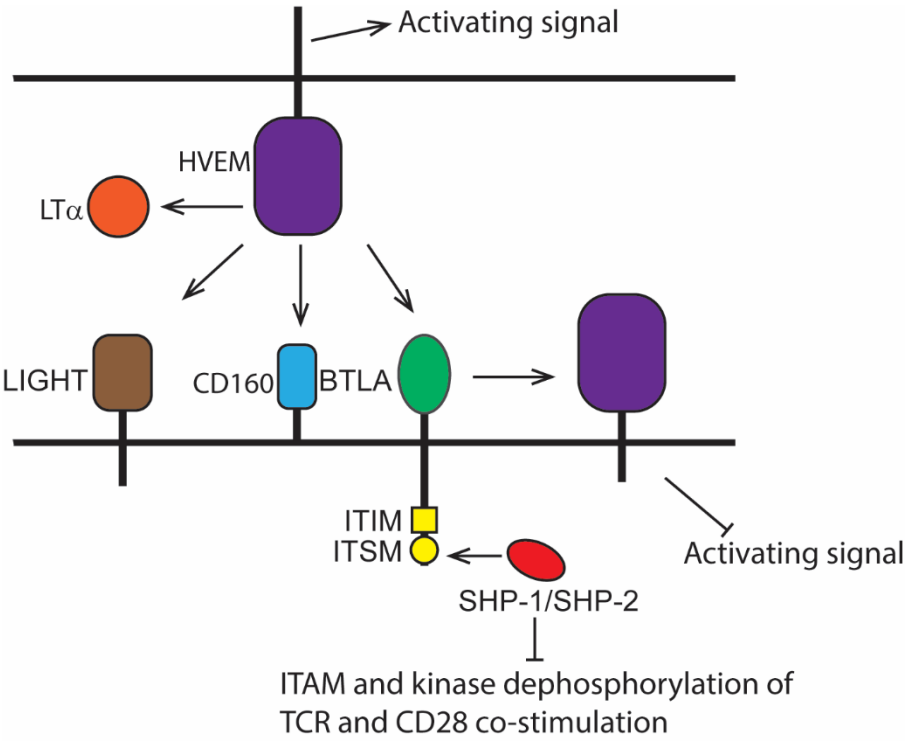


Figure 1.4. BTLA ligand interactions and signalling.

result was found in γδ T-cells wherein BTLA signalling inhibited proliferation and reduced IL-17 and TNF secretion (149). The maintenance of Treg cells was observed to be BTLA dependent, and loss of BTLA in Tregs doubled the number of GC B cells *in vivo* (150). In B cells, SHP-1 recruitment by BTLA has been linked to the reduced activation of downstream mediators of BCR signalling (151). BTLA suppresses IL-21 production by Tfh cells and limits their ability to offer T-cell help to germinal centre B cells, reducing germinal centre B-cell development and proliferation (152,153). BTLA also appears to act on DCs; overexpression of BTLA inhibited their proliferation and maturation. Further, DCs and macrophages from $BTLA^{-/-}$ mice had higher TNFα expression in response to LPS challenge, and $BTLA^{+}$ DCs from human tuberculosis patients had reduced effector cytokine expression and were found to induce a more tolerogenic Treg-Th2 response (154,155). These findings demonstrate a role for BTLA across a variety cell types, suggesting that the agonism of BTLA could be therapeutically effective.

BTLA ligand-based agonists and antibody-based agonists have both been developed. HVEM-Fc fusion proteins have been used to suppress immune responses *in vivo*. The fusion proteins were effective in a model of graft versus host disease (GVHD) and, in combination with cyclosporin, prolonged cardiac allograft survival (156,157). However, HVEM-Fc was also found to exacerbate collagen-induced arthritis in mice, possibly through LIGHT mediated stimulatory signalling (158). Two different anti-BTLA agonist antibodies could suppress GVHD, effects that were lost in $BTLA^{-/-}$ mice (159,160). Similar to the observations with HVEM-Fc, a BTLA agonist antibody prolonged murine cardiac allograft survival by inhibiting alloreactive T-cells and Treg expansion (161). This same antibody also ameliorated a murine model of atherosclerosis and was able to enhance the collagen content in pre-existing lesions, suggesting a stabilising effect (162). An additional anti-BTLA agonist antibody was found to suppress contact hypersensitivity in mice (163).

BTLA agonists therefore show promise in the treatment of autoimmune diseases although caution seems warranted regarding the use of a ligand-based approach, due to ligand reactions with additional receptors.

1.6.3 TIGIT

T-cell immunoreceptor with Ig and ITIM domains (TIGIT or Vstm3, VSIG9, WUCAM) is an inhibitory receptor of the immunoglobulin superfamily and has a single IgV-like extracellular domain, a single pass transmembrane region and a cytoplasmic tail with an ITIM and an immunoglobulin-tail-tyrosine (ITT)-like motif. TIGIT is predominantly expressed on activated T cells, memory T-cells NK cells and Tregs (100).

TIGIT appears to have three ligands in humans although there may be more (Fig. 1.5). The three known ligands are poliovirus receptor (PVR, CD155), PVRL2 (CD112) and nectin-4. The affinity of TIGIT for PVR is much higher than for PVRL2 (100). Moreover, PVR is a shared ligand with other receptors, i.e., the stimulatory CD226 receptor (DNAM-1) and inhibitory CD96 receptor (TACTILE) (100,164,165). PVR therefore appears to play a dual role as a ligand for both stimulatory and inhibitory receptors. However, it has been shown that TIGIT has the highest affinity for PVR and dominates PVR's interaction over all other PVR receptors in NK cell studies (100,166,167). Further, there is evidence that TIGIT can bind CD226 in cis and 'break' the CD226 homodimer inhibiting its signalling (168). TIGIT therefore, like HVEM, appears to inhibit a stimulatory receptor in cis. PVRL2 is also a shared ligand between TIGIT and CD226 as well as the more recently discovered CD112 receptor (169). TIGIT affinity for PVRL2 is very weak and CD112R, which is itself an inhibitory receptor, has the highest affinity for PVRL2 (100,169). Nectin-4 is only known to bind TIGIT and is highly expressed during foetal development (100). Nectin-4 expression

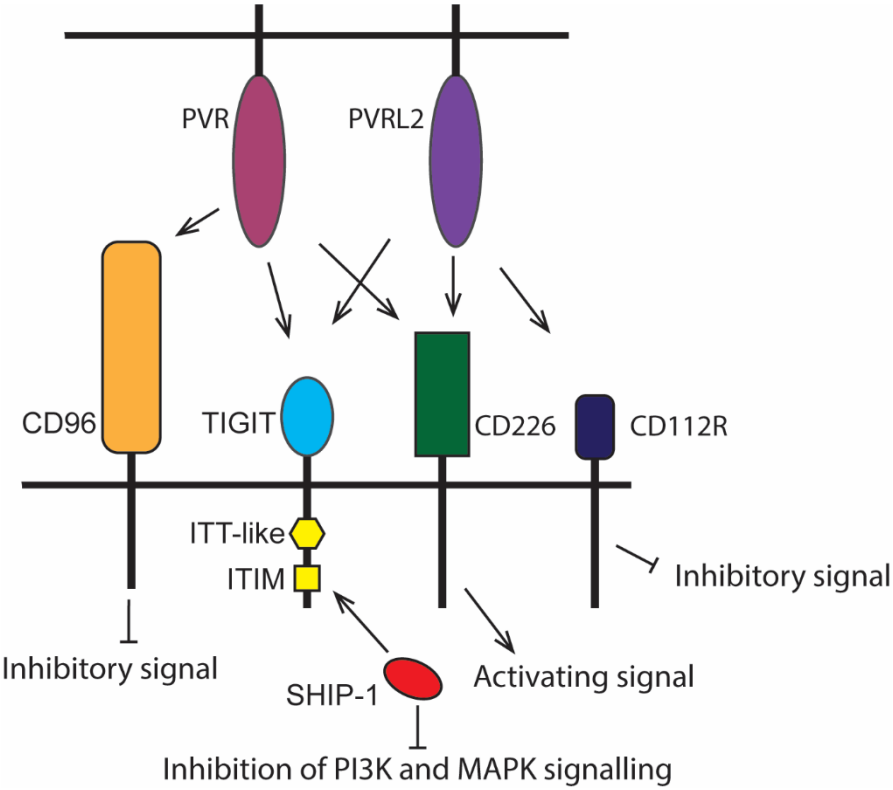


Figure 1.5. TIGIT-ligand interactions and signalling.

has been observed to increase in some tumours suggesting a role for TIGIT in immune evasion (170,171).

Phosphorylation of the TIGIT intracellular tyrosine motifs recruits the phosphatase SHIP-1. SHIP-1 inhibits PI3K and mitogen-activated protein kinase (MAPK) signalling pathways inhibiting NK cells and T cells (172,173). This inhibitory signalling is suggested to control T-cell proliferation as TIGIT$^{-/-}$ mice have hyperproliferative T-cell responses (96). Moreover, TIGITs role as a suppressor of NK and T-cell function has further been supported by studies of the *F. nucleatum* Fap2 protein. Fap2, is another ligand for TIGIT that suppresses the cytotoxic activity of NK cells and the activity of tumour infiltrating CD4^{+} and CD8^{+} T-cells (174). Lastly, Tregs expressing high levels of TIGIT were observed to efficiently suppress Th1 and Th17 T-cells due to the TIGIT induced expression of fibrinogen-like protein 2 (FGL-2), known to reduce effector T-cell proliferation (175).

Taken together, the data suggest that TIGIT agonism could have therapeutic potential. Three agonist anti-TIGIT antibodies were found to reduce disease severity in an EAE model (176).

1.6.4 IL-10R

The IL-10R is composed of two chains, IL-10Rα (CD210a) and IL-10Rβ (CDw210b, CRF2-4) which bind the secreted cytokine IL-10. IL-10Rα engages IL-10 with high affinity and is its private receptor chain. Conversely, IL-10Rβ has a very low affinity for IL-10 alone and is a shared receptor chain with IL-22, IL-26, IL-28 and IL-29. The intracellular domain of IL-10Rα is associated with JAK1 and IL-10Rβ associates with TYK2, and upon receptor dimerisation JAK1 and TYK2 phosphorylate STAT3 (Fig. 1.6). IL-10Rα is mainly expressed by leukocytes with the highest expression found on monocytes and macrophages and to a lower extent on NK cells, DCs, mast cells, T cells and B cells, whereas IL-10Rβ expression is ubiquitous.

IL-10 signalling is pleiotropic and generally immunosuppressive however it also appears to have some stimulatory effects. Upon phosphorylation, STAT3 enters the nucleus where it acts as a transcription factor stimulating STAT3 responsive genes, which perform the effector functions of IL-10 signalling. Additionally, the signalling cascade PI3K/Akt/GSK3β also mediates IL-10 induced transcription in macrophages (177). AMP-activated protein kinase (AMPK) has also been implicated in IL-10 signalling and its absence reduced STAT3 phosphorylation, PI3K pathway activation and the ability of IL-10 to suppress inflammatory gene expression (178). In macrophages IL-10 signalling was found to reduce LPS-induced gene expression by ~20% including expression of MHC-II, pro-inflammatory cytokines, and chemokines (179–183). The main mechanism of suppression was found to be inhibition of transcription (184). Cytokine expression by neutrophils was also inhibited in response to IL-10 (185). IL-10 impairs antigen presentation

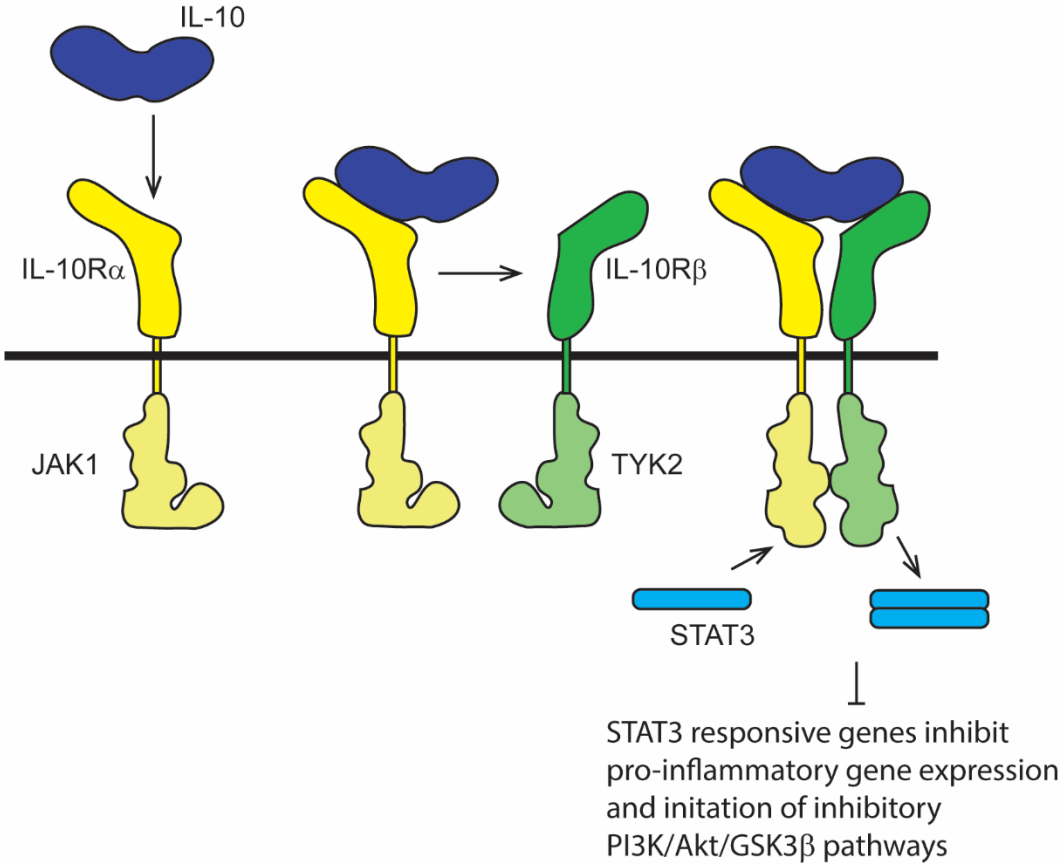


Figure 1.6. IL-10R formation and signalling. IL-10 binds IL-10Rα and this complex recruits IL-10Rβ to form the signalling complex.

by DCs and their maturation is inhibited by IL-10 signalling, reducing their ability to drive a pro-inflammatory T-cell response (186,187). T-cell inhibition by IL-10 occurs indirectly through its actions on APCs; however, IL-10 was also found to directly suppress Th17 cells and Th2 cells (188–191). IL-10 also enhances the survival of Tregs and their ability to inhibit Th17 cells (192,193).

Intriguingly, IL-10 has been found to have stimulatory effects on some effector cell functions: for example, $CD8^+$ T-cell proliferation, IFNγ production and cytotoxicity are increased by IL-10 signalling (194–196). Additionally, B cells and mast cells can also be activated by IL-10 (197–199). Interestingly, IL-10 has also been found to have effects outside of the immune system as reviewed elsewhere (200). The broadly immunosuppressive profile of IL-10 signalling has made it an attractive therapeutic target

for the treatment of autoimmunity. However, it has also been targeted for the treatment of cancers due to its stimulatory effects on $CD8^+$ T-cells.

IL-10R agonists have been trialled in mice and humans to assess their therapeutic potential. Systemic administration of IL-10 was tested in multiple trials in IBD patients, however, it generally did not improve the clinical outcomes (201–204). A reason for the lack of therapeutic activity observed in humans is thought to be the low concentrations of IL-10 achieved locally. *L.lactis,* a gram-positive bacterium, has been engineered to express the IL10 gene for intragastrical delivery. This was found to ameliorate IBD in mice and the clinical disease scores in a small human cohort of Crohn's disease patients (205,206). IL-10 also showed some promising results in human rheumatoid arthritis and psoriasis patients when applied locally (207–209).

Engineering of IL-10 has modified its affinity for the IL-10R receptor chains, particularly IL-10Rβ (210,211). Lowering the affinity of IL-10Rβ restricted IL-10 signalling to the cells with the highest receptor expression levels, i.e., macrophages and monocytes (211). Conversely, increasing IL-10Rβ affinity led to IL-10-mediated stimulatory effects on $CD4^+$ and $CD8^+$ T-cells (210,211). These findings indicate that the affinity of IL-10 for IL-10Rβ, or its concentration, can determine whether IL-10 will inhibit innate immune cells and, indirectly, lymphocytes or whether it will enhance lymphocyte effector function. A bispecific anti-CD86-IL-10 fusion antibody induced IL-10R signalling selectively in $CD86^+$ APCs which promoted the development of Tregs (212). A phase I trial was initiated with anti-CD86-IL-10, however, volunteers developed anti-drug antibodies and development was discontinued (213). Attempts to utilise IL-10 therapeutically in a systemic fashion for the treatment of autoimmunity have mostly been unsuccessful. However, newer findings suggest that selective agonism of IL-10 in immunologically active sites or on specific cell types may have promise.

Due to the increase in $CD8^+$ T-cell cytotoxic activity previously observed it has been suggested that IL-10's immunostimulatory effects could be leveraged in anti-tumour therapy. Seemingly contradictory observations have been made about IL-10 in cancer. Overexpression or administration of IL-10 was associated with a reduction in tumour size, but the presence of IL-10 in the tumour microenvironment has been found to correlate with a worse prognosis (214–217). These findings may be explained by the observations made with the engineered IL-10s described above, i.e., that concentration is key in determining which cells are responsive to IL-10. PEGylated IL-10 (Pegilodecakin), a fusion to improve the pharmacokinetics of IL-10, showed promise in animal models and in phase I clinical trials increasing $CD8^+$ T-cell activity (195,196,218). However, phase II and III trials revealed that there was no increase in efficacy in multiple cancers when PEGylated IL-10 was given in combination with the standard treatments compared to standard treatment alone (219–221).

1.7 Bispecific antibodies

Monoclonal antibodies (mAbs) have antigen binding sites formed by variable heavy (VH) and variable light (VL) domains and an Fc region. Bispecific antibodies can bind two different epitopes simultaneously by combining the antigen binding sites of different antibodies. The bound epitopes can be on different molecules which provides an opportunity to target two different molecules in one therapeutic process. This makes bispecific antibodies particularly interesting as can be seen by the more than 156 clinical trials, recruiting or active, produced by a search of ClinicalTrials.gov with the term "bispecific antibody" (5/2/2023). Further, four of the 12 antibodies approved for use in the US and/or EU were bispecific antibodies in 2022 (222). Bispecifics come in a range of formats which vary in their resemblance to IgG, symmetry, presence of Fc domain, addition of extra

binding domains and valency (as reviewed elsewhere (223). Bispecific antibodies do not occur naturally in humans, except for hIgG4 which is capable of Fab arm exchange (224). The challenge in generating bispecific antibodies is in part due to the variable domains being composed of one VH and one VL chain. Promiscuous pairing of these chains in a conventional antibody format gives 16 possible combinations when all chains are co-expressed. Therefore, if left to assemble randomly, 6.25% of antibodies generated would have the desired bispecificity (225).

The pairing problem represents two distinct challenges: i.e., correct heavy chain (HC) HC heterodimerisation and correct HC light chain (LC) pairing. Various approaches have been developed to guide or enforce correct pairing of these different chains. Heavy-chain pairing is mediated by the third constant region CH3 of IgG and dimerisation is guided by a small number of key residues in CH3, i.e., T366, L368, F405, Y407 and K409 in hIgG1 (226). The introduction of "knob in hole" mutations in CH3 has been a popular approach to guide heterodimeric HC pairing. In this approach the larger amino acid side chains on one CH3 domain are substituted with smaller amino acids to generate a "hole". Conversely, the smaller amino acid side chains on the other CH3 are substituted with larger amino acid side chains to generate a "knob" and heterodimerisation is mostly dependent on hydrophobic interactions between the two different CH3 domains. Early experiments showed >95% heterodimerisation using the knob in hole approach and it has been widely adopted since (223,227,228). The use of electrostatic interactions to guide heterodimeric HC pairing has also proven to be effective. By modifying existing electrostatic interactions or introducing additional electrostatic interactions heterodimerisation can be favoured by generation of one positively charged CH3 and one negatively charged CH3 (229,230). Yet another approach mimicking Fab arm exchange by hIgG4 has also been developed in which K409R and F405L mutations were introduced into hIgG1 which destabilised the homodimeric conformation.

In this case the two monospecific parental antibodies are expressed separately and mixed under mild reducing conditions, which splits the parental homodimers enabling the formation of more stable heterodimers, in a process known as controlled Fab arm exchange (cFAE) (231,232). An advantage of cFAE is the separate expression of the parental antibodies, which ensures that cognate HC/LC is unperturbed.

The light chain problem has also been solved in multiple ways. Affinity chromatography has been used to purify the 25% correctly paired bispecific antibody from the monospecific and non-functional antibody milieu that exists with correct HC heterodimerisation and random LC association (233). The use of two variable domains with one shared LC sequence or the use of single domain antibodies lacking a light chain has also been used to circumvent the light chain pairing problem (227). A solution that had discrete LCs and forced correct pairing was to directly couple the correct LC and HC in an scFv format (234). Similar approaches to those used in overcoming the HC problem have also been used to modify the CH1/CL interaction interface. One such approach swaps CH1 and CL1 in one of the two variable domains used in the desired bispecific antibody resulting in one arm having VL-CH1 and VH-CL1-CH2-CH3 which was found to enhance cognate HC-LC pairing (235). Another effective approach replaced the native disulphide bond in one HC-LC pair with an engineered disulphide bond elsewhere, and a third approach modified the CH1/CL interface to increase the affinity of correct HC-LC binding (236,237). Many ways have been used to guide correct HC-HC and HC-LC pairing, enabling the creation of bispecific antibodies in many different formats and the design of novel bispecific therapeutics.

The unique capabilities of bispecific antibodies have made them attractive for the development of therapeutics. Therapeutic uses include the recruitment and activation of immune cells, and immune checkpoint and inflammatory factor blockade (238–240). One of the earliest bispecific antibodies to be licensed was a bispecific T-cell engager (BiTE)

against CD3 and CD19 (Blinatumomab). Blinatumomab cross-linked T-cells to B-cells resulting in T-cell mediated B-cell destruction for the treatment of advanced acute lymphoblastic leukemia and B-cell precursor acute lymphoblastic leukemia (241,242). The prevention of inhibitory signalling by combinatorial immune checkpoint blockade is being trialled with an anti-PD1 anti-CTLA-4 bispecific antibody, which is showing promise in the treatment of unresectable hepatocellular carcinoma in combination with the kinase inhibitor lenvatinib (243). Most development in the bispecific antibody field has been focused on cancer. However, bispecific antibodies capable of binding two inflammatory cytokines simultaneously for the treatment of autoimmunity are also being investigated as potential treatments for autoimmunity (238).

The improvement and developments in bispecific antibody design make them attractive therapeutics which possess the characteristics of monoclonal antibodies, which have long been used in the clinic and are well tolerated.

1.7.1 Murine Bispecific Antibodies

The testing of novel therapeutics in model systems is crucial to understand their function and while much can be achieved by testing on human cells *in vitro* this approach is limited in its ability to replicate the complexity of intact immune systems. Therefore, testing in animal models is essential to further our understanding of how therapeutics act and predicting their therapeutic potential before testing in humans. Mouse models are normally the first species used for these experiments and, while not a perfect comparison to the human immune system, the two are remarkably similar (244). It is surprising, therefore, that with the advancements in human bispecific antibodies there are only three published approaches for the generation of murine bispecific antibodies (245–247). These murine bispecific antibodies are particularly needed in disease models where repeated dosing is required to

avoid anti-drug responses. This is of particular interest in models of autoimmune disorders as these are chronic conditions and modelling medium to long-term immune suppression is desirable.

This thesis investigates two approaches for making murine bispecifics that have been thoroughly described: one, from Labrijn *et al.*, and the other from Wang *et al.* (245,246). The Labrijn *et al.* approach relies on a process of cross Fab-arm exchange (cFAE) (Fig. 1.7A). In this method both parental antibodies are produced with either F405L-N411T and T370K-K409R mutations in CH3 and purified separately (Fig. 1.7B). Separate expression avoids errant HC-HC and HC-LC pairing while the mutations weaken non-covalent HC-HC homodimer interactions. To form a bispecific antibody the parental antibodies are mixed in mild reducing conditions which, due to the mutations, allow for inter-HC bonds in the homodimer to be broken while maintaining HC-LC bonds, forming half antibodies (Fig. 1.7A). Upon re-oxidation the mutations strongly favour formation of HC-HC heterodimers thus producing bispecific antibodies.

In the second approach, from Wang *et al.*, all bispecific antibody chains are expressed together (Fig. 1.8A) (246). This is enabled by mutations in both CH3 and in one of the HC-LC pairs. Correct heterodimeric HC-HC pairing is guided by E356K-D399K and K409E-K439D mutations in CH3 to electrostatically steer correct pairing (Fig. 1.8B). Correct HC-LC pairing is favoured by moving the cysteines, which form the HC-LC disulphide bond, from the end of the LC and HC hinge to S121C and Y122C, respectively (Fig. 1.8C).

1.8 Work leading up to this thesis

Previous work by the Davis and Cornall groups (described in the PhD theses of Billur Akkaya and Christopher Paluch (248,249)) characterised inhibitory immunoreceptor agonists. An anti-hPD-1 agonist called Clone 19 (Cl.19) inhibited T-cell responses to

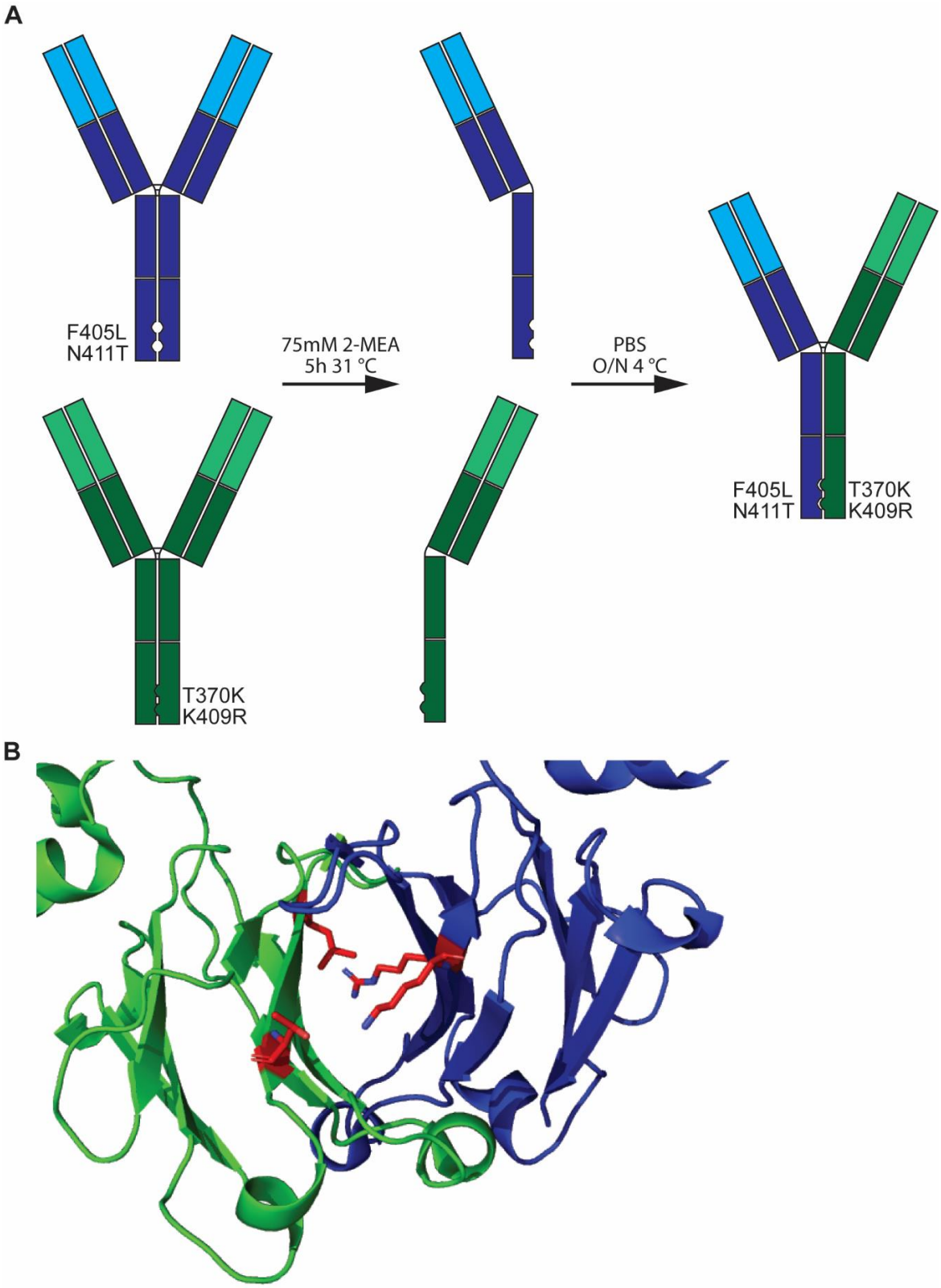


Figure 1.7. Principle of murine bispecific antibody generation by controlled Fab-arm exchange. (A) The process of cFAE. Two parental antibodies (*blue* and *green*), with complementary CH3 mutations, are produced separately. They are mixed and reduced to break inter-heavy chain disulphide bonds and then buffer exchanged to allow formation of heterodimers guided by the mutations in CH3. (B) Ribbon structure of the HC-HC heterodimer with the mutations (*red*) enabling cFAE in mIgG1 CH3 (PDB: 3HKF). Adapted from (245).

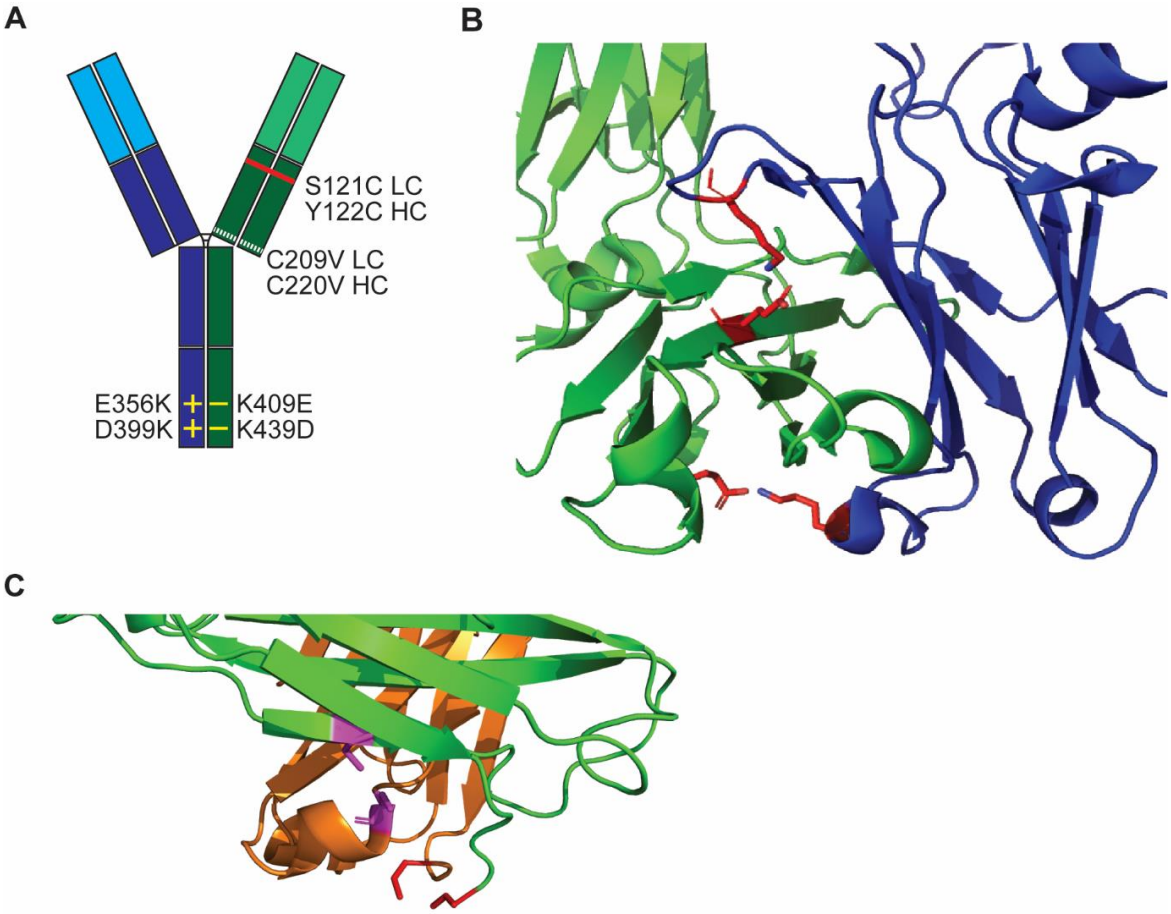


Figure 1.8. **Principle of murine bispecific generation by electrostatic steering.** (A) Schematic of the bispecific antibody with mutations introduced into mIgG1 CH3 and a new disulphide bond between the LC and HC (*red*). The original LC-HC disulphide bond (*dashed line*) is removed by C to V mutations. (B) Ribbon structure of the HC-HC heterodimer with the mutations (*red*) favouring HC-HC heterodimer formation (PDB: 3HKF). (C) Introduction of an inter LC-HC disulphide bond at S121 in CL and Y122 in CH1 (*magenta*) and removal of the native inter LC-HC disulphide bond (*red*) (PDB: 1IGT). Adapted from (246).

various stimuli *in vitro* and *in vivo* but had limited efficacy in an EAE model, a T-cell transfer model of colitis and GVHD. An anti-hBTLA agonist, called 286, inhibited T-cell responses *in vivo* and *in vitro* and ameliorated T-cell transfer-driven colitis and GVHD. The T-cell inhibition by both agonists was found to be Fc receptor dependent. Both antibodies and an anti-TIGIT antibody referred to as CE10 were epitope-mapped and their affinities determined. The affinity of Cl.19 was 27 nM, the affinity of 286 was 0.4 nM and the affinity of CE10 was 0.9 nM. None of these antibodies were ligand blocking, and all were found to have membrane proximal epitopes. Anti-hIL-10Rα hybridomas and anti-mIL10Rβ

hybridomas had been generated for the Davis group by BioGenes GmbH but remained uncharacterised. Humanised inhibitory immunoreceptor receptor "knock-in" C57BL/6 mouse strains were generated for PD-1, BTLA and TIGIT to investigate the therapeutic potential of inhibitory receptor agonists. Strategy and creation of these mice was led by Dr Consuelo Anzilotti and their production was outsourced to InGenious Targeting Laboratory. The strains were designed to express the human extracellular domain of the receptors fused to the murine transmembrane and intracellular signalling domain. The hBTLA and hTIGIT mice were crossed with the hPD-1 mice and characterised in the thesis of Christopher Paluch (249). The mice were found to have normal immune system development and the humanised receptors were cross-reactive with their murine ligands. Consuelo Anzilotti also led the strategy and creation of hIL-10Rα mice which were generated by Taconic Artemis in the manner of the other humanised mice (described in the thesis of Christopher Paluch), but were not cross with hPD-1 (249).

1.9 Aims of thesis

The agonistic activity of inhibitory immunoreceptor agonists is dependent on Fc receptor engagement. This thesis aims to generate murine bispecific antibodies for two purposes. Firstly, the goal is to investigate whether Fc receptor engagement by agonist antibodies can be substituted with the binding of a tissue antigen *in vivo*, and whether this retains the inhibitory activity of the agonists. Secondly, it aims to generate agonistic antibodies against the IL-10R which possess membrane proximal epitopes and can engage Fc receptors, in order to determine whether (a) the principles underlying immunoreceptor superagonism are applicable to cytokine receptors, and (b) this could enhance the agonistic effects of the antibodies at immunologically-active sites *in vivo*. For this, putative IL-10R agonists were tested for their ability to ameliorate IBD in hIL-10Rα mice. For both sets of experiments,

the over-riding goal was to further develop our understanding of the properties and utility of agonistic antibodies.

Chapter 2

Chapter 2 Material and Methods

2.1 Molecular Cloning

Protein sequences were obtained from UniProt and DNA sequences were ordered from GeneArt (Thermo Fisher Scientific), or Genewiz (Azenta). DNA was codon optimised for the intended expression cell line species using the tools provided by the supplier of the DNA sequences. The ordered DNA sequences included 5' and 3' restriction sites for insertion into the desired vector and a TAGTAG sequence at both the 5' and 3' end to ensure efficient restriction digestion. DNA was amplified by PCR with Phusion High-Fidelity DNA polymerase (Thermo Fisher Scientific) and primers complimentary to the 5' and 3' ends of the gene, which had melting temperatures of 65-70°C (calculated using NEB's online Tm calculator). The PCR protocol was varied to meet the requirements of different constructs, in accordance with the manufacturer's guidance.

PCR products of the correct size were isolated by excision from an ethidium bromide stained 2% agarose gel in TBE buffer. PCR products, alongside a DNA size marker, were separated in this gel based on size using 80 mA and the DNA in the excised bands was extracted using a QiaQuick gel extraction kit (Qiagen).

The DNA sequence to be inserted and vectors were digested using restriction enzymes from NEB following the recommended protocols. The digested DNA products were purified using the QiaQuick gel extraction kit.

Ligation of the insert into the vector was performed using T4 DNA ligase (NEB) at 16°C for at least 2 hours, using vector to insert molar ratios of 1:1, 1:3, 1:5 and 1:10. Chemically competent TOP10 *E. coli* were transformed with the ligation product. Transformed cells were spread onto LB-agar plates containing the relevant selection antibiotic and incubated for 16-20 hours at 37°C. Colonies were picked from these plates into selection antibiotic

containing LB broth individually and incubated for 16-20 hours at 37°C. DNA was extracted from the bacterial LB cultures using PureLink HiPure Plasmid Miniprep or Midiprep kits (Thermo Fisher Scientific).

Purified plasmids were sequenced using primers designed to cover the multiple cloning sites and any insertion therein (Sanger sequencing performed by SourceBioscience). Sequences were analysed using SnapGene software to ensure the insertion had the intended sequence.

2.1.1 Design of IL-10Rα mutants

The surface exposure of hIL-10Ra extracellular domain (ECD) amino acids was calculated using the crystal structure (PDB: 1j7v) and the Naccess program (http://www.bioinf.manchester.ac.uk/naccess/). Residues with >50% surface exposure were selected for mutation. Mutants were individually generated by overlap extension PCR with primers designed to change specific amino acids from their WT residues to arginine, except for histidine, lysine and arginine, which were mutated to aspartic acid instead.

The hIL-10Ra ECD mutants were fused to the mCD28 transmembrane and the first 8 cytoplasmic residues. These constructs were cloned into the pGFP^2-N3 vector for transient expression.

The hIL10Rα mutant panel was designed by Susan Yu and Yuan Liu. The hIL10Rα mutants were produced by Heather Brouwer and me.

2.1.2 Bispecific antibody design

Bispecific antibody sequences were produced using mIgG1 sequence from Uniprot (P01868) with the variable sequences from in-house antibodies for 286, 286-scFv, 2C1, 3D7, Nb82, Nb41, 611, 151, 827, Nb5 and Nb6. Kappa light chains were used (P01837). Mutations were introduced into the HC and LC as needed in accordance with Labrijn *et al.*

or Wang *et al.* (245,246). For anti-BTLA*anti-OVA bispecific antibodies the D265A mutations was also included. Each heavy chain of a given bispecific pair expressed a different C-terminal purification tag a His-tag (HHHHHH) or a c-tag (EPEA) for purification purposes.

In cases where a nanobody was incorporated the nanobody sequence was ligated onto the last three residues of CH1 prior to the hinge. In cases where an scFv was incorporated it was directly ligated to the hinge in place of CH1 with a $(G_4S)_2$ glycine serine linker.

2.1.3 IL-10R design

mIL-10Rb and hIL-10Ra extracellular domains were produced for SPR analysis and nanobody generation. A C-terminal His-tag was added for purification. hIL-10Ra was produced by Susan Yu and I. Different versions of mIL-10Rb for anti-mIL-10Rb nanobody identification and selection were produced which included: the addition of a Strep-tag between the ECD sequence and His-tag; the addition of a BirA site for biotinylation between the ECD sequence and His-tag.

The sequences of mIL-10Rb and hIL-10Rb share a conserved sequence between D1 and D2 of DTIIGPP. This was used as the site of fusion for IL-10Rb mD1/hD2 fusion.

2.2 Cell culture

2.2.1 HEK293T

HEK293T cells were cultured in DMEM (Sigma-Aldrich) supplemented with 2 mM L-glutamine, 10% heat-inactivated FCS and 50 units penicillin and 50 µg streptomycin per ml. Prior to harvesting supernatant for protein purification by immobilised metal affinity

chromatography the concentration of FCS was reduced to 2% to minimise bovine serum albumin.

2.2.2 CHO-K1

CHO-K1 cells were cultured in DMEM supplemented with 2 mM L-glutamine, 1 mM Sodium Pyruvate, 1x mixture of non-essential amino acids supplement (Invitrogen), 10% heat-inactivated FCS and 50 units penicillin and 50 µg streptomycin per ml.

2.2.3 ExpiCHO-S

ExpiCHO-S cells were cultured in ExpiCHO expression medium (Thermo Fisher Scientific) supplemented with 2 mM L-glutamine.

2.2.4 Expi293F

Expi293F cells were cultured in Exp293 expression medium (Thermo Fisher Scientific) supplemented with 2 mM L-glutamine.

2.2.5 B-cell hybidromas

B-cell hybridomas were cultured in RPMI-1640 (Sigma-Aldrich) supplemented with 2 mM L-glutamine, 1 mM Sodium Pyruvate, 10 mM HEPES, 100 µM hypoxanthine, 16 µM thymidine supplement (HT supplement), 1x non-essential amino acids supplement (Invitrogen), 15% heat-inactivated FCS and 50 units penicillin and 50 µg streptomycin per ml. Prior to harvesting supernatant for antibody purification FCS was changed to 10% ultra-low IgG FCS.

2.2.6 EL4 cells

EL4 cells were cultured in DMEM (Sigma-Aldrich) supplemented with 2 mM L-glutamine, 10% heat inactivated FCS and 50 units penicillin and 50 µg streptomycin per ml. EL4, specifically EL-4-blue cells expressing plasma membrane markers fused to TagBFP2 were a generous gift from Gillian Griffiths (University of Cambridge).

2.2.7 Primary murine cells

Primary murine cells, e.g., Splenocytes, were cultured in RPMI-1640 supplemented with 2 mM L-glutamine, 100 µM sodium pyruvate, 10 mM HEPES, 50 µM b-mercaptoethanol, 100 uM non-essential amino acid supplement, 10% heat inactivated FCS and 50 units penicillin and 50 ug streptomycin per ml.

2.2.8 Stable transfection of CHO-K1 cells

The IL-10Rb used for generating nanobodies was produced using a stable CHO-K1 cell line. The cell line was produced using the Lonza PEE14 vector, which contains the glutamine synthetase gene. The presence of the glutamine synthetase gene allowed for selection of transfected cells using Methionine sulfoximine (MSX), which is a glutamine synthetase inhibitor, to kill untransfected cells in glutamine free media.

A transfection mixture of 500 µl DMEM, 10 µg PEE14 vector (containing mIL10Rb extracellular domain) and 30 µl Genejuice (Sigma-Aldrich) was made and incubated for 20 minutes at room temperature before adding it to cells. The transfection mixture was added to CHO-K1 cells the day after seeding $4x10^6$ cells in 20 ml glutamine free media in a 75 cm^2 tissue culture flask. The day after transfection, cells were detached using trypsin and media was changed with fresh glutamine free media and plated at $1x10^5$ cells per well in 96-well flat-bottomed plates (100 µl media per well). MSX was added to the wells with a final

concentration of 35 µM, 40 µM, 45 µM, 50 µM and 55 µM (two plates per concentration). Seven days after MSX addition the media was replaced with fresh MSX containing, glutamine free, media. Once supernatants began changing colour towards orange, plates were screened for wells with highly expressing cells.

Protein expression in supernatants was assessed using a dot blot. 5 µl supernatant was pipetted onto a nitrocellulose membrane. The membrane was blocked with 1% skimmed milk in PBS for one hour at room temperature. Subsequently the membrane was incubated in 0.2 µg/ml anti-penta-His antibody (Invitrogen) in blocking buffer for 45 minutes at room temperature. The membrane was then washed with 0.05% Tween-20 (Sigma-Aldrich) in PBS three times followed by incubation with a horseradish peroxidase conjugated antibody at 1 µg/ml in blocking buffer prior to a further three washes in PBS Tween. The membrane was developed using Pierce ECL western blotting substrate and exposed to an X-ray film using darkroom development techniques.

Highly expressing wells were screened for wells containing a single-cell colony and these were selected for further culture and expansion. Supernatants from these cells were harvested for protein purification.

2.2.9 Transduction of HEK293T cells

All proteins for SPR analysis, IL-10Rb used for nanobody screening, Labrijn method-based bispecific antibodies and Wang-based bispecific antibodies were produced using a lentiviral expression system. The lentiviral system, derived from human immunodeficiency virus, is composed of three plasmids which transfected into HEK293T cells together produced self-inactivating virus. This self-inactivating virus was used to transduce fresh HEK293T cells, integrating into the genome and initiating gene of interest expression. The pHR vector has a multiple cloning site into which the gene of interest is inserted under the control of the CMV

promoter. The pMD2G vector contains viral coat proteins for packaging and the p8.91 vector contains the enzymes and structural proteins required to produce infectious viral particles.

On day 0, HEK293T cells were seeded in a 6-well plate in 2 mL medium per well for transfection. On day 1, 100 µL DMEM, 3 µL of GeneJuice transfection reagent (Sigma-Aldrich), 0.5 µg pHR, 0.5 µg p8.91 and 0.25 µg MDG were mixed and incubated at room temperature for 20 minutes prior to addition HEK293T cells. On day 3, the supernatant was harvested and replaced with fresh media for a second harvest on day 4. Harvested supernatant was centrifuged at ~500g for 5 minutes to pellet cells prior to filtration of the supernatant through a 0.45 µm filter. The harvested lentiviral supernatant was stored in the fridge for up to seven days prior to use. HEK293T cells were seeded in a 25 cm^2 flask 24 hours before transduction with lentiviral supernatant. Transduced HEK293T cells were expanded, and supernatant was collect for protein purification.

2.2.10 Transient transfection of HEK293T cells

The $pGFP^2$-N3 vector was used for the expression of hIL-10Ra receptor mutants in HEK293T cells. On day 0, cells were plated in 2 ml of media per well in 6-well plates. Day 1, cells were transfected with 0.5 µg DNA and 1.5 µL of GeneJuice transfection reagent (Sigma-Aldrich) per well. Day 3, cells were harvested in ice-cold PBS by vigorous pipetting. The harvested cells were split into 96-well plates for antibody staining and epitope mapping.

2.2.11 Transient transfection of ExpiCHOs and Expi294

Labrijn method-based antibodies and Wang method-based antibodies were produced using ExpiCHO cells and Wang-method based antibodies were also produced using Expi293 cells. For transfection of ExpiCHO and Expi293 the pcDNA3.1- vector was used, and the transfections were performed in accordance with the relevant expression system user guide

from Thermo Fisher Scientific. For ExpiCHO expression the Max Titer Protocol was followed.

Available at:

- https://assets.thermofisher.com/TFS-Assets/LSG/manuals/MAN0014337_expicho_expression_system_UG.pdf
- https://assets.thermofisher.com/TFS-Assets/LSG/manuals/MAN0019402_Expi293_ExpressionSystem_3L_UG.pdf.

2.3 Protein Purification

2.3.1 Nickel-purification

Proteins expressed with a 6x His-tag were purified by Ni-NTA affinity chromatography. Harvested protein supernatant was centrifuged at 3000 g for 20 minutes to remove cellular debris and adjusted to pH 8. Protein was purified using HisTrap HP 5 ml column (Cytiva) and an AKTA start chromatography system (Cytiva). The column was washed with 5 column volumes (CV) of distilled water, 5 CV of elution buffer (PBS, 0.5 M NaCl, 250 mM imidazole, pH 7.4) and equilibrated with 10 CV of PBS pH 7.4. Supernatant was passed over the equilibrated column followed by 10 CV PBS pH 7.4. Weakly associated proteins were removed by 5 CV of 30 mM imidazole elution buffer or a step-wise gradient of 22.5 mM to 42.5 mM imidazole elution buffer. Desired protein was eluted with 5 CV of elution buffer. The column was stripped and recharged using PBS 0.5 M NaCl 50 mM EDTA, pH 7.4 and 0.1 M $NiSO_4$ in distilled water.

2.3.2 C-tag purification

Proteins expressed with a C-tag (C terminal EPEA) were purified by affinity chromatography using a CaptureSelect C-tag column (Thermo Fisher Scientific) and an AKTA start system (Cytiva). Harvested protein supernatant was centrifuged at 3000 g for 20 minutes to remove cellular debris. The column was washed with 5 CV TBS (20 mM Tris, 150 mM NaCl) prior to sample application followed by 5 CV TBS and elution of the desired protein using a 2 M $MgCl_2$, 20 mM Tris, pH 7.4 elution buffer. Column was cleaned before and after runs with 5 CV 0.2 M glycine pH 2.

2.3.3 Protein-G purification

Murine antibodies from B-cell hybridomas were purified using protein G affinity chromatography. Harvested protein supernatant was centrifuged at 3000 g for 20 minutes to remove cellular debris and diluted in equal volume PBS pH 7.4. Protein G Sepharose beads (Cytiva) were packed in a glass Econo-Column (Bio-Rad). The volume of beads was adjusted based on the volume to be purified but was typically 5 ml for 1 L of supernatant. The column was washed with 10 CV PBS, 0.5 M NaCl, pH 7.4 prior to application of protein supernatant. Subsequently, the column was washed with 5 CV PBS, 0.5 M NaCl, pH 7.4 before elution of the desired antibody using 5 ml fractions of 0.1 M glycine pH 2.5 until no further protein was eluting, assessed by measuring OD at 280 nm with a NanoDrop One. Eluted fractions were immediately neutralised with 200 ul 2.75 M Tris pH 8.5 per fraction. Antibodies from B-cell hybridomas used in this thesis were purified by Heather Brouwer, Christopher Paluch and me.

2.3.4 Controlled Fab arm exchange

Equimolar amounts of parental Labrijn antibodies were incubated together in 75 mM 2-MEA at 31°C at a final concentration of 1 mg/mL. Removal of 2-MEA was performed using PD-10 desalting columns (Cytiva). Samples were stored at 4°C overnight to allow re-oxidation of the disulphide bonds. As described by Labrijn *et al.* (245).

2.3.5 Protein concentration and buffer exchange

Tangential flow filtration was used to reduce large volumes of protein supernatants to smaller volumes for protein purification. A Vivaflow 200, PES, 10,000MWCO (Sartorious) was used for this.

Small volumes of purified proteins were concentrated and/or buffer exchanged using Amicon Ultra-15 centrifugal filter units (Merck) with an appropriate MWCO based on protein size.

2.3.6 Size-exclusion chromotography

Size exclusion chromatography was performed using a Superdex 200 Increase 10/300 GL (Cytiva), a Superdex 75 10/300 GL increase (Cytiva) or a ProteoSEC Size Exclusion column 6-600kDa HR resin 16/600 column (Generon) depending on protein size, volume, and desired resolution. All eluted proteins were buffer exchanged and separated from aggregates by SEC. SEC was performed using either an AKTA start or an AKTA pure chromatography system.

2.3.7 Protein concentration quantification

Protein concentrations were determined by spectrophotometry. A NanoDrop One was used to measure absorbance at 280 nm and relevant protein extinction coefficients were calculated using the ExPASY ProtParam online tool (available: https://web.expasy.org/protparam/)

2.3.8 Polyacrylamide-gel electrophoresis

Mass and purity of purified proteins was assessed after size exclusion chromatography by sodium dodecyl sulfate–polyacrylamide gel electrophoresis (SDS-PAGE). 10 µL of protein sample (at less than 0.5 mg/mL) was diluted in 2x reducing or non-reducing loading buffer. Samples were boiled at 96 °C for 5 minutes prior to loading 15 µL per well of self-made 12% SDS-PAGE gel or NuPAGE 4 to 12% (Thermo Fisher Scientific). A protein ladder of known size was run alongside the proteins of interest. Electrophoresis was carried out at 150 V in a Tris/glycine/SDS-PAGE running buffer. Self-made 12% SDS-PAGE gels consisted of a 12% resolving gel and a 4% stacking gel. Subsequently, gels were subjected to Western blotting, Coomassie Brilliant Blue or Quick Coomassie stain (Generon). Gels were placed in 0.1% Coomassie Brilliant Blue, 40% methanol, 10% acetic acid solution for 15 minutes prior to destaining in a 12% methanol, 10% acetic acid solution to remove background staining. In cases where Quick Coomassie stain was used the gel was placed in the solution for 15-30 minutes before destaining in distilled water.

12% acrylamide resolving gel (recipe for 1 gel): 1.75 ml dH2O, 1.25 ml Tris/HCl pH 8.8 SDS resolving buffer, 2 ml acrylamide/bis-acrylamide 30% solution, 25 µl freshly prepared 10% ammonium persulphate, 5 µl TEMED.

4% acrylamide stacking gel (recipe for 1 gel): 1.55 ml dH2O, 625 µl Tris/HCl pH 6.8 SDS stacking buffer, 325 µl acrylamide/bis-acrylamide 30% solution, 12.5 µl freshly prepared 10% ammonium persulphate, 5 µl TEMED.

2.3.9 Western Blot

Western blots were used to confirm the presence of desired proteins in some supernatants prior to purification and to assess the presence of both antibody heavy chains in purified bispecific antibodies. Proteins were transferred from SDS-PAGE gels (run with Amersham ECL Rainbow Molecular Weight Marker (GE Healthcare) to nitrocellulose membranes (0.45 um, GE Healthcare) by electroblotting using an XCell II Blot module (Invitrogen) at 100 V in transfer buffer (tris-glycine buffer, 20% methanol). Membranes were blocked with PBS 0.1% (v/v) Tween 20 (Sigma Aldrich) and 3% (w/v) BSA (Sigma) for 1 hour at room temperature. HRP-conjugated anti-His-tag antibody (Abcam) diluted (1:5000) in PBS with 3% BSA was used to detect His-tagged proteins. For C-tag detection a primary CaptureSelect biotin anti-C-tag conjugate antibody (Thermo Fisher Scientific) (1:5000) was used with a secondary HRP conjugated anti-biotin antibody (Abcam) (1:5000) both diluted in PBS with 3% BSA. For detection blocked membranes were incubated with primary antibody for 1 hour at room temperature. Membranes were then washed three times with PBS 0.05% Tween-20 three times for 5 minutes prior to development or further incubation with secondary antibody. Immunoblots were developed using a Pierce ECL kit (Thermo Fisher Scientific) and imaged using an iBright FL100 machine (Thermo Fisher Scientific) and exposure time was adjusted as needed.

2.3.10 Endotoxin testing

Pierce Chromogenic Endotoxin Quant Kit (Thermo Fisher Scientific) was used to quantify endotoxin present in purified antibodies for *in vivo* experiments. Experimental procedure was performed on a heat block at 37°C until quantification. In brief, 50 uL of endotoxin standards, blanks and samples were plated in duplicate in a 96-well plate. 50 µL of reconstituted Amebocyte Lysate Reagent was added to each well and mixed. After the time

indicated in the kit 100 µL chromogenic substrate solution was added and mixed. After 6 minutes 50 µL stop solution (25% acetic acid) was added and mixed. Optical density at 405 nm was read after addition of stop solution. Endotoxin units per mL for samples were calculated from the standard curve.

2.3.11 Biotinylation

Biotinylation of a BirA site introduced into mIL-10Rb ECD for nanobody screening was carried out using the BirA biotin-protein ligase standard reaction kit (BirA-500, Avidity) in accordance with the manufacturer's instructions. Size exclusion chromatography (SEC) was used to separate free biotin from the biotinylated protein.

2.4 Surface Plasmon Resonance

Surface plasmon resonance (SPR) experiments were done at 25°C, unless otherwise stated, performed in HBS-P (0.01 M HEPES, 0.15 M NaCl, 0.005% (v/v) surfactant P20) on a Biacore T200 or Biacore 8K (Cytiva). Binding measurements were double reference subtracted, subtracting the signal from the reference channel and the signal from a zero-concentration sample. For experiments determining affinity, i.e., not sandwich SPR experiments, a non-binding protein of similar size was immobilised in the reference channel at approximately equal RU to that of the binding protein in the active channel. For example, an antibody with a different specificity.

Direct immobilisation of purified protein was done using a CM5 sensor chip (Cytiva). Amine coupling was performed as per the manufacturer's instructions with proteins diluted in a 10 mM sodium acetate pH 5 solution. Where no similar non-binding protein was

immobilised in the reference channel the channel still underwent surface activation and de-activation.

Antibodies were indirectly captured onto the sensor surface using a mouse-antibody capture kit (Cytiva). The capture kit was immobilised directly onto a CM5 sensor chip. The kit contains polyclonal anti-Ig antibody and after immobilising it on the sensor chip surface it captures antibodies out of solution passed over it.

Proteins were either used fresh after production without a freeze-thaw cycle or were size excluded a second time after thawing prior to use for SPR. Ovalbumin was purchased from Sigma-Aldrich, IL-10R proteins were produced by Susan Yu and me (as described above) and hBTLA produced by Heather Brouwer and Christopher Paluch.

Binding affinities were determined using either single- or multi-cycle kinetics. For analysis of affinity and binding kinetics a 1:1 binding model was fitted using the Biacore Insight Evaluation Software version 2.0.15.12933 (Cytiva).

The bound antibody for sandwich SPR (RU_{Ab}) was measured 1 second before injection of antigen. Bound antigen (RU_{Ag}) was measured upon the binding curve reaching a plateau. Where RU_{Ag} did not plateau due to dissociation of the antibody from the sensor surface the highest RU_{Ag} achieved was instead used.

For the Rmax comparison SPR method, Rmax was calculated using the Biacore Insight Evaluation Software version 2.0.15.12933. The corrected Rmax of the bispecific antibody (cR_{max}(bAb)) and the parental antibody (cR_{max}(pAb)) were calculated using the non-linear regression (curve fit) one site - Total function of GraphPad Prism.

2.5 Flow Cytometry

Flow cytometry was predominantly done using a BD FACS Canto flow cytometer data was analysed using FlowJo software v10.8 (FlowJo). Specific protocols for each experiment follow.

2.5.1 Fluorescent antibody conjugation

Antibodies were conjugated to Alexa-Fluor® 647 using Antibody Labelling Kit (Thermo Fisher Scientific) according to the manufacturer's instructions, which resulted in ≥ 1 dye per antibody. Labelling efficiency was determined using a NanoDrop One. Fluorescently labelled anitbodies were also used for immunohistochemistry.

2.5.2 Epitope mapping of anti-IL-10Rα antibodies by flow cytometry

The HEK293T cells transiently expressing hIL-10Ra mutants were plated into 96-well plates for flow cytometry at $2.5x10^5$ cells per well and resuspended in 25 mL of hybridoma culture supernatant or purified antibody at 10 mg/ml in FACS buffer. The plates were incubated for 30 minutes on ice before washing three times with FACS buffer and resuspension in 25 mL FACS buffer containing Alexa-Fluor® 647 goat anti-mouse IgG at 1 mg/ml. After a further 30-minute incubation on ice, cells were washed three times and resuspended in 100 ml FACS buffer for acquisition.

Live, GFP^+, cells were gated on and the geometric mean of receptor staining was normalised to the geometric mean of GFP, to adjust for differences in transfection efficiencies. The mutant receptor geometric means were then normalised to the wild-type receptor geometric mean.

2.5.3 *Ex vivo* flow cytometry

0.5 – 1.0x10^6 cells were plated into 96-well plates and washed twice with 200 mL FACS buffer (PBS, 2% FCS, 20 mM HEPES, 0.05% sodium azide). Cells were resuspended in 25-50 μL of antibody staining cocktail for 30 minutes on ice followed by two washes with 200 ml FACS buffer and resuspended in FACS buffer for acquisition on a BD FACS Canto flow cytometer. Supernatant from the 2.4G2 rat-anti mouse CD16/CD32 hybridoma was used 1 in 50 to block Fc-receptor binding.

2.5.4 Phospho-FLOW and intracellular staining

2x10^6 cells were plated into 96-well plates, fixed and permeabilised using BD Cytofix/Cytoperm kit in combination with Cytofix and Perm Wash buffer (BD Bioscienes) prior to staining with an intracellular antibody staining cocktail. Supernatant from the 2.4G2 rat-anti mouse CD16/CD32 hybridoma was used 1 in 50 to block Fc-receptor binding.

2.5.5 mOVA-EL4 binding assay

EL4-blue cells expressing TagBFP2 and mOVA were incubated with self-made anti-OVA antibodies conjugated to Alexa-Fluor®647 (at ~0.05 mg/ml) for 30 minutes on ice prior to acquisition on BD FACS Canto flow.

2.5.6 Legendplex

Serum was incubated with the LEGENDplex mouse inflammation panel (BioLegend) in accordance with the manufacturer's instructions. Analysis was performed using LEGENDplex data analysis software.

2.5.6 Antibodies for flow cytometry

Antibody	Clone	Fluorochrome	Supplier
epitope mapping			
goat anti-mouse IgG	Poly4053	AF647	Biolegend
OT-I RIP-mOVA diabetes			
Anti-OT-I tetramer		PE	Gift from Van den Eynde group, University of Oxford
CD25	PC61	Pacific Blue	Biolegend
CD3	17A2	PE-Cy7	Biolegend
CD4	GK1.5	A700	Biolegend
CD4	GK1.5	BV605	Biolegend
CD44	IM7	PercP-Cy5.5	Life Technologies
CD62L	MEL-14	APC	Biolegend
CD69	H1.2F3	BV605	Biolegend
CD8	53-6.7	APC-Cy7	Biolegend
hBTLA	MIH26	PE	Biolegend
hPD-1	29F.1A12	BV421	Biolegend
hPD-1	29F.1A12	PE	Biolegend
hTIGIT	1G9	PE	Biolegend
mPD-1	RMP1-30	FITC	eBioscience
Near IR Live/Dead		APC-Cy7	Biolegend
OX40	OX-86	PE-Cy7	Biolegend
Va2	B20.1	PE	Biolegend
Vb5	MR9-4	FITC	Biolegend
Zombie Aqua Live/Dead		BV510	Biolegend
OT-I RIP-mOVA co-transfer			
CD45.1	A20	PE-Cy7	Biolegend
CD45.2	104	BV605	Biolegend
CD8	53-6.7	PercP-Cy5.5	Biolegend
CellTraceViolet Kit	N/A	CellTraceViolet	Thermo Fisher Scientific
hBTLA	MIH26	APC	Biolegend
hPD1	29F.1A12	APC	Biolegend
Near IR Live/Dead		APC-Cy7	Biolegend
IL-10 stimulation assays			
B220	RA3-6B2	BV605	Biolegend
CD11b	M1/70	FITC	Biolegend
CD3	17A2	V450	Biolegend
F4/80	BM8	PE	Biolegend
NK1.1	PK136	PercP	Biolegend

pSTAT3	STAT3Y705-B12	APC	Invitrogen
IL-10 *in vivo*			
Ly6C	HK1.4	PercP-Cy5.5	Biolegend
Ly6G	1A8	A700	Biolegend
CD11b	M1/70	APC	Biolegend
CD11c	N418	FITC	Biolegend
CD19	6D5	PE	Biolegend
NK1.1	PK136	PE-Cy7	Biolegend
MHC-II	M5/114.15.2	BV421	Biolegend
B220	RA3-6B2	BV605	Biolegend

2.6 Histology

2.6.1 Tissue fixation and sectioning

Formalin-fixed tissues stored in 70% ethanol were dehydrated using an automated tissue processor which did the following in order: two 70% ethanol baths, two 90% ethanol baths and three 100% ethanol followed by three baths of melted wax, and lastly embedded in paraffin blocks. 5 mm sections were cut using a microtome.

Frozen tissue was embedded in OCT (CellPath) and then 5 mm sections were cut on a Leica Ultracut UCT ultramicrotome then left to dry before storage at -20°C.

2.6.2 H&E staining

Paraffin slides were rehydrated in a series of sequential steps. Two 5 minutes xylene baths, 5 minutes in 100% ethanol, 5 minutes in 95% ethanol, 5 minutes in 70% ethanol and then 5 minutes in 50% ethanol before 5 minutes in distilled water. Slides were then transferred into haemotoxilin for 10s before rinsing in running distilled water. Slides were dehydrated through a series of baths 5 minutes in 50% ethanol, 5 minutes in 70% ethanol, 5 minutes in 95% ethanol, 1 minute in 0.5% eosin 95% ethanol, a quick rinse in 100% ethanol and finally two 5-minute xylene baths. The slides were mounted with DPX for imaging on an Aperio

SlideScanner at 40x magnification. Scoring was as described in Ch.4 and all slides were scored by two people.

2.6.3 Immunohistochemistry

Frozen section slides were fixed in two cold baths of acetone on ice with TBST (20mM TrisHCL pH 7.4., 150 mM NaCl, 0.05% Tween-20) washes in between. After the two acetone baths slides were washed three times with TBST. 10% goat serum was used to block the slides for 1 h at 37 °C in a humidified chamber. The slides were then washed three times in TBST and before incubation with fluorescent primary antibody in 1% BSA TBST overnight at 4°C. After three TBST washes slides were counterstained with DAPI for three minutes at room temperature. After a further three TBST washes. Slides were mounted with Vectashield aqueous medium (Vectorlabs). Antibodies used were rabbit anti-Ovalbumin (Thermo Fisher Scientific) and fluorescently conjugated self-made antibodies.

2.7 *Ex vivo* IL-10 signalling assay

Peritoneal exudate cells (PECs) were collected from a humanely sacrificed mouse by injection of 5 ml ice-cold PBS into the peritoneal cavity. The filled peritoneal cavity was massaged to dislodge cells into the PBS solution and finally the PBS solution was extracted by syringe and the PECs were kept on ice.

For stimulation assays the cells were plated at $5x10^5$ cells per well in a 96-well plate and stimulated with IL-10 for 20 minutes, or for 1h in experiments including antibodies, prior to fixing and intracellular cytokine staining for pSTAT3.

For blocking assays, the cells were pre-incubated with antibody for 4 h prior to the addition of IL-10 for 20 minutes. hIL-10 and mIL-10 were purchased from Biolegend.

2.8 Animal work

All procedures involving animals were carried out in accordance with the Animals (Scientific Procedures) Act 1986, amended 2012. Procedures were reviewed by the clinical medicine animal care and ethical review body (AWERB) and conducted under project licence PPL P79A4C5BA.

Animals were housed in specific pathogen free conditions in individually ventilated cages in social groups and had free access to food and water. Experiments included age and sex matched control animals and treatments were evenly split between cages where possible.

2.8.1 Genotyping of transgenic mice

Transgenic mice were genotyped by Tanya Cheetham by PCR or Sanger sequencing from genetic material using the following primers:

hPD1:

Murine forward - CTC ACA GTG TCA GAG GCA

Murine reverse - ACG GGT TGG CTC AAA CCA TTA C (product 150 bp)

Human forward - TCG TGG TGA CCG AAG GGG AC

Human reverse - GCA GGC TCT CTT TGA TCT GCG (product 300 bp)

hBTLA:

Shared forward - TGT ACC ACA CTG GAA TAC TGA AGG

Murine reverse - TCC TGG CAG ACT GTT TGG AA (product 212 bp)

Human reverse - CCC ATT GTC ATT AGG AAG CAC TGG (product 398 bp)

hTIGIT:

Shared forward - CAG GCA GAG GAA GAA AAA CTC TGG

Murine reverse – ATGACAGAGCCACCTTCCTC (product 249 bp)

Human reverse - GAA AGT ATA GGA ACT TCG CGA CAC GGA C (product 736 bp)

hIL-10Rα:

Shared forward – TCAGGTTGATGTCAAGCTGG

Murine reverse – TGAACTTTAAAGCAACAGAGCG (product 221bp)

Human reverse – CCAGGTTTGCCAGAGTAAGG (product 324bp)

OT-I TCRα Primers:

oIMR1321 CAG CAG CAG GTG AGA CAA AGT transgene

oIMR1322 GGC TTT ATA ATT AGC TTG GTC C transgene (product 350bp)

oIMR8744 CAA ATG TTG CTT GTC TGG TG Int Pos Control For

oIMR8745 GTC AGT CGA GTG CAC AGT TT Int Pos Control Rev (product 200bp)

OT-I TCRβ Primers:

oIMR0675 AAG GTG GAG AGA GAC AAA GGA TTC transgene

oIMR0676 TTG AGA GCT GTC TCC transgene (product 350bp)

oIMR8744 CAA ATG TTG CTT GTC TGG TG Int Pos Control For

oIMR8745 GTC AGT CGA GTG CAC AGT TT Int Pos Control Rev (product 200bp)

PCR programme:

95°C 5min

95°C 30sec}

60°C 30sec} x 36

72°C 60sec}

72°C 10min

16°C hold

2.8.2 RIPmOVA model

hPD-1/hBTLA or hPD1/hTIGIT mice were crossed onto OT-I TCR transgenic mice, which express a T-cell receptor specific for the ovalbumin peptide 257-264 in the context of $H2K^b$. The mice were bread until heterozygous for OT-I and homozygous for both humanised receptors.

$CD8^+$ T-cells were purified by using red blood cell lysis buffer (Thermo Fisher Scientific) before using a $CD8a^+$ T-cell isolation kit (Miltenyi Biotec or Biolegend) by negative selection from the spleens and mesenteric lymph nodes (MLNs) of hPD-1/hBTLA/OT-I or hPD-1/hTIGIT/OT-I mice. Cells were assessed for their purity and $2x10^6$ $CD8^+$ T-cells in PBS were injected IV into female RIP-mOVA or wild type recipient mice. ~18 hours later recipient mice were injected with 200 mg of treatment antibody IP. MOPC21 was used as an isotype control. Mice were weighed and tested for glucosuria daily using One Step G dipsticks (One Step). Mice were culled when they reached a humane endpoint (development of glucosuria or >15% weight loss from starting weight) or on day 20-25 depending on experiment.

For co-transfer experiments $CD45.2^{+/+}$/hPD1/hBTLA/OT-I T-cells and $CD45.1^{+/-}$/$CD45.2^{+/-}$/mPD1/mBTLA/OT-I T-cells were purified as above and then mixed in a 1:1 ratio. The cells were loaded with CTV according to the manufacturer's instructions (Thermo Fisher Scientific) and $1x10^6$ cells were injected IV into RIP-mOVA recipients.

Whole blood, MLNs, spleens and pancreases were collected for analysis. Serum was isolated by centrifuging whole blood at 17000 g for 10 minutes and removing the serum from the cell pellet. This was repeated once, and serum was stored at -20°C. Serum samples were sent to The Mary Lyon Centre, MRC Harwell for glucose analysis on an AU680 analyser. Pancreases were stored in 10% neutral-buffered formalin for 24h before replacing with 70% ethanol for paraffin embedding or frozen in liquid nitrogen for OCT embedding. Spleens

and MLNs were processed into single cell suspensions for flow cytometry. The splenic single cell suspensions were treated with red blood cell lysis buffer prior to staining.

2.8.3 hIL-10Rα mouse model

hIL-10Rα were weighed daily from three weeks of age until 15 weeks of age. At 15 weeks of age, they were culled and colon weight: length ratio was calculated as a measure of gut inflammation. For this, colons were collected from distal caecum to anus, emptied of faeces and weighed and measured.

Mice aged 14-20 weeks were used to investigate antibody tolerability and the effect of anti-IL10R bispecific antibodies. For this they were injected with 200 mg antibody IP and monitored for 7 days prior to humane sacrifice. Whole blood, colons, spleens and MLNs were collected for analysis. Serum was isolated by centrifuging whole blood at 17000 g for 10 minutes and removing the serum from the cell pellet. This was repeated once. Serum was analysed immediately using a LEGENDplex mouse inflammation panel. Colon weight: length ratio was calculated. Spleen and MLNs were processed into single cell suspensions for flow cytometry and the splenic single cell suspensions were treated with red blood cell lysis buffer prior to staining.

2.8.4 MC38 tumour model

The MC38 tumour model was carried out in collaboration with Martin Fellermeyer. C57BL/6 mice humanised for the extracellular regions of PD-1 and CD200R were shaved and subcutaneously injected with 5 x 10^5 MC38 tumour cells in 100 µl ice-cold PBS. This procedure was performed under anaesthesia using isoflurane inhalation. Tumour were measured using calliper every other day. Tumour volume was calculated using the following formula: V in mm^3 = π/6 * length * width * height. On day 7 (average tumour volume 50

mm^3), mice were randomised into groups (n = 8) and treated four times over two weeks with 200 μg/treatment/mice.

Mice were culled when the tumour volume reached 1000 mm^3 or an ulceration persisted over 48 hours.

2.8.5 Immunisation, construction and isolation of nanobodies

Anti-mIL-10Rβ nanobodies were raised and identified by Jiandong Huo and the method used has been described elsewhere (250).

Chapter 3

Chapter 3 Murine bispecific creation and characterisation

3.1 Introduction

For murine bispecific production full length mIgG1 was selected as a backbone. mIgG1 is functionally similar to human IgG4; It does not activate the complement system and binds to the Fc receptors FcγRIIb and FcγRIII (251,252). FcγRIIb is a low affinity, inhibitory Fc receptor, which counteracts the signalling of activatory FcγRs through SHIP-1 recruitment (253). It has been suggested that "knocking out" FcγRIIb increases susceptibility to autoimmunity (254). Conversely, as the bispecific antibodies produced herein are targeted at treating autoimmune diseases engagement of FcγRIIb was thought to be desirable. Fortunately, mIgG1 is one of two mIgGs which have described methods for bispecific antibody generation, along with the much more inflammatory mIgG2a (245,246). A benefit of using a full length mIgG1 molecule is that it has a longer half-life than Fc-less bispecific constructs, without needing further engineering. Again, this is a favourable property in drugs for treating chronic diseases. Fc-less constructs smaller than 50-60 kDa have shorter half-lives and have therefore been coupled to polyethylene glycol (PEG), fused to albumin or multimerised to extend their half-lives (255).

The bispecific antibodies made herein target human BTLA (hBTLA) and ovalbumin (OVA) or human IL-10Rα (hIL-10Rα) and murine IL-10Rβ (mIL-10Rβ). For the anti-hIL-10Rα/anti-mIL-10Rβ bispecific antibodies, retaining Fc receptor engagement to generate close contacts between cells was desired. In contrast, in order to investigate whether hBTLA can be agonised using a tissue antigen (OVA) to create a close contact instead of an antibody Fc-Fc receptor interaction, Fc receptor binding had to be eliminated. To limit Fc-receptor binding in our bispecific antibodies targeting hBTLA and OVA, D265A mutations were inserted into the HCs (Fig. 3.1A, 3.2A and 3.3A). The D265A mutation has been shown to

reduce binding to all murine Fc receptors and was demonstrated by Wang *et al*. to also reduce Fc-receptor binding in their murine bispecific antibody format (246,256–258). The expectation is that D265A will also not change the efficiency of the Labrjin *et al.* bispecific approach due to the distance between D265 and the bispecificity-enabling mutations in CH3 (245).

Lastly, the bispecific antibodies included two different affinity purification tags, a His-tag and a C-tag, one on each heavy chain. The dual-tag approach was used to allow sequential purification of the bispecific antibodies thereby ensuring any contaminating non-bispecific, homodimeric antibodies with only one of the two tags would be removed. Both the His-tag and C-tag are very small tags to avoid immunogenicity when testing in mouse models.

Ideally, the bispecific antibodies produced should express well, form a high fraction of whole, bispecific product, and maintain the binding characteristics of the parental antibodies.

3.2 Production of murine bispecific antibodies

To investigate the Labrijn *et al.* (Fig. 1.7) and Wang *et al.* (Fig. 1.8) bispecific production methods, discussed in chapter 1, bispecific antibodies composed of the anti-hBTLA antibody 286 and the anti-OVA antibody 2C1 were produced using both approaches (245,246). These will be denoted as 286*2C1 (Labrijn) and 286*2C1 (Wang), respectively. Both parental 286 (Labrijn) and 2C1 (Labrijn) antibodies expressed at approximately 1 mg/L in HEK293T cells after affinity chromatography and size exclusion chromatography (SEC) (Fig. 3.1). Some large aggregates were detected during purification of both parental (Labrijn) antibodies, however these could be removed by SEC (Fig. 3.1B, C - Fraction 3-12

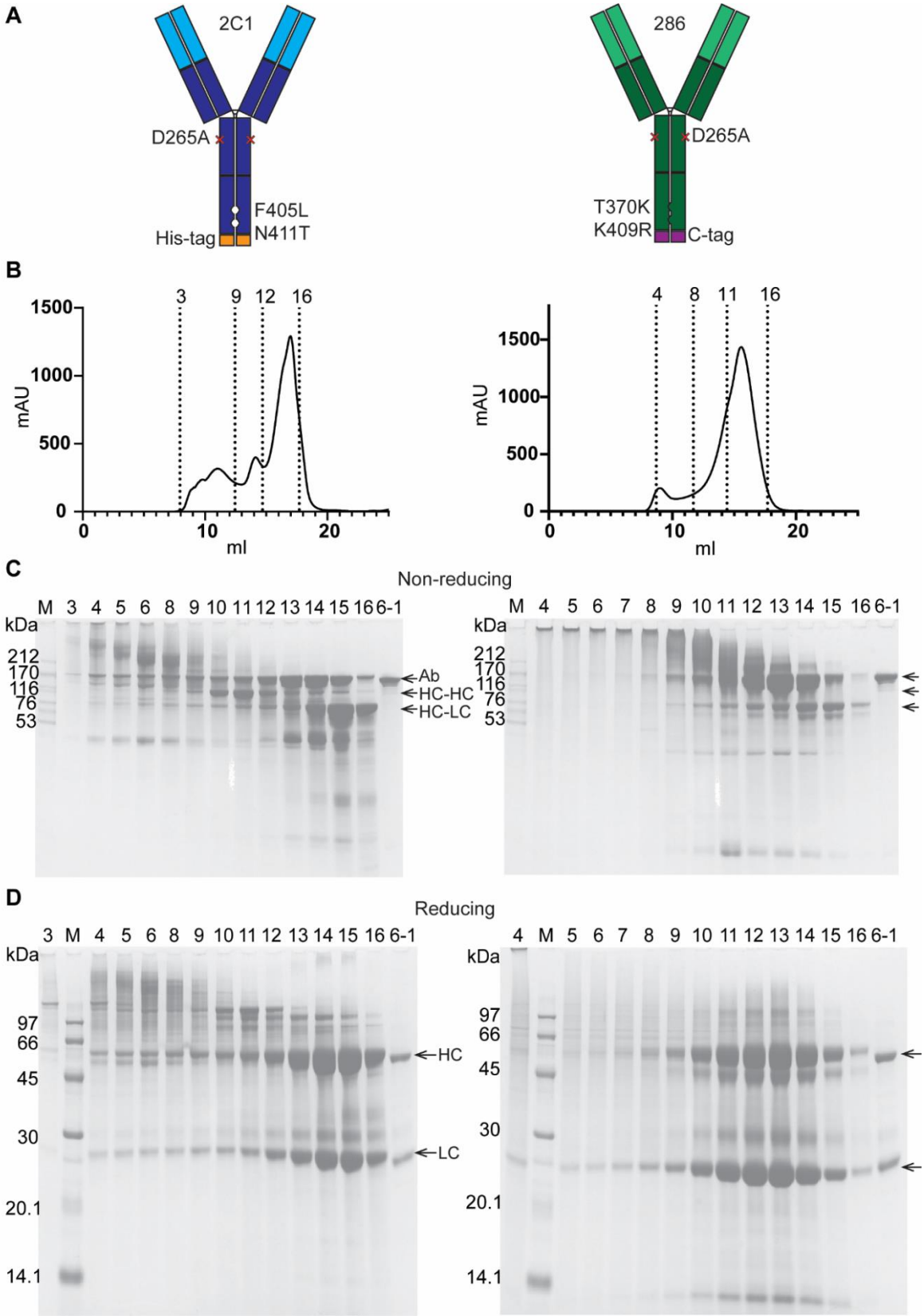


Figure 3.1. **Purification of the parental 2C1 and 286 (Labrijn) antibodies.** (A, B,C,D) *Left panel*: 2C1 and *right panel*: 268. (A) Schematic of 2C1 and 268. (B) SEC profile with numbered fractions. The SEC fractions separated by (C) non-reducing and (D) reducing SDS-PAGE. SDS-PAGE are labelled with band composition (Ab is complete antibody). 6-1 is a non-engineered mIgG1 antibody.

for 2C1 and Fraction 3-11 for 268). Both antibodies did not seem stable in their parental (Labrijn) form as there were two bands on the non-reducing SDS-PAGE at ~160 kDa and ~80 kDa, which represent the expected molecular weight of fully formed antibodies (Ab) and half antibodies (HC-LC), respectively (Fig. 3.1C). In comparison, a non-engineered control mIgG1 (6-1) had no band at ~80 kDa and therefore, it is likely that the F405L-N411T and T370K-K409R mutations in the parental (Labrijn) CH3s were responsible for this behaviour (Fig. 3.1C). The reducing SDS-PAGE shows that most of the product in both the aggregates as well as the antibodies (Labrijn) is composed of HCs and LCs at ~53 kDa and ~27 kDa, respectively (Fig. 3.1D). This suggests that the band seen at ~80 kDa in the non-reducing SDS-PAGE is composed of half antibodies (HC-LC). Lastly, C-tag purification, which was used for the 286 (Labrijn) antibody, appeared to yield fewer impurities than His-tag purification of the 2C1 (Labrijn) antibody, as can be seen by comparing the quantity of products of mass ~97 kDa in the reducing SDS-PAGE of both (Fig 3.1D). This is not unexpected as IMAC binds less selectively than an immunoaffinity resin, which has previously been demonstrated to give high purity (259).

After removal of aggregates, the parental (Labrijn) antibodies were used to produce the bispecific 286*2C1 antibody (Labrijn) by controlled Fab arm exchange (cFAE) followed by re-purification (Fig. 3.2). This yielded a product of ~160 kDa, the expected weight for the bispecific antibody, with some lower intensity bands also present (Fig. 3.2C). When reduced, the 286*2C1 (Labrijn) antibody dissociated into HC and LC bands, which suggests the impurities are single LC, HC polypeptides, or combinations thereof (Fig. 3.2C). The produced 286*2C1 (Labrijn) antibody therefore appears to be unstable as dual purification means any products retained should comprise both HCs and be ≥100 kDa, the estimated weight of HC-HC dimer. To determine whether more stable products could be obtained, reduction times between 3 to 9 hours were used for cFAE. As can be seen in the SEC traces

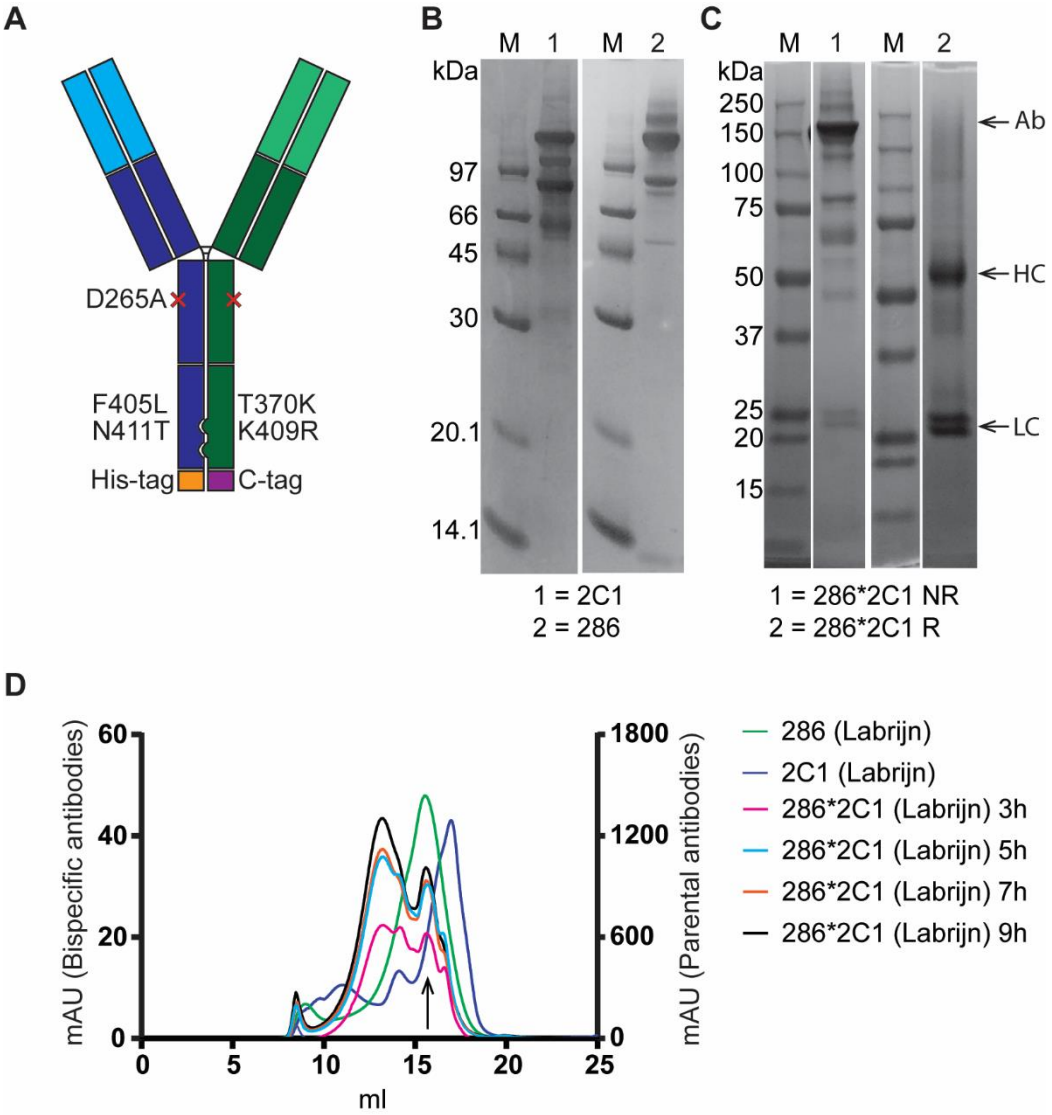


Figure 3.2. Production of the bispecific 286*2C1 (Labrijn) antibody. (A) Schematic of 286*2C1. (B) Non-reducing SDS-PAGE of parental 2C1 (Labrijn) and 286 (Labrijn) antibodies. (C) Non-reducing (NR) and reducing (R) SDS-PAGE of the 286*2C1 antibody (Ab) product after overnight re-oxidation. (D) SEC profiles of 286*2C1, with different reduction durations, and parental 286 (Labrijn) and 2C1 (Labrijn). In (D) the arrow indicates the peak suggested to be 286*2C1.

all reduction times produced a peak appearing to be 286*2C1, as it emerged between the parental 286 (Labrijn) and 2C1 (Labrijn) antibody peaks (Fig. 3.2D). Notably, cFAE appeared to produce a large proportion of aggregates (~10 ml – 14 ml) (Fig. 3.2D).

Purification of the 286*2C1 (Wang) bispecific antibody produced yields of approximately 4.5 mg/L with only small amounts of aggregates eluting at 40-60 ml in the SEC profile

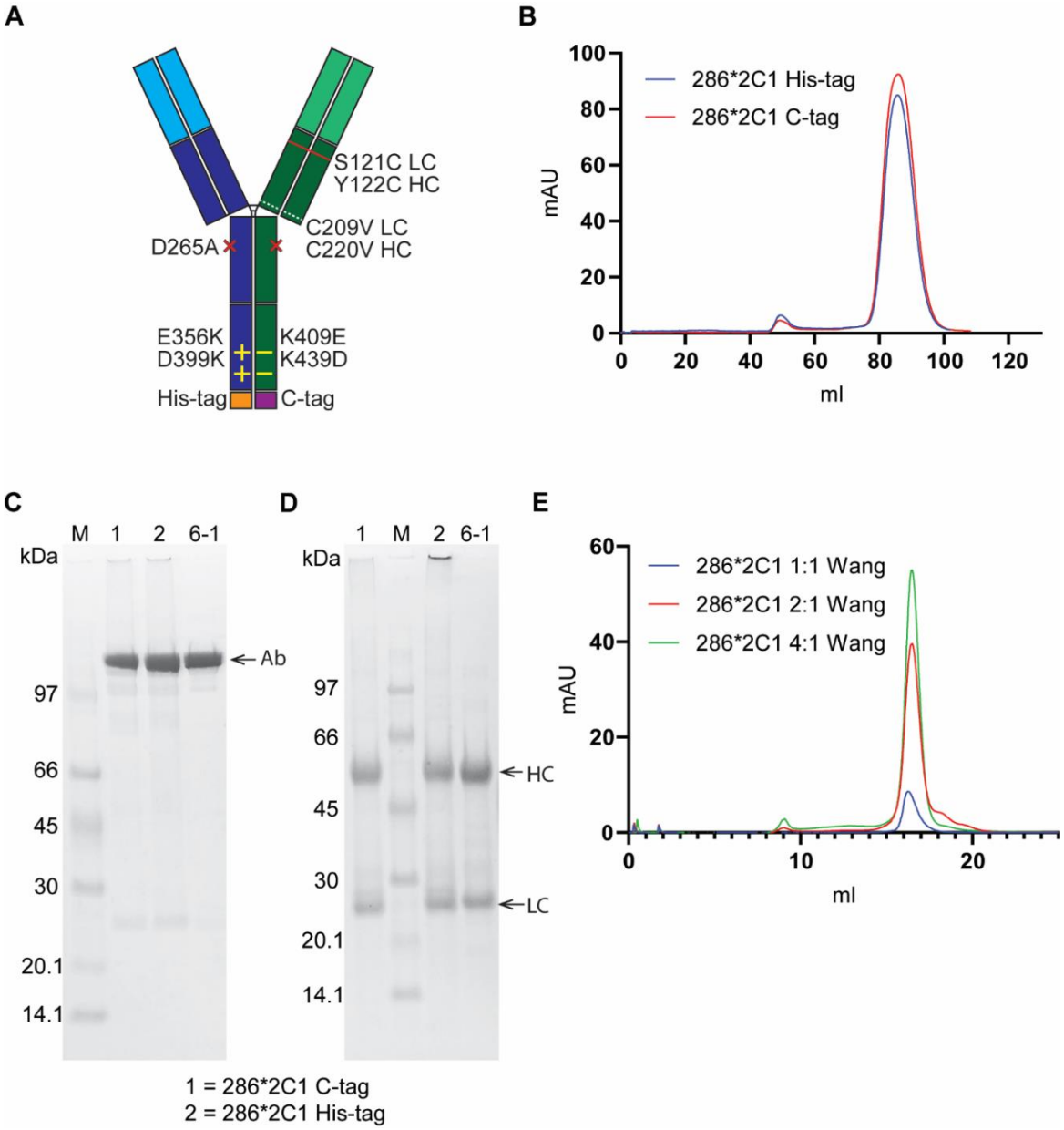


Figure 3.3. **Size exclusion chromatography of the bispecific 286*2C1 (Wang) antibody.** (A) Schematic of 286*2C1. (B) SEC profile. C-tag or His-tag indicates which purification step was performed first during sequential purification. (C) Non-reducing SDS-PAGE. (D) Reducing SDS-PAGE. In (C) and (D) 6-1 is a non-engineered mIgG1 antibody. (E) SEC profile of 286*2C1 produced with different LC:HC DNA ratios.

following dual-tag purification (Fig. 3.3A, B). Both dual purification sequences were used, and no notable difference was found by SEC or SDS-PAGE between purification of the His-tag or C-tag first (Fig. 3.3B-D). Moreover, both produced very similar yields. The antibody was purified with very few impurities and ran similarly to the non-engineered control mIgG1 (6-1) on SDS-PAGE suggesting that the introduced mutations did not negatively impact

stability (Fig. 3.3C, D). Additionally, different LC:HC DNA ratios during transfection were used to produce an excess of LC to ensure every HC had a LC partner. Altering the LC:HC DNA ratios did not result in any notable changes in the SEC profile or SDS-PAGE (Fig. 3.3E). The dual purification strategy ensures both HCs are present after purification and the second column used had little flow through prior to elution suggesting that there was only a small amount of monospecific antibody or protein produced with only one tag (Fig. 3.4). As previously noted, IMAC can bind non-specifically with a low affinity to other proteins containing histidine clusters. Therefore, a stringent stepwise gradient was used for purification, which likely lowered yield but maintained purity and could account for the small amount of C-tag purified protein eluting in the 22.5 mM to 42.5 mM wash steps prior to the 250 mM imidazole elution (Fig. 3.4B).

3.3 Assessing antibody bispecificity using surface plasmon resonance-based assays

3.3.1 Surface Plasmon Resonance

To characterise the antibodies produced, a method for assessing the extent of their bispecific activity was necessary. Multiple methods have been used to assess bispecific antibodies primarily relying on Enzyme-Linked Immunosorbent Assay (ELISA) or Surface Plasmon Resonance (SPR)-based approaches (260). The two approaches used herein rely only on SPR measurements. SPR is a tool to characterise binding interactions between two partners and is widely used to assess the affinity and kinetics of antibody-antigen interactions. In brief, the binding of proteins to a sensor surface can be measured by a change in the angle of reflected light. This is caused by a change in the resonance angle due to a change in refractive index when proteins bind. This change in the angle of reflected light is converted into arbitrary response units (RU) on Biacore instruments such as the ones used in this thesis.

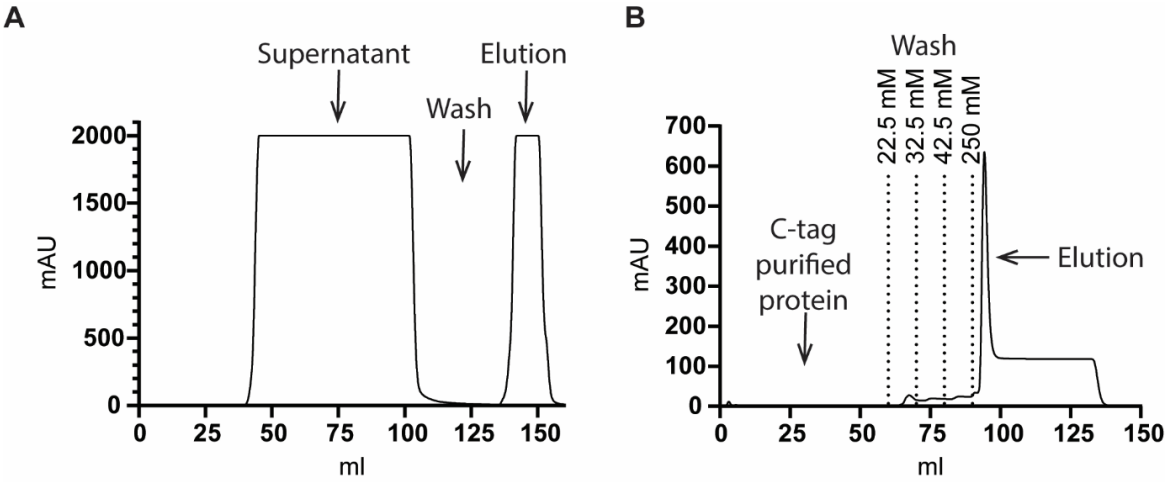


Figure 3.4. Affinity purification of the bispecific 286*2C1 (Labrijn) antibody. (A) C-tag purification from supernatant and (B) His-tag purification from C-tag purified antibody with stringent gradient-wash.

The change in refractive index is linear with the number of protein molecules bound to the sensor surface. The linearity of RU with protein mass allows calculation of the maximal binding response (Rmax) of an antigen to an antibody immobilised on the sensor surface:

$$\text{Rmax (antigen)} = \frac{MW_{Ag} \times RU_{Ab} \times v_{Ab}}{MW_{Ab}}$$

with MW being the molecular weight of the antigen (Ag) or antibody (Ab), RU_{Ab} is the measured RU value of the immobilised antibody and v_{Ab} is the valency of the antibody.

3.3.2 Sandwich SPR assay

The first approach for assessing functional bispecificity of the bispecific antibodies produced is a sandwich SPR assay. In this assay one antigen, antigen A, is immobilised onto the sensor chip surface, which is followed by binding, or capture, of the bispecific antibody to the surface and subsequent binding of a second "free" antigen, antigen B (Fig. 3.5A, B). A similar sandwich SPR approach to the one used here has been described by Gassner *et al.* to measure bispecific antibody binding to two antigens simultaneously (261).

The bispecificity of the antibody is calculated using the experimental and theoretical

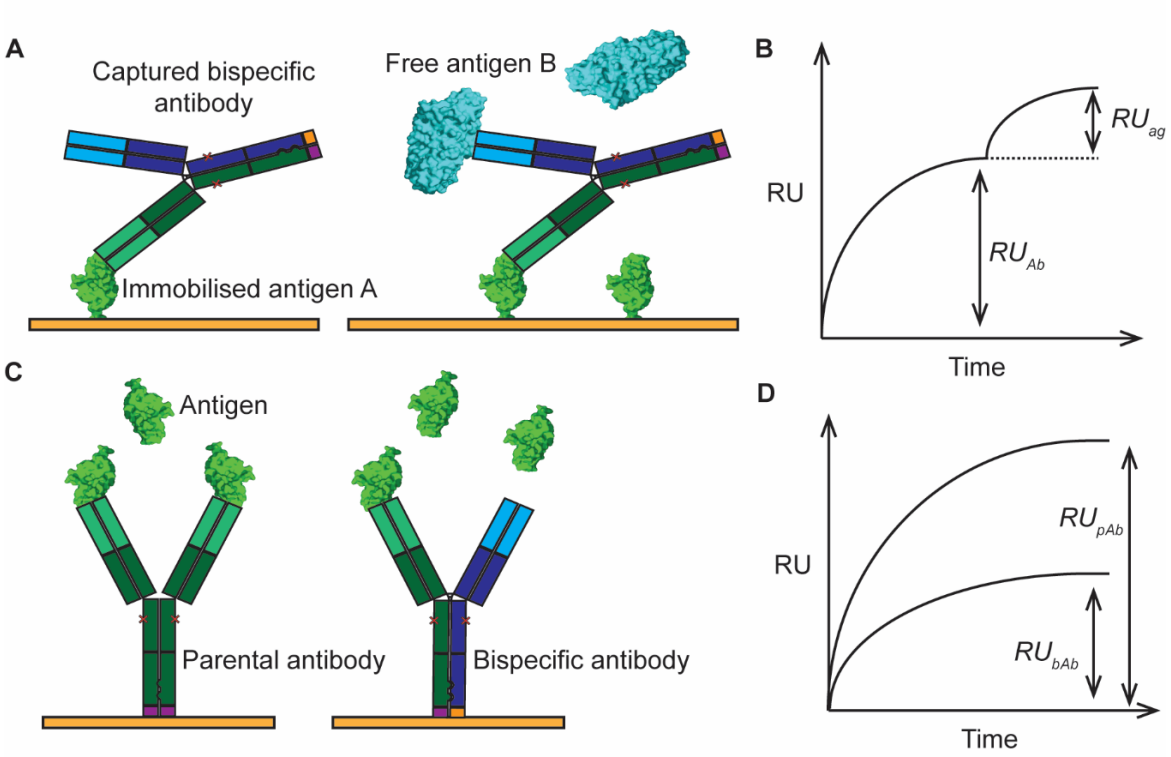


Figure 3.5. **SPR approaches for assessing bispecificity.** (A) In sandwich SPR antigen A (*green*) is immobilised on the chip surface (*gold*). This antigen is then used to capture the bispecific antibody (left panel) followed by binding of a free antigen, antigen B (*blue*, right panel). (B) Model sandwich SPR binding curve showing capture of bispecific antibody (RU_{Ab}) and subsequent binding of free antigen B binding (RU_{Ag}) (C) Rmax comparison SPR in which the parental antibody (left panel) or bispecific antibody (right panel) are captured onto an anti-IgG chip surface (*gold*) and binding to antigen is measured (*green*). (D) Model Rmax comparison SPR binding curves showing binding of antigen to the parental antibody (RU_{pAb}) and to the bispecific antibody (RU_{bAb}) are measured and compared (right panel).

maximum binding of the free antigen B. In SPR, all mass binding to the chip is represented as a change in RU which allows the measurement of the amount of bispecific antibody captured, and of both antigens, A and B. Knowing the amount of captured antibody (obtained from the RU), the valency of the antibody, and the molecular weights of the antibody and antigen B a theoretical value for maximum binding of antigen B (Rmax) to the captured bispecific antibody can be calculated (Eq. 1). At Rmax all binding sites on the captured bispecific antibody are saturated, which can be reached experimentally if the concentration of free antigen B used is sufficiently high. Bispecificity is calculated by the

ratio of the experimentally determined RU of free antigen B at high concentration vs the calculated Rmax, where bispecificity is defined as:

$$\frac{RU_{Ag}}{R_{max}} = \frac{RU_{Ag} \times MW_{Ab}}{RU_{Ab} \times MW_{Ag} \times v_{Ab}}$$

with RU_{Ag} being the measured response of free antigen B. In the case of the sandwich SPR approach, one can assume an antibody valency of one, as one arm of the bispecific antibody is permanently occupied by the immobilised antigen A on the sensor chip. In this case Eq. 2 simplifies to:

$$\frac{RU_{Ag}}{R_{max}} = \frac{RU_{Ag} \times\ MW_{Ab}}{RU_{Ab} \times\ MW_{Ag}}$$

The ratio can be represented as a percentage of bispecificity (p_b) using the sandwich approach:

$$p_b = \frac{RU_{Ag}}{R_{max}} \times 100$$

Bispecific binding capacity, *Bispecific* $B_{C,}$ is a measure of the ability of a bispecific antibody to bind antigen with both arms. The percentage of bispecificity is equal to bispecific binding capacity in the sandwich SPR assay, as free antigen B binding is dependent on the antibody binding the immobilised antigen A. Therefore, the immobilised antigen binding arm of the antibody must bind with 100%.

$$Bispecific\ B_C = p_b(Arm1) \times p_b(Arm2) = p_b(Arm1) \times 1$$

This, sandwich SPR approach can inform about the degree of bispecificity that a bispecific antibody possesses. Further, it confirms whether a bispecific antibody is capable of binding both antigens simultaneously. As this approach relies on binding of an antigen on the sensor chip surface for bispecific antibody capture it selects for functional antibodies. Additionally, its dependence on capturing the bispecific antibody using an immobilised ligand (antigen

A) limits its usefulness in contexts where the antibody immobilised ligand interaction dissociates rapidly.

3.3.3 Rmax comparison SPR assay

The second approach for assessing bispecificity compares the Rmax of the monospecific, divalent parental antibodies with the Rmax of a bispecific antibody (Fig. 3.5C, D). The divalent parental antibodies should have twice the Rmax of the bispecific antibody assuming an equal number of antibody molecules on the sensor chip surface, as they have twice the valency. In this assay the parental or bispecific antibodies are captured by anti-mIgG antibodies immobilised onto the sensor chip surface. A concentration series of the respective antigens is passed over both the captured parental antibodies as well as over the captured bispecific antibody. This can be done using single cycle or multi-cycle kinetics. By fitting these binding curves, Rmax values for each antibody-antigen pair can be obtained, and equal:

$$R_{max}(pAb) = \frac{MW_{Ag} \times RU_{pAb} \times v_{pAb}}{MW_{pAb}}$$

and

$$R_{max}(bAb) = \frac{MW_{Ag} \times RU_{bAb} \times v_{bAb}}{MW_{bAb}}$$

where, $R_{max}(pAb)$ and $R_{max}(bAb)$ are the Rmax values of the parental or bispecific antibody-antigen interactions, respectively. To estimate the quality of the bispecific antibody, both Rmax values need to be corrected for the specific characteristics of each antibody, e.g., valency, *v*, molecular weight, MW, as well as the RU of the parental or bispecific antibody captured, RU_{pAb} and RU_{bAb}, respectively. The corrected Rmax, $cR_{max}(pAb)$, of the parental antibody-antigen interaction, should thereby be equal to the corrected Rmax of the bispecific antibody, $cR_{max}(bAb)$:

$$cR_{max}(pAb) = \frac{R_{max}(pAb) \times MW_{pAb}}{RU_{pAb} \times v_{pAb}} = \frac{R_{max}(bAb) \times MW_{bAb}}{RU_{bAb} \times v_{bAb}} = cR_{max}(bAb)$$

This allows the calculation of binding capacity, B_C, of the bispecific antibody by normalising the corrected Rmax of the bispecific antibody-antigen interaction to the corrected Rmax of the parental antibody-antigen interaction:

$$B_C = \frac{cR_{max}(bAb)}{cR_{max}(pAb)}$$

Since the bispecific antibody binds the antigens on only one arm each, and if the ability of each antibody arm to bind its antigen is independent of each other, the overall percentage of the bispecific binding capacity can be obtained by multiplying the binding capacity, B_C, per arm of both bispecific antibody-antigen interactions.

$$Bispecific\ B_C = B_C\ (Arm1) \times B_C(Arm2) \times 100$$

The Rmax comparison SPR approach alone cannot inform that an antibody is bispecific as the same binding measurements could be achieved using an equal mixture of monospecific divalent antibody. However, by use of a robust bispecific antibody purification process this concern can be alleviated. This approach is also applicable to low-affinity antibody-antigen interactions.

The molecular weights used for all calculations can be seen in Table 3.1.

3.3.3 Bispecificity of the 286*2C1 (Labrijn) antibody

As the Labrijn antibodies produced, using various reduction durations, showed large amounts of aggregation it was decided to change to the Wang *et al*. approach (Fig. 3.2D) (246). However, as the Labrijn bispecific antibodies had been produced and the SPR assays had not yet been tested their characterisation using the bispecific SPR assays was attempted.

Table 3.1. Molecular weights used to determine Rmax

Antibody	Molecular weight (Da)	Antigen	Molecular weight (Da)
286	156778	hBTLA	14734
2C1	159385	OVA	42881
286*2C1	158081	hBTLA/OVA	
Nb82*286	121647	OVA/hBTLA	
2C1*286SvFv	135512	OVA/hBTLA	
Nb82*286ScFv	99078	OVA/hBTLA	
Nb41*286ScFv	98607	OVA/hBTLA	
611	158315	hIL-10Ra	29089
151	155771		
827	157201	mIL-10Rb	28787
827*611	157758	mIL-10Rb/hIL-10Ra	
Nb5*611	122929	mIL-10Rb/hIL-10Ra	
Nb6*611	121586	mIL-10Rb/hIL-10Ra	
827*151	156486	mIL-10Rb/hIL-10Ra	
Nb5*151	121657	mIL-10Rb/hIL-10Ra	
Nb6*151	120314	mIL-10Rb/hIL-10Ra	

For this the SEC peak believed to be bispecific antibodies was isolated as best as possible (Fig. 3.2D). The following results should therefore be treated with caution as they are likely contaminated by some aggregates and different species.

Using Rmax comparison SPR the ability of 286*2C1 to bind hBTLA and OVA was compared to that of the parental antibodies. For this the RU of antigen binding, RU_{hBTLA} or RU_{OVA}, was normalised to the amount of antibody captured and the data are represented in normalised RU_{hBTLA} vs concentration of hBTLA plots (Fig. 3.6A, B). As the valency of the 286 or 2C1 antibody is twice that of the 286*2C1 antibody and the molecular weights are only ~1% different (Table. 3.2), the 286*2C1 antibodies are expected to reach approximately half of the Rmax calculated for the 286 and 2C1 antibodies (Fig. 3.6A, B). When these curves were used to calculate a corrected Rmax for each antibody, the hBTLA binding capacity of the 286*2C1 antibodies was at best 77.8% for the bispecific antibodies, formed using a nine-hour reduction (Table 3.2). The highest binding capacity of OVA, with

110%, was observed when binding to the 286*2C1, obtained after seven hours of reduction (Table 3.2). Taking binding of both arms into account seven hours reduction produced the highest bispecific binding capacity of the antibodies with 77.6%. The other 286*2C1 antibodies obtained from 3-, 5- and 9- hour reductions had bispecific binding capacities of 64.3%, 53.7% and 62.5%, respectively (Table 3.2). Due to the instability seen in the parental antibodies and to see whether the bispecificity could be improved, different fractions from the parental 2C1 and 286 SEC were used in cFAE with a 7-hour reduction. Either early, late or all fractions were mixed from the SEC antibody peaks of the parental antibodies (Fig. 3.1B) and analysed using sandwich SPR (Fig. 3.6C). Early fractions (F) were F10-13 for 2C1 and F10-F12 for 286, and late fractions were F14 onwards for 2C1 and F13 onwards for 286 (Fig. 3.1B). In the sandwich SPR hBTLA is immobilised onto the sensor chip and the 286*2C1 antibodies generated were captured for the first 60s (Fig. 3.6C). At ~60s the free antigen OVA is passed over the surface (Fig. 3.6C). The increase in RU after 60s for the 286*2C1 antibodies shows that binding of OVA occurs and bispecific antibody is present, whereas there is no increase in the RU for the parental anti-hBTLA 286 antibody. When the RU_{OVA} was normalised, the calculated Rmax, based on the RU of captured antibody, 286*2C1 produced from all fractions had the highest percentage bispecific binding capacity with 50.7% (Table 3.3). Interestingly, there is a discrepancy between the bispecific binding capacity obtained in the Rmax comparison SPR for the 286*2C1 after seven hours of reduction and the sandwich SPR of the 286*2C1 made with all fractions, with 77.6% vs 50.7% (Table 3.2). However, given the bispecific antibody material used it is hard to draw conclusions from this.

Table 3.2. Rmax comparison SPR for 286*2C1 (Labrijn) bispecific antibody

Antibody	Reduction time (h)	Antigen	cRmax[#]	B_C (%)	Bispecifi B_C (%)
286		hBTLA	0.137	100	
286*2C1	3	hBTLA	0.099	72.2	64.3 (3 hours)
286*2C1	5	hBTLA	0.085	62.1	
2C1		OVA	0.272	100	
286*2C1	3	OVA	0.243	89.3	53.7 (5 hours)
286*2C1	5	OVA	0.235	86.4	
286[§]		hBTLA	0.123	100	
286*2C1[§]	7	hBTLA	0.086	70.2	77.6 (7 hours)
286*2C1[§]	9	hBTLA	0.095	77.8	
2C1[§]		OVA	0.240	100	
286*2C1[§]	7	OVA	0.266	110.5	62.5 (9 Hours)
286*2C1[§]	9	OVA	0.193	80.3	

All measurements were performed at 25°C

[#]Rmax is corrected for the MW, RU captured and valency of the antibody

[§]Measurements were performed simultaneously

As the sandwich SPR approach selects for functional antibody capable of binding antigen on the sensor chip surface, the finding that it at best bound 50% of the expected second, free antigen was disappointing and suggested that even if aggregation was overcome there were other issues during cFAE. To investigate cFAE more closely different concentrations of the reducing agent, 2-MEA, and different temperatures were used to reduce both parental antibodies used to produce 286*2C1. The different conditions tested were based on those tried by Labrijn *et al.* (245). It was found that under all conditions tested, and without buffer exchange or re-oxidation, there was complete dissociation of HCs and LCs, as seen by non-reducing SDS-PAGE with bands at ~55 kDa and ~27 kDa (Fig. 3.7). Nevertheless, it was found that the Labrijn approach conserved the affinity of both binding arms (Table 3.4).

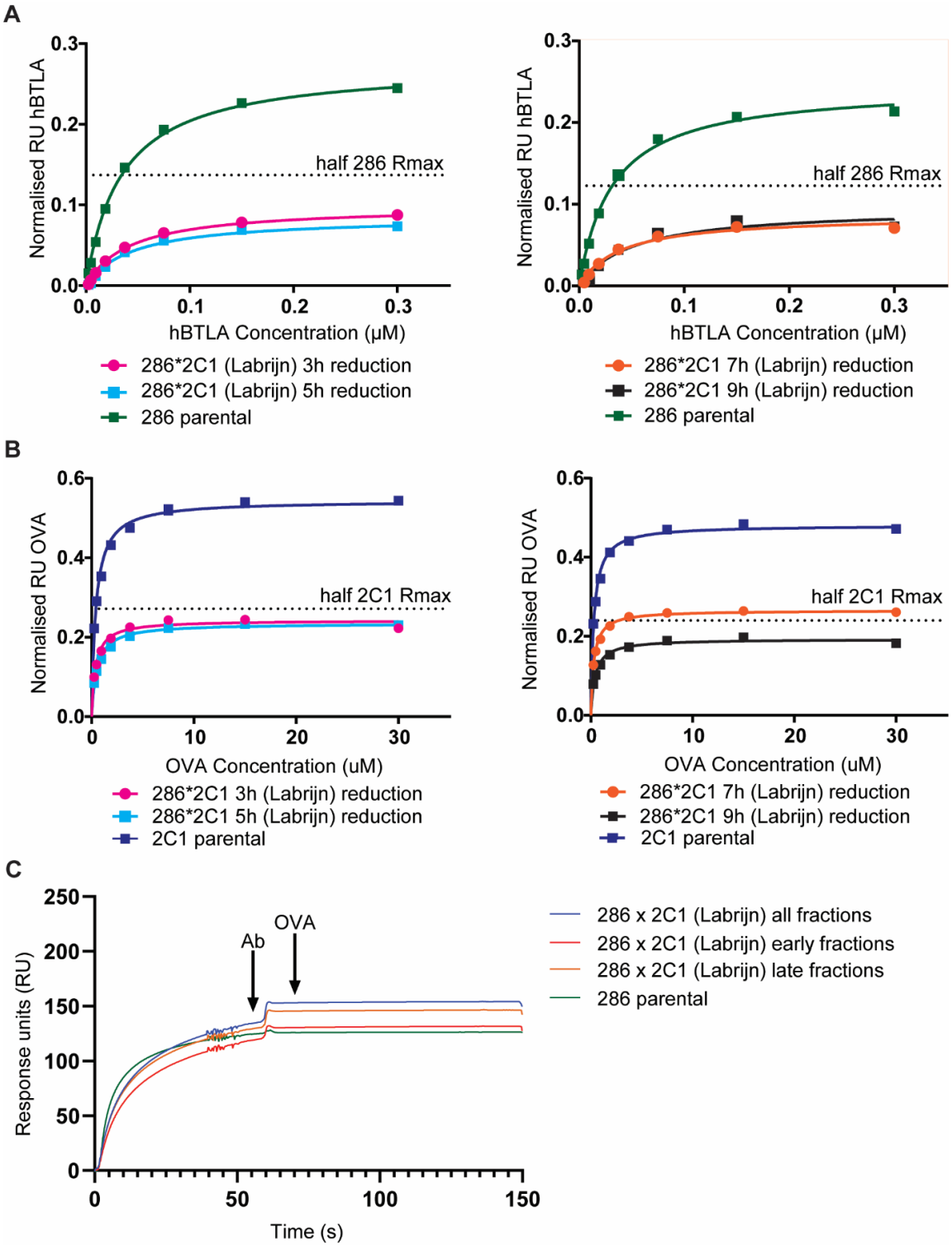


Figure 3.6. Assessment of 286*2C1 bispecific binding capacity (Labrijn). (A,B) Rmax comparison SPR for binding of (A) hBTLA or (B) OVA to either immobilised parental or bispecific antibodies. For (A) and (B) the RU of antigen was normalised to the RU of antibody captured for these plots. (C) Sandwich SPR with immobilised hBTLA, captured parental or bispecific antibodies and OVA as the free antigen. Antibody (Ab) is captured first (0-60s) followed by 30 μM OVA (60s onwards). Arrows indicate where the RUs of capture or binding were measured.

Table 3.3. Sandwich SPR results for 286*2C1 (Labrijn) bispecific antibodies

Antibody	Fractions	RU_{Ab}	RU_{Ag}	Bispecific B_C (%)
286*2C1	all	133.765	18.994	50.7
286*2C1	early	118.478	11.832	35.6
286*2C1	late	128.940	16.214	44.9
286 parental		124.413	0.630	1.8

hBTLA was immobilised and antibody captured. Subsequent binding of the free ligand, OVA, was measured, RU_{Ag}. Measurements were performed at 25°C.

Table 3.4. Steady state affinities comparison table for bispecific production approaches

Antibody	Antigen	K_d ± SD (nM)
Parental 2C1	OVA	2120±1424
Labrijn 286*2C1	OVA	1416±444.5
Wang 286*2C1	OVA	3003±2219
Parental 286	hBTLA	24.9±16.4
Labrijn 286*2C1	hBTLA	47.0±13.3
Wang 286*2C1	hBTLA	31.8±19.3

Measurements were performed at 25°C. The dissociation constant, K_d, is shown in nM ± standard deviation (SD).

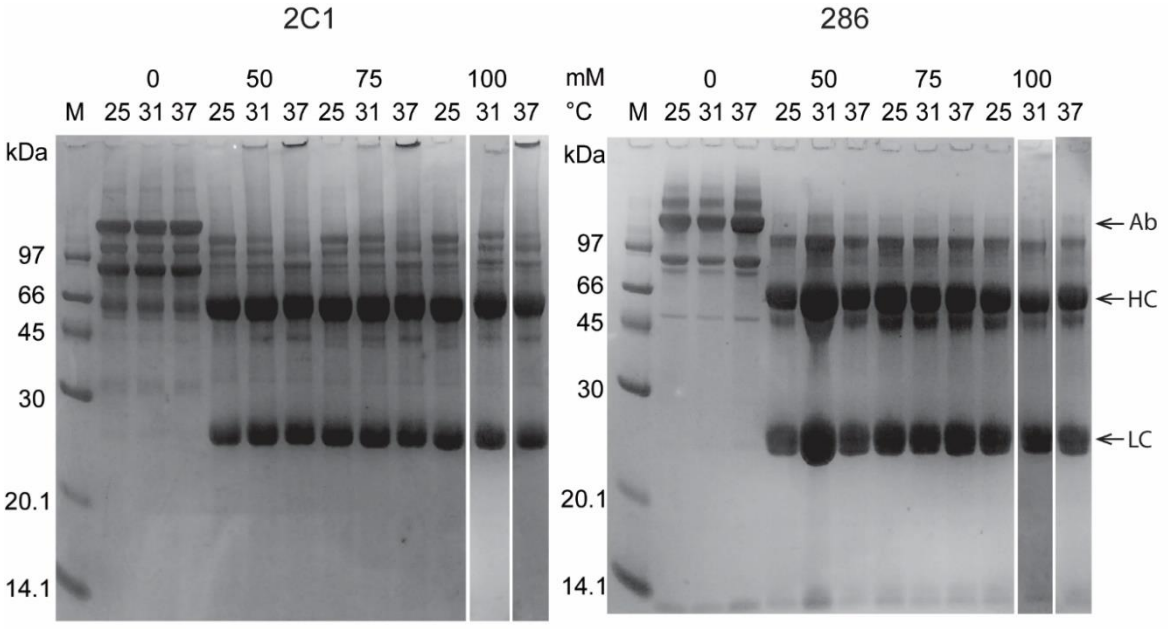


Figure 3.7. Varying reduction conditions of the parental (Labrijn) antibodies. Parental antibodies 2C1 (left panel) and 286 (right panel) on non-reducing SDS-PAGE, after reduction with 2-MEA for seven hours at different temperatures. The concentrations of the reducing agent 2-MEA are shown in mM.

3.3.4 Bispecificity of 286*2C1 (Wang)

The bispecificity of the 286*2C1 antibody was analysed using the Sandwich SPR and Rmax comparison SPR. For the Rmax comparison SPR analysis the 286*2C1 antibody, which had been dual purified in different orders, were pooled. 286*2C1 was found to have a 24% bispecific binding capacity (Table 3.5). This was primarily due to 286*2C1 only achieving 31.1±0.68% binding capacity of OVA when compared with the corrected Rmax of 2C1 (Fig. 3.8A, Table 3.5). The anti-hBTLA arm performed better with a 77.8±1.9% binding capacity (Fig. 3.8B, Table 3.5). 286*2C1 binding to both OVA and hBTLA could be increased by increasing the DNA ratio of LC:HC during transfection. Ratios of both 2:1 and 4:1 were used and increased hBTLA binding to 88.8±2.5% and 87.9±2.3% binding capacity, respectively, reaching close to half of the 286 Rmax (Fig. 3.8D, Table 3.5). Interestingly, the 286 anti-hBTLA arm contained the mutations which relocated the inter HC-LC disulphide bond. The relocation therefore appears to have worked well and without any major drawbacks for the anti- hBTLA arm. The 2:1 LC:HC ratio increased OVA binding capacity from 31.1±0.6% to 69.9±0.3%, resulting in a ~40% increase in bispecific binding capacity obtained using the Rmax comparison SPR method (Fig. 3.8C, Table 3.5). Binding to the anti-OVA-2C1 arm following transfection of LC:HC chain DNA at a ratio of 4:1 resulted in a ~10% lower level of binding than the 2:1 ratio (Fig. 3.8D, Table 3.5). This suggests that LC:HC ratio is not the only factor affecting binding capacity and that maybe at higher LC:HC DNA ratios the ratio of LC:LC starts to play a role too.

The observations during 286*2C1 purification that the order of His-tag and C-tag purification did not make a significant difference to the bispecific antibody production was confirmed when analysing both products using sandwich SPR, as the binding capacity was very similar with 29.7% and 26.4%, respectively (Fig. 3.8E, Table 3.6). Further, a 2:1 DNA ratio also increased the 2C1-arm binding capacity of OVA ~60% to 89.4±5.6% (Fig. 3.8E,

Table 3.5. Rmax comparison SPR for 286*2C1 (Wang) bispecific antibodies

Antibody	Ligand	cRmax	B_C ± SD (%)	Bispecific B_C (%)
2C1	OVA	0.2873 0.2548	100	
286*2C1	OVA	0.0880 0.0805	31.1±0.68	24
286	hBTLA	0.1574 0.1406	100	
286*2C1	hBTLA	0.1204 0.1114	77.9±1.9	24
2C1	OVA	0.2530 0.2654	100	
286*2C1 2:1	OVA	0.1764 0.1862	69.9±0.3	62
286*2C1 4:1	OVA	0.1519 0.1582	59.8±0.3	52
286	hBTLA	0.1281 0.1379	100	
286*2C1 2:1	hBTLA	0.1114 0.1249	88.8±2.5	62
286*2C1 4:1	hBTLA	0.1148 0.1190	87.9±2.3	52

Measurements were performed at 25°C and are grouped together with the parental antibody (2C1 or 286) they were measured with. The binding capacity is shown in percentage ± standard deviation (SD).

Table 3.6). This is 19% larger than the binding capacity of OVA (69.9%, Table 3.5) found using Rmax comparison SPR and 27% higher when considering the bispecific binding capacity (62% vs 89.4±5.56%, Table 3.5, 3.6). This could be due to sandwich SPR relying on an Rmax that was calculated based on the RU of the captured antibody, whereas the Rmax comparison SPR uses the parental Rmax obtained experimentally. To investigate this, the experimentally obtained Rmax for 2C1 was compared to a calculated Rmax for 2C1 based on the RU of 2C1 captured. The experimentally determined Rmax for 2C1 was 96% of the calculated Rmax. Therefore, the sandwich SPR normalisation to a calculated Rmax would underestimate the bispecific binding capacity. Lastly, it was found that the Wang approach conserved the affinity, represented as dissociation constants, K_d, of both binding arms (Table 3.4).

Table 3.6. Sandwich SPR results for the bispecific 286*2C1 (Wang) antibodies

Antibody	RU_{Ab}	RU_{Ag}	Bispecific B_C ± SD (%)
286*2C1 His-tag	528.2 538.4	44.9 41.0	29.7±2.32
286*2C1 C-tag	666.7 676.5	49.2 46.8	26.4±1.17
286*2C1 2:1	130.3 127.2	33.2 29	89.4±5.56
286*2C1 4:1	31.5 29.0	7.7 6.4	85.3±3.65
286 Parental	651.4 520.7	2.0 3.4	1.8±0.92

hBTLA was immobilised and antibody captured. Subsequent binding of the free ligand, OVA, was measured, RU_{Ag}. Measurements were performed at 25°C. Measurements are performed at 25°C. The bispecific binding capacity is shown in percentage ± standard deviation (SD).

3.4 Further bispecific-antibody production

3.4.1 Anti-IL-10 receptor bispecific antibody production

We hypothesised that agonising the IL-10R could be done by engaging both IL-10Rα and IL-10Rβ simultaneously with a bispecific antibody, as this would bring both signalling chains into close proximity. Further, signalling may be potentiated by engagement of Fc receptors on apposing cells creating close contacts resulting in phosphatase exclusion.

Six bispecific antibodies, out of a combination of two anti-IL-10Rα antibodies, one anti-IL-10Rβ antibody and two anti-IL-10Rβ nanobodies, were produced using the Wang mutations (Fig. 3.9). Nanobodies were used due to the difficulty of raising anti-mouse antibodies in mice (see Chapter 5 for Nanobody generation). Nanobodies were fused to KKI-Hinge-CH2-CH3 of mIgG1 for bispecific production (Fig. 3.9A). All nanobody-Fc fusions containing bispecific antibodies produced three bands between 90-150 kDa under non-reducing conditions (Fig. 3.9B). Of these the ~130 kDa band was of the expected size for the full bispecific antibody (Fig. 3.9B). The band at ~110 kDa is suggested to be the bispecific antibody with the nanobody cleaved off or the LC missing and the band at ~95 kDa is likely

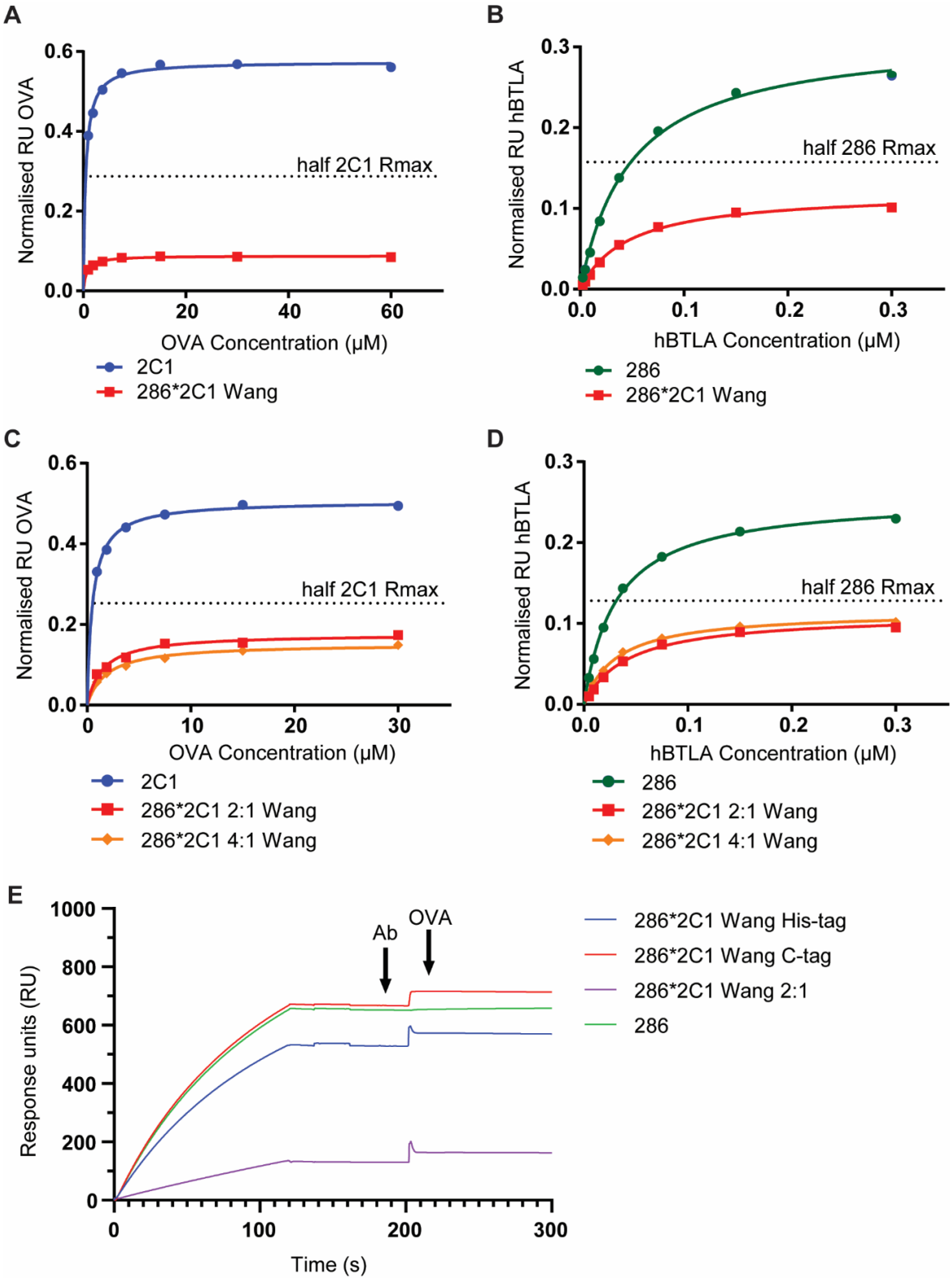


Figure 3.8. Assessment of the 286*2C1 (Wang) bispecific binding capacity. (A, B) Rmax comparison SPR for binding of (A) OVA and (B) hBTLA to the parental or bispecific antibodies. (C, D) Rmax comparison SPR for (C) OVA or (D) hBTLA binding to the antibodies at various LC:HC ratios. For (A-D) the RU of antigen bound was normalised to the RU of antibody captured for these plots. (E) Sandwich SPR for free antigen OVA binding. Antibody (Ab) is captured by immobilised hBTLA for 120s followed 80s later by OVA (at 200s). Arrows indicate the RU of antibody captured and RU of OVA binding.

the HC-HC dimer (Fig. 3.9B). When reduced, the HC, nanobody-Fc fusion (Nb-Fc) and the LC are visible at approximately 50 kDa, 42 kDa, and 25 kDa, respectively (Fig. 3.9B). The reduced product at ~30 kDa was assumed to be hinge-Fc after the Nb was cleaved from it (Fig. 3.9B). The Nb part of the cleavage is not visible at ~15 kDa, suggesting that the cleavage occurred before purification.

The 827*611 or 827*151 bispecific antibodies run at their expected weight at ~160 kDa on the non-reducing SDS-PAGE with HC dimers at ~110 kDa (Fig. 3.9B). In all cases the predominant population appears to be the full bispecific antibody (Fig. 3.9B). The SEC profiles of bispecific antibodies comprising a 611 arm had a lower proportion of impurities than the antibodies containing 151 arms (Fig. 3.9C). This was also reflected in their yields with bispecific antibodies comprising a 611-arm having a yield of >15 mg/L whereas the 151-arm bispecific antibodies produced less than 0.5 mg/L. The high proportion of contaminants and low yield of 151 containing bispecific antibodies suggest that there were folding or stability problems with 151-arm expression. In contrast, the 611-armed antibodies presented a monomeric SEC profile post dual-purification, ran at the expected size and expressed well indicating that any bispecific activity observed was not due to the formation of aggregates.

3.4.2 Other anti-hBTLA*anti-OVA bispecific antibody production

Having established the Wang bispecific antibody generation method and successful incorporation of an Nb-Fc arm, more anti-hBTLA*anti-OVA bispecific antibodies were produced. These antibodies incorporated anti-OVA nanobodies (Nb) and/or an anti-hBTLA 286 single-chain fragment (scFv) (Fig. 3.10A, 3.11A), i.e., Nb82*286, 2C1-286scFv, Nb41-286scFv, Nb82-286scFv to reduce the dimensions of the constructs. When Nb82*286 was produced, aggregates were found and separated by SEC from the bispecific antibody peak

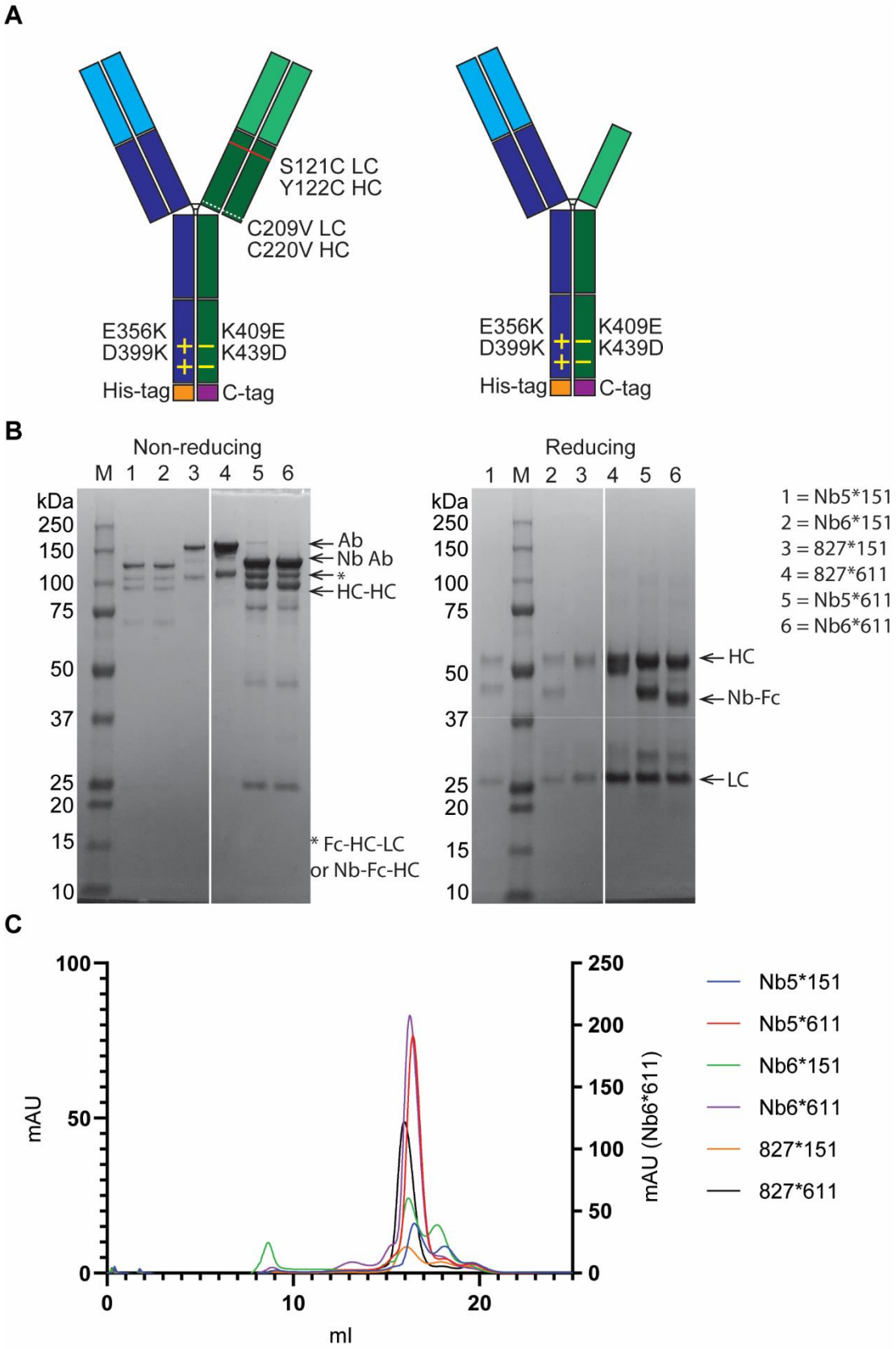


Figure 3.9. Purification of anti-IL-10R bispecific antibodies. (A) Schematic representing both conventional (left) or nanobody fusion (right) bispecific antibodies. (B) Non-reducing (left) and reducing (right) SDS-PAGE of the produced antibodies. (C) SEC profiles of purified proteins.

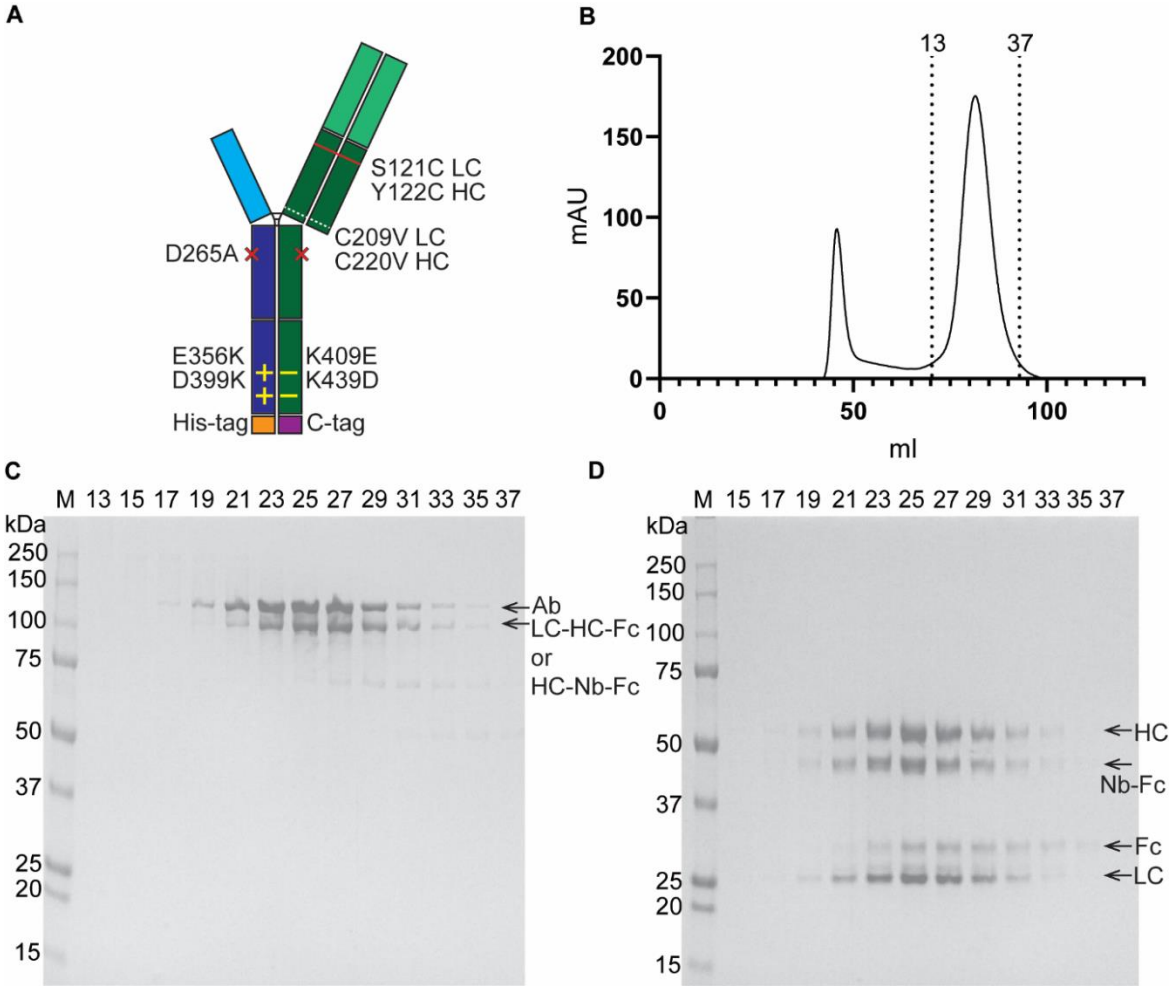


Figure 3.10. Purification of 286*Nb82. (A) Schematic of 286*Nb82. (B) SEC profile. (C) Non-reducing SDS-PAGE SEC fractions. (D) Reducing SDS-PAGE of SEC fractions.

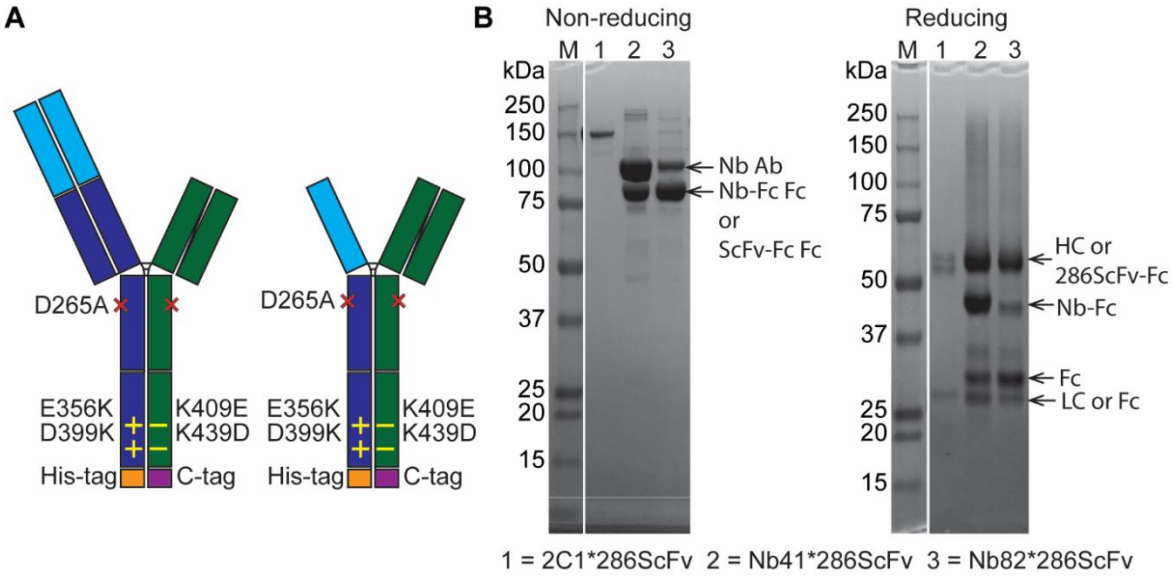


Figure 3.11. Purification of bispecific antibodies with a 286scFv arm. (A) Schematic of 286scFv bispecific antibodies. (B) Non-reducing (left) and reducing (right) SDS-PAGE gels. Nb-Ab is nanobody containing antibody.

(fractions <13 from fractions 13-37 on the SEC trace) (Fig. 3.10B).

The fractions containing the bispecific antibody were analysed using SDS-PAGE and two bands were observed at ~130 kDa and ~105 kDa under non-reducing conditions. These are suggested to be the fully formed bispecific antibody and the bispecific antibody with the nanobody cleaved off, respectively, as SEC produced slight seperation (Fig. 3.10C). The reducing SDS-PAGE showed bands at ~55 kDa, ~42 kDa and ~25 kDa representing the HC, Nb-Fc fusion and LC, respectively (Fig. 3.10D). The band at ~30 kDa is likely the hinge-Fc product after nanobody cleavage, as the His-tag would have retained it but not the nanobody (Fig. 3.10D).

The bispecific antibodies produced including a 286scFv-Fc arm featured either an anti-OVA Fc-nanobody fusion or conventional antibody arm as their partner (Fig. 3.11A). The 2C1*286scFv antibody was visible at ~150 kDa under non-reducing conditions and reduced into the expected constituent chains of HC (~60 kDa), scFv-Fc (~55 kDa) and LC (~27 kDa) (Fig. 3.11B). The scFv-Fc*Nb-Fc bispecific antibodies produced bands of the expected weight at ~100 kDa and a lower band at ~80 kDa which is likely from cleavage of either 286scFv or nanobody (Fig. 3.14B). Upon reduction these bispecific antibodies formed four bands at ~55 kDa, ~43 kDa, ~30 kDa and ~27 kDa (Fig. 3.11B). These bands are assumed to be 286scFv-Fc, Nb-Fc and Fc products from cleavage of either Nb82 and/or 286scFv. It is not possible to tell from the SDS-PAGE whether the two cleaved products come from two cleavage sites on one antibody arm or one cleavage site on both arms. However, the 286scFv*2C1 antibody did not appear to produce 286scFv cleavage product so no additional cleavage would be expected when 286scFv is combined with an Nb-Fc arm (Fig. 3.11B). Interestingly, the ~30 kDa band appears stronger for 286scFv*Nb82 than for 286scFv*Nb41, again suggesting that it is the nanobody arm cleaving rather than the

286scFv arm. If this is true, then the extent of Nb-Fc cleavage appears to be nanobody dependent.

3.5 Western blot analysis of bispecific antibodies

To confirm the identity of the protein bands seen on SDS-PAGE gels for the bispecific antibodies produced, Western blot analysis was done using anti-kappa light chain, anti-His and anti-C-tag detection antibodies (Fig. 3.12). For this analysis, only antibodies used in animal experiments (discussed in Chapters 4 and 5), *i.e.*, the anti-IL-10R Nb5*611, Nb6*611 and 827*611 as well as the OVA/hBTLA Nb82*286, were investigated.

The non-reducing Western blots were harder to interpret than the reducing western blots as the high molecular weight bands were not all distinct upon detection (Fig. 3.12A). Nb82*286 had the most clearly defined bands of the Nb-Fc containing bispecific antibodies (Fig. 3.12A Lanes 1, 2 vs Lane 4). Anti-kappa staining showed bands at ~120 kDa, ~105 kDa and ~75 kDa (Fig. 3.12A). These are suggested to be full bispecific antibody, antibody with the Nb cleaved off and HC-LC, respectively. Anti-His staining for Nb82*286 detected the Nb82-Fc arm which could be detected alone at ~42 kDa. Additionally, His-tag was detected at the weight of full antibody ~120 kDa and two bands smaller than this at ~90 kDa and ~75 kDa believed to be bispecific lacking LC, and bispecific with Nb cleaved off and lacking LC (Fig. 3.12A). C-tag staining of Nb82*286 showed free HC at ~60 kDa (Fig. 3.12A). Additionally, a band at ~75 kDa was observed which could be HC-LC or HC-Fc from nanobody cleavage (Fig. 3.12A). For fragments larger than this the C-tag detection is harder to interpret but the band at ~120 kDa is again present representing the complete antibody (Fig. 3.12A). Staining of Nb5*611 and Nb6*611 was harder to interpret but are suggested to correspond to the same bands as described for Nb82*286 (Fig. 3.12A). 827*611 staining showed complete antibody at ~160 kDa observed with all detection antibodies (Fig. 3.12D).

The reducing anti-kappa Western blots showed LC present at ~30 kDa for all four bispecific antibodies (Fig. 3.12B). Interestingly a band of the same size was seen in the anti-His and anti-C-tag blots as well (Fig. 3.12B). These bands are likely from cleavage at the hinge region in all antibody formats leaving CH2-CH3, which was detected (Fig. 3.12B). For 827*611 anti-His and anti-C-tag Western blot bands at ~60 kDa, ~35 kDa and ~30 kDa can be observed (Fig. 3.12B, Lane 3). These are assumed to be full HC, hinge-CH2-CH3 and CH2-CH3, respectively, suggesting that there is some antibody degradation. However, only the two HCs and the band at ~30 kDa, where LC or CH2-CH3 would be present, could be seen on the reducing SDS-PAGE (Fig. 3.9B). Therefore, the larger degradation products are only detectable due to the much higher sensitivity of a Western blot and represent a very small proportion of overall antibody. Presumably, this is also the case for the CH2-CH3 product seen in the anti-His and anti-C-tag western blots, and the band at ~30 kDa consists predominantly of LC in the SDS-PAGE (Fig. 3.9B). The Nb5*611 and Nb6*611 bispecific antibodies had the C-tag present on each Nb-HC arm. For both of these bispecific antibodies a band at ~36 kDa was seen in the anti-C-tag blot and are suggested to be the nanobody cleavage product, hinge-CH2-CH3 (Fig. 3.12B, Lane 1 and 2). The ~36 kDa band in combination with the ~30 kDa band suggest that the nanobody arm can cleave in two locations, likely before and after the hinge. For Nb5*611 and Nb6*611 the His-tag was present on the full 611 HC. As mentioned above there was a band present at ~30 kDa suggesting cleavage between the hinge and CH2, separating the Fab from the Fc, leaving CH2-CH3 (Fig. 3.12B). The ~36 kDa band could be seen weakly in the SDS-PAGE indicating that hinge-CH2-CH3 was a greater proportion of the overall product than was the case for 827*611, which does not include a Nb-Fc arm (Fig. 3.9B). This suggests that the Nb-hinge junction was being cleaved, rather than the CH1-hinge junction present in all three, in accordance with the suspected Nb cleavage (Table 3.7, Fig. 3.9B). The Nb82*286

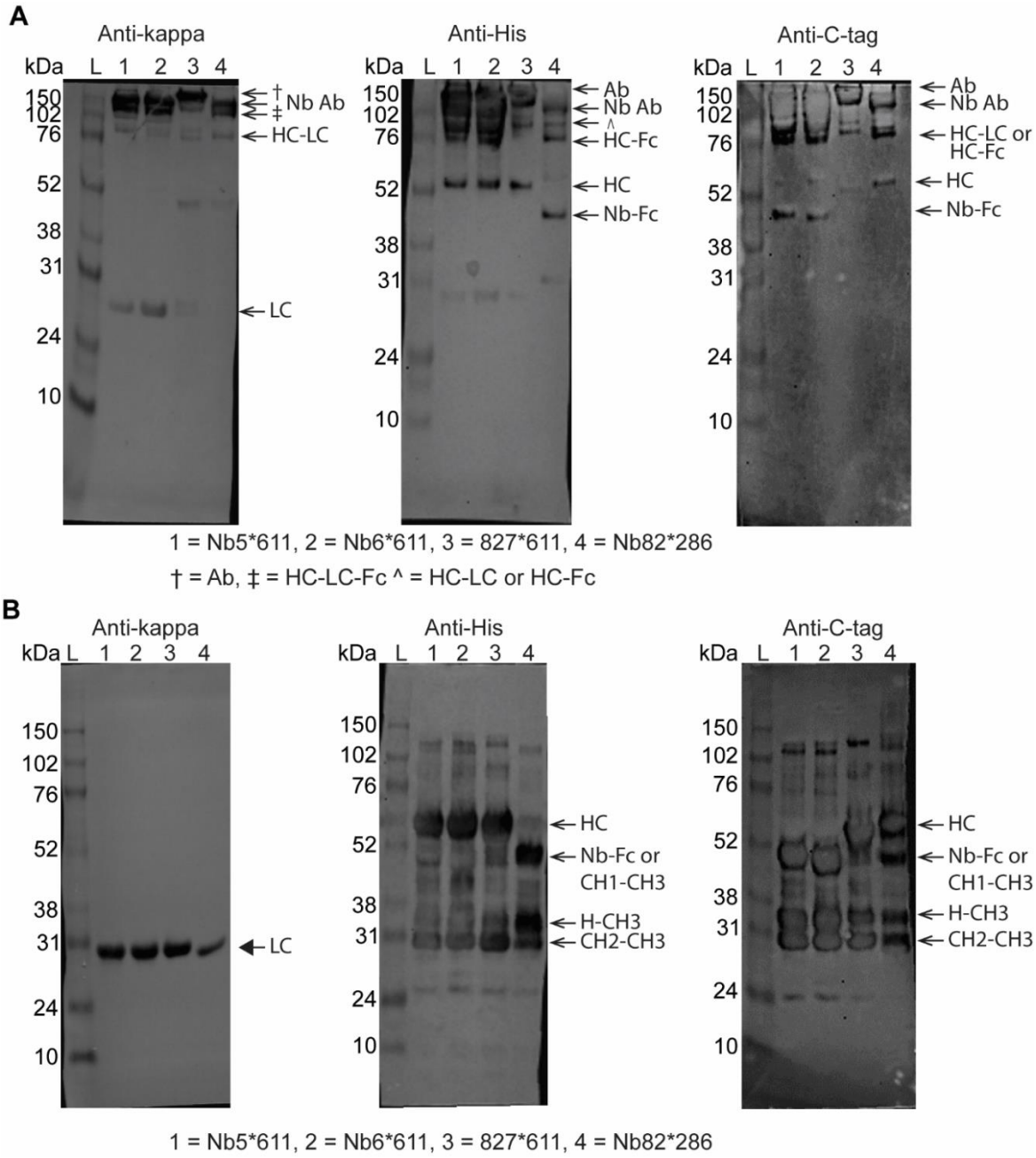


Figure 3.12. Western blots of bispecific antibodies used in animal experiments using anti-kappa, anti-His and anti-C-tag detection antibodies. (A) Non-reducing western blots. (B) Reducing western blots. Western blots are labelled with the likely product at the observed size (H = hinge, CH1-CH3 includes the CH2 domain between them. H-CH3 also includes the domains in between).

antibody had the His-tag present on the Nb82 arm and bands at ~47 kDa, ~36 kDa and ~30 kDa can be seen in the His-tag Western blot (Fig. 3.12B, Lane 4). These are assumed to be Nb82-Fc, hinge-CH2-CH3 and CH2-CH3, respectively. In the C-tag Western blot, detecting the full 286 HC of Nb82*286, there were bands at ~30 kDa, ~36 kDa, ~45 kDa and ~60 kDa

Table 3.7. Rmax comparison SPR of anti-IL-10R bispecific antibodies

Antibody	Antigen	cRmax (bAb)	cRmax (pAb)	B_C ± SD (%)	Bispecific B_C (%)
827*611	mIL-10Rb	0.133	0.182	74.0±1.9	72
827*611	mIL-10Rb	0.138			
Nb6*611	mIL-10Rb	0.208	0.237	84.0±5.8	85
Nb6*611	mIL-10Rb	0.189			
Nb5*611	mIL-10Rb	0.211	0.234	84.3±8.2	82
Nb5*611	mIL-10Rb	0.184			
827*611	hIL-10Ra	0.201	0.184	97.1±17.1	72
827*611	hIL-10Ra	0.157			
Nb6*611	hIL-10Ra	0.244	0.239	101.5±0.9	85
Nb6*611	hIL-10Ra	0.241			
Nb5*611	hIL-10Ra	0.232	0.237	97.4±1.2	82
Nb5*611	hIL-10Ra	0.228			

Measurements were performed at 25°C. The binding capacity is shown in percentage ± standard deviation (SD).

(Fig. 3.12B). These bands are likely to be CH2-CH3, hinge-CH2-CH3, CH1-hinge-CH2-CH3 and full HC, respectively. These bands align in part with the nanobody arm bands in the His-tag Western blot and it is therefore not possible to tell these apart in the reducing SDS-PAGE (Fig. 3.10D). The degradation of the full HC arm of Nb82*286 behaves similarly to 827*611 and degradation products of this arm are therefore suggested to present only a small fraction of the overall protein and that the bands visible on the reducing SDS-PAGE mainly represent HC (~60 kDa), Nb82-Fc (~47 kDa), the hinge-CH2-CH3 product of Nb82 cleavage (~36 kDa) and LC (~30 kDa) (Fig. 3.10D). This is supported by the SPR findings that the Nb82 arm had a binding capacity of 70% whereas the 286-arm had a binding capacity of 105% (Table 3.10, next section). Overall, the Western blot analysis confirmed that complete antibodies were being formed and supported that Nbs were being

cleaved from the FC region. Furthermore, it demonstrated that there was some cleavage across all antibodies at domain junctions, but this is suggested to be occurring only for a small fraction of the total antibody.

3.6 SPR analysis of further bispecific antibodies

3.6.1 Anti-IL-10 receptor bispecific antibody bispecificity

The bispecific antibodies were analysed by SPR to assess their bispecific binding capacity. In the case of the nanobody arms, a calculated Rmax, based on the RU of bispecific antibody captured, was used to estimate the nanobody arms parental *cRmax*, as divalent nanobody-Fc was not produced. For the Rmax comparison SPR, Rmax was determined by fitting the single cycle kinetics binding curves in Fig. 3.13. The 611-arm had 97.1±17.1%, 101.5±0.9% and 97.4±1.2% binding capacity for hIL-10Rα for the 827*611, Nb6*611, Nb5*611 bispecific antibodies, respectively (Table 3.7). For the same bispecific antibodies, the binding capacity of mIL-10Rβ was slightly lower than for hIL-10Rα with 74.0±1.9%, 84.0±5.8% and 84.3±8.2%, respectively (Table 3.7). This observation aligns with the expectation, based on the SDS-PAGE, that either the nanobody was being cleaved off or some 827 LC was missing, both of which could account for the lower binding capacity of mIL-10Rβ. Overall, the bispecific binding capacity was 72% for 827*611, 85% for Nb6*611 and 82% for Nb5*611.

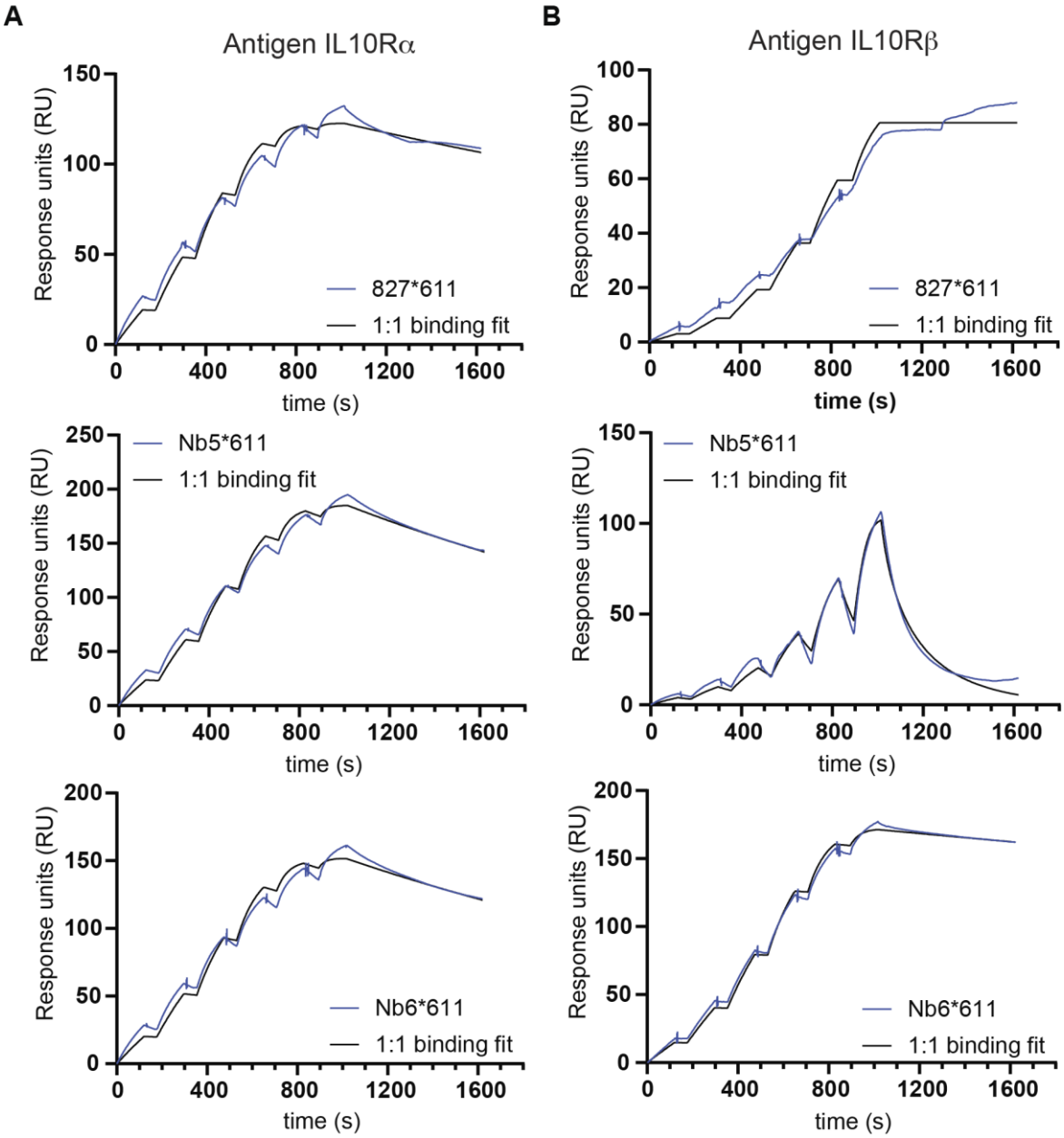


Figure 3.13. SPR analysis of anti-IL-10R bispecific antibodies. (A) Single cycle kinetics of bispecific antibodies binding IL-10Rα (62.5, 125, 250, 500, 1000, 2000 nM). (B) Single cycle kinetics of bispecific antibodies binding to IL-10Rβ (125, 250, 500, 1000, 2000, 4000 nM for 827*611 and 3.125, 6.25, 12.5, 25, 50, 100 nM for Nb5*611 and Nb6*611). Measurements were performed at 25C.

The sandwich SPR for the anti-IL-10R bispecific antibodies used concentrations of 1 µM mIL-10Rb and 10 µM hIL-10Ra. To reach at least 90% of Rmax in the SPR analysis concentrations of at least 10x higher than K_d had to be used. However, the chosen concentrations were limited by the yield of IL-10R chains. This could lead to an underestimation of bispecific binding capacity as the RU of free antigen binding may not

Table 3.8. Sandwich SPR of anti-IL-10R bispecific antibodies

Antibody	Antigen	cRU_{Ag}	cRmax	Bispecific B_C (%)
Nb5*611	hIL-10Rα	0.201	0.237	84.7
Nb6*611	hIL-10Rα	0.221	0.239	92.3
827*611	hIL-10Rα	0.221	0.184	119.7
Nb5*611	mIL-10Rβ	0.173	0.234	73.9
Nb6*611	mIL-10Rβ	0.141	0.237	59.6
827*611	mIL-10Rβ	0.051	0.182	27.8
Nb5*151	hIL-10Rα	0.410	0.237	173.1
Nb6*151	hIL-10Rα	0.344	0.239	143.9
827*151	hIL-10Rα	0.310	0.184	167.9
Nb5*151	mIL-10Rβ	0.175	0.234	74.6
Nb6*151	mIL-10Rβ	0.240	0.237	101.3
827*151	mIL-10Rβ	0.086	0.182	46.9

Either hIL-10Rα or mIL-10Rβ were immobilised and antibody and antigen (1 μM mIL-10Rβ or 10 μM hIL-10Rα) were bound sequentially. Measurements were performed at 25 °C.

approach Rmax. The 827-arm in the bispecific antibodies has the highest K_d and thus, weakest affinity for mIL-10Rb and would be most affected. Therefore, the calculated bispecific binding capacity is likely underestimating the actual bispecificity (Table 3.8). Nevertheless, the binding curves still demonstrate that the bispecific antibodies were able to bind both hIL-10Rα and mIL-10Rβ simultaneously (Fig. 3.14). Further, the affinities of the binding arms in the anti-IL-10R bispecific antibodies were maintained (Table 3.9). Collectively these data show that incorporation of nanobodies into the mIgG1 bispecific antibody is possible. Briefly, the 151 arm bispecific antibodies were screened using the sandwich SPR method with the same caveats mentioned (Table 3.8). hIL-10Rα or mIL-10Rβ were immobilised on the chip surface to select for functional antibody binding. However, the observed hIL-10Rα binding per RU antibody bound was much higher than predicted suggesting possible multivalent contaminants (Table 3.8). The 151 containing bispecific antibodies were not taken any further due to the low yield and contaminants.

Table 3.9. Steady state affinities comparison table for bispecific production approaches

Antibody	Antigen	K_d± SD (nM)
Nb5*611	hIL-10Ra	21.7±2.5
Nb6*611	hIL-10Ra	19.7±0.5
827*611	hIL-10Ra	13.6±4.9
611	hIL-10Ra	23.7±3.9
Nb5*611	mIL-10Rb	107.8±79.8
Nb6*611	mIL-10Rb	3.9±5.8
827*611	mIL-10Rb	102.1±8.2
Nb5	mIL-10Rb	149.6±47.29
Nb6	mIL-10Rb	3.2±0.3
827	mIL-10Rb	107.9

Measurements were performed at 25°C. The dissociation constant, K_d, is shown in nM ± standard deviation (SD).

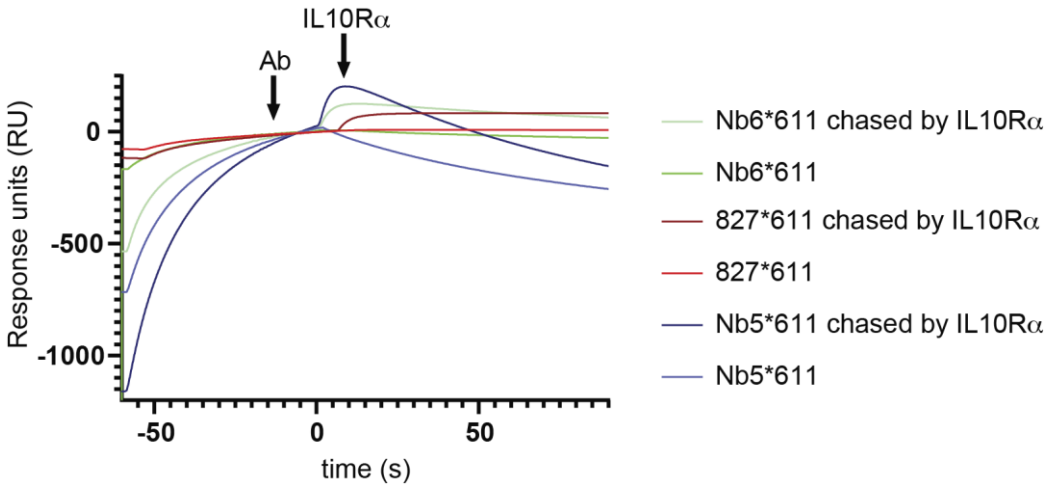


Figure 3.14. Sandwich SPR of anti-IL-10R bispecific antibodies. IL-10Rβ is immobilised on the chip surface. After capture of the various bispecific antibodies (-60s – 0s), IL-10Rα is passed over (0s onwards). Both axes have 0 at beginning of IL-10Rα flow. Measurements were performed at 25°C.

3.6.2 Other anti-hBTLA*anti-OVA bispecific antibody bispecificity

Bispecific binding capacity was assessed using the Rmax comparison SPR method. As 286ScFv, Nb41 and Nb82 were never produced separately as divalent Fc fusions the cRmax obtained experimentally were compared with a calculated parental cRmax based on the RU of antibody captured. Multicycle kinetics for the anti-hBTLA arm of Nb82*286 produced

105% of the expected hBTLA binding, indicating that this arm is fully formed and functional (Fig. 3.15A, Table 3.10). However, the anti-OVA arm of Nb82*286 demonstrated ~70% binding capacity (Fig. 3.15B, Table 3.10), suggesting that some Nb82 is being cleaved off and therefore binding to OVA is lost. OVA binding capacity for Nb82*286ScFv was even lower with 34% when the cRmax was obtained from the binding curve, supporting the idea that the Nb was cleaved off (Fig. 3.15C, Table 3.8). The OVA binding capacity of 286ScFv*Nb41 was higher with 85% than for 286ScFv*Nb82, in agreement with the observation that the Nb41-Fc arm produced less cleavage product than the Nb82-Fc on SDS-PAGE (Fig. 3.11B and Fig. 3.15C, Table 3.8). The 286ScFv*2C1 bound OVA with 76% binding capacity. This is similar to the binding capacity of 286*2C1 (Wang), showing that the reduced OVA binding may be a consistent issue with the 2C1 arm. In all the 286ScFv containing bispecific antibodies hBTLA binding capacity was close to 100% with 95%, 94% and 103% expected binding for 286ScFv*2C1, 286ScFv*Nb41 and 286ScFv*Nb82, respectively (Table 3.10). Overall bispecific binding capacity was estimated to be 73.8% for Nb82*286, 73% for 286ScFv*2C1, 80% for 286ScFv*Nb41 and 34% for 286ScFv*Nb82.

3.7 Endotoxin testing of bispecific antibodies

To ensure that observation from *in vivo* and *ex vivo* experiments using the bispecific antibodies were truly due to the antibodies and not due to the use of endotoxin contaminated material regular endotoxin testing was performed. Endotoxin induces an acute inflammatory response in mice and humans and the pyrogenic threshold in humans is 5 EU/kg which is assumed to be true for mice (262,263). As this thesis examines inhibitory receptor agonists any effect from contaminating endotoxin could mask inhibitory signalling induced by agonists. Therefore, antibodies used in further experiments were confirmed to have

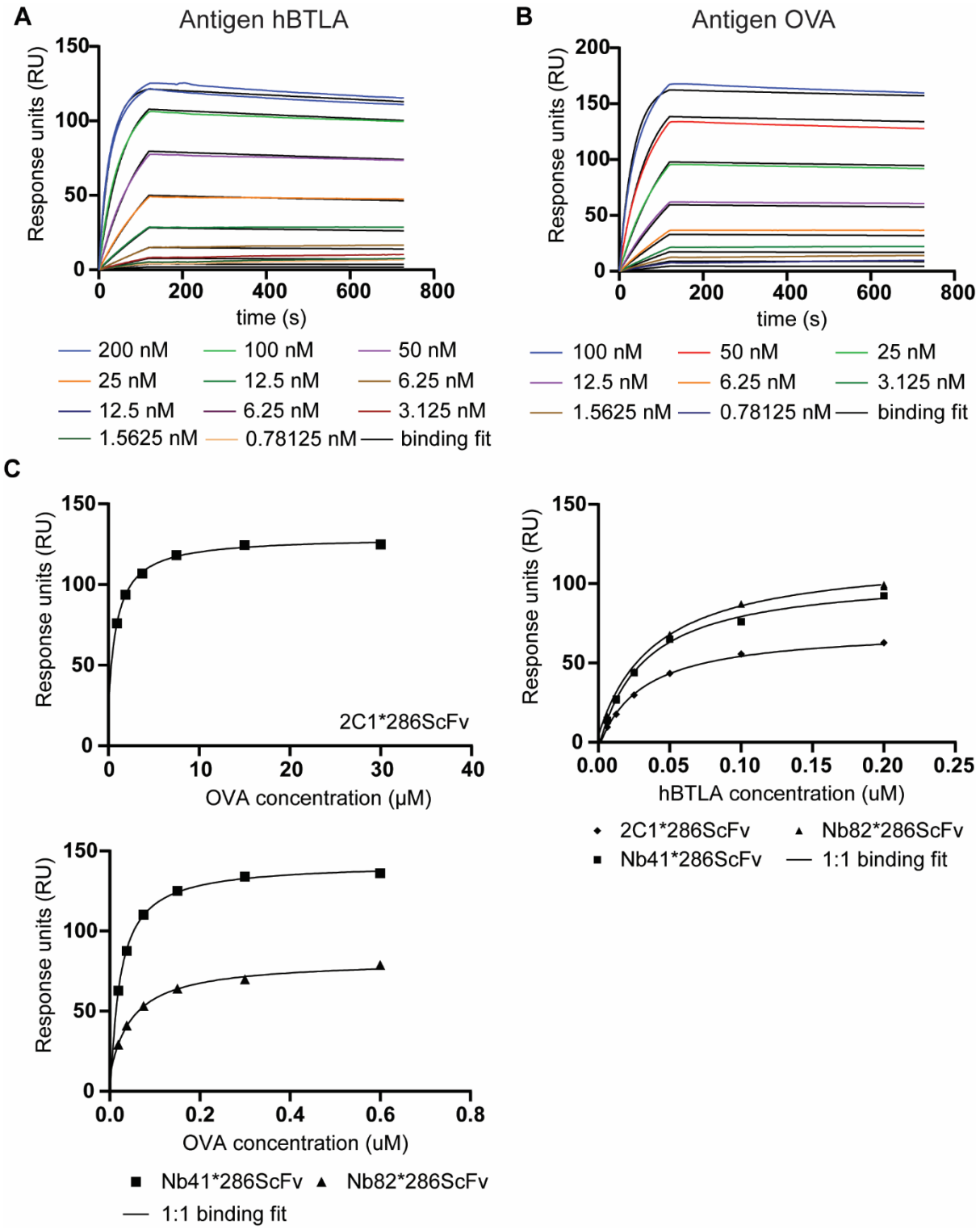


Figure 3.15. SPR analysis of hBTLA/OVA bispecific antibodies. (A) Multicycle kinetic analysis of 286*Nb82 binding hBTLA. (B) Multicycle kinetics analysis of 286*Nb82 binding OVA. (C) SPR analysis of 286-scFv bispecific antibodies binding to OVA (left) or hBTLA (right).

Table 3.10. Rmax comparison SPR of anti-hBTLA*anti-OVA antibodies

Antibody	Antigen	cRmax (bAb)	cRmax (pAb)	B_C (%)	Bispecific B_C (%)
Nb82*286	OVA	0.209	0.299	70.0	73.8
Nb82*286	hBTLA	0.128	0.121	105.4	73.8
286ScFv*2C1	OVA	0.206	0.268	76.7	73.1
286ScFv*Nb41	OVA	0.313	0.368	85.0	79.5
286ScFv*Nb82	OVA	0.124	0.367	33.8	34.7
286ScFv*2C1	hBTLA	0.146	0.153	95.3	73.1
286ScFv*Nb41	hBTLA	0.197	0.211	93.5	79.5
286ScFv*Nb82	hBTLA	0.215	0.210	102.7	34.7

Measurements were performed at 25 °C. The binding capacity is shown in percentage ± standard deviation (SD).

<0.01 endotoxin units (EU) per mL (Fig. 3.16). Doses of at most 200 μL were given to mice weighing ~20 mg or more therefore giving a maximum dose of 1 EU/kg, which is well below the pyrogenic threshold (assuming antibody was at 0.1 EU/ml).

3.8 Discussion

This chapter described the generation of murine bispecific antibodies using two different methods, established by Labrijn *et al.* and by Wang *et al.* (245,246). Using the Labrijn approach, bispecific antibodies were generated and bispecificity was observed in the sandwich SPR-based assay. However, the process of cFAE exchange used in this method produced a large amount of aggregated material. Thus, it was unclear if binding was due to the presence of monomeric and correctly folded bispecific antibodies or due to (at least partially) functional but aggregated multimeric protein. Furthermore, complete dissociation of the heavy and light chains was observed, presumably allowing the heavy and light chains to freely reassociate giving, at best, 25% bispecific product (245). Interestingly, Labrijn *et al.* have shown that no LC-HC dissociation occurs when cFAE is used to produce human IgG1 bispecific antibodies; however, this was not shown in their work describing the use of

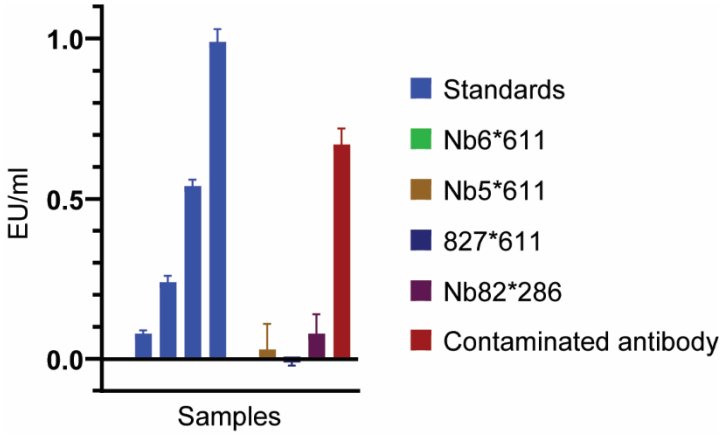


Figure 3.16 Endotoxin quantification of bispecific antibodies used in animal experiments. EU = endotoxin units. Testing was done by Martin Fellermeyer and myself.

cFAE for the creation of murine bispecific antibodies (232,245,264). Thus, the bispecific activity Labrijn *et al.* observed might arise from bispecific antibody with correct HC-HC heterodimerisation but random light chain association. However, it is also possible that the hydrophobic interaction chromatography used by Labrijn *et al.* to purify their bispecific antibody post cFAE selected for correctly-associated antibodies. In the future it might be possible to reduce HC-LC dissociation during cFAE by lowering the concentrations of 2-MEA further, but this was not explored. Notwithstanding all this, functional bispecific antibodies were produced in a much more straightforward manner using the Wang *et al.* method (246). The repositioning of the HC-LC disulphide bond to stabilise the construct was tolerated across all tested bispecific antibodies, in keeping with the observations of Wang *et al.* (246).

A dual-purification approach was used to isolate bispecific antibodies and it is assumed that this selectively purifies molecules expressing both purification tags. This is supported by others using a similar approach that effectively removed homodimeric contaminants (265). Additionally, bispecific antibodies comprising one nanobody- or scFv-arm and one conventional antibody-arm produced antibody of the expected intermediate size between a homodimeric conventional antibody and a homodimeric antibody with nanobody arms. Only

faint traces of homodimeric, full-length antibody were observable using SDS-PAGE, indicating that this species was not a major contaminant. It is not possible to exclude the creation of homodimeric nanobody-arm antibody in this manner, as this would have the same size as the products believed to result from LC dissociation or cleavage on SDS-PAGE gels. However, the 2C1*286scfv antibody did not produce any smaller products than expected on SDS-PAGE and therefore the smaller products seen with the Nb-arm containing bispecifics are believed to be cleavage products and not homodimers. A shortcoming of the dual-purification approach is that aggregates which contain both HCs could have been purified. Therefore, SEC was used post-purification to remove large aggregates, mitigating this. Overall, the high yields and purity of 2C1*286scFv, as seen by SDS-PAGE, suggests that dual purification was selectively purifying bispecific antibody, and that the Wang *et al.* mutations introduced to favour heterodimerisation were highly effective (246).

The bispecific binding capacity of the new antibodies was assessed using SPR assays. Bispecific binding capacity was consistently slightly higher when measured using the sandwich SPR-based assay compared to the Rmax comparison assay. This discrepancy could arise due to the immobilised antigen on the chip surface in the sandwich SPR-based assay selecting for well-formed antibodies, capable of binding antigen, whereas the Rmax-based comparison, which used anti-IgG to capture antibody onto the sensor chip surface would have also captured contaminating non-functional fragments, such as HC-HC dimers. This would increase the measured RU of bispecific antibody captured while not increasing antigen binding, resulting in a lower effective bispecific binding capacity. Thus, the Rmax-based approach might be more informative regarding the quality of the entire bispecific antibody mixture.

Wang *et al.* increased the LC to HC DNA ratio during their bispecific antibody production and found that this increased the proportion of functional bispecific antibody. Similarly, a

2:1 LC to HC DNA ratio was found to increase bispecific binding capacity measured using both SPR-based assays demonstrating the ability of both methods to capture these effects.

A shortcoming of the Rmax SPR-based approach is that it is unable to distinguish between an equal mix of two divalent monospecific antibodies and a bispecific antibody. However, this possibility is eliminated by the combination of the sandwich SPR-based assay and the two-tag purification scheme. The bispecific binding capacities obtained using the Rmax SPR-based assay should therefore be reliable. The sandwich SPR-based method, on the other hand, cannot be used to determine the proportion of bispecific antibody present in the mixture. Rather, it is only informative about the protein that is bound to the immobilised antigen. Additionally, the sandwich SPR-based assay produced some unrealistically high bispecific binding capacities (>100%). This could be due to the binding of a fraction of aggregated free antigen which would inflate all measured bispecific binding capacities, even though the antigen was subjected to size-exclusion chromatography prior to SPR in mitigation. Importantly, the sandwich SPR-based assay demonstrated that the new bispecific antibodies were capable of binding both antigens. However, this does not necessarily apply to the case when both antigens are membrane bound, as binding one membrane restricted antigen may limit the freedom of the second antibody-arm to reach and bind its epitope.

Overall, the bispecific antibodies produced in this chapter appeared to be highly bispecific in nature and highly pure. The antibodies were therefore taken forward into experiments in Chapters 4 and 5 to examine their effects.

Chapter 4

Chapter 4 Effects of inhibitory immunoreceptor agonists in the OT-I RIP-mOVA diabetes mouse model

Previously hBTLA, hPD-1 and hTIGIT agonists have been developed (described in the thesis of Christopher Paluch (249)). Of these the hBTLA antibody 286 has been shown to ameliorate disease in a $CD4^+$ T-cell driven model of colitis (249). Further, in a model of graft versus host disease (GVHD), in which bone marrow and splenocytes from hBTLA donor mice were injected into MHC haplotype-mismatched recipients, the 286 antibody significantly increased survival and reduced weight loss and colon inflammation (249). Interestingly, 286 agonism of hBTLA was found to be Fc receptor dependent. hBTLA signalling is believed, therefore, to be triggered by 286 through creation of a "close contact" between two cells, mediated by antibody engagement of hBTLA and Fc receptor in trans. Creation of a close contact results in a change of the local kinase/phosphatase balance by exclusion of large protein receptor tyrosine phosphatases, resulting in kinase activity predominating and signalling being initiated (Lippert *et al.*, manuscript submitted).

To investigate whether hBTLA agonism by 286 could be achieved in a tissue-specific, Fc receptor independent manner, it was hypothesised that Fc receptor binding could be replaced with binding to another membrane bound antigen in a bispecific antibody format. The membrane bound form of OVA (mOVA) was selected as the antigen. OVA does not have a naturally occurring membrane-bound form, therefore mOVA used in the following experiments represents a fusion protein between OVA and the transmembrane and stalk of the human transferrin receptor (266).

There were two primary benefits of using mOVA as a model tissue antigen. Firstly, the availability of anti-OVA antibody sequences in the literature, which could be incorporated into a bispecific antibody format (267–270). Secondly, mice expressing mOVA under the

rat insulin promoter (RIP-mOVA) have been used to investigate antigen presentation, T-cell tolerance and T-cell homing by adoptively transferring OVA specific OT-I and OT-II T-cells into these mice (266,271–277). OT-I T-cells are $CD8^+$ T-cells with a transgenic TCR, composed of the Vα2 and Vβ5 chains, reactive with the OVA derived peptide SIINFEKL (amino acids 257-264) bound to the MHC class I molecule $H\text{-}2K^b$ (278). OT-II T-cells are $CD4^+$ T-cells reactive to an OVA peptide (amino acids 323-339) presented by the MHC class II molecule $I\text{-}A^b$ (279). Therefore, when OT-I and OT-II T-cells are adoptively transferred into RIP-mOVA mice on a C57BL/6 background they respond to mOVA initiating a T cell driven immune response against the mOVA expressing cells.

Under the rat insulin promotor, mOVA is expressed in beta cells present in the pancreatic islets of Langerhans and in renal proximal tubular cells (266). The beta cells are responsible for insulin production and regulate blood glucose. Transferred OT-I and OT-II T-cells infiltrate the islets and destroy the beta cells resulting in insufficient insulin production and the breakdown of blood glucose regulation, causing diabetes (272–277). This is similar to the development of type I diabetes in humans in which auto-reactive T-cells destroy beta cells leading to loss of insulin production (280).

Both PD-1 and BTLA have been shown to be important regulators of OT-I T-cell activity in the OT-I RIP-mOVA diabetes model (273,274). BTLA knock out OT-I T-cells adoptively transferred into RIP-mOVA mice increased the incidence of diabetes when compared with wild type (WT) OT-I T-cells (274). Further, blockade of PD-1 by antagonist antibodies was shown to increase the occurrence of diabetes and increase expression of IL-2, IFNγ and granzyme B in OT-I T-cells (273). These findings suggest that agonism of BTLA and PD-1 could ameliorate disease progression and suppress OT-I T-cell activity in the OT-I RIP-mOVA diabetes model, making it a suitable model to investigate inhibitory immunoreceptor agonism.

To allow assessment of anti-human inhibitory immunoreceptor receptor agonists, mice expressing the human extracellular domain of the inhibitory immunoreceptors fused to the murine intracellular domain were crossed to OT-I mice. These humanised receptors have previously been shown to maintain binding to the murine ligands and no significant changes in response to immunisation or immune system development were found (described in the thesis of Christopher Paluch (249)).

The OT-I RIP-mOVA diabetes model was used to investigate agonism of the previously developed hBTLA, hPD-1 and hTIGIT agonists, 286, Cl.19 and CE10, respectively, as well as the OVA/hBTLA bispecific antibody Nb82*286.

4.1 OT-I RIP-mOVA diabetes model pilot study

To establish the OT-I RIP-mOVA diabetes model $2x10^6$ OT-I T-cells were adoptively transferred into RIP-mOVA and WT, C57BL/6 ($H\text{-}2K^b$) mice. This number of OT-I T-cells had previously been shown to cause diabetes in 90% of RIP-mOVA mice (277). OT-I T-cells were harvested from the spleens and lymph nodes of OT-I donor mice and injected intravenously into RIP-mOVA or WT recipient mice (Fig. 4.1A).

To confirm OT-I T-cells were successfully purified prior to intravenous injection the presence of Vα2 and Vβ5, the two OT-I T-cell TCR chains, was confirmed by flow cytometry (Fig. 4.1B). Cells were counted and $2x10^6$ cells were adoptively transferred. The mice were monitored daily for glycosuria as well as weight loss and humanely sacrificed if positive for glycosuria or if weight loss exceeded 15% of the starting weight (or 20% in the

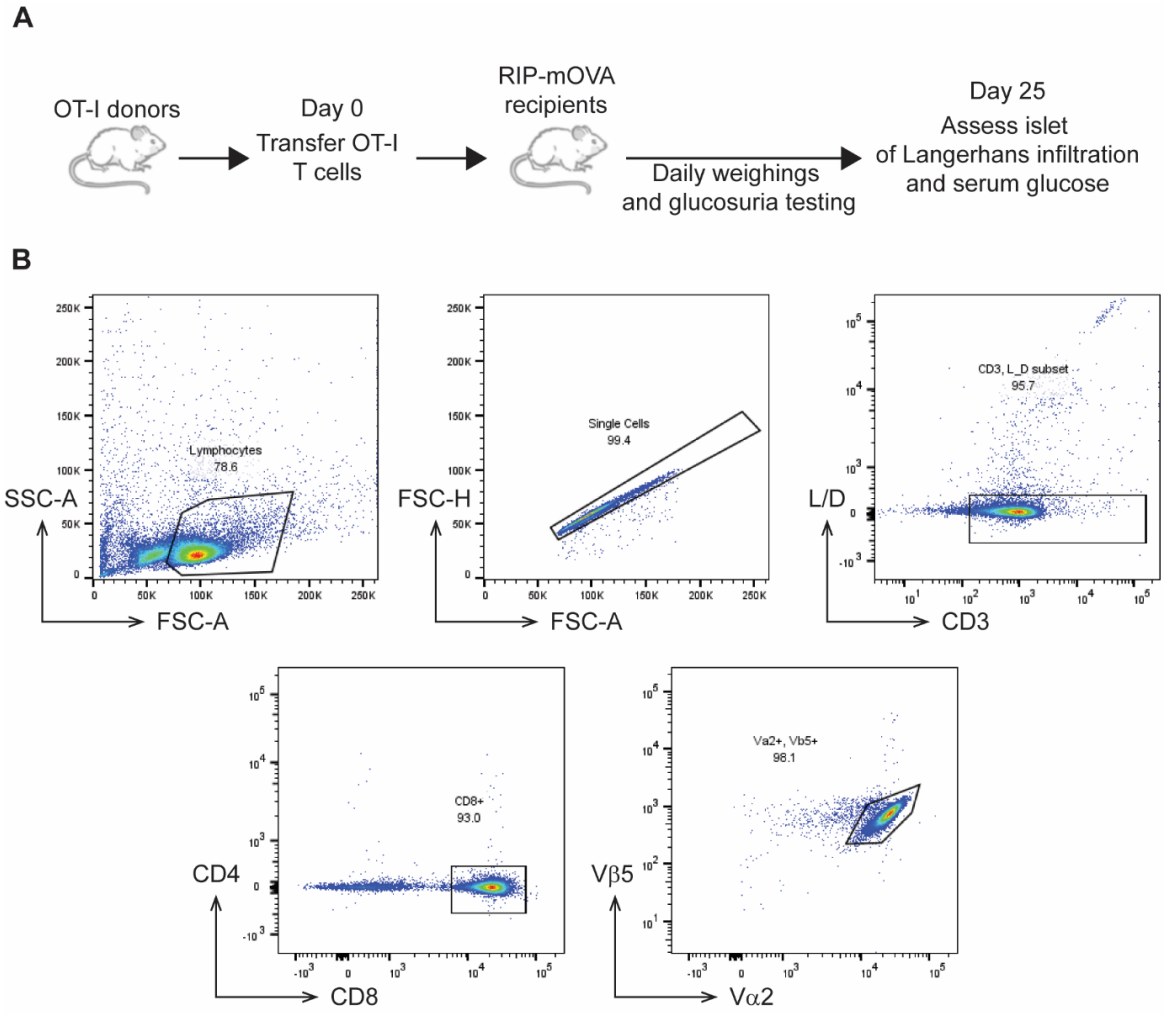


Figure 4.1. Model of autoimmune diabetes in RIP-mOVA mice by transfer of OT-I CD8⁺ T-cells. (A) Experimental procedure for OT-I RIP-mOVA diabetes model pilot. (B) Gating of OT-I CD8⁺ T-cells post purification, prior to transfer.

first two weeks). After 25 days or at the defined humane endpoints islets of Langerhans inflammation was assessed by scoring islet infiltration from 1-4, with 1 being no infiltration and 4 being inflammatory cells surrounding and permeating the islet (Fig. 4.2A-D).

Over 25 days the RIP-mOVA mice lost more weight in comparison to the WT mice (Fig. 4.3A). One of six mice in the RIP-mOVA group was humanely sacrificed after exceeding the 15% weight-loss threshold at Day 18 (Fig. 4.3A, B). Severe weight loss was unexpected but possible due to activation of the transferred OT-I cells and subsequent immune response.

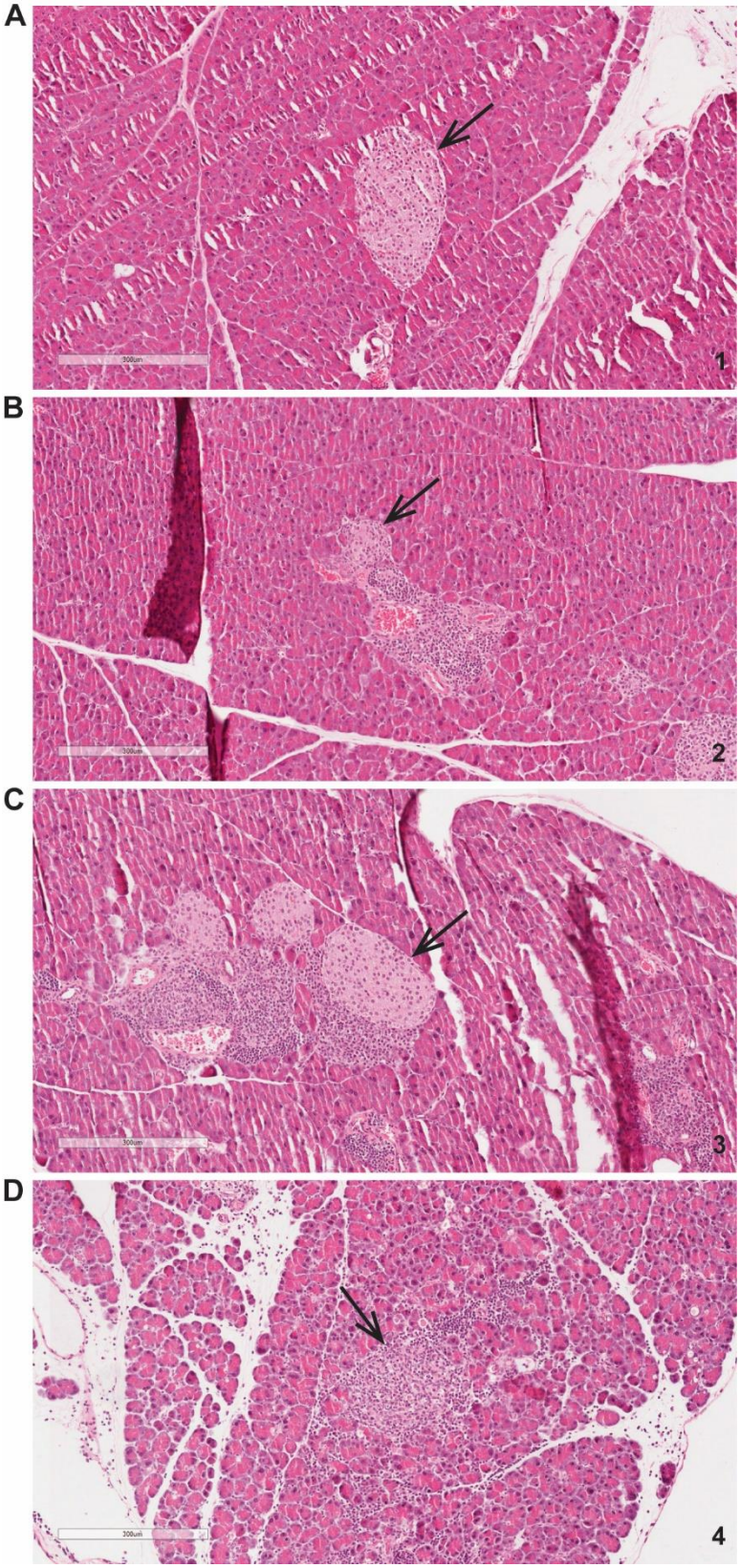


Figure 4.2. Exemplar histology sections of RIP-mOVA islet of Langerhans infiltrate scoring. (A) No signs of inflammation or immune infiltrate around the islet (score = 1). (B) Periductular/perivascular mononuclear cell inflammation (score = 2). (C) Early-stage insulitis (score = 3). (D) Severe insulitis (score = 4). Arrows highlight the islet being scored and the score is indicated in the bottom right-hand corner of each image.

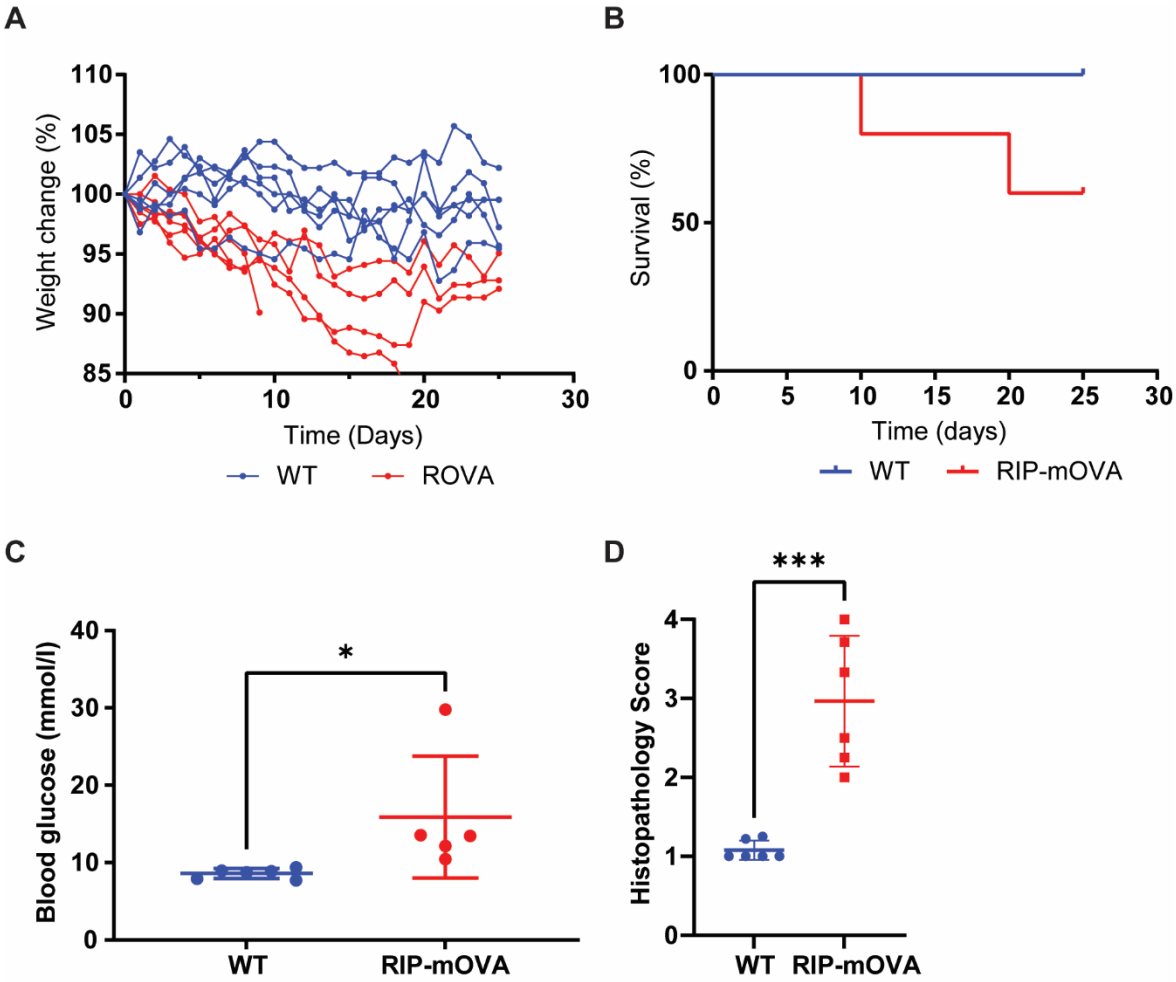


Figure 4.3. Assessment of RIP-mOVA and WT mice after OT-I T-cell transfer. (A) Weight of individual mice over time. (B) Kaplan-Meier survival curve (analysed by Log-rank test, p = 0.1010). (C) Blood glucose of individual mice. (D) Histopathology scores of islets of Langerhans infiltration in pancreatic tissue sections. (C, D) Statistical analysis was performed using unpaired student's t-test (* p ≤ 0.05, ** p ≤ 0.01, **** p ≤ 0.0001). WT n = 6 and RIP-mOVA n = 6 (the mouse culled in error was removed from this analysis in all cases except D).

Two further mice were culled after testing positive for glycosuria, however one of these was later found to be sacrificed in error due to a lack of familiarity with the strips used for testing. This mouse was removed from the Kaplan-Meier survival curve, which showed that two of five RIP-mOVA mice reached their humane end points prior to Day 25 (Fig. 4.3B). None of the WT mice developed glycosuria or exceeded the weight loss threshold (Fig. 4.3A, B). Blood glucose was analysed and found to exceed the reference range in all RIP-mOVA mice, except the mouse culled in error (281). Blood glucose levels were found to differ

significantly from the WT mice demonstrating that the transferred OT-I T-cells had caused blood glucose dysregulation as expected (Fig. 4.3C). Lastly, scoring of islet infiltration in pancreas tissue sections showed significantly more cell infiltrate in the RIP-mOVA mice than the WT mice (Fig. 4.3D). As expected, H&E-stained pancreatic sections of both RIP-mOVA mice and WT mice with and without OT-I T-cell transfer showed that this is not due to either the expression of mOVA or OT-I T-cell transfer alone but rather a combination effect (Fig. 4.4A, B).

This pilot showed that the transfer of $2x10^6$ OT-I T-cells into the RIP-mOVA mice was sufficient for future experiments. This was because there was significant islet infiltration and, while most mice did not develop glycosuria, it would be possible to detect OT-I T-cell inhibition and a reduction in disease progression by histology. Conversely, it would also allow for the detection of increased OT-I T-cell activity via an increase in mice developing glycosuria. Therefore, it would be possible to identify both successful inhibitory antibodies and detect agonist antibodies which do not produce inhibition as expected.

4.2 Anti-mOVA antibody selection

To use mOVA as the model tissue antigen required an antibody capable of binding mOVA. mOVA is a human transferrin receptor/OVA fusion protein comprising amino acids 1-118 of the human transferrin receptor and amino acids 139-385 of OVA. As such, approximately a third of OVA was removed in the creation of mOVA (Fig. 4.5A) (266). This is likely to have had a large impact on the structure of the OVA fragment present in mOVA. Therefore, an antibody was sought that bound within amino acids 139-385. The epitopes of five anti-OVA antibodies had previously been determined using a binding screen to an OVA mutant library (267). These mapped antibodies appeared to bind three distinct epitopes. Of these epitopes,

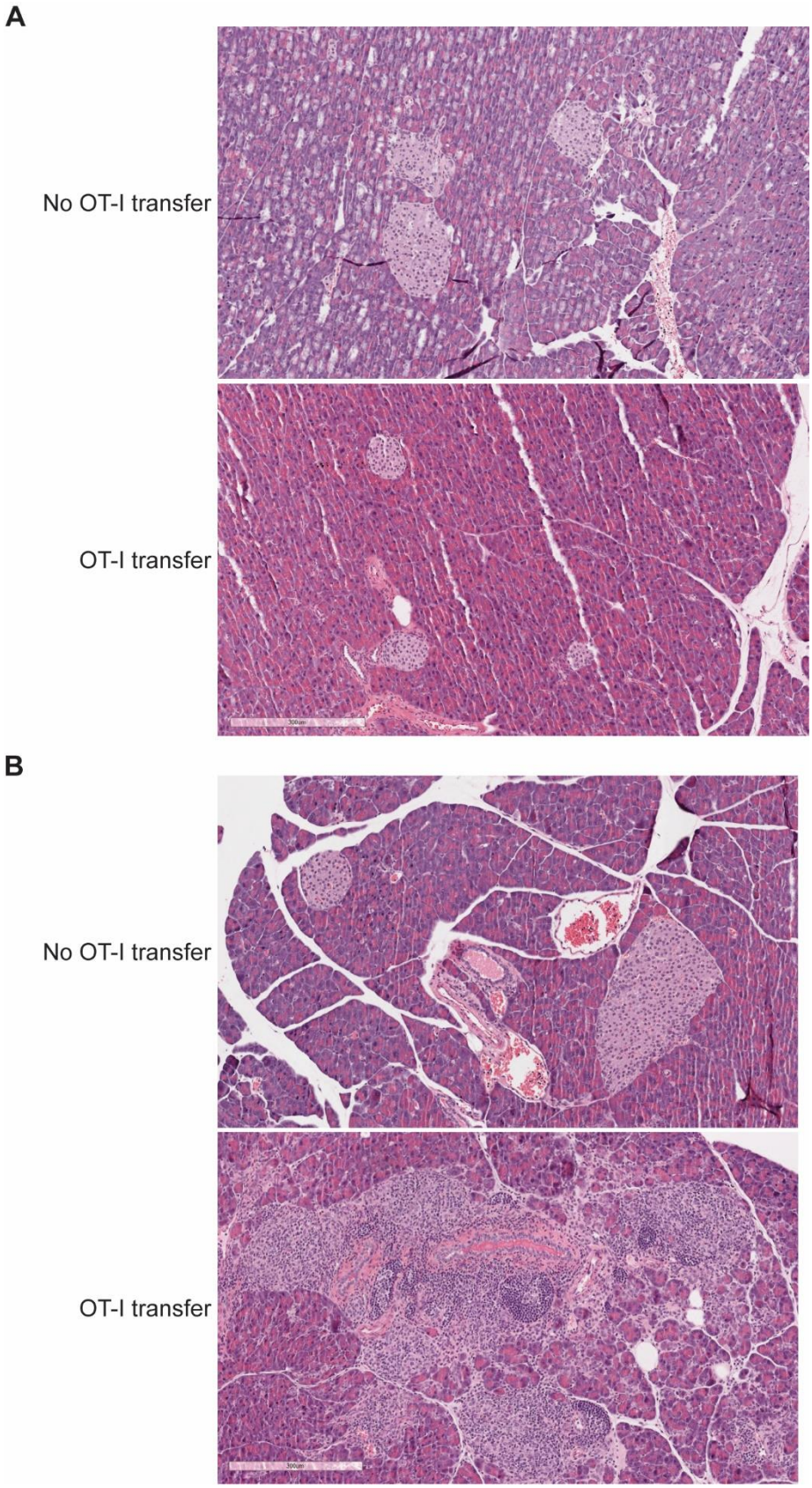


Figure 4.4. Comparison of RIP-mOVA and WT pancreas histology sections with and without OT-I transfer. (A) WT pancreas. (B) RIP-mOVA pancreas. Islet infiltration was assessed at day 25 or after development of glycosuria.

one was found at amino acids 65-67 of OVA which is not present in the mOVA sequence, excluding this as a candidate. The two other epitopes were present in the mOVA sequence and two antibodies which bound these epitopes, 2C1 and 3D7, were selected as candidate detection reagents (267). 2C1 was selected as it appeared to bind a cluster of amino acids of OVA, i.e., residues 203-205, possibly representing a linear epitope. A linear epitope was preferred due to the possible or likely change in the OVA structure in mOVA. The second candidate, 3D7, had its binding reduced by multiple different mutants of OVA, the primary cluster appearing between amino acids 179-194 of OVA, suggesting it bound a non-linear epitope (267). However, with so few antibodies having known epitopes and binding within the sequence used in mOVA, both antibodies were taken forward (267–270).

After production of both 3D7 and 2C1 it was found that 2C1 bound OVA using SPR (Fig. 3.7), whereas 3D7 did not (data not shown). However, 2C1 did not appear to bind mOVA expressing EL4 cells, a murine T-lymphoblast cell line, or to cryosections of RIP-mOVA pancreases (Fig 4.5B, C). Thus, neither 2C1 nor 3D7 were capable of binding mOVA.

Two nanobodies, Nb41 and Nb82, had previously been described as binding OVA, although their epitopes had not been identified (270). These nanobodies were incorporated into hBTLA/OVA bispecific antibodies to investigate their ability to bind mOVA. Of these two, Nb82*286, labelled with AF647, was found to bind EL4 mOVA cells and RIP-mOVA pancreas cryosections (Fig. 4.5B, C). In both cases no binding to WT EL4 cells or pancreas was observed indicating that the binding of Nb82*286 was antigen-specific (Fig. 4.5B, C). Further, no binding was seen for the other two bispecific antibodies, *i.e.,* Nb41*286 and 286*2C1, indicating that the Nb82 arm alone was responsible for binding (Fig. 4.5B, C).

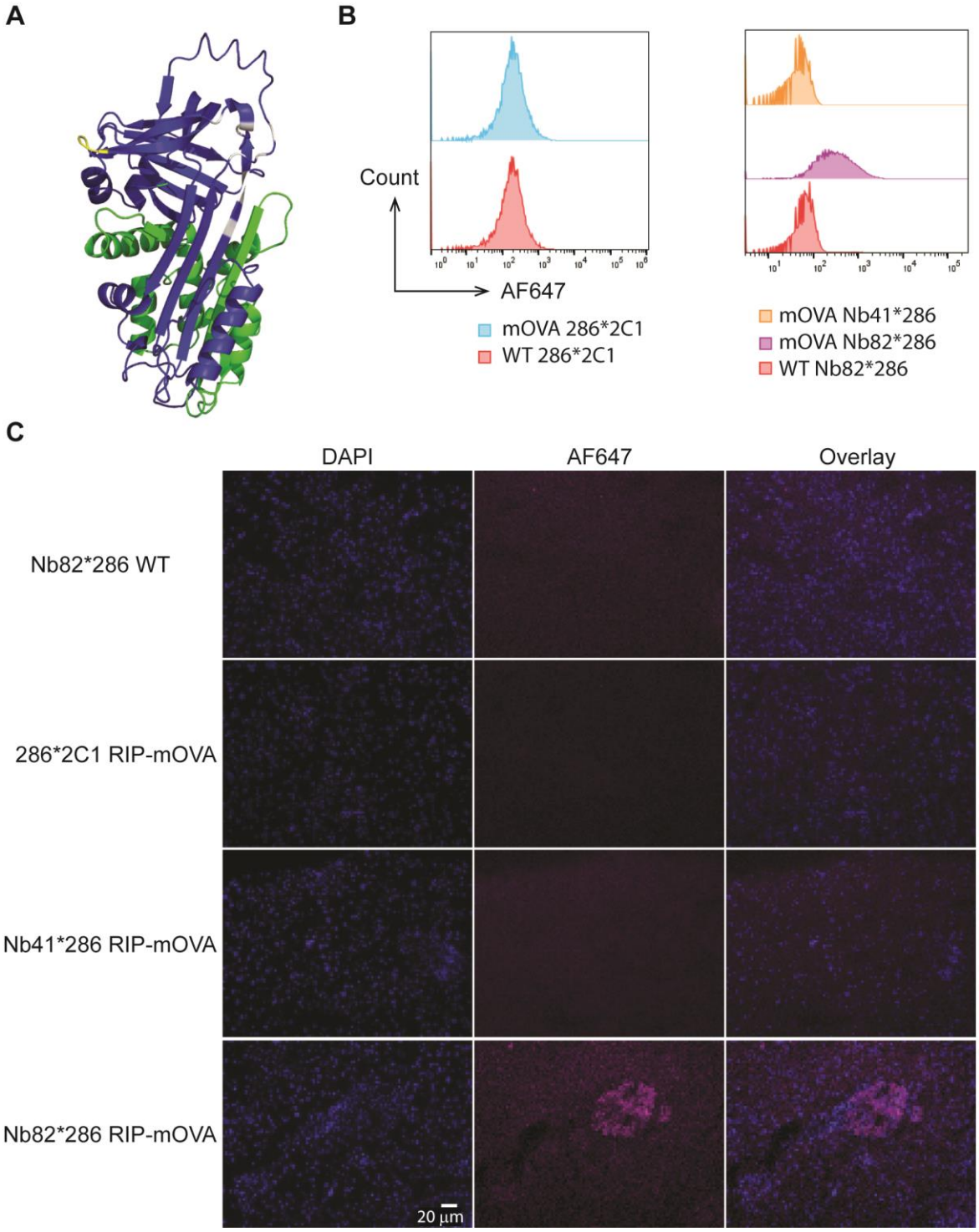


Figure 4.5. Antibody and nanobody binding of mOVA. (A) Crystal structure of OVA with residues present in mOVA (*blue*) and those removed in mOVA (*green)* (PDB: 1OVA). Additionally, putative binding sites for anti-OVA antibodies 3D7 (*white*) and 2C1 (*yellow*) (267). (B) Binding of AF647 labelled antibodies to EL4 cells (WT) and EL4 cells expressing mOVA (mOVA). (C) Binding of AF647 labelled antibodies to cryosections of RIP-mOVA pancreas sections.

4.3 hBTLA, hPD-1 and hTIGIT agonists in the OT-I RIP-mOVA mouse model

The pilot experiment established that the transfer of $2x10^6$ OT-I T-cells into the RIP-mOVA mice was sufficient to produce significant pancreatic infiltration. This model was next used for investigating the treatment of OT-I RIP-mOVA diabetic mice with inhibitory immunoreceptor agonist antibodies against hBTLA, hPD-1 and hTIGIT as well as the hBTLA/OVA bispecific, Nb82*286. The hBTLA agonist was 286, the hPD-1 agonist Cl.19 and the hTIGIT agonist CE10. These antibodies had previously been identified by the Davis laboratory as promising candidate agonists. Alongside these antibodies the isotype-control antibody, MOPC21, was used.

For these experiments the humanised inhibitory immunoreceptor receptor knock-in mice were crossed with OT-I mice generating hPD-1/hTIGIT/OT-I and hPD-1/hBTLA/OT-I mice. TIGIT and BTLA are located close together on chromosome 16 and therefore generating crosses of these strains to produce triple-humanised mice was not possible. Thus, hTIGIT/hPD-1/OT-I or hBTLA/hPD-1/OT-I T-cells were transferred into RIP-mOVA recipients and on Day 1 200 μg of antibody was injected intraperitoneally (Fig. 4.6A). The humane endpoints were the same as in the pilot experiment. At the end of the experiment, or upon reaching a humane endpoint, islet infiltration was assessed along with an analysis of the $V\alpha2^+$ T-cell population in the mesenteric lymph nodes (MLNs) (Fig. 4.6A). The proportion of $V\alpha2^+$ T-cells in the MLNs was used as a possible indicator of inhibition, as it had previously been shown that expansion of labelled OT-I T-cells was detectable in the MLNs 60 hours after transfer in RIP-mOVA mice but not detectable in WT mice (273). However this expansion in the MLNs was not observed in all earlier work (266).

In these experiments no mice lost more than 15% of their initial weight, and so mice were humanely sacrificed only because they tested positive for glycosuria. No experimental group had more than a ~5% body weight change (Fig. 4.6B). Unexpectedly, mice treated with the

hPD-1 agonist Cl.19 developed glycosuria significantly more frequently than any other group with 10 out of 12 mice developing glycosuria within 15 days (Fig. 4.6C). All other groups had no mice test positive for glycosuria except for one mouse treated with the hTIGIT agonist CE 10 (Fig. 4.6C).

Histology scoring of islet infiltration showed that the MOPC21, Cl.19 and CE 10-treated mice had significantly higher levels of infiltrate when compared with WT recipient mice, indicating that none of these antibodies completely ameliorated islet infiltration (Fig. 4.6D). The two lowest histopathology scores in the Cl.19-treated group were from the mice which did not develop glycosuria and therefore survived until the end of the experiment (Fig. 4.6C, D).

Mice treated with 286, the hBTLA agonist, were found to have statistically indistinguishable levels of infiltrate versus WT recipient mice ($p = 0.4398$) (Fig. 4.6D). Nevertheless, nor did 286 recipient mice have a significantly lower histopathology score than those treated with isotype control, MOPC21 ($p = 0.1651$) (Fig. 4.6D). However, the 286-treated mice did have significantly reduced infiltration in comparison to the Cl.19-treated mice, which had the most pronounced infiltrate ($p = 0.0033$) (Fig. 4.6D). Taken together, 286 may have an effect on reducing islet infiltration, but further repeat experiments would be needed to confirm this observation.

The scoring for the hBTLA/OVA bispecific antibody, Nb82*286, treated mice followed the trend established for 286-treated mice, showing no significant differences to WT recipients ($p = 0.088$) or MOPC21-treated mice ($p = 0.60$) and being significantly different from Cl.19-treated mice ($p = 0.0357$) (Fig. 4.6D). The data for Nb82*286-treated mice had a greater level of variation than 286 treated mice making the data harder to interpret (Fig. 4.6D). Overall, the data for Nb82*286 treatment appeared to follow a similar pattern to 286 treatment ($p = 0.9917$), suggesting that it may be agonising hBTLA and reducing OT-I T-

cell activity (Fig. 4.6D). Again, more repeat experiments would be required to confirm this observation.

Given the similarity between the histopathological scores of the two anti-hBTLA antibody treatment groups and the fact they agonise the same receptor, the histopathological scores of 286-treated and Nb82*286-treated mice were combined to increase the statistical power of hBTLA agonism as a whole. When this combined hBTLA agonist group was compared with isotype control treated mice it was found to be significantly different ($p = 0.0165$). Therefore, hBTLA agonism was effective in reducing immune infiltration.

Data for both the hTIGIT/hPD-1/OT-I and hBTLA/hPD-1/OT-I experiments were pooled to increase the power for analysis as the Kaplan-Meier survival curves and histopathology scores of WT recipients, MOPC21-treated, and Cl.19-treated mice overlapped closely (Fig. 4.6D).

Lastly, the proportions of $CD8^+$ T-cells and $V\alpha2^+$ $CD8^+$ T-cells in MLNs were assessed by flow cytometry (Fig. 4.7A). No significant increase in the proportion of $CD8^+$ T-cells was observed between any treatment groups (Fig. 4.7B). However, the $V\alpha2^+$ TCR chain-expressing population present among the $CD8^+$ T-cells was found to be significantly larger in the Cl.19-treated mice in comparison to the WT recipient mice and the MOPC21-treated mice, revealing an expansion of mOVA binding $CD8^+$ OT-I T-cells (Fig. 4.7C). The two Cl.19 mice, which had the lowest $V\alpha2^+$ populations, were the mice that did not develop glycosuria (Fig. 4.7C). The expansion of the $V\alpha2^+$ population could therefore be due to Cl.19 treatment. Alternatively, it could be due to the $V\alpha2^+$ population being assessed at the humane end point which was at an earlier time point for most of the Cl.19-treated mice than

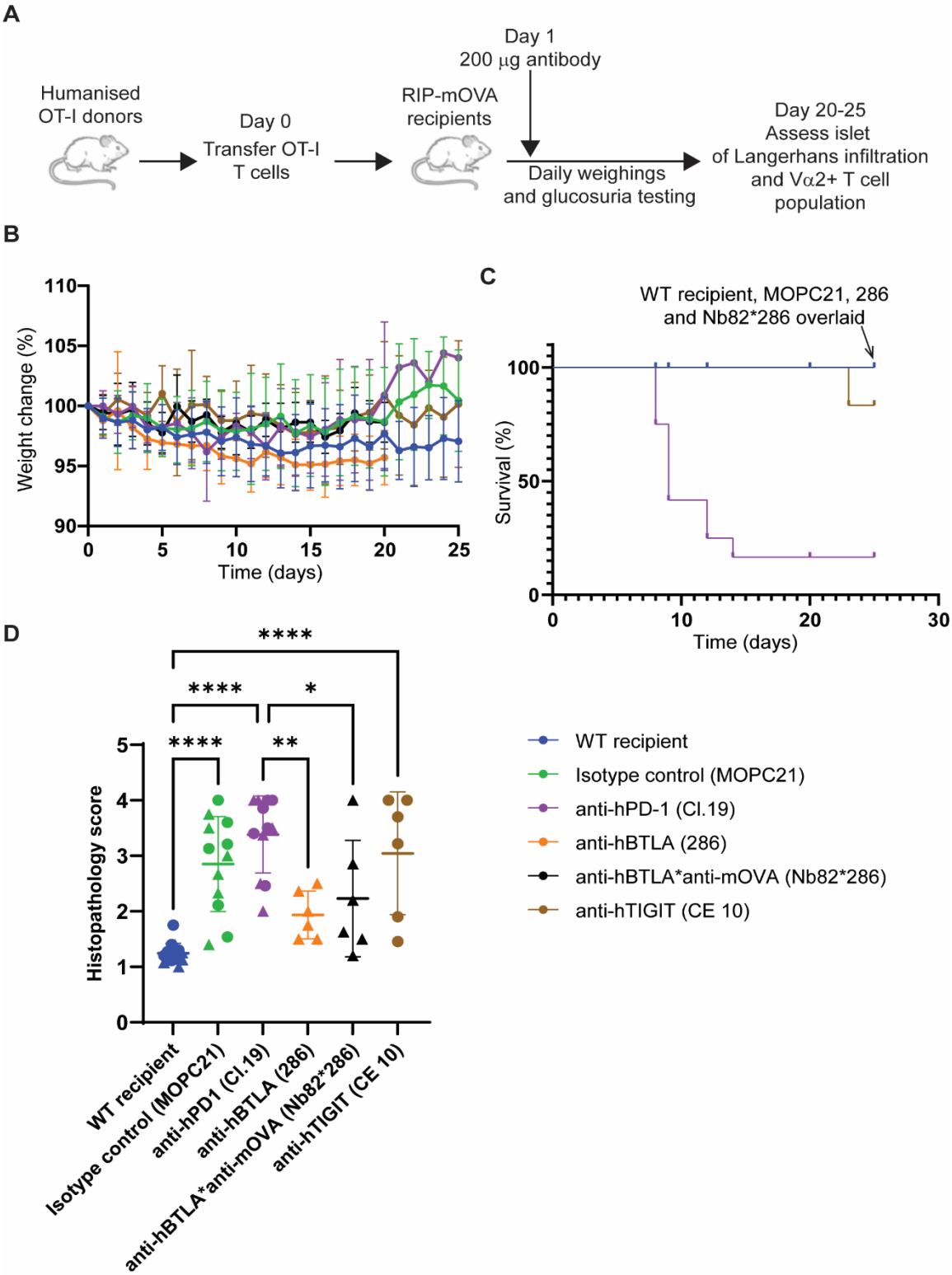


Figure 4.6. Antibody treatment of OT-I RIP-mOVA diabetes mice. (A) Experimental procedure for treatment of OT-I RIP-mOVA diabetes mice. (B) Mouse weight over time grouped by antibody treatment. (C) Kaplan Meier survival curve grouped by antibody treatment. (D) Histopathology scores of islets of Langerhans infiltration in pancreatic tissue sections. Data represent two experiments for WT recipient (n = 15), MOPC-21 (n = 12), Cl.19 (n = 12) and one experiment for 286 (n = 6), Nb82*286 (n = 6), CE 10 (n = 6). Circles and triangles represent the two experimental cohorts. Statistical analysis was performed using Tukey's multiple comparison test (* $p \leq 0.05$, ** $p \leq 0.01$, **** $p \leq 0.0001$).

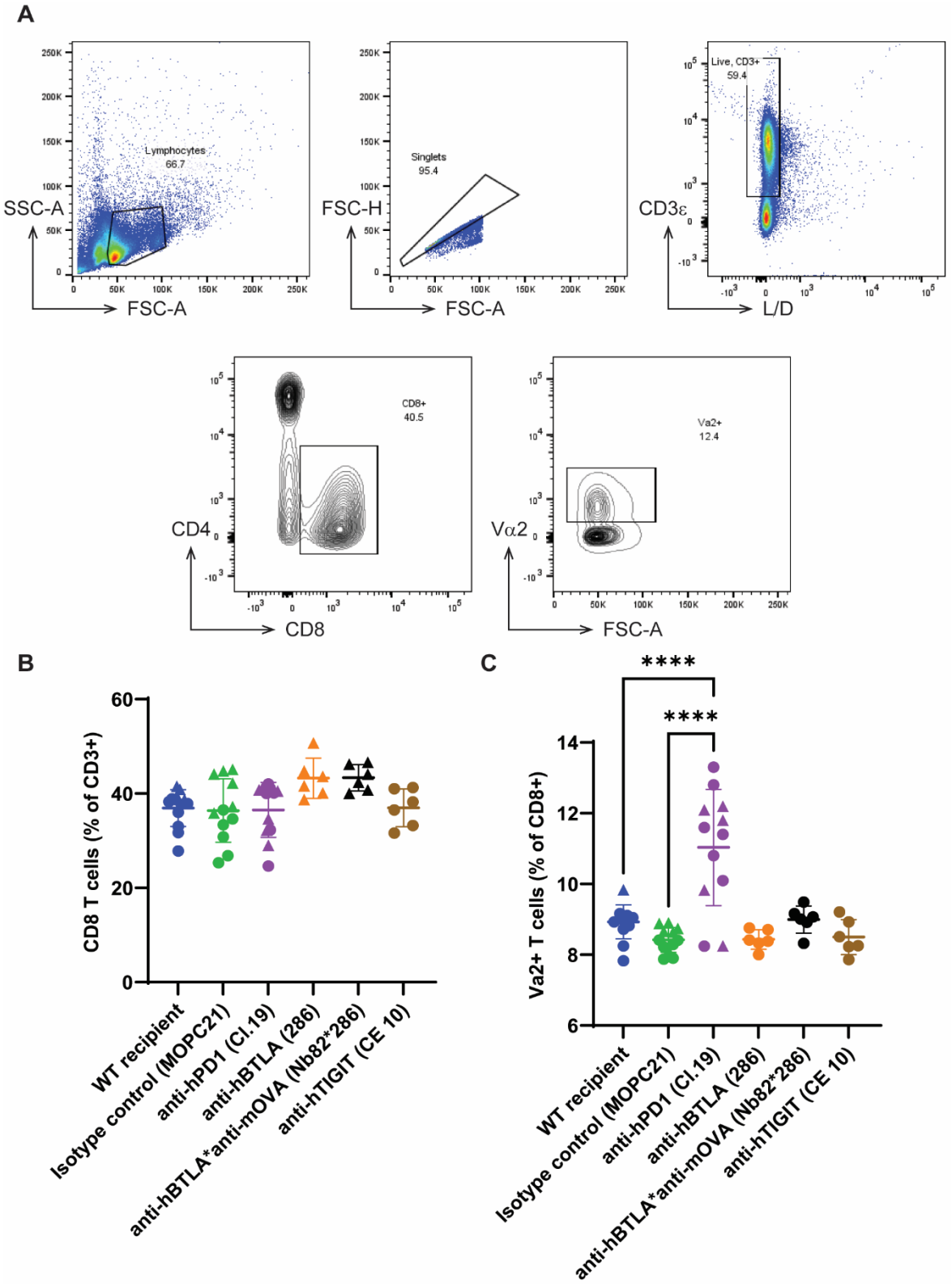


Figure 4.7. Vα2⁺ T-cell flow cytometry analysis of OT-I RIP-mOVA diabetes mice after antibody treatment. (A) Gating strategy. (B) MLN CD8⁺ T-cell population for all treatment groups as a percentage of CD3⁺ cells. (C) MLN Vα2⁺ positive T-cells as a percentage of CD8⁺ T-cells. Data represent two experiments for WT recipient (n = 15), MOPC-21 (n = 12), Cl.19 (n = 12) and one experiment for 286 (n = 6), Nb82*286 (n = 6), CE 10 (n = 6). Circles and triangles represent the two experimental cohorts. Statistical analysis was performed using Tukey's multiple comparison test (**** $p \leq 0.0001$).

for the other treatment groups. The Vα2^{+} expansion could therefore have occurred across all groups prior to Day 15 and contracted by the end of the experiments. Taken together, the results of the Cl.19 treatment suggest that agonism of hPD-1 was enhancing OT-I T-cell activity instead of suppressing it, whereas hBTLA agonism by 286 and Nb82*286 may have been suppressing OT-I T-cell activity.

4.4 OT-I T-cell expansion *in vivo* in the presence of hPD-1 and hBTLA agonists

To investigate the observed Vα2^{+} T-cell expansion in the Cl.19-treated mice as well as to investigate the suppression of OT-I T-cell expansion by the hBTLA agonist 286, the expansion of humanised and non-humanised OT-I T-cells was compared in RIP-mOVA recipients. In this experiment, CD45.2$^{+/+}$/hPD-1/hBTLA/OT-I T-cells and CD45.1$^{+/-}$/CD45.2$^{+/-}$/mPD-1/mBTLA/OT-I T-cells were co-transferred into RIP-mOVA recipients (Fig. 4.8A). Cells were labelled with cell trace violet (CTV) and mixed in a one-to-one ratio prior to intravenous injection. On Day 1 mice were injected with 200 μg of antibody and monitored until being humanely sacrificed on Day 4. The difference in CD45 isoform expression allowed for humanised and non-humanised OT-I T-cells to be distinguished by flow cytometry.

The mixed population prior to injection was found to be 50.5% CD45.2$^{+/+}$/hPD-1/hBTLA/OT-I T-cells and 49.5% CD45.1$^{+/-}$/CD45.2$^{+/-}$/mPD-1/mBTLA/OT-I, giving a ratio of humanised to non-humanised OT-I cells of 0.98 (Fig. 4.8B). As both Cl.19 and 286 bind the humanised receptors and are not cross reactive with the murine receptors, a difference in the relative expansion of the two cell subsets can be attributed to the antibody treatment when compared to the isotype control MOPC21. Suppression of humanised OT-I T-cell expansion would increase the non-humanised to humanised OT-I T-cell ratio.

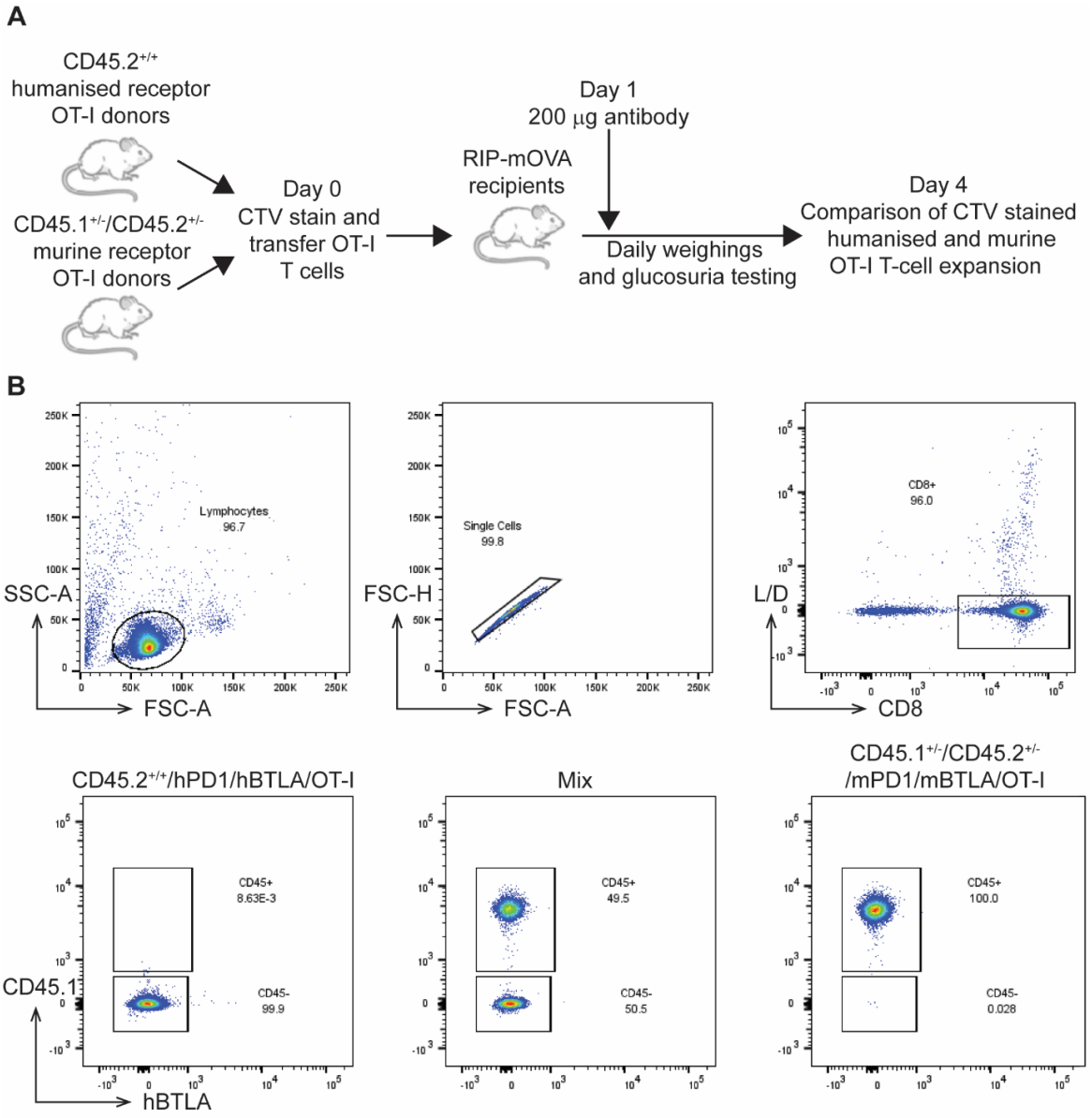


Figure 4.8. *In vivo* comparison of humanised and murine OT-I T-cell expansion in RIP-mOVA mice. (A) Experimental procedure for co-transfer of humanised and murine OT-I T-cells. (B) Flow cytometry gating strategy of CD45.2$^{+/+}$ humanised OT-I T-cells, CD45.1$^{+/-}$ /CD45.2$^{+/-}$ murine OT-I T-cells and the 1:1 mixed population used for adoptive transfer.

To identify the transferred OT-I T-cells after four days, the proportion of CD8^{+} Vα2^{+} Vβ5^{+} CTV^{+} cells in MLNs was obtained and the ratio of CD45.1/2 to CD45.2$^{+/+}$ cells was assessed by flow cytometry (Fig. 4.9A). Day 4 (~84 hours) was selected as the end point because OT-I T-cell proliferation had previously been observed to take 50 and 60 hours, and an additional day was added as antibody treatment was administered on Day 1 (273,274).

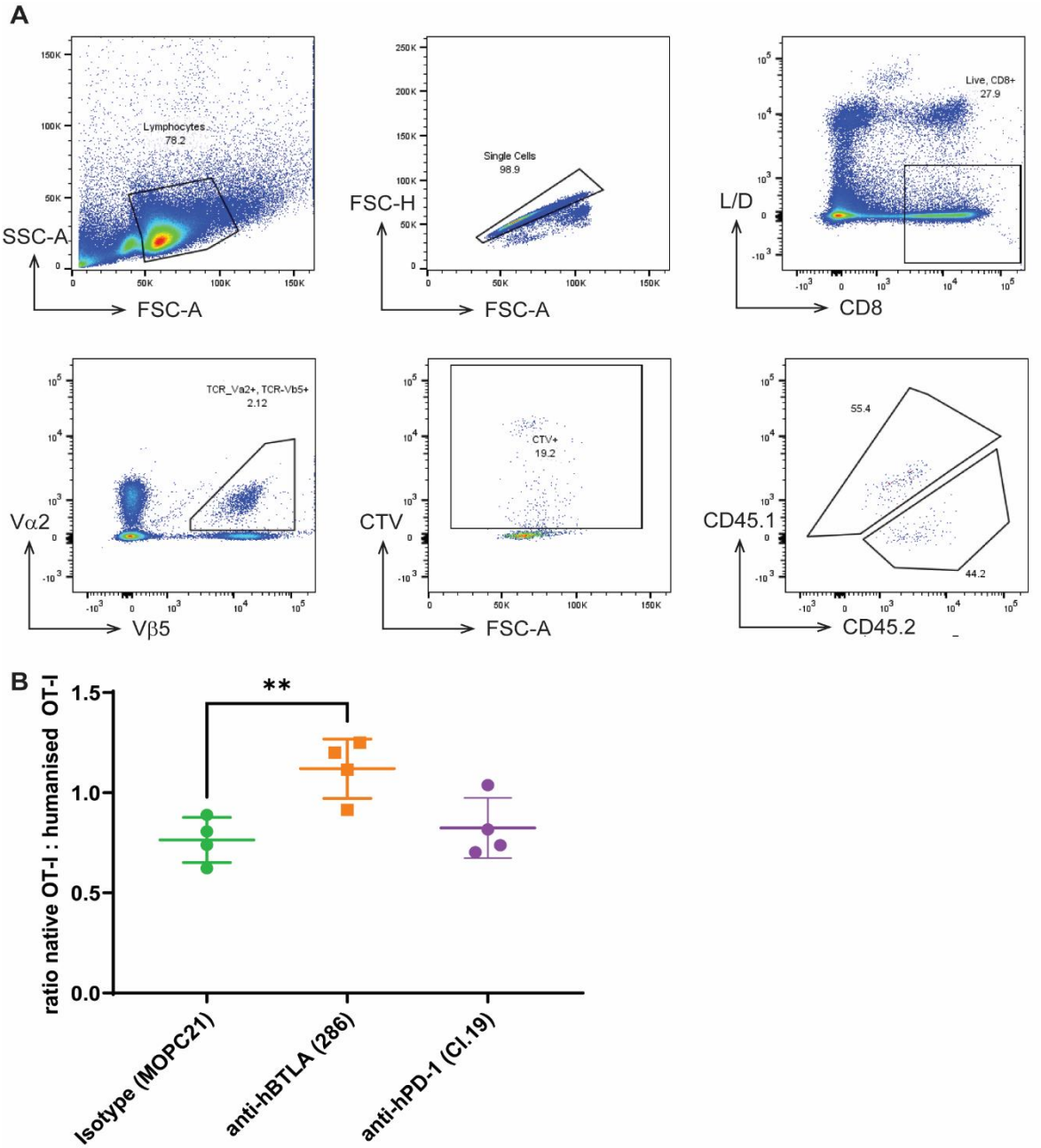


Figure 4.9. Analysis of *in vivo* comparison of humanised and native OT-I T-cell expansion in RIP-mOVA mice after four days. (A) Flow cytometry gating strategy to compare CD45.2$^{+/+}$ humanised OT-I T-cells and CD45.1$^{+/-}$/CD45.2$^{+/-}$ OT-I T-cells. (B) Ratio of CD45.1$^{+/-}$/CD45.2$^{+/-}$ OT-I T-cells to CD45.1$^{+/+}$ humanised OT-I T-cells by antibody treatment. Statistical analysis was performed using Tukey's multiple comparison test (**** $p \leq 0.0001$).

The ratio of non-humanised CD45. 1/2 to humanised CD45.2$^{+/+}$ cells was compared between the MOPC21 treatment group and those that received Cl.19 or 286 treatment (Fig. 4.9B). In the isotype group it appeared that humanised cells had proliferated more than the non-humanised cells, as the ratio at transfer was 0.98 and after four days had reduced to 0.76. Of

the two agonist antibody treatment groups, Cl.19 did not exhibit a significant difference to MOPC21 ($p = 0.7717$). However, 286 was found to have significantly increased the non-humanised to humanised OT-I T-cell ratio in comparison to MOPC21 ($p = 0.0098$) from 0.76±0.11 to 1.12±0.15, indicating that hBTLA agonism had reduced humanised OT-I T-cell proliferation (Fig. 4.9B). 286 treatment in this model thus supported the notion that hBTLA agonism was suppressing OT-I T-cell activity as suggested for the hBTLA agonists in the RIP-mOVA mouse model (see Section 3.3).

Cl.19 treatment did not increase humanised OT-I T-cell expansion in comparison to the isotype control (Fig. 4.9B). Indicating that the previously observed $V\alpha2^{+}$ T-cell expansion (Fig. 4.7C) was likely antibody independent.

4.5 Effects of other anti-hPD-1 antibodies in the OT-I RIP-mOVA model

Having observed that Cl.19 was unexpectedly enhancing OT-I T-cell activity, other hPD-1-targeting antibodies were investigated for comparison. The first of these was ANB030, also known as Rosnilimab, which was developed by AnaptysBio (282,283). ANB030 is another hPD-1 agonist which is dependent on Fc receptor engagement for agonism, like Cl.19, and is therefore believed to rely on the same signalling mechanism as Cl.19 (282). ANB030 is currently set to enter a phase two clinical trial for moderate to severe alopecia areata, an autoimmune mediated form of hair loss due to a breakdown of tolerance, with T cells being the major driver of the disease (ClinicalTrials.gov identifier: **NCT05205070)**.

The second anti-hPD-1 antibody included was a murinised version of the hPD-1 antagonist Nivolumab. This was to examine whether the effects of a bona fide PD-1 blocking antibody were similar to those observed in Cl.19-treated RIP-mOVA mice. Additionally, to remove any signalling occurring due to Nivolumab co-engagement of hPD-1 and Fc receptors a D265A mutation was included in the mIgG1 of Nivolumab (Lippert *et al.*, manuscript

submitted). Nivolumab D265A has been shown to be a more effective antagonist than Nivolumab, producing tumour suppression in the MC38 cancer model and increasing OT-II T-cell expansion in response to OVA immunisation above that achieved by Nivolumab (Fellermeyer *et al.*, unpublished, Lippert *et al.*, manuscript submitted, (284)). Therefore, both the second hPD-1 agonist antibody ANB030, and the improved hPD-1 antagonist Nivolumab D265A, were used in comparison to Cl.19.

The experimental setup was as previously described with the exception that an anti-OT-I tetramer was included in the flow cytometry panel instead of anti-Vα2 for more selective staining of OT-I T-cells (Fig. 4.6A). No treatment group experienced more than 5% weight loss from their initial starting weight, except for mice treated with Nivolumab D265A (Fig. 4.10A). All Nivolumab D265A treated mice developed glycosuria and rapidly lost condition (Fig. 4.10B). This was in contrast to the Cl.19-treated mice in previous experiments (Section 4.3), which had developed glycosuria at similar time points but maintained their condition. All other mice humanely sacrificed before the end point of the experiment at Day 22 also developed glycosuria. This included three of seven Cl.19-treated mice and three of seven ANB030-treated mice although the survival curves of both groups were not found to be significantly different from isotype control-treated mice (both $p = 0.0597$) (Fig. 4.10C).

Lastly OT-I staining of MLNs using an anti-OT-I tetramer revealed significantly expanded OT-I T-cell populations in the Nivolumab D265A-treated mice (Fig. 4.10C, D). The previously observed expansion of OT-I T-cells following Cl.19 treatment (Fig. 4.7C), however, was not observed in this experiment. Additionally, fewer Cl.19-treated mice developed glycosuria (3/7 vs 10/12). For both the Cl.19 and ANB030 treatment groups, the mice that developed glycosuria earliest also had the highest OT-I T-cell populations in the $CD8^+$ T-cell compartment (Fig. 4.10C). Overall, both hPD-1 agonist antibodies produced

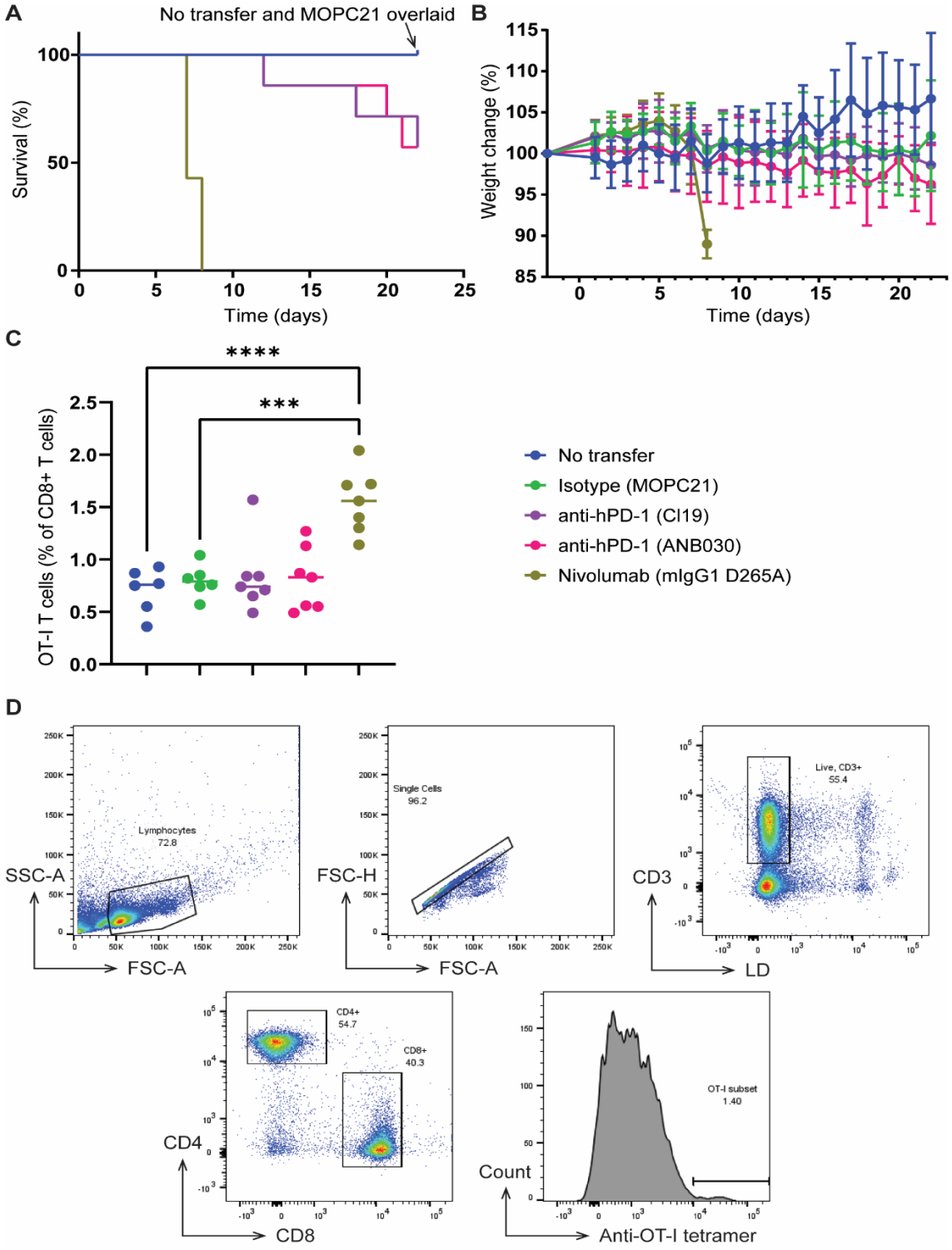


Figure 4.10. The effect of anti-hPD-1 antibodies in an autoimmune diabetes model using humanised OT-I T-cells. (A) Kaplan Meier survival curve (analysed by Log-rank test with antibody treatments compared to MOPC21, Cl.19 p = 0.0597, ANB030 p = 0.0597, Nivolumab D265A p = 0.0003) (B) Weight change of mouse weights grouped by treatment. (C) OT-I T-cell populations as a percentage of $CD8^+$ T-cells grouped by treatment (analysis by Tukey's multiple comparison test (**** $p \leq 0.0001$)). (D) Gating of OT-I T-cells using an anti-OT-I tetramer. RIP-mOVA mice not receiving an OT-I T-cell transfer (n = 6) are denoted as No transfer (*blue*). The remaining treatment groups contained the same number of mice (n = 7). This work was done in collaboration with L.Cox and C. Paluch (Mirobio, Oxford).

increased disease, although the effects just failed to reach significance. Thus, indicating that PD-1 agonism was having a net antagonistic effect and inhibiting PD-1 function.

4.6 Effects of anti-hPD-1 antibodies in a MC38 tumour model.

Nivolumab enhances T-cell activity by blocking hPD-1 and has been shown to suppress tumour growth in mice injected with MC38 tumour cells (284,285). As Cl.19 appeared to be enhancing T-cell activity in the OT-I RIP-mOVA mouse model it was next tested whether Cl.19 could suppress tumour growth in the MC38 mice. For this $0.5x10^6$ MC38 tumour cells were injected subcutaneously into hPD-1/hCD200R mice (Fig. 4.11A). On Day 7, the mice were given four doses over two weeks of 200 µg of antibody injected intraperitoneally. Tumours were measured every two days and humanely sacrificed upon the tumour volume reaching 1000 mm^3 or ulceration persisting over 48 hours.

Immune system development in hCD200R chimeric receptor mice was previously shown to be normal and immune responses to be comparable with WT mice (249). Therefore, the presence of hCD200R was not expected to influence this experiment.

Mice treated with the isotype control MOPC21 either exceeded 1000 mm^3 or developed ulcerations by day 26 (Fig. 4.11B, C). Nivolumab D265A treatment was able to completely suppress tumour growth in three of seven mice over 60 days and greatly delayed tumour growth in a fourth mouse, indicating that it was enhancing T-cell activity (Fig. 4.11B, D). Cl.19 treatment completely suppressed tumour growth for 60 days in only one of eight mice (Fig. 4.11B, E). This experiment was done in collaboration with Martin Fellermeyer who has used the same MOPC21 isotype control treatment in his own MC38 tumour model studies. Across his experiments a total of 54 mice have been treated with MOPC21 and none of these mice were able to suppress tumour growth (Fellermeyer *et al.*, unpublished data).

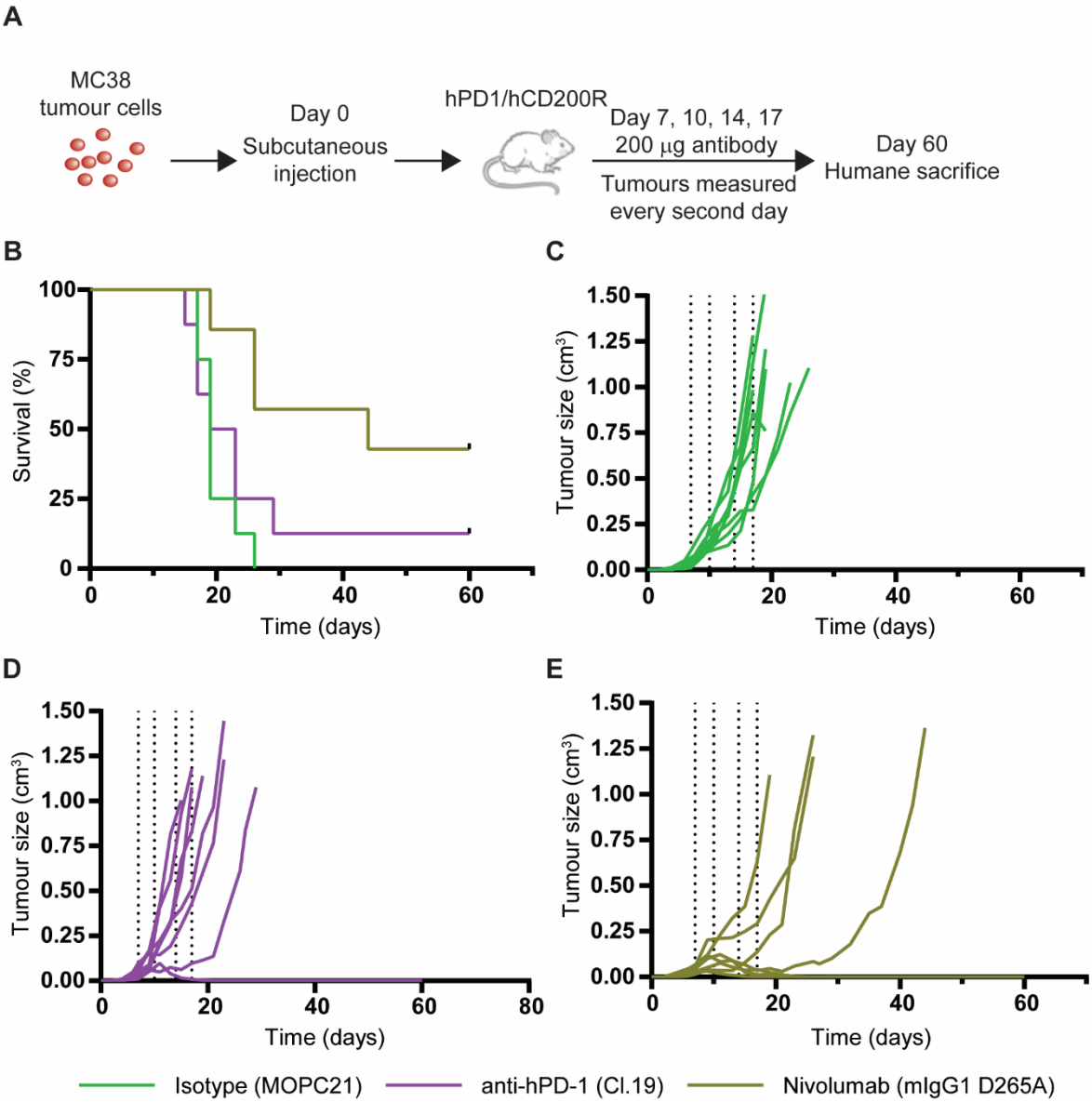


Figure 4.11. The effect of anti-hPD-1 antibodies in an MC38 tumour mouse model. (A) Experimental procedure outline for the MC38 tumour mouse model (B) Kaplan Meier survival curve (analysed by Log-rank test with antibody treatments compared to MOPC21, Cl.19 p = 0.5216, Nivolumab D265A p = 0.0026). (C) Tumour size of MOPC21-treated mice (n = 8). (D) Tumour size of Cl.19-treated mice (n = 8). (E) Tumour size of Nivolumab (mIgG1 D265A)-treated mice (n = 7). In (B-D) dotted lines indicate the antibody injection time points. This work was done in collaboration with Martin Fellermeyer (Davis Lab, Oxford).

Additionally, Nivolumab on a mIgG1 backbone only had a response rate of 20% (Fellermeyer *et al.*, unpublished data). Nevertheless, more experiments would need to be done to determine whether Cl.19 treatment had any effect in this model. It does look inferior to straightforward blocking antibodies.

4.7 Conclusion

The main aim of this chapter was to investigate whether existing inhibitory immunoreceptor agonist antibodies could suppress T-cell activity in a disease model with a known tissue antigen and whether agonism could be achieved by engaging a tissue antigen rather than Fc receptors. To this end the OT-I RIP-mOVA diabetes mouse model and inhibitory immunoreceptor agonists for hPD-1, hTIGIT and hBTLA were selected. For the Fc receptor-independent approach, the tissue antigen dependent bispecific antibody Nb82*286 was tested and shown to bind mOVA. The mOVA antigen was expected to substitute for Fc receptor engagement in close contact formation. Although it is not a native tissue antigen, it models how a tissue specific antigen could be utilised to agonise inhibitory immunoreceptors in an Fc-receptor independent manner.

The monoclonal antibodies Cl.19, which binds to hPD-1, CE 10 which binds to hTIGIT, and 286 which binds to hBTLA were investigated in the OT-I RIP-mOVA model. The time point of antibody treatment, one day after cell transfer but prior to the onset of clinical symptoms, was chosen to assess whether an ongoing immune response could be suppressed. In the cases of both the Fc-engaging antibody 286 as well as the bispecific antibody binding to hBTLA, a degree of immune suppression was observed as the immune infiltrate was reduced *in vivo* compared to the isotype control. However, the results were more variable for the bispecific construct and Nb82*286 was not produced in time to investigate its effect on proliferation in the hBTLA OT-I/mBTLA co-transfer model. Nevertheless, the RIP-mOVA model appears to be a reasonable setting within which to explore Fc receptor independent BTLA agonism.

This was not the case for CE 10 or Cl.19, which had no effect or worsened the disease outcome. As disease development could occur within seven days it is possible that greater suppression of immune infiltration could have been achieved by treating mice

prophylactically. In initial experiments, hPD-1 agonism by Cl.19 increased the occurrence of glycosuria and pancreatic immune infiltration was consistently very high. This was unexpected as PD-1 agonism was thought to inhibit OT-I T-cell activity and not enhance it. It is important to note that a subsequent experiment produced slightly different responses, with 3/7 mice developing glycosuria (vs 10/12) after Cl.19 treatment. The later experiment were performed using $CD8^+$ T-cell purification kits from different manufacturers (Miltenyi Biotec vs Biolegend) and the cells to be injected were counted by a different individual. Previous literature has suggested the model is quite sensitive to the number and purity of $CD8^+$ T-cells transferred with different groups reporting different cell counts required to achieve the same disease incidence (274,277). Therefore, it is possible that the observed discrepancy is due to the difference in purification kits and operator. Nevertheless, in all experiments, Cl.19 treatment appeared to make disease worse, and it appeared that a further PD-1 agonist ANB030 did likewise. hPD-1 blockade also increased disease incidence although the Nivolumab D265A antibody appeared to enhance OT-I T-cell activity much more than Cl.19. Antagonism through Cl.19 agonism therefore appears to be either less potent or is more delayed than direct hPD-1 blockade, or a combination of both.

To investigate the effect of inhibitory immunoreceptor agonist antibodies on OT-I cell proliferation after transfer, CTV was used to distinguish donor from recipient cells. CTV staining was sufficient to observe a difference in proliferation between humanised and murine receptor OT-I cells. However, an expansion of OT-I T-cells after Cl.19 treatment was not evident at Day 4. Longer term tracking of cells could further elucidate whether Cl.19 is affecting OT-I T-cell expansion or whether its OT-I T-cell enhancing activity is through increased effector function. To improve cell tracking it would be ideal to cross mice further to generate humanised and murine OT-I donors and RIP-mOVA recipients, which can all be distinguished by CD45 isoforms, ie. $CD45.1^{+/+}$, CD45.1/CD45.2 and $CD45.2^{+/+}$. This would

avoid any ambiguity due to loss of CTV during proliferation and allow long term tracking of transferred cells.

The use of humanised receptor mice allowed the assessment of anti-human receptor antibodies, and generated results more directly relevant to human therapeutic approaches. Two main limitations were found with this model. The first was the use of $2x10^6$ OT-I T-cells for transfer in the OT-I RIP-mOVA model. Even though this allowed detection of both enhancement of OT-I T-cell activity and inhibition thereof, the transfer of more cells may have made the effect of BTLA agonism more pronounced when compared with isotype control-treated mice, both in development of glycosuria and immune infiltrate. However, had this been the case the enhancement of OT-I T-cell activity by Cl.19 might not have been discovered. Another limitation, as referred to above, is that the OT-I RIP-mOVA model has a limited subset of cells that were potentially responsive to the treatment. The transferred cells were only enriched for $CD8^+$ T-cells and thus an effect of antibody treatment on other cell types could not be determined. The addition of $CD4^+$ OT-II T-cells alongside $CD8^+$ OT-I T-cells would allow investigation of the antibody effect on the combination of these T-cell subsets.

While mouse models cannot precisely reproduce human disease, they provide useful insight into whether the inhibitory immunoreceptor pathways can be exploited to regulate immune responses *in vivo*.

Chapter 5

Chapter 5 Bispecific agonism of the interleukin-10 receptor

5.1 Introduction

To investigate whether bipartite cytokine receptors could be triggered using a bispecific antibody the IL-10 receptor (IL-10R) was selected as a target for agonism. This choice was driven by the small size of the receptor, potentially allowing phosphatase exclusion, and the important role IL-10 has in regulating and terminating inflammation making it an attractive therapeutic target (200,286–288).

The aim is to develop an anti-IL-10R bispecific antibody capable of mimicking the action of IL-10 by bringing the IL-10R chains close together to initiate phosphorylation and signalling. Although IL-10 is a homodimer it has been shown to retain its activity in monomeric form (289). Therefore, an antibody capable of co-localising one of each receptor chain is expected to be sufficient to initiate signalling.

This chapter will discuss the characterisation of the anti-IL-10Rα and anti-IL-10Rβ antibodies as well as the signalling and *in vivo* assays used to examine their effects. Humanised IL10Rα mice, with the human extracellular domain and murine intracellular domain of IL-10Rα, have previously been generated for *in vivo* experiments. The hIL10Rα mice maintained the murine IL-10Rβ therefore the bispecific antibodies generated are anti-hIL-10Rα with anti-mIL-10Rβ.

5.2 Characterisation of anti-hIL-10Rα antibodies

To produce anti-hIL-10Rα antibodies mice had previously been immunised with the extracellular domain of hIL-10Rα to generate anti-hIL-10Rα antibodies. The immunisation, performed by the contract research organisation (CRO), BioGenes GmbH, generated eight

candidate antibodies. To select which anti-hIL-10Rα antibodies to incorporate into anti-IL-10R bispecific antibodies the eight antibodies were characterised.

5.2.1 Affinity

Using SPR the antibodies were screened for binding to 2 μM hIL-10Rα (Fig. 5.1A). Antibodies were captured using a chip coated with anti-mIgG antibody. This was to ensure candidate antibodies were oriented to maximise antigen binding. 2 μM represents a high enough concentration able to detect binding of antibodies with micromolar and stronger affinities. Of eight antibodies, four antibodies were found to bind hIL10Rα and more detailed kinetic analysis was performed on these (Fig. 5.1B, Table 5.1). All four antibodies displayed similar binding kinetics with at most a ~3-fold difference in affinity. The kinetics did not greatly differentiate the candidate antibodies.

5.2.2 Epitope mapping

To further characterise the anti-hIL-10Rα antibodies their epitopes were investigated. The epitope can significantly impact the outcome of an antibody receptor interaction. An epitope which overlaps with the ligand binding site is likely to block ligand receptor interaction inhibiting signalling. However, as the aim was to produce agonist anti-IL-10R bispecific antibodies blocking endogenous signalling was not thought to be a concern. Antibodies with membrane proximal epitopes were sought as these may produce more potent agonism by excluding receptor protein tyrosine phosphatases thus reducing receptor dephosphorylation. To identify the epitopes of the anti-hIL-10Rα antibodies, site directed mutagenesis was used to mutate 37 surface exposed residues of the membrane proximal domain of hIL-10Rα. Each

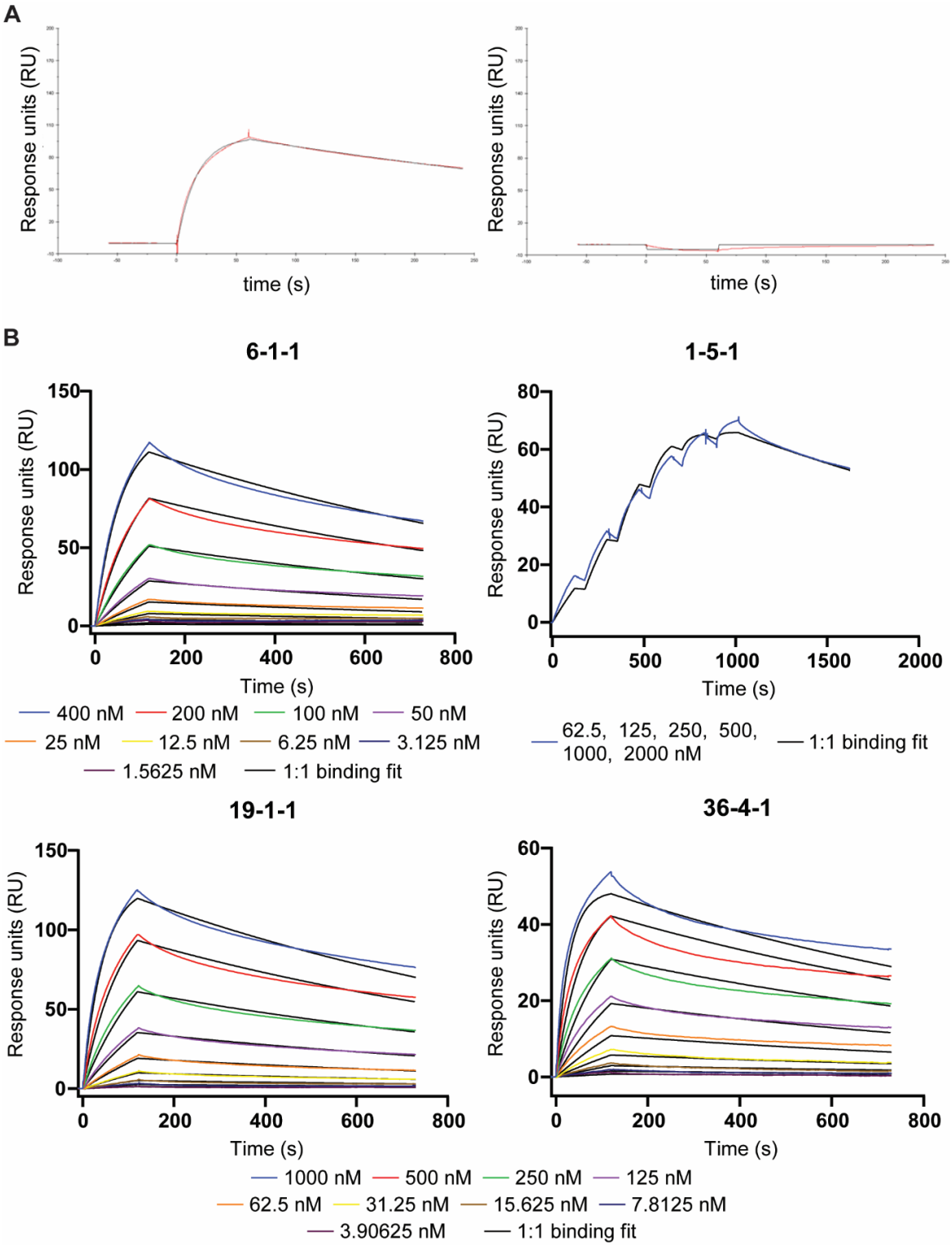


Figure 5.1 SPR analysis of anti-hIL-10Rα antibodies binding to hIL-10Rα. Candidate anti-hIL-10Rα antibodies were captured onto the sensor chip. (A) Screening for binding to 2 μM hIL-10Rα. Representative examples of a binder, 6-1-1 (left) and a non-binder, 28-9-1 (right). (B) Multi-cycle SPR, using an increasing concentration of hIL-10Rα was used to measure the kinetics of the anti-hIL-10Rα / hIL10Rα interaction. Curves were fitted with a 1:1 binding fit (*red* for A and B, *black* for C).

Table 5.1 Binding kinetics of anti-hIL-10Rα antibodies to hIL-10Rα

Antibody	k_{on} ± SD ($M^{-1}s^{-1}$)	k_{off} ± SD (s^{-1})	K_d ± SD (nM)
6-1-1	2.24±0.45 x10^4	5.62±4.37 x10^{-4}	23.8±13.4
1-5-1	2.72±0.04 x10^4	3.60±1.23 x10^{-4}	13.3±0.5
19-1-1	2.11±0.85 x10^4	8.69±0.17 x10^{-4}	41.2±0.9
36-4-1	3.49±0.57 x10^4	13.1±6.71 x10^{-4}	37.3±18.6

Measurements performed at 25°C.

mutant receptor was expressed with an intracellular green fluorescent protein (GFP) tag on the surface of HEK293T cells. GFP tagged wild type receptor-expressing HEK293T cells were also produced. The receptor cell lines were stained with each anti-hIL-10Rα antibody followed by a fluorescently labelled secondary antibody. Antibody binding to the mutant receptors was assessed by normalising the staining (geometric mean) of mutant receptor cells to that of the wild-type (WT) receptor cells (Fig. 5.2A, Table 5.2). The GFP tag was used to ensure comparison of only the successfully transfected cells (Fig. 5.2A). Residues which greatly reduced binding in comparison to WT (< 20%) and clustered together were the suggested epitope.

The binding of the antibodies, 1-5-1 and 6-1-1, was greatly reduced for the same mutants (amino acids E147, E137, W197 and E200) and therefore these antibodies are suggested to share a similar membrane proximal epitope (Fig. 5.2B, Table 5.2). 19-1-1 followed a similar binding trend to 1-5-1 and 6-1-1, with reduced binding to E147, E137, W197 and E200 but the binding of this antibody was not greatly reduced by any mutations, and it exhibited reduced binding across more mutants than 1-5-1 and 6-1-1; the location of the epitope of 19-1-1 was therefore not clear (Table 5.2). The binding of 36-4-1 was not reduced for any mutants (Table 5.2), suggesting that 36-4-1 binds the membrane distal domain, which was unmutated. Further, the binding of 36-4-1 suggested that all the mutants expressed and

folded correctly as it was able to bind all constructs. Strictly speaking, 36-4-1 could in principle bind a linear epitope, although it seems very unlikely that all of the mutated proteins would fold equally poorly.

1-5-1 and 6-1-1 were selected as lead candidates for incorporation into anti-IL-10R bispecific antibodies as they bound a membrane proximal epitope which could be clearly identified. To determine the variable domain sequences of 1-5-1 and 6-1-1 for bispecific antibody generation both were sequenced by the CRO, Absolute Antibody.

5.3 Characterisation of anti-hIL-10Rβ antibodies

Anti-mIL-10Rβ antibodies were also raised by the CRO, Biogenes GmbH. Rats were immunised with a chimaeric rat/mouse IL-10Rβ extracellular domain protein constituting the rat membrane distal domain and murine membrane proximal domain. This was done to favour the generation of antibodies which bound the membrane proximal domain.

Three candidate antibodies were screened using SPR and only the antibody 8-2-7 was found to bind (Fig. 5.3A). As there was only one binding antibody the integrity of IL-10Rβ was confirmed using a commercial monoclonal antibody against IL-10Rβ, MAB53681 (Fig. 5.3B). The binding antibody, 8-2-7, was found to have a K_d of 101 nM (Fig. 5.3C, Table 5.3). As 8-2-7 was the only mIL-10Rβ binding antibody its variable domain sequence was determined (by Absolute Antibody).

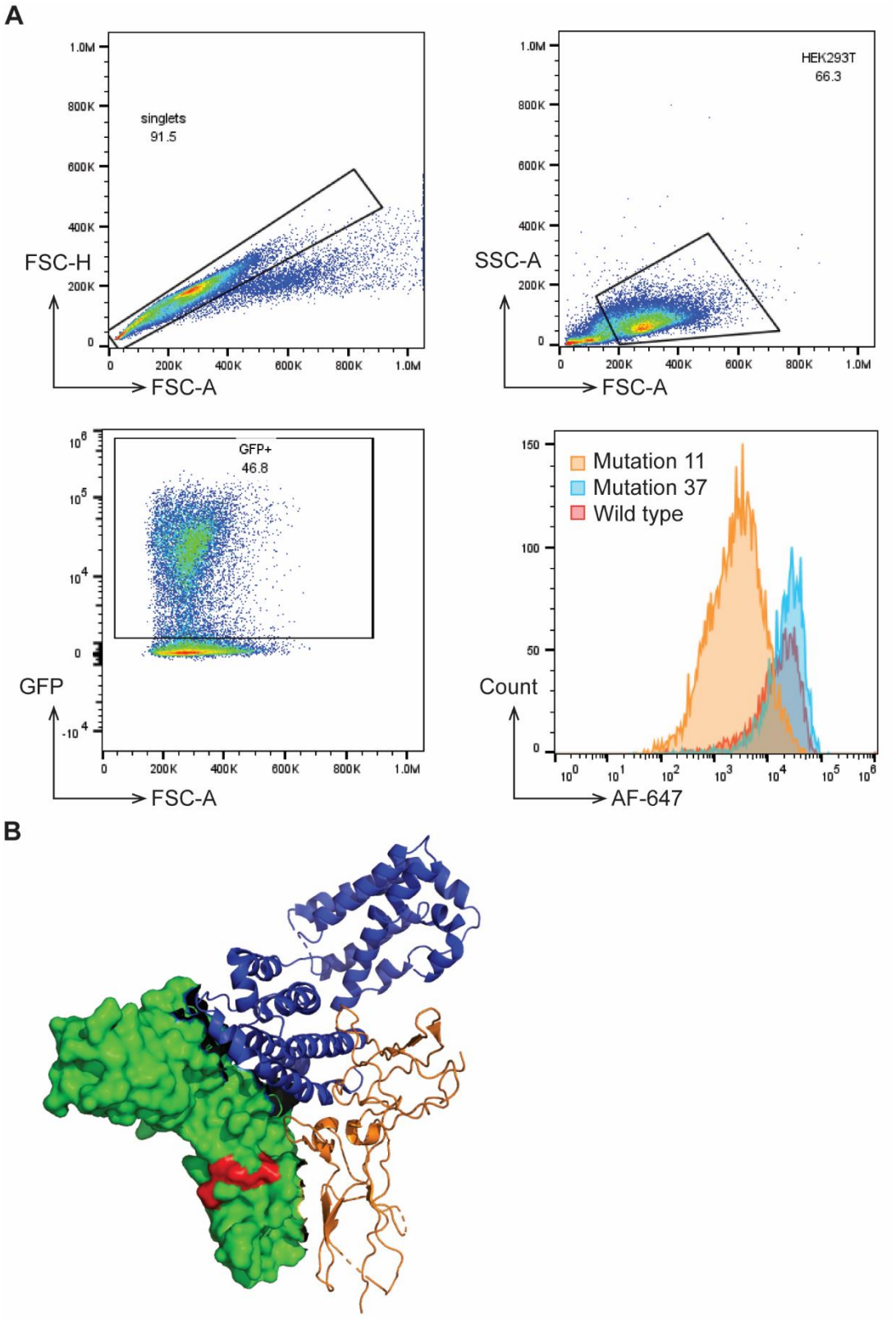


Figure 5.2 Epitope mapping of anti-hIL-10Rα antibodies. (A) Gating strategy selecting for successfully transfected cells and comparisons of the anti-hIL-10Rα antibody 6-1-1 staining of different mutant (*blue* and *orange*) and wild type (*red*) receptors (bottom right panel). (B) IL-10R crystal structure showing residues which greatly reduced binding (to <20% of wild type binding) for 6-1-1 and 1-5-1 in *red* with the IL-10Rα subunit in *green*, IL-10Rβ subunit in *orange* and IL-10 in *blue*.

Table 5.2 Percentage binding of four anti-hIL-10Rα antibodies to hIL-10Rα mutants normalised to binding of WT hIL-10Rα

Mutation	Residue	Amino acid	1-5-1	6-1-1	19-1-1	36-4-1
1	108	S	72.24645	112.7128	149.5649	284.8986
2	110	N	122.2687	228.732	97.2837	172.3647
3	112	E	84.43392	130.4744	53.12601	268.3045
4	113	I	101.3873	176.7987	102.7282	169.7261
5	115	N	66.14616	82.91367	51.00544	199.2565
6	119	L	54.29852	70.21015	82.46082	179.1475
7	123	Q	131.6672	208.696	48.13365	213.1537
8	126	R	21.08258	24.87973	27.14028	209.7564
9	142	H	45.22941	99.77868	380.5818	126.9833
10	143	F	37.73332	61.44943	199.8764	166.0659
11	147	E	6.70036	6.401324	27.80897	94.78971
12	152	K	35.64187	42.70796	88.00889	266.0187
13	154	P	34.59885	52.93882	23.55907	153.0784
14	157	F	45.92569	107.8518	84.5871	187.1022
15	132	A	86.75603	233.2111	71.47969	179.0596
16	128	K	91.99556	239.8014	95.2114	163.2844
17	129	M	49.44819	99.05335	45.13006	286.9986
18	137	E	10.47533	9.275918	25.18577	85.22724
19	138	S	61.03019	121.1385	123.1024	143.4948
20	158	T	40.03302	68.32561	75.47012	173.0425
21	160	T	40.31213	82.53161	104.7258	186.8338
22	161	H	41.64903	76.21488	52.17319	234.6519
23	162	K	93.21997	248.8508	78.8253	172.8384
24	165	K	23.03916	40.06934	30.97294	573.7522
25	166	H	79.25935	126.5021	152.5147	94.08497
26	170	S	88.02993	128.9009	106.7208	128.9352
27	172	L	73.97757	149.7616	107.3196	168.3069
28	174	S	79.42202	157.9172	93.45014	129.5472
29	189	A	73.42334	131.8677	150.5199	131.1089
30	192	S	46.73878	77.4137	351.0057	106.1154
31	194	K	33.60931	51.09283	28.14172	165.2122
32	196	M	94.42145	242.1424	212.7949	89.42966
33	197	W	7.524028	6.709217	21.39362	91.56573
34	199	K	151.7653	406.642	47.51521	208.6169
35	200	E	17.47465	17.99863	22.35963	102.4334
36	202	C	110.9784	129.3807	38.03859	122.0735
37	204	S	134.0463	279.1304	113.1778	131.7253

Residues were mutated from their WT residues, shown in the table, to arginine, except for histidine, lysine and arginine, which were mutated to aspartic acid instead. Colour gradient represents percentage of relative binding ranging from red (0) to green (≥100%).

5.4 Characterisation of anti-mIL-10Rβ nanobodies

The immunisation of rats with chimaeric rat/mouse IL-10Rβ extracellular domains had only produced one anti-mIL-10Rβ antibody, 8-2-7. As affinity and epitope could play a crucial role in determining whether a bispecific antibody is agonistic, having only one anti-IL-10Rβ was limiting. Therefore, more anti-IL-10Rβ antibodies were generated enabling the production of diverse bispecific molecules.

The small number of antibodies raised in rats was suggested to be due to the high levels of IL-10Rβ sequence homology (86%) between the two species. Therefore, the more distantly related llama was selected for immunisation with mIL-10Rβ.

An advantage of choosing llamas is that camelids produce heavy chain only antibodies (HC-Abs). HC-Abs lack light chains and incorporating the variable domains of HC-Abs, *i.e.*, V_HHs, also known as nanobodies, into bispecific antibodies diminishes the need to pair cognate heavy and light chains, thereby greatly simplifying antibody isolation. Additionally, V_HHs are stable and small, ~15 kDa, and bispecific antibodies incorporating these may be able to bring receptor chains closer together or create closer contacts between cells, both of which may potentiate signalling. To immunise llamas the mIL-10Rβ extracellular domain was produced in CHO cells. A broad, diffuse band of the expected size between ~35 kDa and ~45 kDa was observed on SDS-PAGE (Fig. 5.4A). The diffuse band is thought to be due to variable glycosylation of mIL-10Rβ. mIL10-Rβ was further purified using SEC and the monomeric mIL10-Rβ fraction was pooled and used for immunisation (Fractions 12-24, Fig. 5.4B). Immunisation, initial screening of anti-mIL-10Rβ nanobodies and sequencing was done in collaboration with Jiandong Huo (R. Owens laboratory, University of Oxford).

Table 5.3 Binding kinetics of anti-mIL-10Rβ antibody to mIL-10Rβ

Antibody	k_{on} ± SD ($M^{-1}s^{-1}$)	k_{off} ± SD (s^{-1})	K_d ± SD (nM)
8-2-7	4.57±0.35 x10^3	4.59±0.51 x10^{-4}	101±10.6

Measurements performed at 25°C.

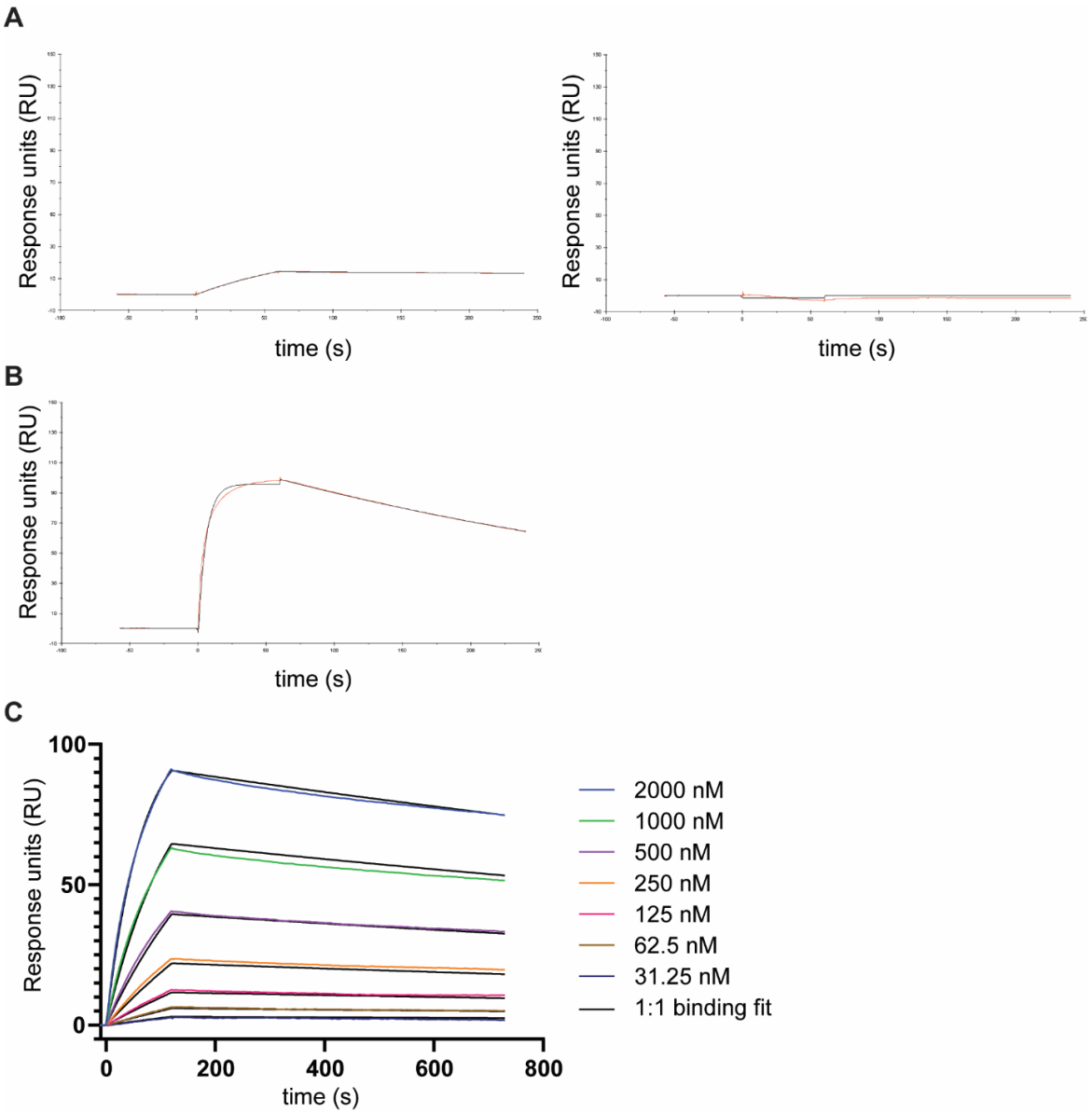


Figure 5.3 SPR analysis of anti-mIL-10Rβ antibodies binding to mIL-10Rβ. Candidate anti-mIL-10Rβ antibodies were captured onto the sensor chip. (A) Screening of antibodies 8-2-7 (*left*) and 14-2-2 (*right*) for binding to 2 μM mIL-10Rβ. (B) Binding of the mIL-10Rβ by the monoclonal antibody R&D MAB53681. (C) Multi-cycle kinetic analysis of the anti-mIL-10Rβ antibody 8-2-7. Curves were fitted with a 1:1 binding fit (*red* for A and B, *black* for C).

The first immunisation did not yield any anti-IL-10Rβ nanobodies. However, a second immunisation in a different Llama produced six nanobodies.

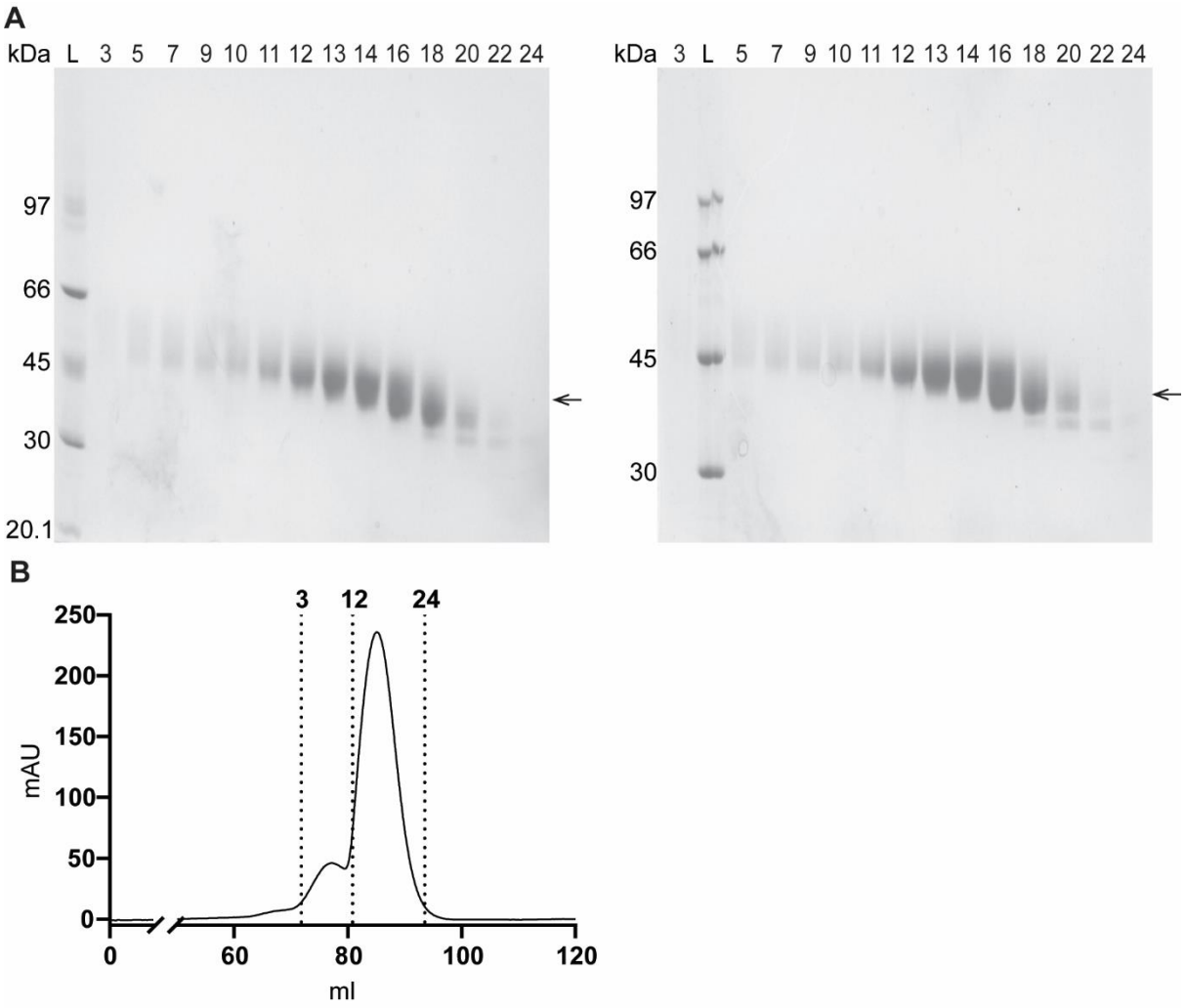


Figure 5.4 Production of the mIL-10Rβ extracellular domain. (A) Non-reducing (*left*) and reducing (*right*) SDS-PAGE of mIL-10Rβ (arrows indicate mIL-10Rβ). (B) SEC of mIL-10Rβ. Lane numbers and dotted lines on the SEC trace indicate fractions from SEC. Fractions 12-24 are the monomeric mIL10Rβ peak.

5.4.1 Affinity

The six anti-mIL-10Rβ nanobodies ran at the expected size of ~15 kDa on SDS-PAGE and were all monomeric in the SEC profile (Fig. 5.5A, B). The six nanobodies were found to have low nanomolar affinities spanning a ~20-fold affinity range (Fig. 5.6, Table 5.4). Variation in on- and off-rates was observed with Nb5 and Nb7 displaying faster kinetics, while Nb3 and Nb6 had slower kinetics (Fig. 5.6, Table 5.4).

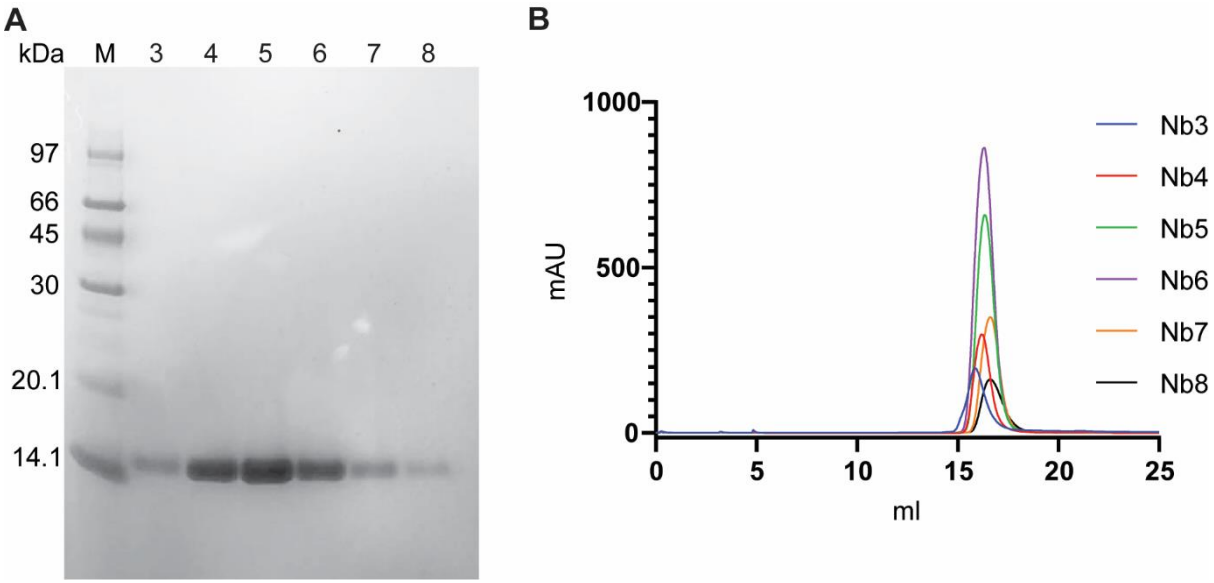


Figure 5.5 Anti-mIL-10Rβ nanobody production. (A) Non-reducing SDS-PAGE of anti-mIL-10Rβ nanobodies. (B) SEC of anti-mIL-10Rβ nanobodies.

5.4.2 Domain mapping

To determine which of the two mIL-10Rβ domains the anti-mIL-10Rβ nanobodies bound, two chimaeric human/mouse IL-10Rβs were produced (either hD1/mD2 or mD1/hD2) (Fig. 5.7A). Chimaeric IL-10Rβ was generated instead of single domains to increase the probability of producing correctly folded, stable IL-10Rβ. Nanobodies which lost binding to one of the chimaeric IL-10Rβ were suggested to bind within the domain that had been humanised. The sequence homology of the extracellular domains of hIL-10Rβ and mIL-10Rβ is 73%. Therefore, some anti-mIL-10Rβ nanobodies may retain binding to both chimaeras, binding a conserved region between the mouse and human proteins.

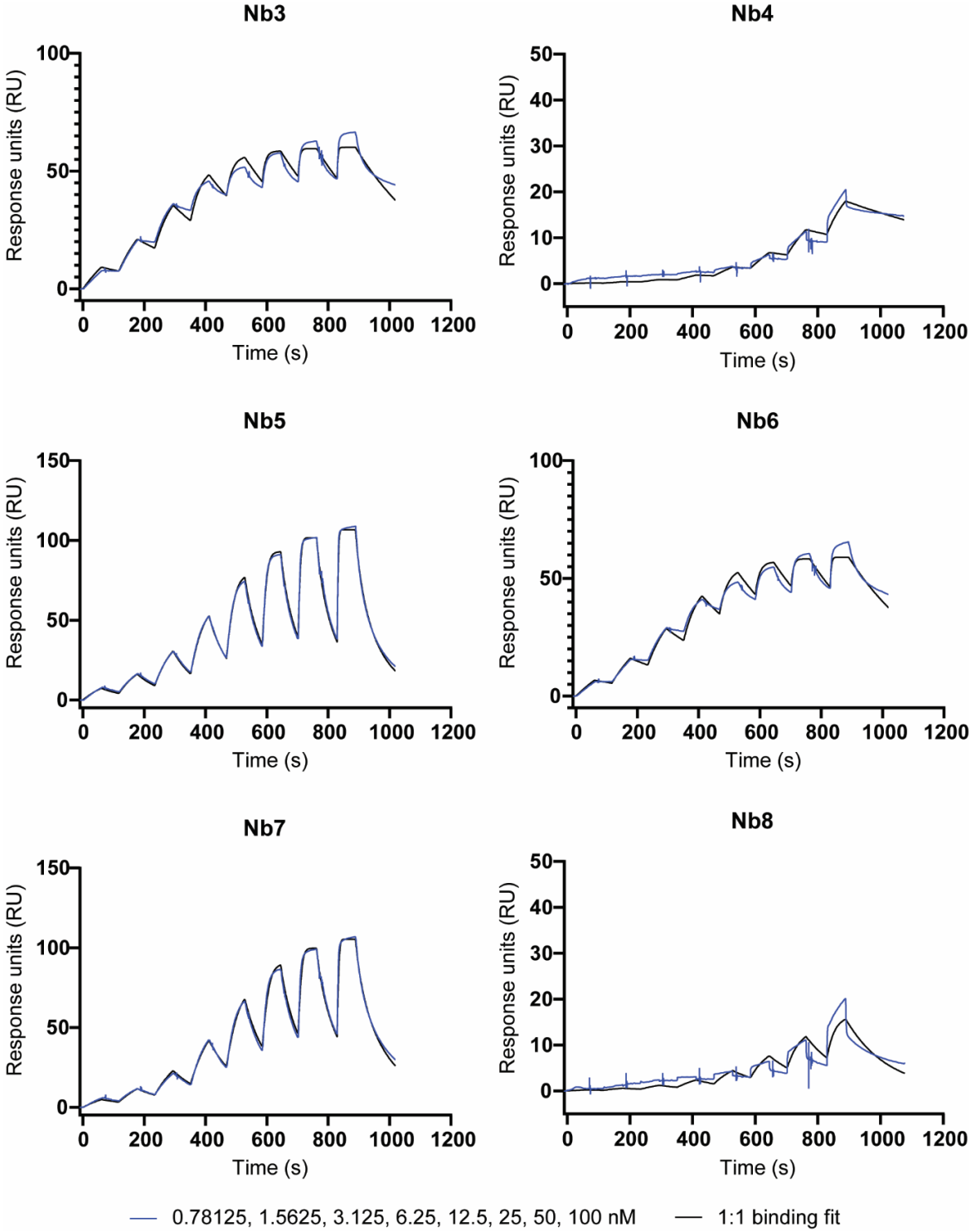


Figure 5.6 Anti-mIL-10Rβ nanobody kinetic analysis. Single cycle SPR, using an increasing concentration of nanobody (*blue*), was used to measure the binding of nanobodies to mIL-10Rβ immobilised on the sensor chip surface. Curves were fitted with a 1:1 binding fit (*black*).

Table 5.4 Kinetics for anti-mIL-10Rβ nanobody binding to mIL-10Rβ.

Antibody	k_{on} ± SD ($M^{-1}s^{-1}$)	k_{off} ± SD (s^{-1})	K_d ± SD (nM)
Nb3	33.5±8.4 x10^5	3.19±0.58 x10^{-3}	0.96±0.068
Nb4	1.30±0.14 x10^5	1.73±0.49 x10^{-3}	13.1±2.26
Nb5	53.7±0.57 x10^5	60.2±5.94 x10^{-3}	11.2±1.22
Nb6	26.1±3.11 x10^5	6.30±4.01 x10^{-3}	2.52±1.84
Nb7	44.6±9.12 x10^5	23.8±0.99 x10^{-3}	5.43±0.89
Nb8	3.77±0.50 x10^5	7.78±0.40 x10^{-3}	20.8±1.7

Measurements performed at 25°C.

The IL-10Rβ hD1/mD2 protein expressed well and showed the same broad band observed in the production of mIL-10Rβ (Fig. 5.7B). Additionally, no contaminants or aggregates were observed on SDS-PAGE, and SEC revealed negligible aggregates for IL-10Rβ hD1/mD2 (Fig. 5.7B, C). On the other hand, IL-10Rβ mD1/hD2 did not express well and while there was a broad band at the expected size of ~40 kDa there was also evidence of a large quantity of aggregate on SDS-PAGE as well as in SEC (Fig. 5.7B, C). By SEC this aggregate was removed for SPR analysis, however questions over the integrity of the IL-10Rβ mD1/hD2 remained given its poor expression and tendency to aggregate.

Anti-mIL-10Rβ nanobodies were screened for binding to both chimaeric IL-10Rβ and WT mIL-10Rβ (Fig 5.8). For this the IL-10Rβ constructs were biotinylated and captured on the SPR sensor surface using streptavidin. Nb4 and Nb8 showed dramatically reduced or loss of binding to IL-10Rβ hD1/mD2 when compared with binding to the WT mIL-10Rβ, suggesting that these nanobodies bind to the membrane distal domain, D1. Nb3, Nb5, Nb6, Nb7 all retained their binding to IL-10Rβ hD1/mD2 therefore these nanobodies either bind the membrane proximal mD2 or a conserved region in D1. All nanobodies showed reduced

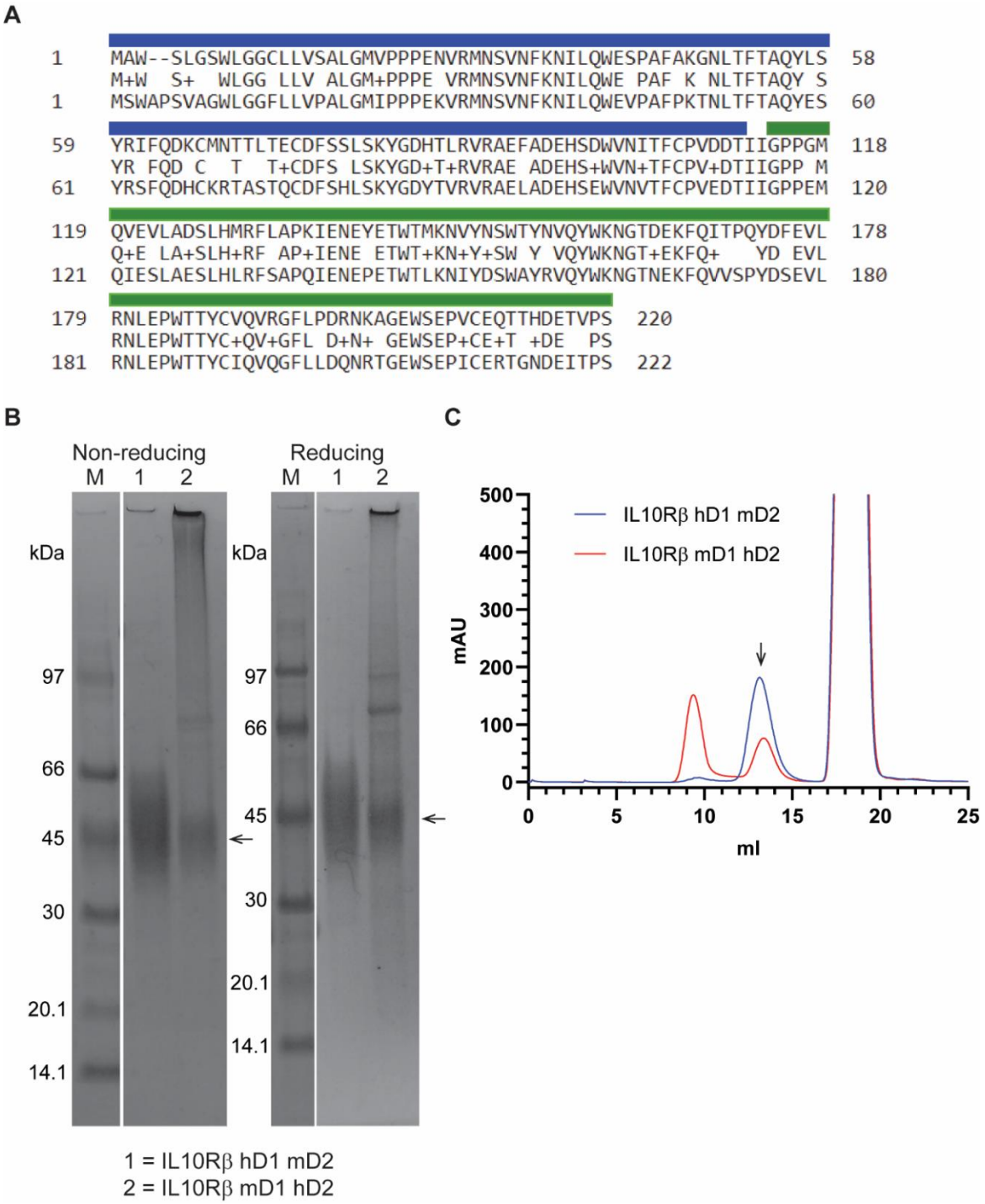


Figure 5.7 Chimaeric human/murine IL-10Rβ production. Alignment of human (*top*) and murine (*bottom*) IL-10Rβ extracellular domain 1 (*blue*) and domain 2 (*green*). (B) SDS-PAGE of the chimaeric IL-10Rβ constructs comprised of hD1/mD2 or mD1/hD2. Arrows indicate monomeric chimaeric IL-10Rβ. (C) SEC of chimaeric IL-10Rβ constructs wherein they were separated from free biotin post biotinylation. Peaks before 16 ml represent chimaeric IL-10Rβ and the 17-20 ml is free biotin. Arrows indicate the monomeric form of the receptor subunit.

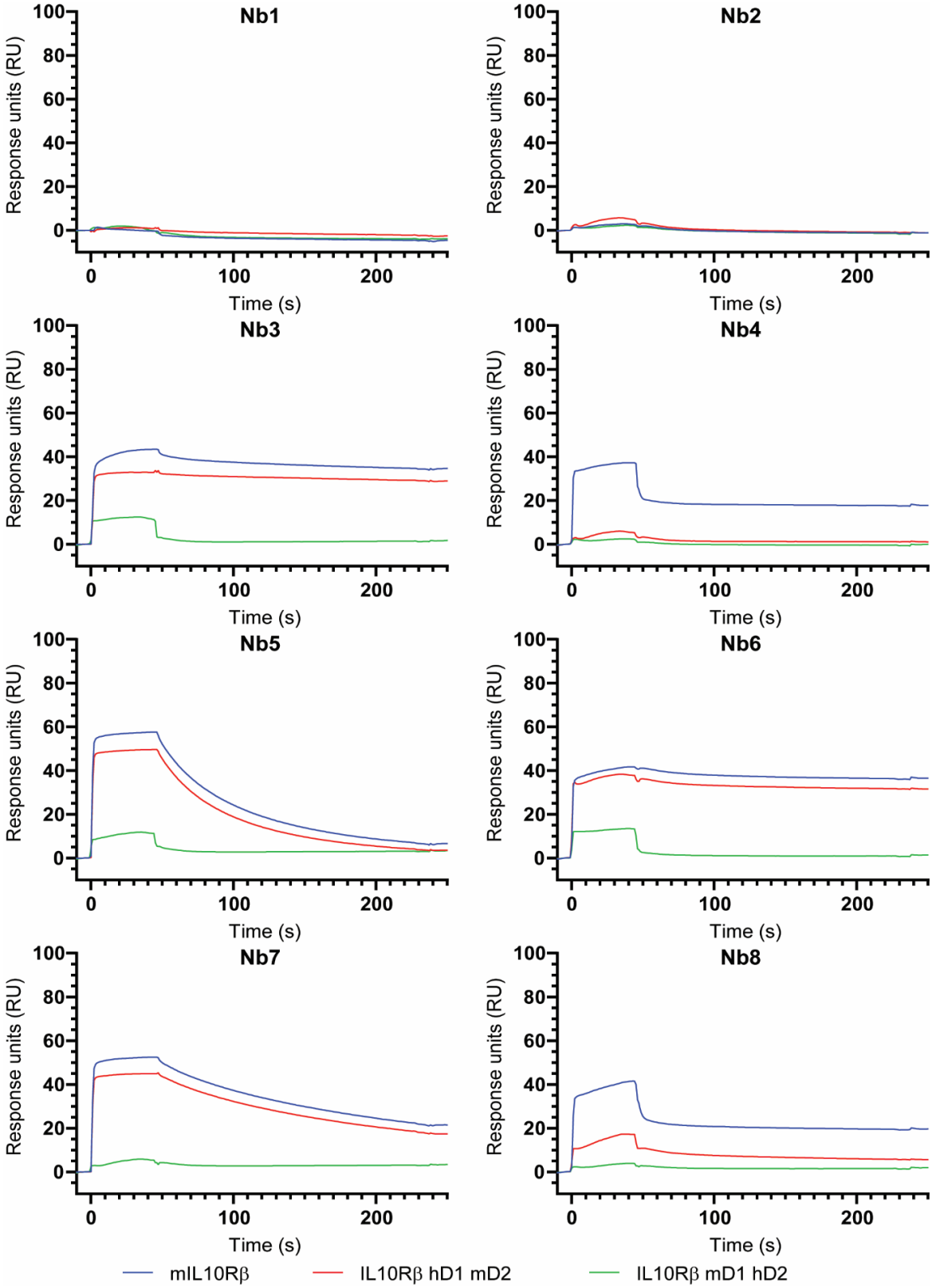


Figure 5.8 Screen of anti-mIL-10Rβ nanobody binding to chimaeric and wild-type mIL-10Rβ. ~200 RU of either WT mIL-10Rβ (*blue*), IL-10Rβ hD1/mD2 (*red*) or mD1/hD2 (*green*) were immobilised in different channels on the sensor surface. 100 nM nanobody was then screened for binding in each channel.

binding to IL-10Rβ mD1/hD2, which in combination with the poor expression and aggregation of IL-10Rβ mD1/hD2 indicates that IL-10Rβ mD1/hD2 is misfolded. The domain of binding therefore had to be based on only the comparison between nanobody binding of IL-10Rβ hD1/mD2 and WT.

Following this, Nb5 and Nb6 were selected as lead candidates. This was for three reasons. Firstly, they were among the best expressing nanobodies. Secondly, these two nanobodies had different binding kinetics with Nb5 having faster on- and off-rates and Nb6 having slower kinetics. Thirdly, both appeared to bind the membrane proximal domain of mIL-10Rβ.

5.5 *Ex vivo* IL-10 signalling assays

To investigate the anti-IL-10R antibodies, nanobodies and bispecific antibodies for their ability to agonise the IL-10R and treat disease, humanised IL-10Rα (hIL-10Rα) mice had previously been produced by the Davis and Cornall groups. These animals were engineered by replacement to express the human extracellular domains of the human IL-10Rα (Anzilotti, C, unpublished). They are described in more detail later.

5.5.1 IL-10 signalling in hIL10Rα peritoneal exudate cells

To examine whether these hIL-10Rα mice had retained their ability to signal, peritoneal exudate cells (PECs) where investigated for their ability to respond to hIL-10 and mIL-10. PECs are primarily innate immune cells such as macrophages and neutrophils and have previously been shown to be responsive to mIL-10, insofar as it inhibited their ability to produce TNFα in response to LPS *ex vivo* (290). Additionally, PECs were chosen as there are Fc receptors present that enable antibodies to potentially generate close contacts through

the interaction of cells expressing the IL-10R and others expressing Fc receptors, with the receptors interacting in trans.

The IL-10 JAK-STAT signalling pathway involves the phosphorylation of STAT3, which dimerises and functions as a transcription factor. With the use of an antibody specific to phosphorylated STAT3 it was possible to assess whether signalling was occurring using the immediate downstream signalling mediator from the IL-10R (Fig. 5.9A). hIL10Rα PECs stimulated with hIL-10 showed an increase in pSTAT3 whereas PECs stimulated with mIL-10 did not (Fig. 5.9B). The hIL-10 responsive cells were predominantly CD11b+, F4/80+ indicating they are macrophages or other innate cell subsets (Fig. 5.9A). This demonstrated that the intracellular signalling machinery had not been perturbed by the humanisation. However, the humanised receptor was no longer capable of binding mIL-10 and is therefore unable to respond to endogenous signalling.

5.5.2 Antibody agonism of the IL-10R

To investigate whether the anti-hIL-10Rα antibodies or anti-mIL-10Rβ antibodies were able to agonise the IL-10R in their monospecific form, PECs were incubated with these antibodies prior to staining for pSTAT3. The monospecific antibodies and nanobodies against hIL-10Rα or mIL-10Rβ were not expected to be agonistic, as IL-10 naturally forms heterodimeric complexes to induce signalling. Nevertheless, the ability of these antibodies and nanobodies to induce signalling was examined to exclude the possibility that they have unexpected agonistic qualities and to demonstrate that any signalling observed with the anti-IL-10R bispecific antibodies was due to their bispecific nature. None of the antibodies or nanobodies were able to stimulate the phosphorylation of STAT3 above the level of an

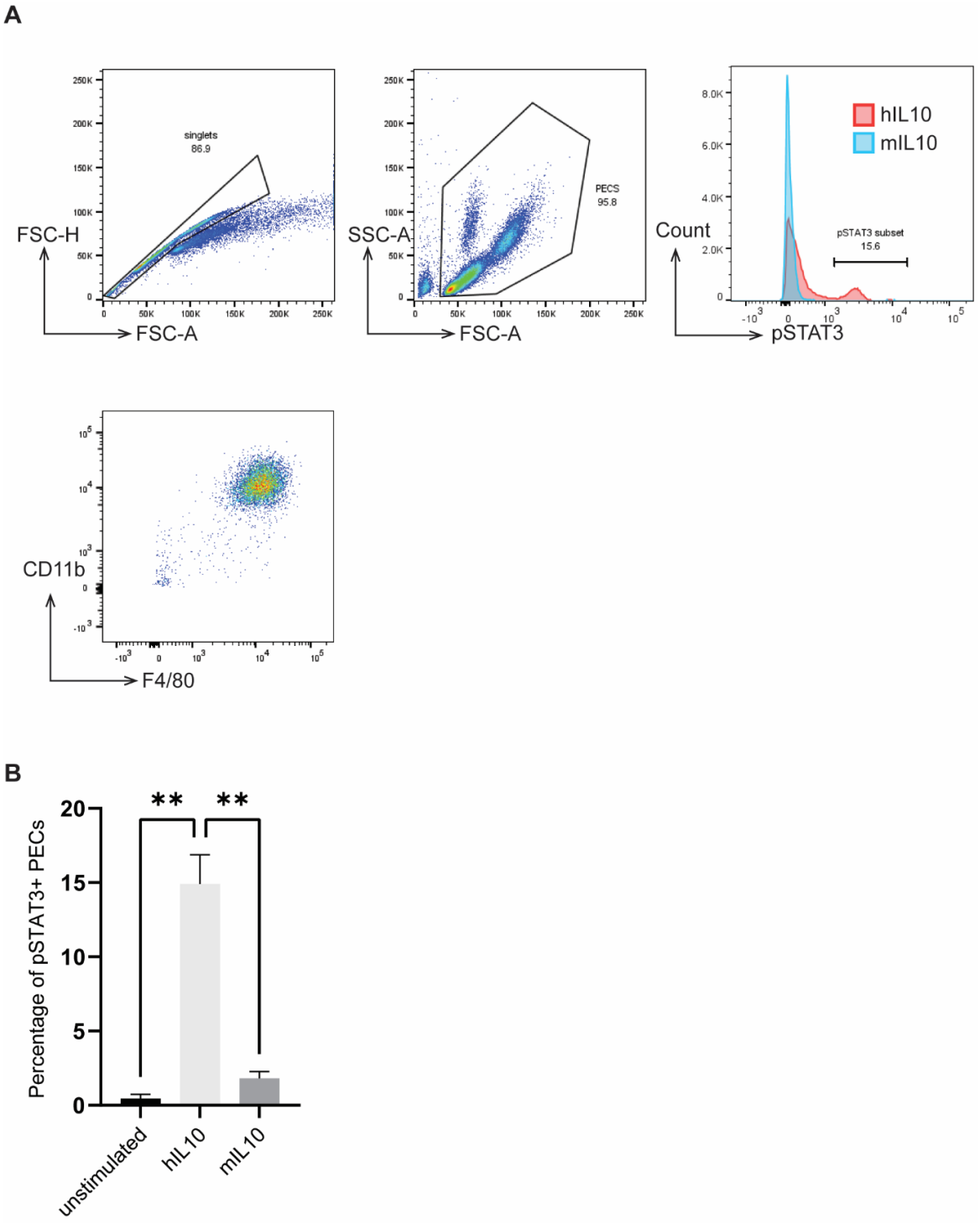


Figure 5.9 Ability of IL-10 to agonise peritoneal exudate cells from hIL10Rα mice. PECs were stimulated with IL-10 for 20 minutes prior to fixing and intracellular staining of pSTAT3. (A) Gating of pSTAT3+ PECs and plot of pSTAT3+ cells by CD11b and F4/80. (B) Percentage of pSTAT3+ PECs after stimulation with hIL-10 or mIL-10 (data analysis using Tukey's multiple comparison test (** $p \leq 0.01$)). Error bars represent standard deviation.

isotype control demonstrating their expected lack of agonistic ability (Fig. 5.10A, B). Using the same PEC assay, the anti-IL-10R bispecific antibodies Nb5*611, Nb6*611 and 827*611 (production discussed in Chapter 3), capable of binding both IL-10R chains and therefore potentially acting as agonists, were tested for induction of STAT3 phosphorylation. None of the bispecific antibodies tested were able to stimulate phosphorylation of STAT3 (Fig. 5.10C).

5.5.3 Antibody blockade of the IL-10R

Having observed that none of the antibodies were able to agonise the IL-10R their ability to block signalling was examined. This was done using the same hIL-10Rα PEC assay with four hours of antibody incubation prior to stimulation with hIL-10. All the antibodies and nanobodies tested blocked signalling to varying extents compared to the isotype control (Fig. 5.11A, B, C). Of the anti-IL-10Rα antibodies 6-1-1 showed the greatest blockade of IL-10 activity, reducing the percentage of pSTAT3+ PECs from 15.6% in the MOPC21 to 0.4%, a 97.5% reduction (Fig. 5.11A). The remaining antibody or nanobody incubated cells were also compared with MOPC21 to assess the reduction in pSTAT3+ PECs. The other anti-IL-10Rα antibodies 1-5-1, 19-1-1 and 36-4-1 reduced the percentage of pSTAT3+ PECs by 31.1%, 22.1% and 46.1%, respectively, demonstrating partial blockade of IL-10 signalling (Fig. 5.11A). The anti-IL-10Rβ antibody 8-2-7 reduced pSTAT3+ PECs by 63.8% (Fig. 5.11B), whereas the anti-IL-10Rβ nanobodies Nb4 and Nb8 greatly reduced the percentage of pSTAT3+ PECs by 94.7% and 94.6%, respectively (Fig. 5.11B). The remaining nanobodies (Nb3, 5, 6, 7) showed less blockade reducing pSTAT3+ PECs by < 68% (Fig. 5.11B). Lastly, the bispecific antibodies against both IL-10R chains reduced the percentage

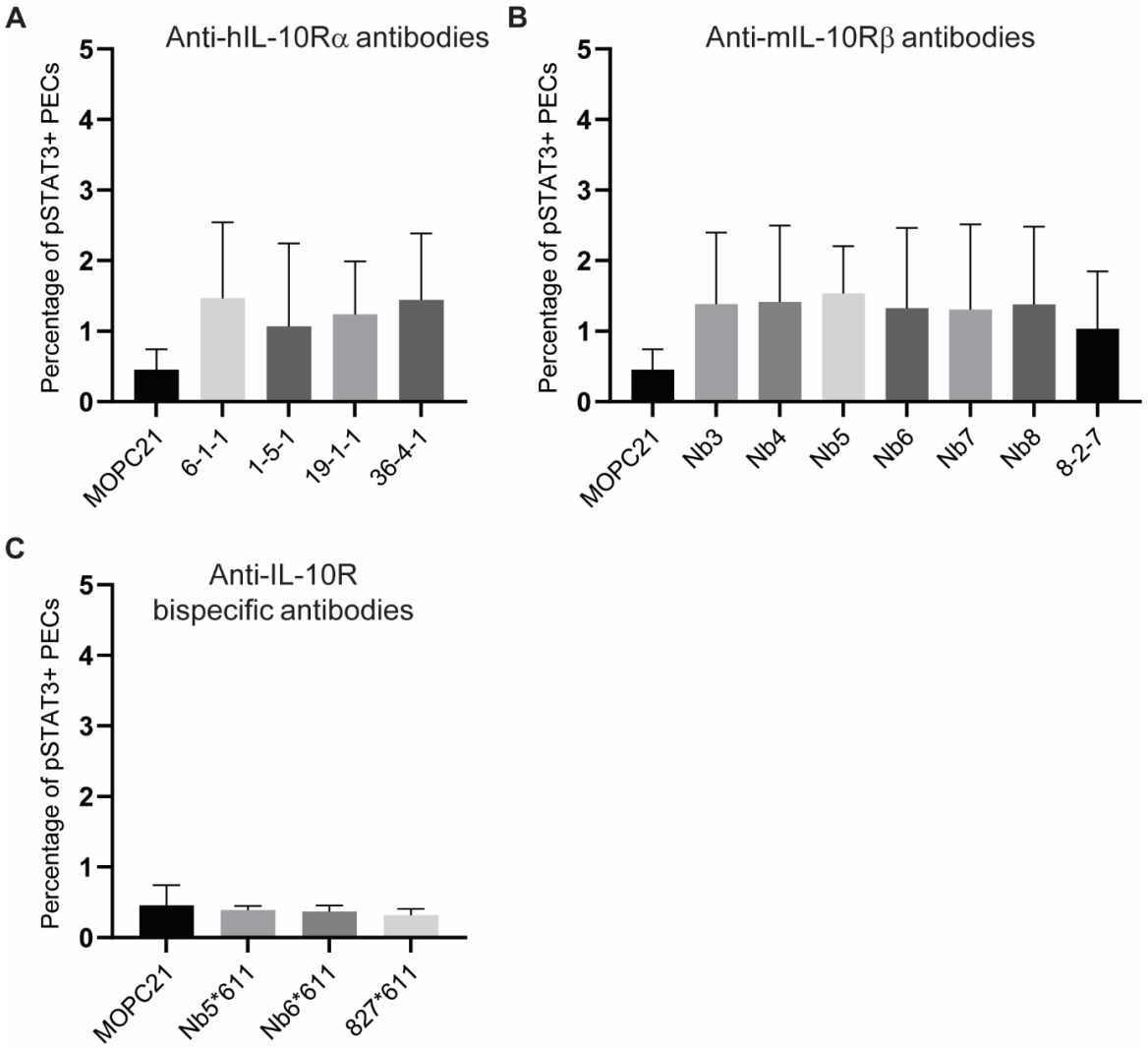


Figure 5.10 Ability of IL-10 antibodies to stimulate hIL10Rα peritoneal exudate cells. PECs were stimulated with antibody for one hour prior to fixing and intracellular staining of pSTAT3. (A) Stimulation with anti-hIL-10Rα antibodies. (B) Stimulation with anti-IL-10Rβ nanobodies and antibody. (C) Stimulation with anti-IL-10R bispecific antibodies. Data are analysed using Tukey's multiple comparison test (significance at $p \leq 0.05$). Error bars represent standard deviation.

of pSTAT3+ cells by 67.3%, 52.5% and 41.1% for Nb5*611, Nb6*611 and 827*611, respectively (Fig. 5.11C), which was significantly less inhibition than was observed for the most potent monomeric antibodies or nanobodies.

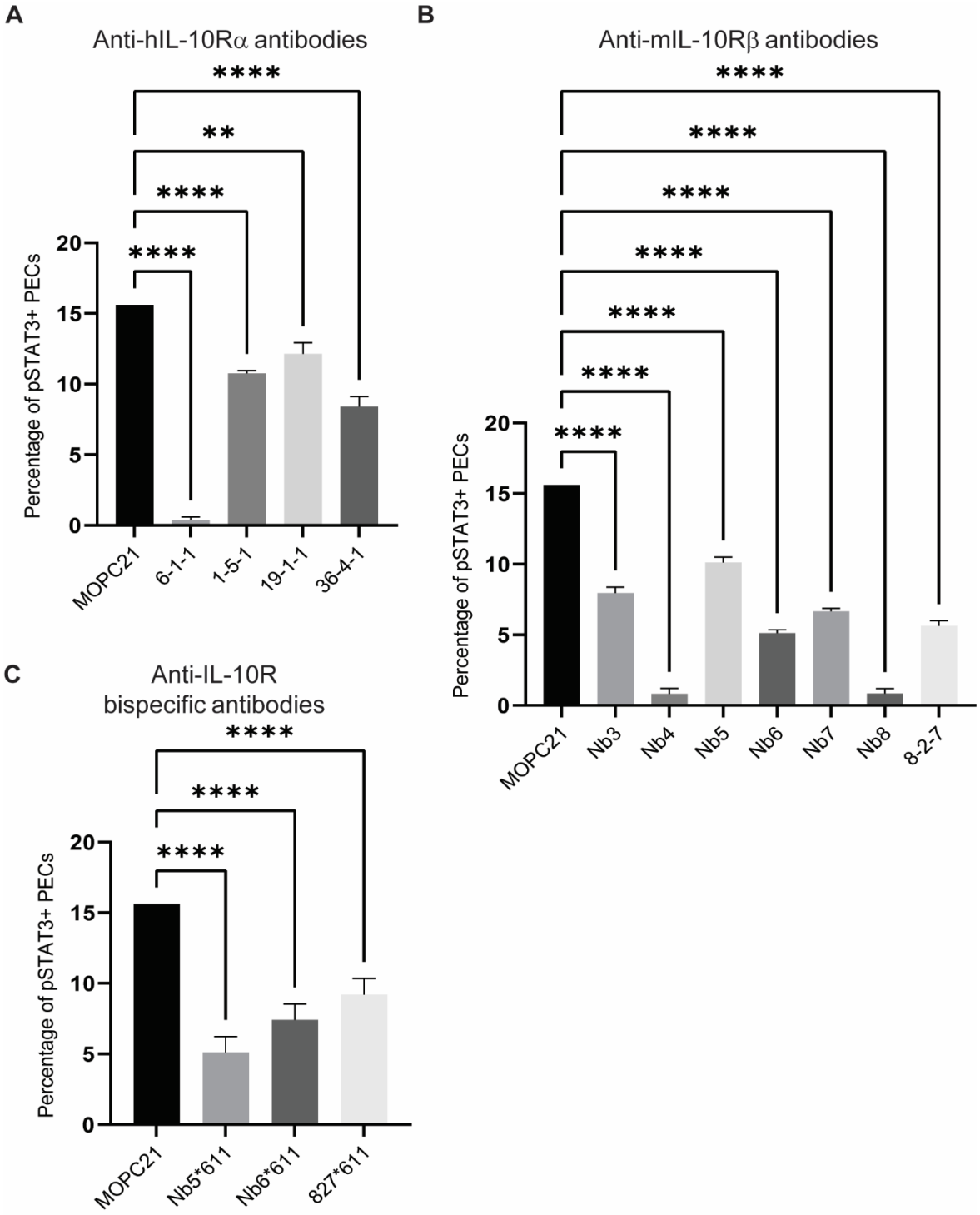


Figure 5.11 Ability of anti-IL-10 antibodies to block hIL-10 signalling in hIL10Rα PECs. PECs were incubated with (A) anti-hIL-10Rα antibodies, (B) anti-IL-10Rβ nanobodies and antibody, or (C) anti-IL-10R bispecific antibodies for four hours prior to stimulation with hIL-10 for 20 minutes. The level of phosphorylated STAT3 was subsequently determined by intracellular staining. Data are analysed using Tukey's multiple comparison test with comparisons to MOPC21 shown (* $p \leq 0.05$, ** $p \leq 0.01$, **** $p \leq 0.0001$). Error bars represent standard deviation.

5.6 Bispecific anti-IL-10R *in vivo*

In vitro studies of the agonistic potential of antibodies can provide insight into the effects on particular signalling pathways or cell types. However, *in vivo* studies are needed to provide information on their therapeutic efficacy, as *in vitro* assays cannot replicate the complex interplay between cell types and the cumulative outcome of a therapeutic when all its effects are combined. This is particularly important in the case of IL-10R agonism as it is known to be a highly pleiotropic cytokine impacting a wide range of different cell types. For these studies hIL10Rα knock-in mice had been generated.

5.6.1 hIL10Rα mouse phenotype

The inability of endogenous mIL-10 to signal in hIL10Rα-expressing cells, noted in the *in vitro* experiments, generated a phenotype consistent with the development of IBD in hIL10Rα mice. Homozygous, hIL10R$\alpha^{+/+}$, were found to have retarded growth compared to heterozygous hIL10Rα mice (Fig. 5.12A), and some developed rectal prolapses (Fig. 5.12B). Colon inflammation was assessed using colon weight: length ratios, which has previously been shown to correlate strongly with histological scoring (291). The homozygous mice had significantly greater colon weight: length ratios indicating greater inflammation (Fig. 5.12B). Additionally, when excising the colons, enlarged mesenteric lymph nodes were observed in the hIL10R$\alpha^{+/+}$ mice suggesting higher immune activity. A further sign of intestinal inflammation in the hIL10R$\alpha^{+/+}$ mice was the observation of a looser stool.

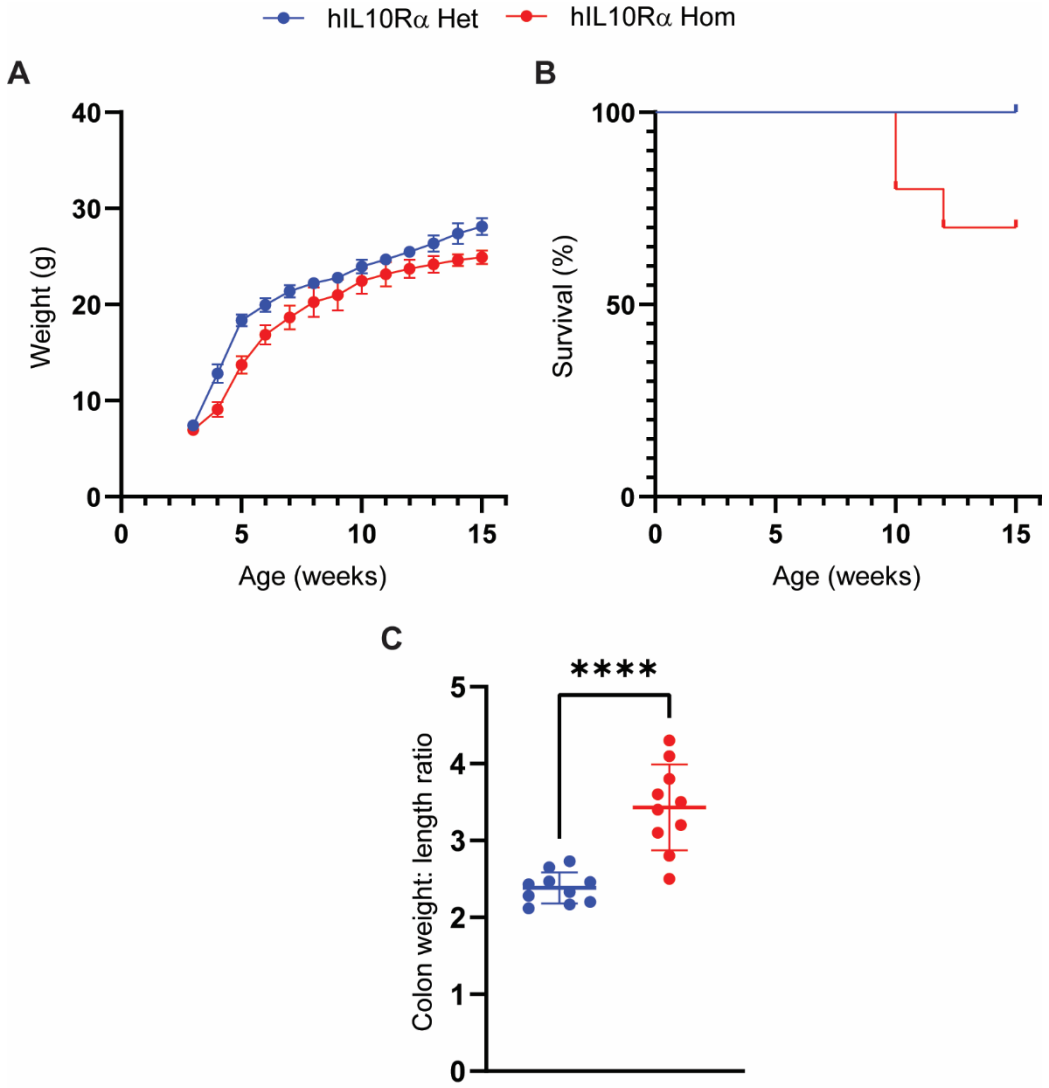


Figure 5.12 Humanised IL10Rα mouse phenotype comparison. (A) Mouse weights over time, from 3-15 weeks of age. (B) Kaplan-Meier survival curve (Log rank test, p = 0.0676). (C) Colon inflammation assessed by colon weight: length ratio (unpaired t test, p = <0.0001). The phenotype was compared between 10 female heterozygous (het, *blue*) and 10 female homozygous (hom, *red*) hIL10Rα mice. Litter- and cage-mates were used where possible.

5.6.2 Anti-IL-10R bispecific antibody tolerability in hIL10Rα mice

To establish whether the anti-IL-10R bispecific antibodies could be tolerated *in vivo,* groups of three mice, aged 14-20 weeks, were injected with 200 μg of antibody and monitored for one week. As the IL-10Rβ chain is shared with other cytokine receptors and the bispecific anti-IL-10R antibodies may block the IL-10Rβ function in these signalling pathways, there was a concern that antibody treatment might have wider ranging effects than blocking IL-

10 signalling alone. Whilst studies in IL10Rβ$^{-/-}$ mice have shown that they share the IBD phenotype with IL10Rα$^{-/-}$ mice (292), which suggests that blocking of IL-10Rβ by the bispecific antibodies would not cause additional adverse outcomes, other effects needed to be eliminated.

hIL10Rα mice treated with bispecific antibody did not appear different to isotype control treated mice upon daily visual inspection. Further, the groups of mice did not show any weight loss except for one mouse in the Nb6*611 treatment group which lost 5% of its starting weight over the seven-day period (Fig. 5.13A). After one week the mice were killed and their colon weight: length ratio was measured. Mice treated with Nb5*611 and 827*611 both had significantly higher colon weight: length ratios indicating more inflammation was occurring than for the isotype control treated mice (Fig. 5.13B).

The levels of pro-inflammatory cytokines in the serum of mice after one week were also analysed, alongside the levels in the three heterozygous hIL10Rα litter and cage mates as a reference. Cytokines typically have half-lives ranging from minutes to tens of hours so IL-10 agonism could reasonably be expected to reduce the level of pro-inflammatory cytokines over a week (293). Heterozygous hIL10Rα mice were used to assess the concentration of cytokines in healthy mice although for all but IL-6, IL12p70, IL-23 and IL27 levels in these mice were below the limit of detection (Fig. 5.14). Legendplex beads were used to assess cytokines including TNFα, IL-1β, IL-1α IL-6, IFNγ, IL-12p70, IL-17, IL-23, IL-27, MCP-1, IL-10, IFNβ, GM-CSF. No significant change was found across these cytokines between the isotype control group and any treatment group and examples are shown in Fig. 5.14.

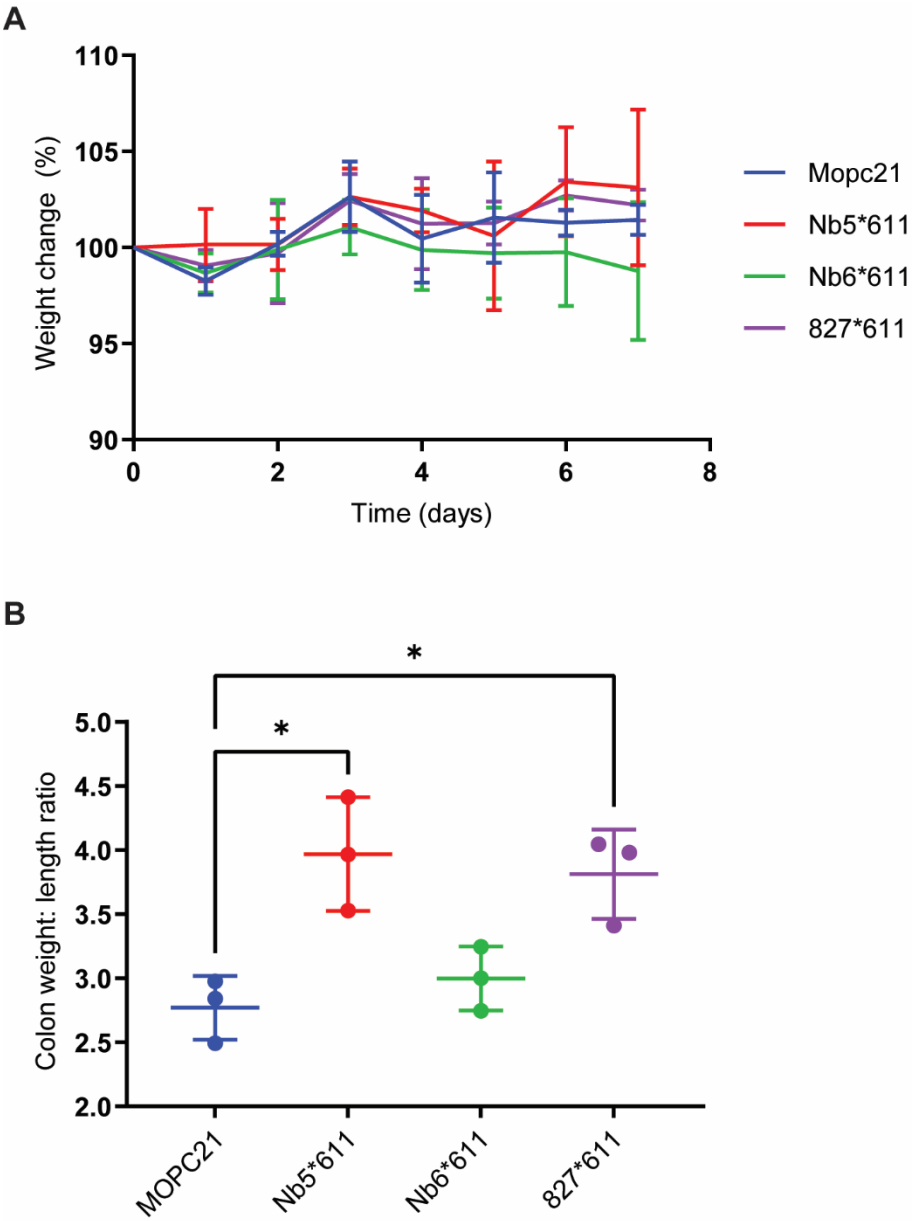


Figure 5.13 Anti-IL-10R bispecific antibody tolerability study. Groups of three mice treated with 200 μg anti-IL-10R bispecific antibody or isotype control (MOPC21) were monitored daily. (A) Weight change by group from starting weight. (B) Colon weight: length ratio of different groups. Data are analysed using Tukey's multiple comparison test (* $p \leq 0.05$). Error bars represent standard deviation.

Lastly, IL-10 is known to reduce MHC II expression on macrophages and monocytes which was examined by flow cytometry (Fig. 5.15A). The macrophage/monocyte population was identified using an approach which excluded B cells, T cells, NK cells, eosinophils, basophils, neutrophils and dendritic cells by gating for B220- CD19- CD11b+ NK1.1- CD11c- Ly6g- SSCLo cells, which has been shown to select for a mixed macrophage/mono-

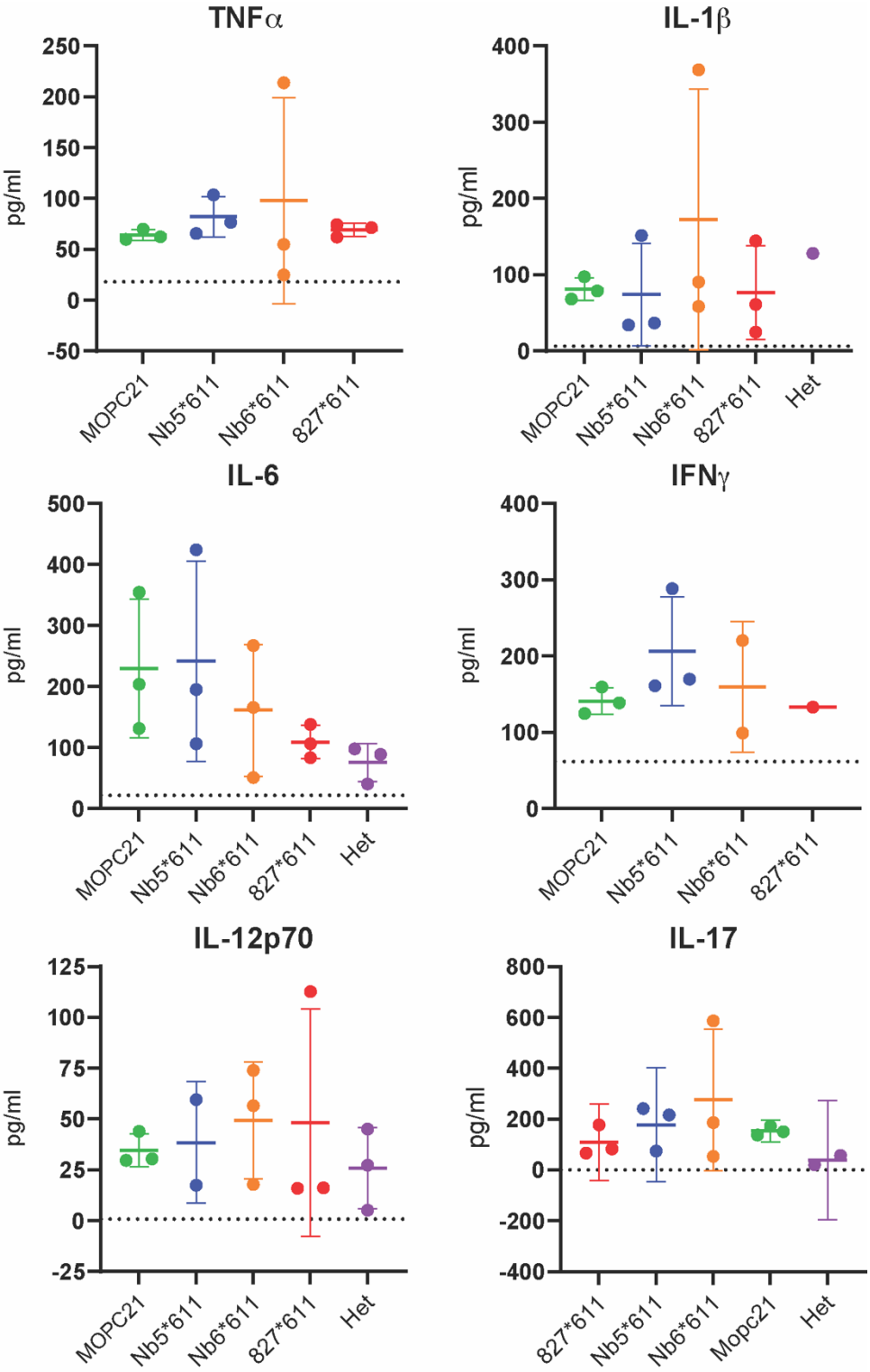


Figure 5.14 Serum cytokines in homozygous hIL10Rα mice seven days post anti-IL-10R bispecific antibody treatment and untreated heterozygous hIL10Rα mice. Levels of TNFα, IL-1β, IL-6, IFNγ, IL-12p70 and IL-17A were assessed using Legendplex beads. Groups of three homozygous mice were injected with 200 μg bispecific antibody or isotype control (MOPC21). Data points below the limit of detection (dotted line) were not included. Where no heterozygous data is present this is because the levels were below the limit of detection. Data analysed using Tukey's multiple comparison test (* $p \leq 0.05$). Error bars represent standard deviation.

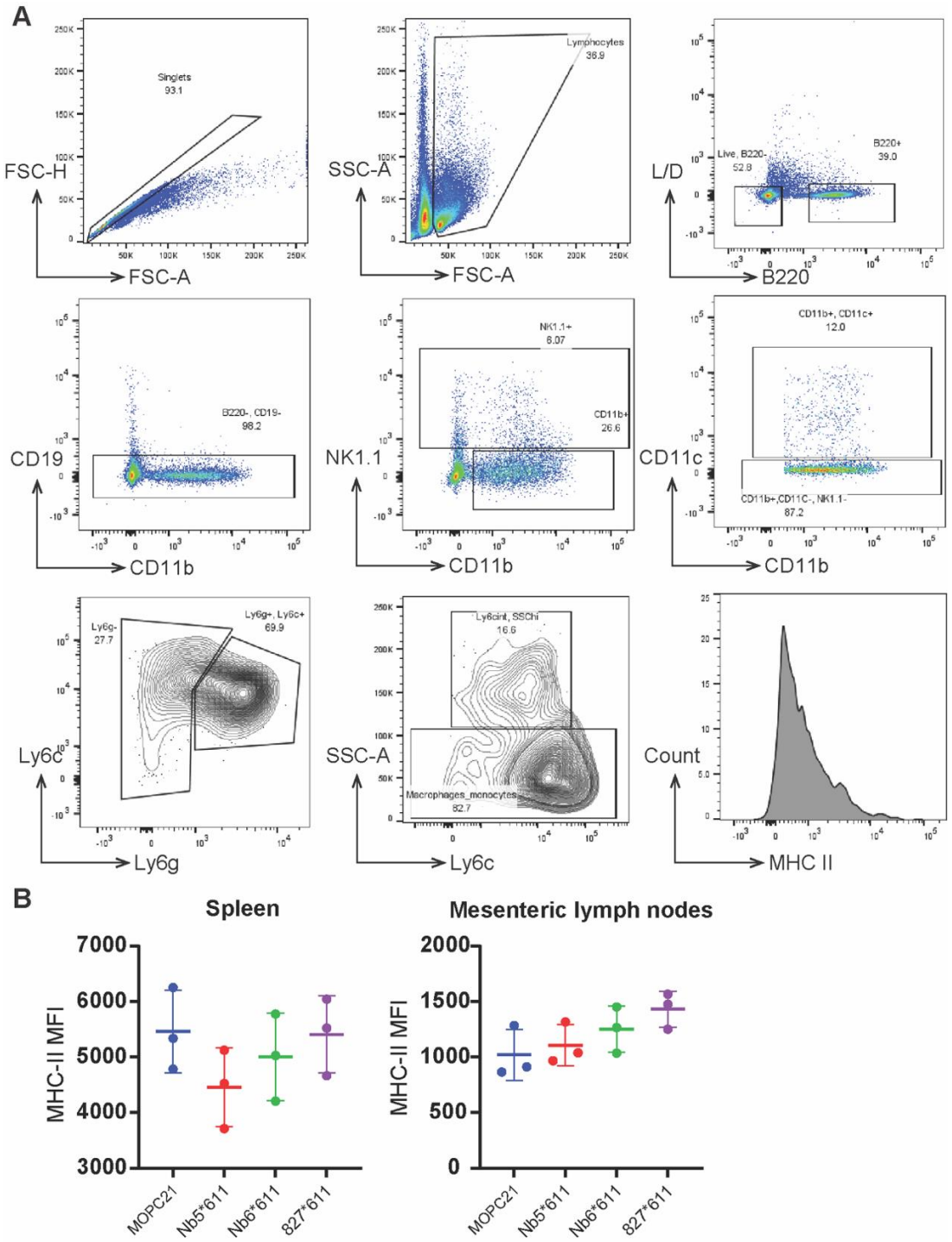


Figure 5.15 MHC II expression on mixed macrophage/monocyte populations of hIL10Rα mice treated with anti-IL-10R bispecific antibodies. Four groups of three mice were injected with 200 μg anti-IL-10R bispecific antibody and sacrificed on Day 7. (A) Gating strategy for mixed macrophage/monocyte population based on ref. (294). Panels in order top-left to bottom-right. The first four gates excluded doublets, debris, dead cells, B220+, and CD19+ cells. CD11b+, NK1.1-, CD11c- cells were gated followed by gating of Ly6g- cells. SSCHi cells were excluded and the remaining cells (B220-, CD19-, CD11b+, NK1.1-, CD11c-, Ly6g-, SSCLo) were the mixed macrophage/monocyte population whose MHC II-MFI was measured. (B) The MHC II-MFI organised by treatment group isolated from spleen or mesenteric lymph nodes. Data analysed using Tukey's multiple comparison test (* $p \leq 0.05$). Error bars represent standard deviation.

cyte population (294). No significant differences in MHC II expression were observed in the mixed macrophage/monocyte populations across treatment groups in splenocytes or mesenteric lymph node (MLN) cells. The MHC II expression in the MLN was notably higher than in splenocytes possibly due to the MLNs containing more activated monocytes and macrophages.

5.7 Discussion

In experiments described in this chapter, the affinities and epitopes of anti-IL-10Rα and anti-IL-10Rβ antibodies and nanobodies were investigated. This was to select those with favourable binding characteristics expected to induce agonism of the IL-10R when combined in a bispecific format. Antibodies were selected for membrane proximal binding and for variety in binding kinetics where possible.

The generation of anti-IL-10Rβ antibodies and nanobodies proved challenging as immunisation of rats did not produce many antibodies. Nonetheless, one of two llamas immunised with mIL-10Rβ produced six anti-IL-10Rβ nanobodies. The lack of immunogenicity of IL-10Rβ may be explained by the relatively high degree of structural similarity predicted for IL-10R, reflecting that of IL-10 (295). It should, however, be noted that just one attempt was made to produce rat anti-IL-10Rβ antibodies by conventional methods.

Two approaches were used to determine the binding locations of antibodies and nanobodies. The first used point mutations in the IL-10Rα chain to discover which mutations reduced antibody binding. The second used chimaeric IL-10Rβ to eliminate binding to one domain at a time. The first approach gives a higher resolution of the epitope whereas the chimaeras merely indicated the domain which was bound. The latter approach was used to more

quickly identify nanobodies which bound membrane proximally. While both approaches identified antibodies likely to bind membrane proximally, the detailed orientation of binding cannot be assessed with either approach. The binding orientation may be crucial as antibodies, which bind the same location, can orient in different directions and permit or prevent close interactions with other molecules. For example, this may explain the difference in the ability of the anti-IL-10Rα antibodies 1-5-1 and 6-1-1 to block IL-10 signalling *in vitro* although both bind the same epitope, which was found to be outside the IL-10Rα IL-10Rβ binding site. Anti-mIL-10Rβ nanobodies Nb4 and Nb8, both effective blockers of IL-10 signalling, were found to bind D1 and their effective blockade of IL-10 signalling supports an epitope preventing IL-10Rα IL-10 binding in D1.

These considerations likely apply to the lack of agonism observed using the bispecific antibodies. These antibodies are capable of binding both IL-10R chains simultaneously. This should allow them to co-localise both chains when binding in cis on a cell. However, colocalising both chains may not be sufficient if they are not brought into close enough proximity for their intracellular domains to interact. The proximity of the intracellular domains is dependent on the spacing of the two antibody arms and the orientation with which these antibodies bind the receptor.

The signalling potential of the bispecific antibodies was assessed using hIL10Rα mice. The humanisation of the extracellular domain of the alpha chain did not impair the signalling machinery, evident by STAT3 phosphorylation in response to hIL-10. This indicates that the lack of agonism by the bispecific antibodies is very likely an antibody-intrinsic effect, such as those discussed above, rather than an inability to detect signalling.

The hIL-10Rα mice were found to be unresponsive to mIL-10, which led to the development of an IBD phenotype in the homozygous mice. Previous work has shown that the development of IBD in IL-10 signalling knockout models is microbiome dependent (296).

The development of IBD in these mice was therefore thought to be due to a combination of the absence of IL-10 signalling and the flora present in the animal facility. Further, the phenotype development was similar to those noted by other researchers (101,297). IL-10 signalling in animal models of IBD has been shown to be effective in ameliorating disease and therefore the hIL-10Rα mice are a good candidate model for assessing the therapeutic potential of IL-10R agonists *in vivo*. Additionally, the use of a humanised extracellular domain would allow successful anti-hIL-10Rα antibodies to be carried forward to experiments on PBMCs or other human tissue.

The tolerability study showed significant differences in the colon weight: length ratios of Nb5*611- and 827*611-treated mice in comparison to isotype control treated mice. However, there was no significant differences noted in MHC-II expression or cytokine levels which have been shown to be IL-10 signalling dependent (180,298). Given the only trend was towards worsening, it was decided not to repeat the experiment on grounds of animal welfare.

Chapter 6

Chapter 6 Discussion

The work in this thesis builds on previous studies of antibody agonists targeting immune checkpoint receptors (Lippert et al., manuscript submitted; ref 1). These studies leveraged antibody cross linking of cells in an Fc receptor-dependent manner to agonise small, monomeric, immunoreceptors. To investigate whether the Fc receptor-dependence of previously developed checkpoint agonists could be circumvented by substituting binding to a tissue antigen, 286 and Nb82*286 (BTLA agonists), Cl.19 (a PD1 agonist) and CE10 (a TIGIT agonist) were tested for their ability to ameliorate disease in a GVHD model, i.e., the RIP-mOVA diabetes model. Murine IgG1 bispecific antibodies were generated using two different published approaches. The approach described by Labrijn *et al.* relying on controlled Fab arm exchange was found to produce antibodies with unstable characteristics (245). The more-recently described approach from Wang *et al.* successfully yielded stable bispecific antibodies capable of binding both targets, demonstrated using a novel SPR-based approach (246). BTLA agonism appeared to reduce disease progression in the RIP-mOVA diabetes model and the data also suggested that subverting the Fc receptor dependency may be possible. Unexpectedly, PD-1 agonism enhanced disease progression similarly to that observed with a PD-1 blocking antibody. Using bispecific antibodies, antibody agonism of bipartite receptors with intrinsic catalytic activity was also attempted, however agonism of the IL-10R was not achieved with the initial set of constructs. One explanation is that the bispecific antibodies did not meet the possibly strict geometric requirements needed to initiate signalling and therefore warrants further investigation.

6.1 Fc-receptor independent BTLA agonism

BTLA agonists have previously been shown to ameliorate GVHD in mouse models (160,299). Similarly, the anti-BTLA agonist used herein, 286, had been shown to prevent colitis in a T-cell transfer model of the disease and prevented disease in a GVHD model wherein MHC mismatched bone marrow and splenocytes were injected into irradiated recipient mice (249). The use of 286 was therefore expected to ameliorate another T-cell driven GVHD, the OT-I RIP-mOVA model, in which transferred MHC Class I OVA-specific CD8 T-cells recognise OVA expressed in the pancreas under the rat insulin promoter and cause diabetes. Indeed, BTLA agonism reduced inflammation and disease progression in the RIP-mOVA model.

The finding that 286 could ameliorate disease raised the question of whether the Fc receptor dependency of 286 agonism could be circumvented by the engagement of a tissue antigen instead. Hypothetically, this would focus the immunosuppression with increased safety, and removal of the Fc receptor binding dependency would avoid potential concerns associated with agonist antibodies requiring Fc receptors for co-engagement, which might be limited. Secondly, Fc receptors can themselves signal and their engagement may result in unintended signalling in Fc receptor-expressing cells. As the majority of Fc receptors have pro-inflammatory functions this is undesirable for the development of immune checkpoint agonists, whose net effects are intended to be inhibitory (252,300). Therefore, development of agonists for testing in mouse models has thus far relied on the use of the mIgG1 backbone, which predominantly binds the inhibitory FcγR2b receptor. However, mIgG1 is capable of engaging the activatory FcγRIII, albeit with a lower affinity (252). Therefore, removing the requirement for Fc receptor engagement allows, in principle, future development of agonists which can utilise tissue antigens to create the close contacts expected to be needed for signalling thereby removing countervailing Fc receptor signalling. Results obtained with the

bispecific anti-OVA anti-BTLA antibody, Nb82*286, produced similar results to 286 treatment in a first experiment, but cannot be considered conclusive without further repeats. The possibility that close contact formation, likely necessary for 286 agonism, could be achieved in an FcR-independent manner creates an opportunity to consider targeting other treatments locally to tissues of interest. This would allow lower treatment doses to be given as the active reagent would bind locally, increasing the local concentration of antibody in the targeted tissue. Tissue targeted agonism would also allow targeting of receptors on cells in tissues where less Fc receptor is present such as in the periphery and in non-immunologically active tissues. The small amounts of Fc receptor present in these regions may limit Fc receptor dependent antibody agonism and by developing agonist antibodies that rely on a tissue antigen for close contact formation, this limitation could be overcome.

It may also be possible to agonise two receptors simultaneously and bidirectionally, only in locations where both receptors are present, by using a bispecific antibody targeting two immunoreceptors. For example, the actions of a PD-1 agonist and BTLA agonist could be combined in one antibody. The benefit of combination drug activity would need to be assessed but it could lead to very potent inhibition. Agonism of both receptors would require the antibody to bind cells in trans to maintain close contact formation. As such, the degree to which the bispecific antibody binds in cis, if both receptors are present on the same cell, would need to be considered to ensure agonism occurs rather than simply occupying all the receptors in cis and potentially antagonising the receptors instead.

Immune checkpoint receptors are not the only targets of antibody agonists which have been described to be Fc receptor-dependent. TNF superfamily receptor agonists have also been shown to require Fc receptor engagement to achieve agonism (301). TNF superfamily receptor signalling is initiated upon receptor trimerization which creates the docking sites for downstream adaptor proteins (302). The Fc receptor dependency of TNF superfamily

receptor agonist antibodies is therefore believed to be due to the ability of Fc receptor binding to help cluster the TNF superfamily receptor on an opposing cell, mimicking the effects of natural ligand binding, rather than due to phosphatase exclusion (303). As the mechanism underlying Fc receptor dependency differs between the TNF superfamily receptors and immunoreceptors, findings with one of these signalling systems cannot be extrapolated to the other. However, use of a tissue antigen to enable agonism could conceivably be used to replace the requirement for Fc receptor binding for both these receptor families. Medler *et al*. demonstrated that Fc receptor-dependent TNF superfamily receptor agonist antibodies which had anti-CD20 single chain variable fragments fused to their C-termini were able to agonise TNF superfamily receptors in an Fc receptor independent manner (304). Interestingly, the same group demonstrated that TNF superfamily receptor agonists could also be made Fc receptor independent by fusing the cytokine IL-2 to the agonist antibody C-termini (304). The use of an antibody/cytokine fusion could be extended to agonise immunoreceptors independent of Fc receptor binding, using an antibody with one cytokine arm and one conventional antibody arm. This combination could be useful to deliver both the action of the cytokine and agonist antibody simultaneously and would give the cytokine the therapeutically desirable pharmacokinetics of an antibody therapeutic, assuming that trans binding occurs and that the intercellular dimensions are small enough.

The potency of immune checkpoint agonism appears to depend on the intercellular distance in the cell-cell contact and the consequent levels of phosphatase exclusion created by the antibody (Lippert *et al.*, manuscript submitted). The potency is therefore determined by the dimensions of the antibody used. Herein 286, a membrane proximal binder and Nb82, which binds mOVA at an unknown epitope but likely binds near the membrane due to the small size of mOVA, were used. This was on a conventional mIgG1 backbone with an estimated

arm reach of ~12-15 nm, which is small enough to mimic the dimensions of an immune cell synapse (~15 nm), known to exclude receptor tyrosine phosphatases (31). It seems likely that this criterion will be important to bear in mind during the development of future immunoreceptor agonists. In support of this are findings obtained with the use of T-cell bispecific antibodies or fragments thereof used to recruit T cells to target cancer cells and to eliminate them, often known as bispecific T-cell engagers (BiTE). Using T-cell-binding bispecific antibodies it has been found that the more compact the intercellular space generated by a BiTE the more potent they are at eliminating the target cells, with a reduction in dimensions from 9-11 nm to 5-6 nm allowing the generation of a BiTE that was 35-fold more potent (305). In contrast, the constructs used for Fc receptor independent TNF receptor superfamily agonism, discussed above, are unlikely to translate directly to immunoreceptor agonism, as these are likely too large to form a <15 nm intercellular distance (304). The intercellular distance generated by an antibody agonist utilising a membrane antigen will be dependent on the proximity of the epitopes to the membrane, the size of the antigen and the distance between variable domains. As such, future development of immunoreceptor agonists should focus on generating compact cell-cell contacts with bispecific antibody formats with low inter variable-domain distances and could include Fc-less bispecific antibodies, if appropriate distances can be reached.

6.2 PD-1 agonism exacerbated OT-I T cell driven diabetes

PD-1 is currently the best target for antagonism in cancer treatment and blockade of PD-1 signalling has been found to cause immune related adverse events in some patients (306). These immune related adverse events stem from lowering the threshold for immune activation, causing errant autoimmune responses. This suggests that it might be possible to achieve the inverse effect by agonising PD-1 to inhibit autoimmune responses. Previous

work had demonstrated that Cl.19 inhibited CD4 OT-II T-cell expansion and reduced markers of systemic lupus erythematosus (SLE) in a BM12 transfer model of the disease (Lippert *et al.* manuscript submitted). Further, low expression of PD-1 in the presence of ligand has been found to be sufficient to inhibit proliferation of both $CD4^+$ and $CD8^+$ T-cells, with increasing expression inhibiting cytokine expression and cytotoxicity, suggesting that PD-1 signalling would be able to inhibit OT-I T-cell activity and suppress GvHD (307). Therefore, the finding that Cl.19 agonism resulted in the exacerbation of OT-I T-cell driven diabetes in RIP-mOVA mice was unexpected.

Cl.19 has previously been shown not to compete with PD-L1 or PD-L2 for PD1 binding (Lippert et al., manuscript submitted). Similarly, ANB030, a functionally similar PD-1 agonist to Cl.19, also does not compete with PD-L1 (282). Therefore, the observed increase in glycosuria in Cl.19 treated mice cannot be explained by preventing PD-1 interacting with its ligands. Additionally, as the anti-BTLA antibody, 286, reduced inflammation and both 286 and Cl.19 likely rely on phosphatase exclusion through binding of Fc receptors to achieve signalling, the apparent activating effect observed on PD-1 signalling with Cl.19 is unlikely to be due to a lack of Fc receptor being present. The difference also cannot be explained by the engagement of different Fc receptors as both antibodies are mIgG1.

One possibility is that agonistic Cl.19-induced signalling resulted in the downregulation of the PDCD1 gene reducing PD-1 expression. Alternatively, antibody binding may result in receptor-mediated endocytosis internalising the Cl.19 PD-1 complex as observed for other monoclonal antibodies and used in some instances to deliver drugs intracellularly using antibody-drug conjugates (308,309). Both outcomes would reduce surface expression of PD-1, thereby reducing both PD-1 signalling from Cl.19 and signalling from natural ligands. In both cases there would presumably be a spike in initial inhibitory signalling, followed by a reduction in PD-1 signalling from baseline. Nivolumab D265A is a very potent blocker of

PD-1 signalling and while Cl.19 did increase the incidence of glycosuria it appeared less potent than Nivolumab D265A, suggesting that there might have been some PD-1 signalling consistent with receptor down regulation or internalisation. If PD-1 downregulation is due to receptor mediated endocytosis, rather than downregulation of PD-1 expression, it could be possible to develop PD-1 agonist antibodies which induce less internalisation (309). Dimerisation of receptors by antibodies has been reported to increase receptor internalisation. For example, the fibroblast growth factor receptor, which possesses intrinsic kinase activity, has been found to endocytose upon dimerisation independently of activation (310). Additionally, antibody receptor complexes which internalise and dissociate within two hours have been found to enable recycling of the human epidermal growth factor receptor 2 to the cell surface, whereas antibody receptor complexes which did not dissociate were ubiquitinated (311). While these receptors function differently to PD-1, the mechanism by which they are internalised may be similar. These examples suggest that an antibody with an anti-PD-1 valency of one with a faster off-rate may reduce receptor internalisation and increase receptor recycling both acting to maintain more PD-1 on the cell surface. Experiments exploring the expression of PD-1 on OT-I T-cells post transfer in the RIP-mOVA model may help to better understand the observations made with Cl.19 treatment.

In support of the hypothesis that Cl.19 reduces PD-1 on the cell surface are findings obtained with ANB030. ANB030 has been found to decrease the proportion of PD-1 expressing CD4 and CD8 T cells by ~50% while total T-cell numbers remained unchanged (312). The reduction in the proportion of PD-1 expressing cells was most marked for cells expressing high levels of PD-1 which was reduced by ~90% (312). The size of the reduction was proposed to correlate with receptor occupancy indicating a need for ongoing antibody presence to maintain the reduction in PD-1. These findings support the idea that the increase in OT-I T-cell activity may be due to PD-1 receptor downregulation. Further, in combination

with previous findings that cytotoxicity is inhibited by PD-L1 only at intermediate to high levels of PD-1 expression, the transferred OT-I cells may lose PD-1 expression and signalling beyond the threshold necessary to inhibit cytotoxic activity (307).

Comparing the adverse findings for Cl.19 treatment in the RIP-mOVA model with the beneficial findings in the BM12 model suggests that the distinct outcomes could be linked to the cell types responsible for disease in each case (Lippert *et al.*, manuscript submitted). In the BM12 model, SLE can be caused solely by a transfer of $CD4^+$ T-cells into an MHC mismatched recipient (313). The $CD4^+$ T-cells of particular importance include T follicular helper (Tfh) cells, which express a lot of PD-1 and have B-cell helper functions that support the development of antibody-producing cells (313). On the other hand, $CD8^+$ T-cells drive glycosuria in the RIP-mOVA model (277). PD-1 has been shown to play an active role in the early stages of a $CD8^+$ T-cell response with PD-1 expression occurring as soon as four hours post cognate peptide (gp33) injection into transgenic P14 mice (314). Further, blockade of PD-1 signalling in mice infected with lymphocytic choriomeningitis virus (LCMV) was found to increase granzyme B expression in antigen-specific $CD8^+$ T-cells and increases the rate of viral clearance (314). The Cl.19 PD-1 agonism-driven antagonism of $CD8^+$ T-cells could therefore be increasing the activity of effector $CD8^+$ T-cells in this new setting in a similar manner.

Tfh cells, unlike $CD8^+$ T-cells, do not act directly on their targets, rather they support the development of antibody forming cells in germinal centres, leading to an increase in antibody production (122). It is these plasma cells which are the effector cells. Experiments have found that PD-1 signalling in Tfh cells performs a role that supports, rather than suppresses, the actions of Tfh cells and the high expression of PD-1 on Tfh cells indicates the likely importance of this signalling axis in these cells (122,123). The primary source of PD-1 signalling to Tfh cells appears to come from B cells which express PD-L1 and/or PD-

L2 (123). By deleting PD-1 in a Tfh cell-specific manner it has been shown that removing PD-1 signalling increased Tfh cell numbers (123). However, these PD-1 "knockout" Tfh cells were found to synthesise less IL-4 and IL-21 (123). Further, a reduction in development of long-lived plasma cells was observed suggesting that despite their increased number the PD-1-depleted Tfh cells were less effective at supporting plasma cell development (123). IL-4 and IL-21 have both been reported to support the development of antibody forming cells with mice deficient in either IL-4Rα or IL-21R *in vivo* having fewer germinal centre B-cells with a reduction in B-cell differentiation and proliferation compared to wild type mice (315,316). Similarly, the study which eliminated PD-1 signalling in Tfh cells found that there was an increase in germinal centre B-cell death, which could account for the observed reduction in long lived plasma cells (123). These results could also be reproduced by eliminating PD-L2 expression in a B-cell specific manner further supporting the importance of the Tfh/B cell PD-1/PD-L2 interactions in the production of long-lived plasma cells (123). The positive effects of Cl.19 treatment in the BM12 SLE model could therefore be accounted for by a reduction in PD-1 signalling which reduces the ability of Tfh cells to support plasma cell development, which in turn would reduce disease severity. It should be noted that the loss of PD-1 signalling did not completely remove the antibody response; rather, it reduced the response (123). However, this reduction could be sufficient to ameliorate SLE in the BM12 model. Interestingly, another subset of follicular $CD4^+$ T-cells could also account for the outcome of Cl.19 treatment in the BM12 SLE model. T follicular regulatory (Tfr) cells also express PD-1 and would also be transferred in the BM12 SLE model. PD-1 deficient Tfr cells have been found to have enhanced suppressive abilities in mice and inhibited the production of antibody more potently than wild type Tfr cells (317). Therefore, the action of PD-1 agonism-driven antagonism in Tfh cells and/or in Tfr cells

could account for the amelioration of disease in Cl.19-treated mice observed in the BM12 SLE model.

Alternatively, it may be that Cl.19 agonism does not antagonise PD-1 signalling in Tfh cells and that this is unique to $CD8^+$ OT-I T-cells. In this case reduced Tfh cell activity would account for the amelioration seen in the BM12 SLE model.

The contrasting roles that PD-1 can play on different cell types demonstrates the need to further understand immune checkpoint signalling outcomes across different cell types and highlights also that there is unlikely to be a single solution for all autoimmune conditions. Rather the development of a range of inhibitory agonists against different targets is likely needed to deliver appropriate agonism depending on disease aetiology and the tissue setting. For example, BTLA and PD-1 vary in their expression on different cell types and during different stages of T-cell activation, suggesting they may be exploited for the treatment of different conditions (57,134). Further, different checkpoint receptors may have different rates of internalisation and receptors which remain available at the cell surface for continued inhibitory signalling would be more appealing targets.

6.3 Ligand vs antibody-based approaches for checkpoint agonism

Other approaches to trigger checkpoint receptors like BTLA and PD-1 have been considered using ligand-Fc fusion proteins (57). These ligand-Fc fusion proteins are also capable of engaging Fc receptors and can likely achieve phosphatase exclusion in this manner. A fusion of human or murine HVEM, the BTLA ligand, to the Fc of human or murine IgG1 was able to reduce proliferation of both human and murine CD4 T-cells *in vitro* when the HVEM-Fc fusions were cross linked using an anti-Fc antibody (140). Further, in an *in vivo* model of GVHD, in which irradiated mice were injected with MHC-II mismatched splenocytes and bone marrow cells, treatment with mHVEM-hIgG1 Fc fusion reduced weight loss and

intestinal pathology scores (156). PD-L1, the PD-1 ligand, has also been investigated in an Fc-fused format. Murine PD-L1 fused to a mutated form of mIgG2a Fc (mutated to remove C1q and FcγRI binding and to remove antibody and complement dependent cytotoxicity) was found to ameliorate both acute DSS colitis and chronic T-cell transfer colitis in mice (127). A similar construct with mPD-L1 fused to hIgG Fc also reduced clinical arthritis scores and histology in the joints of mice in a collagen-induced arthritis model (125).

The use of natural ligands as agonists has some disadvantages compared to an antibody agonist. Many ligands are shared by multiple receptors, for example, the BTLA ligand HVEM is also capable of binding the activatory receptor LIGHT (318). This makes using the natural ligands for inhibitory agonism challenging as treatment may induce counterproductive activatory signalling, weakening or negating the inhibitory effect. Antibodies can be generated with specificity to only the inhibitory receptor and can be selected for higher affinity than the affinity of the natural ligand. It is feasible that natural ligands could be engineered to have greater affinity and specificity for the inhibitory receptor. This has been achieved with a modified version of HVEM-Fc capable of binding BTLA selectively with a 10-fold higher affinity than WT HVEM. Further, this mutated HVEM-Fc was capable of inhibiting T, B and NK cell cytokine production (319). However, this approach is more labour-intensive than selecting an antibody with the desired characteristics and competes directly with the natural inhibitory ligands which may reduce net inhibitory activation. The use of an antibody agonist may also be preferable as it could be capable of binding mutated receptors in which natural ligand binding is perturbed. Additionally, there is an existing precedent of using monoclonal antibodies as therapeutics, which means that antibodies may encounter fewer regulatory obstacles in moving to the clinic in comparison to ligand-Fc fusions.

6.4 Lessons learned from bispecific antibody IL-10R agonism

The anti-IL-10R bispecific antibodies described in this thesis failed to agonise the IL-10R. Simultaneous binding was demonstrated using SPR in which the receptors are not constrained by their binding to a membrane; however it is possible that a physiological complex could not be formed at the cell surface, i.e. that binding of one receptor subunit precludes the other bispecific arm from binding its epitope on the other receptor chain, for topological reasons. On the face of it, this seems unlikely because receptors in the membrane can freely rotate on a membrane plane-orthogonal axis. It is more likely that the receptor chains were engaged and co-localised by the bispecific antibodies on the cell but co-localisation was insufficient to induce agonism.

The lack of signalling may therefore be expected to be due to the inability of the bispecific to bring the intracellular domains close enough together to interact with one another. This could be due to (1) the binding of the receptor chains in an orientation that prevents the intracellular domains being functional or, (2) the distance between the antibody arms and bound receptor chains not being permissive of intracellular domain interactions (Fig. 6.1).

Computational modelling of how IL-10, IL-10Rα and IL-10Rβ dock together showed that the distance between the C-termini of the extracellular domains, IL-10Rα (residue T206) and IL-10Rβ (residue T194), was 23Å indicating that the intracellular domains may have to be very closely aligned to achieve signalling (320). A structure of the active JAK1-IFNλR1 dimer has shown how JAKs dimerise using their inactive pseudokinase domains (71). From this it has been proposed that pseudokinase binding releases the active tyrosine kinase domain from inhibition allowing transphosphorylation (71). The structure also highlighted how the FERM domain of JAKs associates with the membrane proximal portion of the receptor's cytoplasmic tail, suggesting a limited range of motion intracellularly (71).

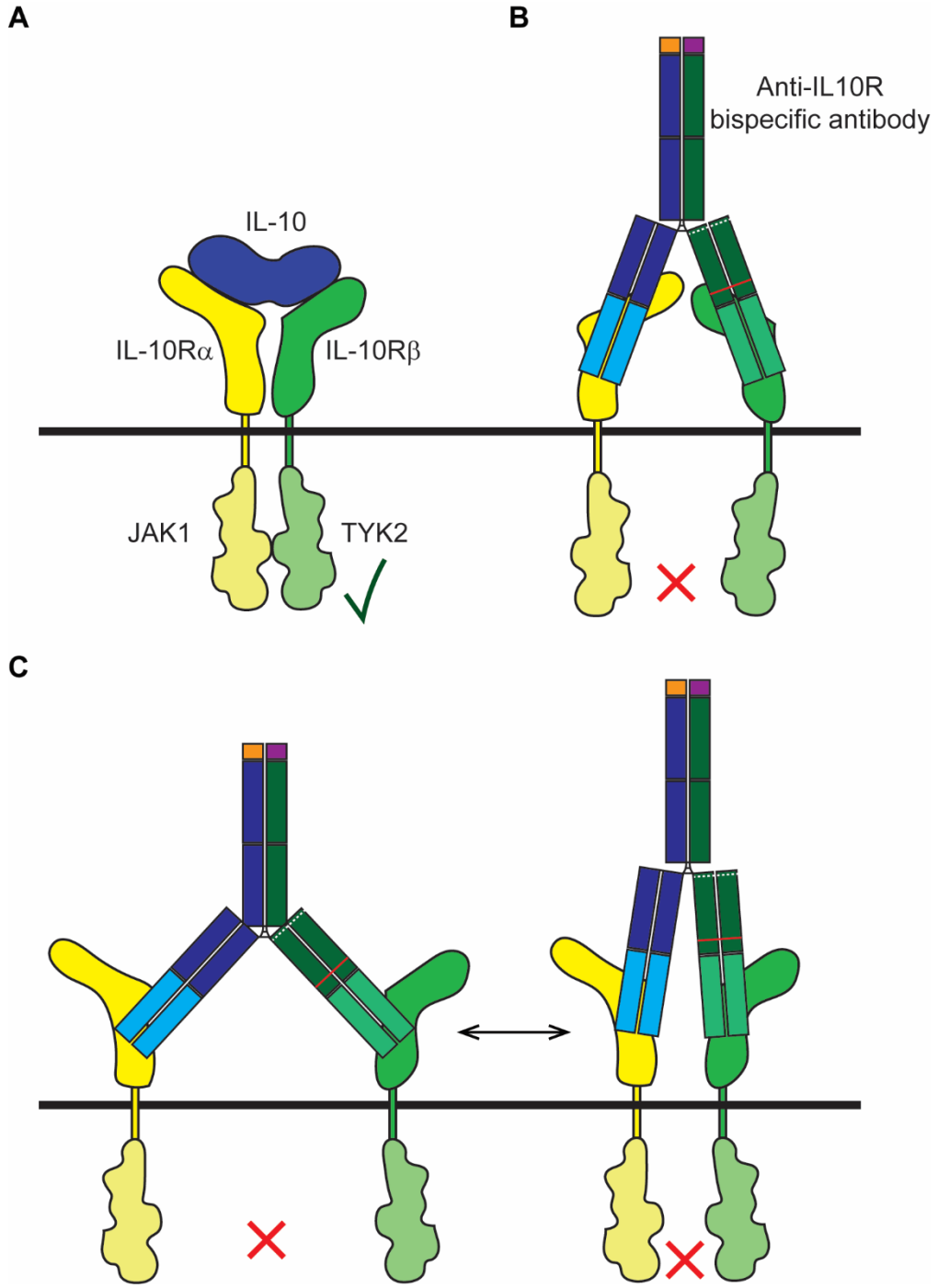


Figure. 6.1. Possible non-signalling conformations of the anti-IL10R bispecific antibody IL-10R complex. (A) The native conformation of the IL-10R complex which meets the requirements for kinase interaction and signalling. (B) Both IL-10R chains bound by an anti-IL10R bispecific antibody in a conformation which does not permit kinase interactions due to the orientations of the IL-10R chains. (C) Both IL-10R chains held apart by the anti-IL10R bispecific antibody preventing intrinsic kinase interaction either due to hinge flexibility (left) or steric restrictions preventing close enough apposition of the intracellular domains (right).

Further, previous molecular dynamics simulations found that mutations in the JAK2 FERM domain disrupt its interaction with the membrane causing it to change orientation (69). This change in orientation reduced receptor dimerisation and signalling likely by disrupting pseudokinase domain alignment and interaction (69). These findings demonstrate the need to bring the receptor transmembrane domains into close proximity, as the associated kinases likely have a limited range of motion and the requirement for this to be in an orientation permissive of pseudokinase domain interaction to release the tyrosine kinase domains from their inhibition.

It is unknown whether the natural IL-10Rα/IL-10Rβ interface in the IL-10/IL-10Rα/IL-10Rβ complex must be maintained to achieve productive kinase interaction and signalling or not. There are other orientations which may permit the intracellular signalling chains to align as closely as the natural conformation suggesting that these alternative conformations could result in signalling. Therefore, antibodies that block the natural interface between the two IL10R chains may still be agonists in the right bispecific pairing. A study of the homodimeric receptor thrombopoietin (TpoR), which is associated with JAK2, has shown that multiple dimeric conformations which were rotated on their membrane plane-orthogonal axis were capable of signalling and promoting cell growth (321). Four of seven conformations investigated were able to promote growth equivalent to the wild type receptor and two other conformations could promote reduced growth and only one conformation did not stimulate growth. These findings were mirrored by the activity of the downstream mediators of TpoR signalling, STAT3 and STAT5 (321). This demonstrates that transphosphorylation of receptor chains by JAKs is possible in multiple receptor orientations. Therefore, the IL-10R may similarly have multiple rotational conformations permissive of signalling and that the native orientation may not be requisite for signalling. The IL-10R is associated with different JAKs than TpoR associating with JAK1 and TYK2

instead of JAK2. However, they all likely possess similar requirements in regard to the orientation-dependence of their signaling functions.

The recently patented findings of Synthekine, a company which develops engineered cytokines and cytokine agonists, demonstrates linker lengths which brought the intracellular receptor chains and their associated kinases into close enough proximity for signalling (322). The patent deals with IL-10R agonists produced using two nanobodies linked by a short serine-glycine linker, with one nanobody binding IL-10Rα and the other binding IL-10Rβ. The authors of the work demonstrated that adjustments in linker length from between 0 – 10 residues had dramatic effects on the agonistic potential of their constructs. A 10 amino acid linker reduced the agonistic activity, presumably due to the distance between intracellular domains being too great, whereas linkers of zero and two residues also reduced the activity, likely due to their being too restrictive of the nanobody's binding ability or linker flexibility. Linkers of between four and eight amino acids appeared to function best. With an approximation of 3.5Å per amino acid in the unstructured glycine-serine linker, this results in a small range of distances with optimal signalling. These findings support the notion that the anti-IL-10R bispecific antibodies produced in this thesis did not signal as they did not bring the signalling domains of the two receptor chains close enough together, in the manner of the Synthekine constructs with ten residue linkers. However, their work emphasizes that the IL-10R can be agonised using antibodies to artificially co-localise both receptor chains, and suggests that there aren't strict conformational requirements on signalling by the cytoplasmic kinases, that are determined by the extracellular regions of the receptor.

During the course of the research described in this thesis, Harris *et al.* published findings in which the heterodimeric IL-2 receptor was triggered using a bispecific antibody (323). The IL-2R agonist bispecific antibodies utilised heavy chain only variable domains, generated in rats, fused onto the hIgG1 Fc region at the hinge in place of CH1. The Fc also contained

"knob in hole" mutations to guide Fc heterodimerisation and bispecific antibody formation. The antibody constructs were similar to the constructs generated in this thesis for antibodies containing a nanobody arm. However, in this thesis only one arm was a nanobody and the second anti-IL10Rα arm was a conventional antibody arm which likely caused too large a distance between the binding sites. However, the IL-2R bispecific antibodies demonstrated that a bispecific antibody on an Fc backbone rather than with a short glycine serine linker is also capable of agonising JAK STAT signalling. Therefore, the role of Fc receptor binding and large receptor protein tyrosine phosphatase exclusion and its influence on cytokine receptor agonists can still be explored using these constructs.

The IL-10R agonists developed by Synthekine and the IL-2R agonists developed by Harris *et al.* highlight the challenges faced in generating antibody agonists against cytokine receptors. Many constructs which were permissive of signalling regarding their dimensions did not show agonistic activity. Only 23 of 98 IL-10R agonists showed agonistic potential and of these only 11 were strong agonists with equivalent or greater activity than IL-10. This highlights that other factors, such as epitope position and/or affinity, must also play a role in receptor agonism. It is therefore important to gain a greater understanding of what characteristics differentiate cytokine receptor agonist antibodies from non-agonistic antibodies. For example the epitope positions of some bispecific antibodies may be unfavourable as binding to one epitope could restrict the antibodies ability to bind its second epitope in cis.

This may be due to steric restrictions upon binding of one receptor chain limiting the ability of the molecules to bind the second chain required for signalling. This highlights the need to better understand other factors influencing agonism, such as epitope position and affinity. As this work was unsuccessful in generating bispecific IL-10R agonists, it was not possible to explore the role of large receptor protein tyrosine phosphatase exclusion on the signalling

of these receptors. This might be possible now by combining the nanobody-hinge-CH2-CH3 construct used by Harris *et al.*, nanobodies from the Synthekine patent and the variable domains of the antibodies characterised in this thesis in the smaller ScFv format. Alternatively, the antibodies and nanobodies characterised in this thesis could be used in a dual variable domain immunoglobulin construct, in which an anti-IL-10Rβ nanobody could be linked to the N-terminus of an anti-IL-10Rα antibody sequence. The linker length between antibody variable domain and nanobody could be varied and this construct would allow IL-10Rα and IL-10Rβ to be brought into very close proximity with one another. All these constructs would have an Fc capable of binding Fc receptors and thereby excluding receptor protein phosphatases. These constructs, if agonistic, could then be used to examine the role of phosphatase exclusion by testing the effects of Fc mutations on their activity (Lippert et al., manuscript submitted, 3).

Agonists against the IL-10R have been tested in clinical trials for over 20 years and their efficacy has been limited. However, the recent findings that have begun to understand how altering the affinity of IL-10 for the IL-10Rβ chain modulates signalling outcomes in different cell types may help to design new therapeutics that decouple the anti-inflammatory effects on myeloid cells from the stimulatory effects on lymphocytes (298). It may therefore be possible to generate bispecific antibodies which can either enhance lymphocyte function to help eliminate tumours or deliver inhibitory signalling to the myeloid compartment.

6.5 Closing remarks

This thesis has begun to iterate and develop agonist antibodies against inhibitory immune receptors with both extrinsic and intrinsic kinase activity, building on the principles of the kinetic-segregation model. Agonism of inhibitory receptors affords an opportunity to treat

autoimmunity through pathways not directly involved in the development of disease. This approach seeks to exploit regulatory signalling pathways to suppress aberrant immune responses and to restore homeostasis, and by improving our understanding of the mechanisms of receptor signalling, this approach could be applied more systematically. We can learn many lessons through the development of agonist antibodies where these give fundamental insights into the mechanisms regulating cell signalling. For example, by understanding the need for close contact formation, the Fc receptor dependency could be circumvented or optimised. This in turn opens the possibility for the generation of even more potent agonists. The large number of bispecific and multispecific antibody formats could be used, and the ongoing development of other non-antibody formats, suggests that there is considerable scope for generating a large variety of potentially useful therapeutic agonists.

Chapter 7

Chapter 7 Appendix

7.1 hIL10Ra mouse generation

Gene information:

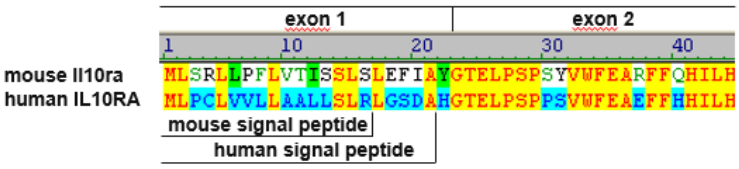
Mouse Il10ra gene:

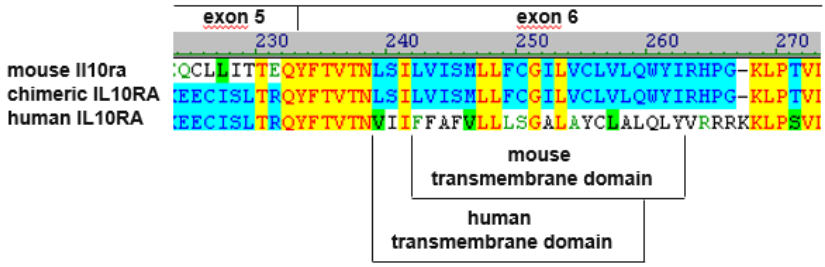
- official gene symbol: **Il10ra**
- official gene name: **interleukin 10 receptor, alpha**
- located on mouse chromosome **9**
- Ensembl gene ID: **ENSMUSG00000032089**
- NCBI gene ID: **16154**
- C57BL/6 BAC-IDs: **RP23-288M22, RP23-357H21, RP23-397G16**

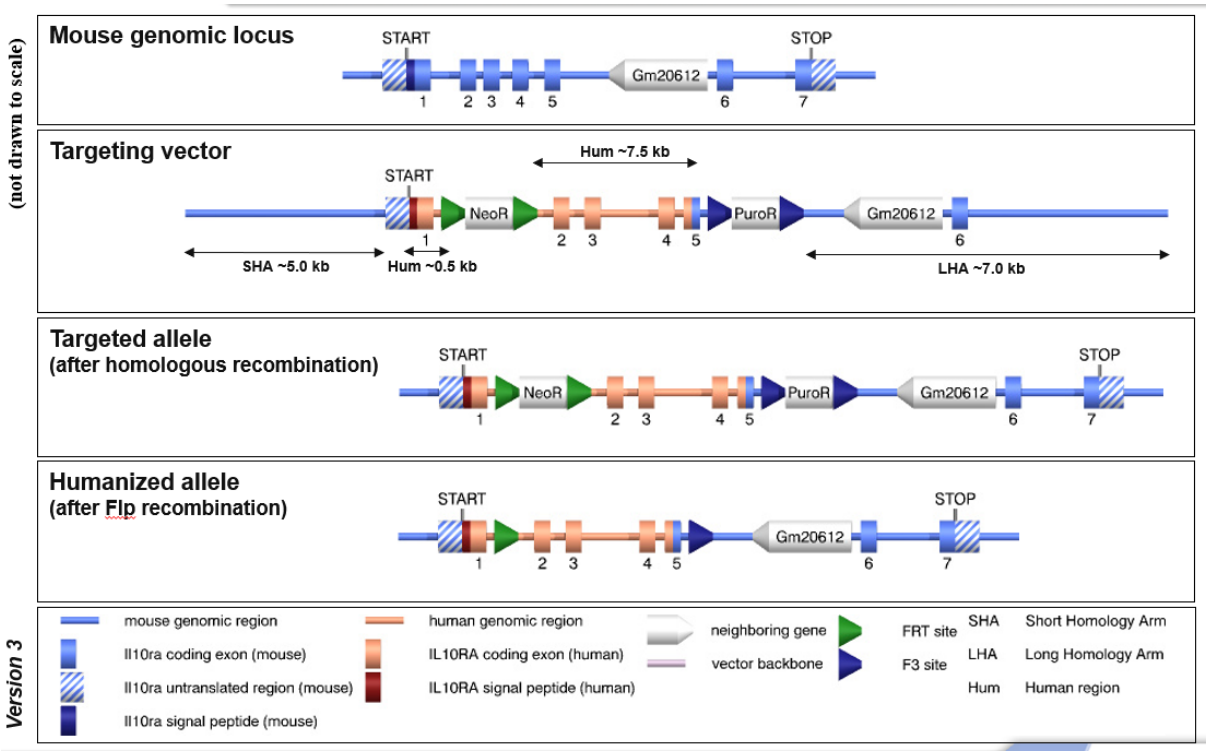
Human IL10RA gene:

- official gene symbol: **IL10RA**
- official gene name: **interleukin 10 receptor, alpha**
- Ensembl gene ID: **ENSG00000110324**
- NCBI gene ID: **3587**
- human BAC-IDs: **RP11-278M6, RP11-484N10, RP11-786F19**

Sequence conservation between mouse Il10ra and human IL10RA proteins:







8.2 Publications relating to SARS-CoV-2

During the university building closures due to the outbreak of SARS-CoV-2 I worked in the lab of Alain Townsend to help with anti-SARS-CoV-2 antibody production and characterisation. Some of the work I contributed to has been published in the following references:

1. Huang KA, Zhou D, Tan TK, Chen C, Duyvesteyn HME, Zhao Y, Ginn HM, Qin L, Rijal P, Schimanski L, Donat R, Harding A, Gilbert-Jaramillo J, James W, Tree JA, Buttigieg K, Carroll M, Charlton S, Lien CE, Lin MY, Chen CP, Cheng SH, Chen X, Lin TY, Fry EE, Ren J, Ma C, Townsend AR, Stuart DI. Structures and therapeutic potential of anti-RBD human monoclonal antibodies against SARS-CoV-2. Theranostics. 2022 Jan 1;12(1):1-17. doi: 10.7150/thno.65563. PMID: 34987630; PMCID: PMC8690919.

2. Zhou D, Duyvesteyn HME, Chen CP, Huang CG, Chen TH, Shih SR, Lin YC, Cheng CY, Cheng SH, Huang YC, Lin TY, Ma C, Huo J, Carrique L, Malinauskas T, Ruza RR, Shah PNM, Tan TK, Rijal P, Donat RF, Godwin K, Buttigieg KR, Tree JA, Radecke J, Paterson NG, Supasa P, Mongkolsapaya J, Screaton GR, Carroll MW, Gilbert-Jaramillo J, Knight ML, James W, Owens RJ, Naismith JH, Townsend AR, Fry EE, Zhao Y, Ren J, Stuart DI, Huang KA. Structural basis for the neutralization of SARS-CoV-2 by an antibody from a convalescent patient. Nat

Struct Mol Biol. 2020 Oct;27(10):950-958. doi: 10.1038/s41594-020-0480-y. Epub 2020 Jul 31. PMID: 32737466.

Chapter 8

Chapter 8 References

1. Miller FW. The increasing prevalence of autoimmunity and autoimmune diseases: an urgent call to action for improved understanding, diagnosis, treatment, and prevention. Current Opinion in Immunology. 2023 Feb 1;80:102266.
2. Wang L, Wang FS, Gershwin & ME, Wang A, Wang L, Me G. Human autoimmune diseases: a comprehensive update. Journal of Internal Medicine. 2015 Oct 1;278(4):369–95.
3. Smith-Garvin JE, Koretzky GA, Jordan MS. T Cell Activation. Annual review of immunology. 2009;27:591.
4. Chen L, Flies DB. Molecular mechanisms of T cell co-stimulation and co-inhibition. Nature Reviews Immunology 2013 13:4. 2013 Mar 8;13(4):227–42.
5. Urtsinger J, Schmidt C, Mondino A, Lins D, Kedl R, Jenkins M, et al. Inflammatory cytokines provide a third signal for activation of naive CD4+ and CD8+ T cells. J Immunol. 1999;162(6):3256–62.
6. Uings IJ, Farrow SN. Cell receptors and cell signalling. Molecular Pathology. 2000;53(6):295.
7. Dushek O, Goyette J, van der Merwe PA. Non-catalytic tyrosine-phosphorylated receptors. Immunological Reviews. 2012 Nov 1;250(1):258–76.
8. Isakov N. Immunoreceptor tyrosine-based activation motif (ITAM), a unique module linking antigen and Fc receptors to their signaling cascades. Journal of leukocyte biology. 1997;61(1):6–16.
9. Daëron M, Jaeger S, Du Pasquier L, Vivier E. Immunoreceptor tyrosine-based inhibition motifs: a quest in the past and future. Immunological reviews. 2008 Aug;224(1):11–43.
10. Le Borgne M, Shaw AS. SAP Signaling: A Dual Mechanism of Action. Immunity. 2012 Jun 29;36(6):899–901.
11. Nika K, Soldani C, Salek M, Paster W, Gray A, Etzensperger R, et al. Constitutively active Lck kinase in T cells drives antigen receptor signal transduction. Immunity. 2010 Jun;32(6):766–77.
12. Imbert V, Peyron JF, Farahi Far D, Mari B, Auberger P, Rossi B. Induction of tyrosine phosphorylation and T-cell activation by vanadate peroxide, an inhibitor of protein tyrosine phosphatases. Biochemical Journal. 1994 Jan 1;297(Pt 1):163.
13. Fernandes RA, Su L, Nishiga Y, Ren J, Bhuiyan AM, Cheng N, et al. Immune receptor inhibition through enforced phosphatase recruitment. Nature 2020 586:7831. 2020 Oct 21;586(7831):779–84.
14. Chakraborty AK, Weiss A. Insights into the initiation of TCR signaling. Nature Immunology. 2014 Sep 19;15(9):798–807.
15. Goyette J, Nieves DJ, Ma Y, Gaus K. How does T cell receptor clustering impact on signal transduction? Journal of Cell Science. 2019;132(4):jcs226423.
16. Ihle JN. Cytokine receptor signalling. Nature 1995 377:6550. 1995 Oct 19;377(6550):591–4.
17. Lemmon MA, Schlessinger J. Cell signaling by receptor-tyrosine kinases. Cell. 2010 Jun 6;141(7):1117.
18. Van Wauwe J, Goossens J, Beverley P. Human T lymphocyte activation by monoclonal antibodies; OKT3, but not UCHT1, triggers mitogenesis via an interleukin 2-dependent mechanism. J Immunol. 1984;133(1):129–32.
19. Manz BN, Jackson BL, Petit RS, Dustin ML, Groves J. T-cell triggering thresholds are modulated by the number of antigen within individual T-cell receptor clusters.

Proceedings of the National Academy of Sciences of the United States of America. 2011 May 31;108(22):9089–94.
20. Erlandson SC, McMahon C, Kruse AC. Structural Basis for G Protein-Coupled Receptor Signaling. Annual review of biophysics. 2018 May 20;47:1–18.
21. Traynelis SF, Wollmuth LP, McBain CJ, Menniti FS, Vance KM, Ogden KK, et al. Glutamate Receptor Ion Channels: Structure, Regulation, and Function. Pharmacological Reviews. 2010 Sep;62(3):405.
22. Call ME, Pyrdol J, Wiedmann M, Wucherpfennig KW. The organizing principle in the formation of the T cell receptor-CD3 complex. Cell. 2002 Dec 27;111(7):967–79.
23. Xu C, Gagnon E, Call ME, Schnell JR, Schwieters CD, Carman C V., et al. Regulation of T cell receptor activation by dynamic membrane binding of the CD3epsilon cytoplasmic tyrosine-based motif. Cell. 2008 Nov 14;135(4):702–13.
24. Beddoe T, Chen Z, Clements CS, Ely LK, Bushell SR, Vivian JP, et al. Antigen Ligation Triggers a Conformational Change within the Constant Domain of the αβ T Cell Receptor. Immunity. 2009 Jun 19;30(6):777–88.
25. Sušac L, Vuong MT, Thomas C, von Bülow S, O'Brien-Ball C, Santos AM, et al. Structure of a fully assembled tumor-specific T cell receptor ligated by pMHC. Cell. 2022 Aug 18;185(17):3201-3213.e19.
26. Dong D, Zheng L, Lin J, Zhang B, Zhu Y, Li N, et al. Structural basis of assembly of the human T cell receptor–CD3 complex. Nature 2019 573:7775. 2019 Aug 28;573(7775):546–52.
27. Dobbins J, Gagnon E, Godec J, Pyrdol J, Vignali DAA, Sharpe AH, et al. Binding of the cytoplasmic domain of CD28 to the plasma membrane inhibits Lck recruitment and signaling. Science signaling. 2016 Jul 26;9(438).
28. Kim ST, Takeuchi K, Sun ZYJ, Touma M, Castro CE, Fahmy A, et al. The αβ T cell receptor is an anisotropic mechanosensor. Journal of Biological Chemistry. 2009 Nov 6;284(45):31028–37.
29. Göhring J, Kellner F, Schrangl L, Platzer R, Klotzsch E, Stockinger H, et al. Temporal analysis of T-cell receptor-imposed forces via quantitative single molecule FRET measurements. Nature Communications 2021 12:1. 2021 May 4;12(1):1–14.
30. Chang VT, Fernandes RA, Ganzinger KA, Lee SF, Siebold C, McColl J, et al. Initiation of T cell signaling by CD45 segregation at "close contacts." Nature Immunology. 2016 May 21;17(5):574–82.
31. Davis SJ, van der Merwe PA. The kinetic-segregation model: TCR triggering and beyond. Nature Immunology. 2006 Aug 1;7(8):803–9.
32. Anton van der Merwe P, McNamee PN, Davies EA, Barclay AN, Davis SJ. Topology of the CD2-CD48 cell-adhesion molecule complex: implications for antigen recognition by T cells. Current Biology. 1995 Jan 1;5(1):74–84.
33. Junghans V, Santos AM, Lui Y, Davis SJ, Jönsson P. Dimensions and Interactions of Large T-Cell Surface Proteins. Frontiers in Immunology. 2018 Sep 27;9:2215.
34. Symons A, Willis AC, Barclay AN. Domain organization of the extracellular region of CD45. Protein Engineering, Design and Selection. 2002 Oct 1;12(10):885–92.
35. Choudhuri K, van der Merwe PA, Dustin ML, Basat AB, Bridge M, Cordoba SP, et al. The large ectodomains of CD45 and CD148 regulate their segregation from and inhibition of ligated T-cell receptor. Blood. 2013 May 23;121(21):4295–302.
36. Mørch AM, Bálint Š, Santos AM, Davis SJ, Dustin ML. Coreceptors and TCR Signaling – the Strong and the Weak of It. Frontiers in Cell and Developmental Biology. 2020 Oct 16;8:1147.

37. Junghans V, Hladilkova J, Santos AM, Lund M, Davis SJ, Jönsson P. Hydrodynamic trapping measures the interaction between membrane-associated molecules. Scientific reports. 2018 Dec 1;8(1).
38. Choudhuri K, Wiseman D, Brown MH, Gould K, Van Der Merwe PA. T-cell receptor triggering is critically dependent on the dimensions of its peptide-MHC ligand. Nature. 2005 Jul 28;436(7050):578–82.
39. Choudhuri K, Parker M, Milicic A, Cole DK, Shaw MK, Sewell AK, et al. Peptide-major histocompatibility complex dimensions control proximal kinase-phosphatase balance during T cell activation. The Journal of biological chemistry. 2009 Sep 18;284(38):26096–105.
40. Chen KY, Jenkins E, Körbel M, Ponjavic A, Lippert AH, Santos AM, et al. Trapping or slowing the diffusion of T cell receptors at close contacts initiates T cell signaling. Proceedings of the National Academy of Sciences of the United States of America. 2021 Sep 28;118(39):e2024250118.
41. Fernandes RA, Ganzinger KA, Tzou J, Jönsson P, Lee SF, Palayret M, et al. A cell-topography based mechanism for ligand discrimination by the T-cell receptor. bioRxiv. 2017;
42. Felce JH, Sezgin E, Wane M, Brouwer H, Dustin ML, Eggeling C, et al. CD45 exclusion– and cross-linking–based receptor signaling together broaden FceRI reactivity. Vol. 11, Science Signaling. 2018.
43. Köhler K, Xiong S, Brzostek J, Mehrabi M, Eissmann P, Harrison A, et al. Matched sizes of activating and inhibitory receptor ligand pairs are required for optimal signal integration by human natural killer cells. Zimmer J, editor. PLoS ONE. 2010 Nov 5;5(11):e15374.
44. Hudecek M, Lupo-Stanghellini MT, Kosasih PL, Sommermeyer D, Jensen MC, Rader C, et al. Receptor affinity and extracellular domain modifications affect tumor recognition by ROR1-specific chimeric antigen receptor T cells. Clinical cancer research : an official journal of the American Association for Cancer Research. 2013 Jun 15;19(12):3153–64.
45. Hudecek M, Sommermeyer D, Kosasih PL, Silva-Benedict A, Liu L, Rader C, et al. The nonsignaling extracellular spacer domain of chimeric antigen receptors is decisive for in vivo antitumor activity. Cancer immunology research. 2015 Feb 1;3(2):125–35.
46. Finnern R, Gilham DE, Abken H, Hombach AA, Schildgen V, Heuser C. Redirected T Cells Determines the Efficiency of Activation of Binding Epitope within the Target Molecule Immunoreceptors: The Position of the T Cell Activation by Antibody-Like. J Immunol References. 2007;178:4650–7.
47. James SE, Greenberg PD, Jensen MC, Lin Y, Wang J, Till BG, et al. Antigen sensitivity of CD22-specific chimeric TCR is modulated by target epitope distance from the cell membrane. Journal of immunology (Baltimore, Md : 1950). 2008 May 15;180(10):7028–38.
48. Li J, Stagg NJ, Johnston J, Hö I, James JR, Correspondence TTJ. Membrane-Proximal Epitope Facilitates Efficient T Cell Synapse Formation by Anti-FcRH5/CD3 and Is a Requirement for Myeloma Cell Killing In Brief. Cancer Cell. 2017;31:383–95.
49. Geppert TD, Lipsky PE, Simmons HC. Activation of T lymphocytes by immobilized monoclonal antibodies to CD3. Regulatory influences of monoclonal antibodies to additional T cell surface determinants. Activation of T Lymphocytes by Immobilized Monoclonal Antibodies to CD3 Regulatory Influences of

Monoclonal Antibodies to Additional T Cell Surface Determinants. J Clin Invest. 1988;81(5):1497.
50. Suntharalingam G, Perry MR, Ward S, Brett SJ, Castello-Cortes A, Brunner MD, et al. Cytokine storm in a phase 1 trial of the anti-CD28 monoclonal antibody TGN1412. The New England journal of medicine. 2006 Sep 7;355(10):1018–28.
51. Tacke M, Hanke G, Hanke T, Hünig T. CD28-mediated induction of proliferation in resting T cellsin vitro andin vivo without engagement of the T cell receptor: Evidence for functionally distinct forms of CD28. European Journal of Immunology. 1997 Jan 1;27(1):239–47.
52. Lühder F, Huang Y, Dennehy KM, Guntermann C, Müller I, Winkler E, et al. Topological requirements and signaling properties of T cell-activating, anti-CD28 antibody superagonists. The Journal of experimental medicine. 2003 Apr 21;197(8):955–66.
53. Evans EJ, Esnouf RM, Manso-Sancho R, Gilbert RJC, James JR, Yu C, et al. Crystal structure of a soluble CD28-Fab complex. Nature Immunology. 2005 Mar 6;6(3):271–9.
54. Bartholomaeus P, Semmler LY, Bukur T, Boisguerin V, Römer PS, Tabares P, et al. Cell contact-dependent priming and Fc interaction with CD32+ immune cells contribute to the TGN1412-triggered cytokine response. Journal of immunology (Baltimore, Md : 1950). 2014 Mar 1;192(5):2091–8.
55. Hussain K, Hargreaves CE, Roghanian A, Oldham RJ, Claude Chan HT, Mockridge CI, et al. Upregulation of FcγRIIb on monocytes is necessary to promote the superagonist activity of TGN1412. Blood. 2015 Jan 1;125(1):102–10.
56. Dudek S, Weißmüller S, Anzaghe M, Miller L, Sterr S, Hoffmann K, et al. Human Fcγ receptors compete for TGN1412 binding that determines the antibody's effector function. European journal of immunology. 2019 Jul 1;49(7):1117–26.
57. Paluch C, Santos AM, Anzilotti C, Cornall RJ, Davis SJ. Immune checkpoints as therapeutic targets in autoimmunity. Frontiers in Immunology. 2018 Oct 8;9(OCT):2306.
58. Suzuki K, Tajima M, Tokumaru Y, Oshiro Y, Nagata S, Kamada H, et al. Anti-PD-1 antibodies recognizing the membrane-proximal region are PD-1 agonists that can down-regulate inflammatory diseases. Science immunology. 2023 Jan 13;8(79):eadd4947.
59. Barr AJ, Ugochukwu E, Lee WH, King ONF, Filippakopoulos P, Alfano I, et al. Large-Scale Structural Analysis of the Classical Human Protein Tyrosine Phosphatome. Cell. 2009 Jan 23;136(2):352–63.
60. Saxton RA, Glassman CR, Garcia KC. Emerging principles of cytokine pharmacology and therapeutics. Nature Reviews Drug Discovery 2022 22:1. 2022 Sep 21;22(1):21–37.
61. Zheng X, Wu Y, Bi J, Huang Y, Cheng Y, Li Y, et al. The use of supercytokines, immunocytokines, engager cytokines, and other synthetic cytokines in immunotherapy. Cellular & Molecular Immunology 2021 19:2. 2022 Jan 4;19(2):192–209.
62. Villarino A V., Kanno Y, O'Shea JJ. Mechanisms and consequences of Jak-STAT signaling in the immune system. Nature Immunology. 2017 Mar 22;18(4):374–84.
63. Chow D chone, He X lin, Snow AL, Rose-John S, Garcia KC. Structure of an Extracellular gp130 Cytokine Receptor Signaling Complex. Science. 2001 Mar 16;291(5511):2150 LP – 2155.
64. Saharinen P, Silvennoinen O. The pseudokinase domain is required for suppression of basal activity of Jak2 and Jak3 tyrosine kinases and for cytokine-inducible

activation of signal transduction. Journal of Biological Chemistry. 2002 Dec 6;277(49):47954–63.
65. Lupardus PJ, Ultsch M, Wallweber H, Kohli PB, Johnson AR, Eigenbrot C. Structure of the pseudokinase-kinase domains from protein kinase TYK2 reveals a mechanism for Janus kinase (JAK) autoinhibition. Proceedings of the National Academy of Sciences of the United States of America. 2014 Jun 3;111(22):8025–30.
66. Saharinen P, Takaluoma K, Silvennoinen O. Regulation of the Jak2 Tyrosine Kinase by Its Pseudokinase Domain. Molecular and Cellular Biology. 2000 May 1;20(10):3387.
67. Cunningham BC, Ultsch M, De Vos AM, Mulkerrin MG, Clauser KR, Wells JA. Dimerization of the extracellular domain of the human growth hormone receptor by a single hormone molecule. Science (New York, NY). 1991;254(5033):821–5.
68. Brooks AJ, Dai W, O'Mara ML, Abankwa D, Chhabra Y, Pelekanos RA, et al. Mechanism of activation of protein kinase JAK2 by the growth hormone receptor. Science. 2014 May 16;344(6185).
69. Wilmes S, Hafer M, Vuorio J, Tucker JA, Winkelmann H, Löchte S, et al. Mechanism of homodimeric cytokine receptor activation and dysregulation by oncogenic mutations. Science. 2020 Feb 7;367(6478):643–52.
70. Caveney NA, Saxton RA, Waghray D, Glassman CR, Tsutsumi N, Hubbard SR, et al. Structural basis of Janus kinase trans-activation. Cell Reports. 2023 Mar 28;42(3).
71. Glassman CR, Tsutsumi N, Saxton RA, Lupardus PJ, Jude KM, Christopher Garcia K. Structure of a Janus kinase cytokine receptor complex reveals the basis for dimeric activation. Science. 2022 Apr 8;376(6589).
72. Levy DE, Darnell JE. STATs: transcriptional control and biological impact. Nature Reviews Molecular Cell Biology 2002 3:9. 2002;3(9):651–62.
73. Morris R, Kershaw NJ, Babon JJ. The molecular details of cytokine signaling via the JAK/STAT pathway. Protein Science. 2018 Dec 1;27(12):1984–2009.
74. Hu X, li J, Fu M, Zhao X, Wang W. The JAK/STAT signaling pathway: from bench to clinic. Signal Transduction and Targeted Therapy 2021 6:1. 2021 Nov 26;6(1):1–33.
75. Kershaw NJ, Murphy JM, Liau NPD, Varghese LN, Laktyushin A, Whitlock EL, et al. SOCS3 binds specific receptor-JAK complexes to control cytokine signaling by direct kinase inhibition. Nature structural & molecular biology. 2013 May;20(4):469–76.
76. Böhmer FD, Friedrich K. Protein tyrosine phosphatases as wardens of STAT signaling. 2014;
77. Irie-Sasaki J, Sasaki T, Matsumoto W, Opavsky A, Cheng M, Welstead G, et al. CD45 is a JAK phosphatase and negatively regulates cytokine receptor signalling. Nature. 2001 Jan 18;409(6818):349–54.
78. Ghoreschi K, Laurence A, O'Shea JJ. Janus kinases in immune cell signaling. Immunological Reviews. 2009;228(1):273–87.
79. Kojima R, Scheller L, Fussenegger M. Nonimmune cells equipped with T-cell-receptor-like signaling for cancer cell ablation. Nature Chemical Biology. 2018;14(1):42–9.
80. Boyman O, Kovar M, Rubinstein MP, Surh CD, Sprent J. Selective stimulation of T cell subsets with antibody-cytokine immune complexes. Science. 2006 Mar 31;311(5769):1924–7.

81. Létourneau S, Van Leeuwen EMM, Krieg C, Martin C, Pantaleo G, Sprent J, et al. IL-2/anti-IL-2 antibody complexes show strong biological activity by avoiding interaction with IL-2 receptor α subunit CD25. Proceedings of the National Academy of Sciences of the United States of America. 2010 Feb 2;107(5):2171.
82. VanDyke D, Iglesias M, Tomala J, Young A, Smith J, Perry JA, et al. Engineered human cytokine/antibody fusion proteins expand regulatory T cells and confer autoimmune disease protection. Cell Reports. 2022 Oct 18;41(3):20.
83. Guo Y, Kang W, Zhong Y, Li R, Li G, Shen Y, et al. Purification and characterization of human IL-10/Fc fusion protein expressed in Pichia pastoris. Protein Expression and Purification. 2012 Jun 1;83(2):152–6.
84. Zheng X, Steele A, Hancock W, Stevens A, Nickerson P, Roy-Chaudhury P, et al. A noncytolytic IL-10/Fc fusion protein prevents diabetes, blocks autoimmunity, and promotes suppressor phenomena in NOD mice. J Immunol. 1997;158(9):4507–13.
85. Gillies SD. A new platform for constructing antibody-cytokine fusion proteins (immunocytokines) with improved biological properties and adaptable cytokine activity. Protein Engineering, Design and Selection. 2013 Oct 1;26(10):561–9.
86. Kuehn HS, Ouyang W, Lo B, Deenick EK, Niemela JE, Avery DT, et al. Immune dysregulation in human subjects with heterozygous germline mutations in CTLA4. Science (New York, NY). 2014 Sep 9;345(6204):1623.
87. Tivol EA, Borriello F, Schweitzer AN, Lynch WP, Bluestone JA, Sharpe AH. Loss of CTLA-4 leads to massive lymphoproliferation and fatal multiorgan tissue destruction, revealing a critical negative regulatory role of CTLA-4. Immunity. 1995;3(5):541–7.
88. Lee YH, Bae SC, Kim JH, Song GG. Metaanalyse von Genpolymorphismen beim programmierten Zelltod 1: Assoziationen mit der Suzeptibiliät für rheumatoide Arthritis, ankylosierende Spondylitis und Typ-1-Diabetes. Zeitschrift fur Rheumatologie. 2015 Apr 1;74(3):230–9.
89. Dong H, Strome SE, Matteson EL, Moder KG, Flies DB, Zhu G, et al. Costimulating aberrant T cell responses by B7-H1 autoantibodies in rheumatoid arthritis. The Journal of clinical investigation. 2003;111(3):363–70.
90. Nishimura H, Nose M, Hiai H, Minato N, Honjo T. Development of lupus-like autoimmune diseases by disruption of the PD-1 gene encoding an ITIM motif-carrying immunoreceptor. Immunity. 1999 Aug 1;11(2):141–51.
91. Nishimura H, Okazaki T, Tanaka Y, Nakatani K, Hara M, Matsumori A, et al. Autoimmune dilated cardiomyopathy in PD-1 receptor-deficient mice. Science. 2001 Jan 12;291(5502):319–22.
92. Lin SC, Kuo CC, Chan CH. Association of a BTLA gene polymorphism with the risk of rheumatoid arthritis. Journal of Biomedical Science. 2006 Nov 6;13(6):853–60.
93. Watanabe N, Oki M, Owada T, Oya Y, Ikeda K, Saito Y, et al. A Functional Polymorphism in B and T Lymphocyte Attenuator Is Associated with Susceptibility to Rheumatoid Arthritis. Clinical and Developmental Immunology. 2011;2011.
94. Sawaf M, Fauny JD, Felten R, Sagez F, Gottenberg JE, Dumortier H, et al. Defective BTLA functionality is rescued by restoring lipid metabolism in lupus CD4+ T cells. JCI Insight. 2018 Jul 12;3(13).
95. Oya Y, Watanabe N, Owada T, Oki M, Hirose K, Suto A, et al. Development of Autoimmune Hepatitis-like Disease and Autoantibody Production to Nuclear Antigens in Mice Lacking B and T Lymphocyte Attenuator (BTLA). Arthritis and rheumatism. 2008 Aug;58(8):2498.

96. Joller N, Hafler JP, Brynedal B, Kassam N, Spoerl S, Levin SD, et al. Cutting edge: TIGIT has T cell-intrinsic inhibitory functions. Journal of immunology (Baltimore, Md : 1950). 2011 Feb 1;186(3):1338–42.
97. Lucca LE, Axisa PP, Singer ER, Nolan NM, Dominguez-Villar M, Hafler DA. TIGIT signaling restores suppressor function of Th1 Tregs. JCI Insight. 2019 Feb 2;4(3).
98. Deng Y, Huang F, Wang J. A narrative review of PD-1 and autoimmune diseases. Annals of Blood. 2022 Sep 1;7(0).
99. Ning Z, Liu K, Xiong H. Roles of BTLA in Immunity and Immune Disorders. Frontiers in Immunology. 2021 Mar 29;12:990.
100. Yue C, Gao S, Li S, Xing Z, Qian H, Hu Y, et al. TIGIT as a Promising Therapeutic Target in Autoimmune Diseases. Frontiers in Immunology. 2022 Jun 3;13:2848.
101. Kühn R, Löhler J, Rennick D, Rajewsky K, Müller W. Interleukin-10-deficient mice develop chronic enterocolitis. Cell. 1993 Oct;75(2):263–74.
102. Glocker EO, Kotlarz D, Klein C, Shah N, Grimbacher B. IL-10 and IL-10 receptor defects in humans. Annals of the New York Academy of Sciences. 2011;1246(1):102–7.
103. Glocker EO, Kotlarz D, Boztug K, Gertz EM, Schäffer AA, Noyan F, et al. Inflammatory Bowel Disease and Mutations Affecting the Interleukin-10 Receptor A bs tr ac t. N Engl J Med. 2009;361:2033–78.
104. Moran CJ, Walters TD, Guo CH, Kugathasan S, Klein C, Turner D, et al. IL-10R polymorphisms are associated with very-early-onset ulcerative colitis. Inflammatory Bowel Diseases. 2013 Jan;19(1):115–23.
105. Engelhardt KR, Grimbacher B. IL-10 in humans: Lessons from the Gut, IL-10/IL-10 receptor deficiencies, and IL-10 polymorphisms. Current Topics in Microbiology and Immunology. 2014;380:1–18.
106. Ouyang W, Rutz S, Crellin NK, Valdez PA, Hymowitz SG. Regulation and Functions of the IL-10 Family of Cytokines in Inflammation and Disease. https://doi.org/101146/annurev-immunol-031210-101312. 2011 Mar 22;29:71–109.
107. Mortaz E, Tabarsi P, Mansouri D, Khosravi A, Garssen J, Velayati A, et al. Cancers Related to Immunodeficiencies: Update and Perspectives. Frontiers in Immunology. 2016 Sep 20;7(SEP):1.
108. Jiang T, Zhou C, Ren S. Role of IL-2 in cancer immunotherapy. Oncoimmunology. 2016 Jun 2;5(6).
109. Robert C, Long G V., Brady B, Dutriaux C, Maio M, Mortier L, et al. Nivolumab in Previously Untreated Melanoma without BRAF Mutation . New England Journal of Medicine. 2015 Jan 22;372(4):320–30.
110. Hodi FS, O'Day SJ, McDermott DF, Weber RW, Sosman JA, Haanen JB, et al. Improved Survival with Ipilimumab in Patients with Metastatic Melanoma. New England Journal of Medicine. 2010 Aug 19;363(8):711–23.
111. Conroy M, Naidoo J. Immune-related adverse events and the balancing act of immunotherapy. Nature Communications 2022 13:1. 2022 Jan 19;13(1):1–4.
112. Edner NM, Carlesso G, Rush JS, Walker LSK. Targeting co-stimulatory molecules in autoimmune disease. Nature Reviews Drug Discovery 2020 19:12. 2020 Sep 16;19(12):860–83.
113. Patsoukis N, Wang Q, Strauss L, Boussiotis VA. Revisiting the PD-1 pathway. Science Advances. 2020 Sep 1;6(38).
114. Okazaki T, Chikuma S, Iwai Y, Fagarasan S, Honjo T. A rheostat for immune responses: the unique properties of PD-1 and their advantages for clinical application. Nature Immunology 2013 14:12. 2013 Nov 15;14(12):1212–8.

115. Bally APR, Austin JW, Boss JM. Genetic and epigenetic regulation of PD-1 expression. Journal of immunology (Baltimore, Md : 1950). 2016 Mar 3;196(6):2431.
116. Agata Y, Kawasaki A, Nishimura H, Ishida Y, Tsubata T, Yagita H, et al. Expression of the PD-1 antigen on the surface of stimulated mouse T and B lymphocytes. International Immunology. 1996 May 1;8(5):765–72.
117. Xu X, Hou B, Fulzele A, Masubuchi T, Zhao Y, Wu Z, et al. PD-1 and BTLA regulate T cell signaling differentially and only partially through SHP1 and SHP2. The Journal of Cell Biology. 2020 Jun 6;219(6).
118. Xu X, Masubuchi T, Cai Q, Zhao Y, Hui E. Molecular features underlying differential SHP1/SHP2 binding of immune checkpoint receptors. eLife. 2021 Nov 1;10.
119. Hui E, Cheung J, Zhu J, Su X, Taylor MJ, Wallweber HA, et al. T cell costimulatory receptor CD28 is a primary target for PD-1–mediated inhibition. Science (New York, NY). 2017 Mar 3;355(6332):1428.
120. Wang L, Pino-Lagos K, De Vries VC, Guleria I, Sayegh MH, Noelle RJ. Programmed death 1 ligand signaling regulates the generation of adaptive Foxp3+CD4+ regulatory T cells. Proceedings of the National Academy of Sciences of the United States of America. 2008 Jul 8;105(27):9331–6.
121. Stathopoulou C, Gangaplara A, Mallett G, Flomerfelt FA, Liniany LP, Knight D, et al. PD-1 Inhibitory Receptor Downregulates Asparaginyl Endopeptidase and Maintains Foxp3 Transcription Factor Stability in Induced Regulatory T Cells. Immunity. 2018 Aug 21;49(2):247-263.e7.
122. Shi J, Hou S, Fang Q, Liu X, Liu X, Qi H. PD-1 Controls Follicular T Helper Cell Positioning and Function. Immunity. 2018 Aug 8;49(2):264.
123. Good-Jacobson KL, Szumilas CG, Chen L, Sharpe AH, Tomayko MM, Shlomchik MJ. PD-1 regulates germinal center B cell survival and the formation and affinity of long-lived plasma cells. Nature Immunology 2010 11:6. 2010 May 9;11(6):535–42.
124. Lu J, Wu J, Mao L, Xu H, Wang S. Revisiting PD-1/PD-L pathway in T and B cell response: Beyond immunosuppression. Cytokine & Growth Factor Reviews. 2022 Oct 1;67:58–65.
125. Wang G, Hu P, Yang J, Shen G, Wu X. The effects of PDL-Ig on collagen-induced arthritis. Rheumatology International. 2011 Apr 25;31(4):513–9.
126. Raptopoulou AP, Bertsias G, Makrygiannakis D, Verginis P, Kritikos I, Tzardi M, et al. The programmed death 1/programmed death ligand 1 inhibitory pathway is up-regulated in rheumatoid synovium and regulates peripheral T cell responses in human and murine arthritis. Arthritis and rheumatism. 2010 Jul;62(7):1870–80.
127. Song MY, Hong CP, Park SJ, Kim JH, Yang BG, Park Y, et al. Protective effects of Fc-fused PD-L1 on two different animal models of colitis. Gut. 2015 Feb 1;64(2):260–71.
128. Bryan CM, Rocklin GJ, Bick MJ, Ford A, Majri-Morrison S, Kroll A V., et al. Computational design of a synthetic PD-1 agonist. Proceedings of the National Academy of Sciences of the United States of America. 2021 Jul 20;118(29):e2102164118.
129. Curnock AP, Bossi G, Kumaran J, Bawden LJ, Figueiredo R, Tawar R, et al. Cell-targeted PD-1 agonists that mimic PD-L1 are potent T cell inhibitors. JCI Insight. 2021 Oct 22;6(20).
130. Helou DG, Shafiei-Jahani P, Lo R, Howard E, Hurrell BP, Galle-Treger L, et al. PD-1 pathway regulates ILC2 metabolism and PD-1 agonist treatment ameliorates

airway hyperreactivity. Nature Communications 2020 11:1. 2020 Aug 10;11(1):1–15.
131. Kasagi S, Kawano S, Okazaki T, Honjo T, Morinobu A, Hatachi S, et al. Anti-Programmed Cell Death 1 Antibody Reduces CD4+PD-1+ T Cells and Relieves the Lupus-Like Nephritis of NZB/W F1 Mice. The Journal of Immunology. 2010 Mar 1;184(5):2337–47.
132. Watanabe N, Gavrieli M, Sedy JR, Yang J, Fallarino F, Loftin SK, et al. BTLA is a lymphocyte inhibitory receptor with similarities to CTLA-4 and PD-1. Nature Immunology. 2003 Jul 8;4(7):670–9.
133. Ning Z, Liu K, Xiong H. Roles of BTLA in Immunity and Immune Disorders. Frontiers in Immunology. 2021 Mar 29;12:990.
134. Fuertes Marraco SA, Neubert NJ, Verdeil G, Speiser DE. Inhibitory receptors beyond T cell exhaustion. Frontiers in Immunology. 2015 Jun 26;6(JUN):310.
135. Hurchla MA, Sedy JR, Gavrielli M, Drake CG, Murphy TL, Murphy KM. B and T lymphocyte attenuator exhibits structural and expression polymorphisms and is highly Induced in anergic CD4+ T cells. Journal of immunology (Baltimore, Md : 1950). 2005 Mar 15;174(6):3377–85.
136. Sedy JR, Gavrieli M, Potter KG, Hurchla MA, Lindsley RC, Hildner K, et al. B and T lymphocyte attenuator regulates T cell activation through interaction with herpesvirus entry mediator. Nature Immunology 2004 6:1. 2004 Nov 28;6(1):90–8.
137. Murphy TL, Murphy KM. Slow Down and Survive: Enigmatic Immunoregulation by BTLA and HVEM. Annual Review of Immunology. 2010 Mar;28(1):389–411.
138. Rodriguez-Barbosa JI, Schneider P, Weigert A, Lee KM, Kim TJ, Perez-Simon JA, et al. HVEM, a cosignaling molecular switch, and its interactions with BTLA, CD160 and LIGHT. Cellular & Molecular Immunology 2019 16:7. 2019 Jun 3;16(7):679–82.
139. Cai G, Anumanthan A, Brown JA, Greenfield EA, Zhu B, Freeman GJ. CD160 inhibits activation of human CD4+ T cells through interaction with herpesvirus entry mediator. Nature Immunology 2008 9:2. 2008 Jan 13;9(2):176–85.
140. Gonzalez LC, Loyet KM, Calemine-Fenaux J, Chauhan V, Wranik B, Ouyang W, et al. A coreceptor interaction between the CD28 and TNF receptor family members B and T lymphocyte attenuator and herpesvirus entry mediator. Proceedings of the National Academy of Sciences of the United States of America. 2005 Jan 1;102(4):1116.
141. Cheung TC, Oborne LM, Steinberg MW, Macauley MG, Fukuyama S, Sanjo H, et al. T cell intrinsic heterodimeric complexes between HVEM and BTLA determine receptivity to the surrounding microenvironment. Journal of immunology (Baltimore, Md : 1950). 2009 Dec 1;183(11):7286–96.
142. Battin C, Leitner J, Waidhofer-Söllner P, Grabmeier-Pfistershammer K, Olive D, Steinberger P. BTLA inhibition has a dominant role in the cis-complex of BTLA and HVEM. Frontiers in Immunology. 2022 Aug 23;13:4831.
143. Gavrieli M, Watanabe N, Loftin SK, Murphy TL, Murphy KM. Characterization of phosphotyrosine binding motifs in the cytoplasmic domain of B and T lymphocyte attenuator required for association with protein tyrosine phosphatases SHP-1 and SHP-2. Biochemical and Biophysical Research Communications. 2003 Dec 26;312(4):1236–43.
144. Gavrieli M, Murphy KM. Association of Grb-2 and PI3K p85 with phosphotyrosile peptides derived from BTLA. Biochemical and biophysical research communications. 2006 Jul 14;345(4):1440–5.

145. Hurchla MA, Sedy JR, Murphy KM. Unexpected role of B and T lymphocyte attenuator in sustaining cell survival during chronic allostimulation. Journal of immunology (Baltimore, Md : 1950). 2007 May 15;178(10):6073–82.
146. Han P, Goularte OD, Rufner K, Wilkinson B, Kaye J. An Inhibitory Ig Superfamily Protein Expressed by Lymphocytes and APCs Is Also an Early Marker of Thymocyte Positive Selection. The Journal of Immunology. 2004 May 15;172(10):5931–9.
147. Grabmeier-Pfistershammer K, Stecher C, Zettl M, Rosskopf S, Rieger A, Zlabinger GJ, et al. Antibodies targeting BTLA or TIM-3 enhance HIV-1 specific T cell responses in combination with PD-1 blockade. Clinical Immunology. 2017 Oct 1;183:167–73.
148. Otsuki N, Kamimura Y, Hashiguchi M, Azuma M. Expression and function of the B and T lymphocyte attenuator (BTLA/CD272) on human T cells. Biochemical and Biophysical Research Communications. 2006 Jun 16;344(4):1121–7.
149. Bekiaris V, Šedý JR, Macauley MG, Rhode-Kurnow A, Ware CF. The Inhibitory Receptor BTLA Controls γδ T Cell Homeostasis and Inflammatory Responses. Immunity. 2013 Dec 12;39(6):1082–94.
150. Stienne C, Virgen-Slane R, Elmé L, Murphy KM, Ware CF, Sedy´correspondence JR, et al. Btla signaling in conventional and regulatory lymphocytes coordinately tempers humoral immunity in the intestinal mucosa. CellReports. 2022;38:110553.
151. Vendel AC, Calemine-Fenaux J, Izrael-Tomasevic A, Chauhan V, Arnott D, Eaton DL. B and T Lymphocyte Attenuator Regulates B Cell Receptor Signaling by Targeting Syk and BLNK. The Journal of Immunology. 2009 Feb 1;182(3):1509–17.
152. Kashiwakuma D, Suto A, Hiramatsu Y, Ikeda K, Takatori H, Suzuki K, et al. B and T Lymphocyte Attenuator Suppresses IL-21 Production from Follicular Th Cells and Subsequent Humoral Immune Responses. The Journal of Immunology. 2010 Sep 1;185(5):2730–6.
153. Mintz MA, Felce JH, Chou MY, Mayya V, Xu Y, Shui JW, et al. The HVEM-BTLA Axis Restrains T Cell Help to Germinal Center B Cells and Functions as a Cell-Extrinsic Suppressor in Lymphomagenesis. Immunity. 2019 Aug 20;51(2):310-323.e7.
154. Kobayashi Y, Iwata A, Suzuki K, Suto A, Kawashima S, Saito Y, et al. B and T lymphocyte attenuator inhibits LPS-induced endotoxic shock by suppressing Toll-like receptor 4 signaling in innate immune cells. Proceedings of the National Academy of Sciences of the United States of America. 2013 Mar 26;110(13):5121–6.
155. Zhang JA, Lu Y Bin, Wang WD, Liu G Bin, Chen C, Shen L, et al. BTLA-Expressing Dendritic Cells in Patients With Tuberculosis Exhibit Reduced Production of IL-12/IFN-α and Increased Production of IL-4 and TGF-β, Favoring Th2 and Foxp3+ Treg Polarization. Frontiers in Immunology. 2020 Mar 31;11:518.
156. Brown GR, Lee EL, El-Hayek J, Kintner K, Luck C. IL-12-Independent LIGHT Signaling Enhances MHC Class II Disparate CD4+ T Cell Alloproliferation, IFN-γ Responses, and Intestinal Graft-versus-Host Disease. The Journal of Immunology. 2005 Apr 15;174(8):4688–95.
157. Ye Q, Fraser CC, Gao W, Wang L, Busfield SJ, Wang C, et al. Modulation of LIGHT-HVEM costimulation prolongs cardiac allograft survival. The Journal of experimental medicine. 2002 Mar 18;195(6):795–800.
158. Pierer M, Schulz A, Rossol M, Kendzia E, Kyburz D, Haentzschel H, et al. Herpesvirus entry mediator-Ig treatment during immunization aggravates

rheumatoid arthritis in the collagen-induced arthritis model. Journal of immunology (Baltimore, Md : 1950). 2009 Mar 1;182(5):3139–45.
159. Albring JC, Sandau MM, Rapaport AS, Edelson BT, Satpathy A, Mashayekhi M, et al. Targeting of B and T lymphocyte associated (BTLA) prevents graft-versus-host disease without global immunosuppression. The Journal of experimental medicine. 2010 Nov 22;207(12):2551–9.
160. Sakoda Y, Park JJ, Zhao Y, Kuramasu A, Geng D, Liu Y, et al. Dichotomous regulation of GVHD through bidirectional functions of the BTLA-HVEM pathway. Blood. 2011 Feb 24;117(8):2506–14.
161. Uchiyama M, Jin X, Matsuda H, Bashuda H, Imazuru T, Shimokawa T, et al. An agonistic anti-BTLA mAb (3C10) induced generation of IL-10-dependent regulatory CD4+ T cells and prolongation of murine cardiac allograft. Transplantation. 2014 Feb 15;97(3):301–9.
162. Douna H, Amersfoort J, Schaftenaar FH, Kröner MJ, Kiss MG, Slütter B, et al. B- and T-lymphocyte attenuator stimulation protects against atherosclerosis by regulating follicular B cells. Cardiovascular Research. 2020 Feb 1;116(2):295–305.
163. Nakagomi D, Suzuki K, Hosokawa J, Kobayashi Y, Suto A, Takatori H, et al. Therapeutic potential of B and T lymphocyte attenuator expressed on CD8+ T cells for contact hypersensitivity. Journal of Investigative Dermatology. 2013 Mar 1;133(3):702–11.
164. Gao J, Zheng Q, Xin N, Wang W, Zhao C. CD155, an onco-immunologic molecule in human tumors. Cancer Science. 2017 Oct 1;108(10):1934–8.
165. Meyer D, Seth S, Albrecht J, Maier MK, Du Pasquier L, Ravens I, et al. CD96 interaction with CD155 via its first Ig-like domain is modulated by alternative splicing or mutations in distal Ig-like domains. Journal of Biological Chemistry. 2009 Jan 23;284(4):2235–44.
166. Yu X, Harden K, Gonzalez LC, Francesco M, Chiang E, Irving B, et al. The surface protein TIGIT suppresses T cell activation by promoting the generation of mature immunoregulatory dendritic cells. Nature Immunology 2008 10:1. 2008 Nov 16;10(1):48–57.
167. Stanietsky N, Rovis TL, Glasner A, Seidel E, Tsukerman P, Yamin R, et al. Mouse TIGIT inhibits NK-cell cytotoxicity upon interaction with PVR. European Journal of Immunology. 2013 Aug 1;43(8):2138–50.
168. Johnston RJ, Comps-Agrar L, Hackney J, Yu X, Huseni M, Yang Y, et al. The Immunoreceptor TIGIT Regulates Antitumor and Antiviral CD8+ T Cell Effector Function. Cancer Cell. 2014 Dec 8;26(6):923–37.
169. Zhu Y, Paniccia A, Schulick AC, Chen W, Koenig MR, Byers JT, et al. Identification of CD112R as a novel checkpoint for human T cells. The Journal of Experimental Medicine. 2016 Feb 2;213(2):167.
170. Challita-Eid PM, Satpayev D, Yang P, An Z, Morrison K, Shostak Y, et al. Enfortumab Vedotin Antibody-Drug Conjugate Targeting Nectin-4 Is a Highly Potent Therapeutic Agent in Multiple Preclinical Cancer Models. Cancer research. 2016 May 15;76(10):3003–13.
171. Reches A, Ophir Y, Stein N, Kol I, Isaacson B, Charpak Amikam Y, et al. Nectin4 is a novel TIGIT ligand which combines checkpoint inhibition and tumor specificity. Journal for Immunotherapy of Cancer. 2020 Jun 4;8(1):266.
172. Li M, Xia P, Du Y, Liu S, Huang G, Chen J, et al. T-cell immunoglobulin and ITIM domain (TIGIT) receptor/poliovirus receptor (PVR) ligand engagement suppresses interferon-γ production of natural killer cells via β-arrestin 2-mediated negative signaling. Journal of Biological Chemistry. 2014 Jun 20;289(25):17647–57.

173. Liu S, Zhang H, Li M, Hu D, Li C, Ge B, et al. Recruitment of Grb2 and SHIP1 by the ITT-like motif of TIGIT suppresses granule polarization and cytotoxicity of NK cells. Cell Death & Differentiation 2013 20:3. 2012 Nov 16;20(3):456–64.
174. Gur C, Ibrahim Y, Isaacson B, Yamin R, Abed J, Gamliel M, et al. Binding of the Fap2 protein of fusobacterium nucleatum to human inhibitory receptor TIGIT protects tumors from immune cell attack. Immunity. 2015 Feb 17;42(2):344–55.
175. Joller N, Lozano E, Burkett PR, Patel B, Xiao S, Zhu C, et al. Treg cells expressing the coinhibitory molecule TIGIT selectively inhibit proinflammatory Th1 and Th17 cell responses. Immunity. 2014 Apr 17;40(4):569–81.
176. Dixon KO, Schorer M, Nevin J, Etminan Y, Amoozgar Z, Kondo T, et al. Functional Anti-TIGIT Antibodies Regulate Development of Autoimmunity and Antitumor Immunity. The Journal of Immunology. 2018 Apr 15;200(8):3000–7.
177. Antoniv TT, Ivashkiv LB. Interleukin-10-induced gene expression and suppressive function are selectively modulated by the PI3K-Akt-GSK3 pathway. Immunology. 2011 Apr 1;132(4):567–77.
178. Zhu YP, Brown JR, Sag D, Zhang L, Suttles J. Adenosine 5′-Monophosphate–Activated Protein Kinase Regulates IL-10–Mediated Anti-Inflammatory Signaling Pathways in Macrophages. The Journal of Immunology. 2015 Jan 15;194(2):584–94.
179. Fiorentino DF, Zlotnik A, Mosmann TR, Howard M, O'Garra A. IL-10 inhibits cytokine production by activated macrophages. Journal of immunology (Baltimore, Md : 1950). 1991 Dec 1;147(11):3815–22.
180. Waal Malefyt R De, Haanen J, Spits H, Koncarolo MG, Te Velde A, Figdor C, et al. Interleukin 10 (IL-10) and viral IL-10 strongly reduce antigen-specific human T cell proliferation by diminishing the antigen-presenting capacity of monocytes via downregulation of class II major histocompatibility complex expression. Journal of Experimental Medicine. 1991 Oct 1;174(4):915–24.
181. Bogdan C, Vodovotz Y, Nathan C. Macrophage deactivation by interleukin 10. Journal of Experimental Medicine. 1991 Dec 1;174(6):1549–55.
182. Ding L, Shevach' EM. IL-10 INHIBITS MITOGEN-INDUCED T CELL PROLIFERATION BY SELECTIVELY INHIBITING MACROPHAGE COSTIMULATORY FUNCTION. 1992;
183. Lang R, Patel D, Morris JJ, Rutschman RL, Murray PJ. Shaping Gene Expression in Activated and Resting Primary Macrophages by IL-10. The Journal of Immunology. 2002 Sep 1;169(5):2253–63.
184. Conaway EA, de Oliveira DC, McInnis CM, Snapper SB, Horwitz BH. Inhibition of Inflammatory Gene Transcription by IL-10 Is Associated with Rapid Suppression of Lipopolysaccharide-Induced Enhancer Activation. The Journal of Immunology. 2017 Apr 1;198(7):2906–15.
185. Cassatella MA, Meda L, Bonora S, Ceska M, Constantin G. Interleukin 10 (IL-10) inhibits the release of proinflammatory cytokines from human polymorphonuclear leukocytes. Evidence for an autocrine role of tumor necrosis factor and IL-1 beta in mediating the production of IL-8 triggered by lipopolysaccharide. Journal of Experimental Medicine. 1993 Dec 1;178(6):2207–11.
186. De Smedt T, Van Mechelen M, De Becker G, Urbain J, Leo O, Moser M. Effect of interleukin-10 on dendritic cell maturation and function. European journal of immunology. 1997;27(5):1229–35.
187. Bhattacharyya S, Sen P, Wallet M, Long B, Baldwin AS, Tisch R. Immunoregulation of dendritic cells by IL-10 is mediated through suppression of

the PI3K/Akt pathway and of IκB kinase activity. Blood. 2004 Aug 15;104(4):1100–9.
188. Grünig G, Corry DB, Leach MW, Seymour BWP, Kurup VP, Rennick DM. Interleukin-10 Is a Natural Suppressor of Cytokine Production and Inflammation in a Murine Model of Allergic Bronchopulmonary Aspergillosis. Journal of Experimental Medicine. 1997 Mar 17;185(6):1089–100.
189. Coomes SM, Kannan Y, Pelly VS, Entwistle LJ, Guidi R, Perez-Lloret J, et al. CD4 + Th2 cells are directly regulated by IL-10 during allergic airway inflammation. Mucosal Immunology. 2017 Jan 1;10(1):150–61.
190. Huber S, Gagliani N, Esplugues E, O'Connor W, Huber FJ, Chaudhry A, et al. Th17 Cells Express Interleukin-10 Receptor and Are Controlled by Foxp3- and Foxp3+ Regulatory CD4+ T Cells in an Interleukin-10-Dependent Manner. Immunity. 2011 Apr 22;34(4):554–65.
191. Kamanaka M, Huber S, Zenewicz LA, Gagliani N, Rathinam C, O'Connor W, et al. Memory/effector (CD45RBlo) CD4 T cells are controlled directly by IL-10 and cause IL-22–dependent intestinal pathology. Journal of Experimental Medicine. 2011 May 9;208(5):1027–40.
192. Murai M, Turovskaya O, Kim G, Cheroutre H, Kronenberg M, Madan R. Interleukin 10 acts on regulatory t cells to maintain expression of the transcription factor foxp3 and suppressive function in mice with colitis. Nature Immunology. 2009;10(11):1178–84.
193. Chaudhry A, Samstein RM, Treuting P, Liang Y, Pils MC, Heinrich JM, et al. Interleukin-10 Signaling in Regulatory T Cells Is Required for Suppression of Th17 Cell-Mediated Inflammation. Immunity. 2011 Apr 22;34(4):566–78.
194. Groux H, Bigler M, de Vries JE, Roncarolo MG. Inhibitory and Stimulatory Effects of IL-10 on Human CD8+ T Cells. The Journal of Immunology. 1998 Apr 1;160(7):3188–93.
195. Mumm JB, Emmerich J, Zhang X, Chan I, Wu L, Mauze S, et al. IL-10 Elicits IFNγ-Dependent tumor immune surveillance. Cancer Cell. 2011 Dec 13;20(6):781–96.
196. Naing A, Infante JR, Papadopoulos KP, Chan IH, Shen C, Ratti NP, et al. PEGylated IL-10 (Pegilodecakin) Induces Systemic Immune Activation, CD8+ T Cell Invigoration and Polyclonal T Cell Expansion in Cancer Patients. Cancer Cell. 2018 Nov 12;34(5):775-791.e3.
197. Itoh K, Hirohata S. The role of IL-10 in human B cell activation, proliferation and differention. J Immunol. 1995;154(9):4341–50.
198. Thompson-Snipes L, Dhar V, Bond MW, Mosmann TR, Moore KW, Rennick DM. Interleukin 10: a novel stimulatory factor for mast cells and their progenitors. Journal of Experimental Medicine. 1991 Feb 1;173(2):507–10.
199. Rousset F, Garcia E, Defrance T, Peronne C, Vezzio N, Hsu DH, et al. Interleukin 10 is a potent growth and differentiation factor for activated human B lymphocytes. Proceedings of the National Academy of Sciences. 1992 Mar 1;89(5):1890–3.
200. Saraiva M, Vieira P, O'Garra A. Biology and therapeutic potential of interleukin-10. Journal of Experimental Medicine. 2020 Jan 6;217(1).
201. Schreiber S, Fedorak RN, Nielsen OH, Wild G, Williams CN, Nikolaus S, et al. Safety and efficacy of recombinant human interleukin 10 in chronic active Crohn's disease. Gastroenterology. 2000 Dec 1;119(6):1461–72.
202. Colombel JF, Rutgeerts P, Malchow H, Jacyna M, Nielsen OH, Rask-Madsen J, et al. Interleukin 10 (Tenovil) in the prevention of postoperative recurrence of Crohn's disease. Gut. 2001 Jul 1;49(1):42–6.

203. Van Deventer SJH, Elson CO, Fedorak RN. Multiple doses of intravenous interleukin 10 in steroid-refractory Crohn's disease. Gastroenterology. 1997 Aug 1;113(2):383–9.
204. Fedorak RN, Gangl A, Elson CO, Rutgeerts P, Schreiber S, Wild G, et al. Recombinant human interleukin 10 in the treatment of patients with mild to moderately active Crohn's disease. Gastroenterology. 2000 Dec 1;119(6):1473–82.
205. Braat H, Rottiers P, Hommes DW, Huyghebaert N, Remaut E, Remon JP, et al. A Phase I Trial With Transgenic Bacteria Expressing Interleukin-10 in Crohn's Disease. Clinical Gastroenterology and Hepatology. 2006 Jun 1;4(6):754–9.
206. Steidler L, Hans W, Schotte L, Neirynck S, Obermeier F, Falk W, et al. Treatment of murine colitis by Lactococcus lactis secreting interleukin-10. Science. 2000 Aug 25;289(5483):1352–5.
207. McInnes IB, Illei GG, Danning CL, Yarboro CH, Crane M, Kuroiwa T, et al. IL-10 Improves Skin Disease and Modulates Endothelial Activation and Leukocyte Effector Function in Patients with Psoriatic Arthritis. The Journal of Immunology. 2001 Oct 1;167(7):4075–82.
208. Trachsel E, Bootz F, Silacci M, Kaspar M, Kosmehl H, Neri D. Antibody-mediated delivery of IL-10 inhibits the progression of established collagen-induced arthritis. Arthritis Research and Therapy. 2007 Jan 29;9(1):1–9.
209. Galeazzi M, Bazzichi2 L, Sebastiani GD, Neri D, Garcia Gonzalez E, Ravenni N, et al. A Phase IB Clinical Trial with Dekavil (F8-Il10), an Immunoregulatory "Armed Antibody" for the Treatment of Rheumatoid Arthritis, Used in Combination with Methotrexate. 2014;16.
210. Gorby C, Bellón JS, Wilmes S, Warda W, Pohler E, Fyfe PK, et al. Engineered il-10 variants elicit potent immunomodulatory effects at low ligand doses. Science Signaling. 2020 Sep 15;13(649):653.
211. Saxton RA, Tsutsumi N, Su LL, Abhiraman GC, Mohan K, Henneberg LT, et al. Structure-based decoupling of the pro- And anti-inflammatory functions of interleukin-10. Science. 2021 Mar 19;371(6535).
212. Pellerin L, Chen P, Gregori S, Hernandez-Hoyos G, Bacchetta R, Roncarolo MG. APVO210: A Bispecific Anti-CD86-IL-10 Fusion Protein (ADAPTIR^{TM}) to induce antigen-specific T regulatory type 1 cells. Frontiers in Immunology. 2018 May 25;9(MAY):25.
213. Aptevo Therapeutics Provides Corporate and Pipeline Update. Bloomberg. 2019 Oct 3;
214. Berman RM, Suzuki T, Tahara H, Robbins PD, Narula SK, Lotze MT. Systemic administration of cellular IL-10 induces an effective, specific, and long-lived immune response against established tumors in mice. The Journal of Immunology. 1996 Jul 1;157(1):231–8.
215. Zheng LM, Ojcius DM, Garaud F, Roth C, Maxwell E, Li Z, et al. Interleukin-10 inhibits tumor metastasis through an NK cell-dependent mechanism. Journal of Experimental Medicine. 1996 Aug 1;184(2):579–84.
216. Nemunaitis J, Fong T, Shabe P, Martineau D, Ando D. Comparison of Serum Interleukin-10 (IL-10) Levels Between Normal Volunteers and Patients with Advanced Melanoma. http://dx.doi.org/101081/CNV-100102550. 2001;19(3):239–47.
217. Mannino MH, Zhu Z, Xiao H, Bai Q, Wakefield MR, Fang Y. The paradoxical role of IL-10 in immunity and cancer. Cancer Letters. 2015 Oct 28;367(2):103–7.
218. Naing A, Wong DJ, Infante JR, Korn WM, Aljumaily R, Papadopoulos KP, et al. Pegilodecakin combined with pembrolizumab or nivolumab for patients with

advanced solid tumours (IVY): a multicentre, multicohort, open-label, phase 1b trial. The Lancet Oncology. 2019 Nov 1;20(11):1544–55.
219. Spigel D, Jotte R, Nemunaitis J, Shum M, Schneider J, Goldschmidt J, et al. Randomized Phase 2 Studies of Checkpoint Inhibitors Alone or in Combination With Pegilodecakin in Patients With Metastatic NSCLC (CYPRESS 1 and CYPRESS 2). Journal of Thoracic Oncology. 2021 Feb 1;16(2):327–33.
220. Hecht JR, Lonardi S, Bendell J, Sim HW, Macarulla T, Lopez CD, et al. Randomized Phase III Study of FOLFOX Alone or With Pegilodecakin as Second-Line Therapy in Patients With Metastatic Pancreatic Cancer That Progressed After Gemcitabine (SEQUOIA). Journal of Clinical Oncology. 2021 Apr 1;39(10):1108–18.
221. Cavallazzi Sebold B, Ni G, Li J, Li H, Liu X, Wang T. PEGylated IL-10: Clinical Development in Cancer Immunotherapy, Where to Go? Current Oncology Reports. 2023 Feb 1;25(2):115–22.
222. Kaplon H, Crescioli S, Chenoweth A, Visweswaraiah J, Reichert JM. Antibodies to watch in 2023. https://doi.org/101080/1942086220222153410. 2022 Dec 31;15(1).
223. Brinkmann U, Kontermann RE. mAbs The making of bispecific antibodies. 2017;
224. Kolfschoten MVDN, Schuurman J, Losen M, Bleeker WK, Martínez-Martínez P, Vermeulen E, et al. Anti-inflammatory activity of human IgG4 antibodies by dynamic Fab arm exchange. Science. 2007 Sep 14;317(5844):1554–7.
225. Schaefer W, Völger HR, Lorenz S, Imhof-Jung S, Regula JT, Klein C, et al. Heavy and light chain pairing of bivalent quadroma and knobs-into-holes antibodies analyzed by UHR-ESI-QTOF mass spectrometry. mAbs. 2016 Jan 1;8(1):49.
226. Dall'Acqua W, Simon AL, Mulkerrin MG, Carter P. Contribution of Domain Interface Residues to the Stability of Antibody CH3 Domain Homodimers. Biochemistry. 1998 Jun 30;37(26):9266–73.
227. Merchant AM, Zhu Z, Yuan JQ, Goddard A, Adams CW, Presta LG, et al. An efficient route to human bispecific IgG. Nature Biotechnology 1998 16:7. 1998 Jul;16(7):677–81.
228. Kreudenstein TS Von, Escobar-Carbrera E, Lario PI, D'Angelo I, Brault K, Kelly J, et al. Improving biophysical properties of a bispecific antibody scaffold to aid developability: Quality by molecular design. mAbs. 2013 Sep;5(5):646–54.
229. Gunasekaran K, Pentony M, Shen M, Garrett L, Forte C, Woodward A, et al. Enhancing antibody Fc heterodimer formation through electrostatic steering effects: Applications to bispecific molecules and monovalent IgG. Journal of Biological Chemistry. 2010 Jun 18;285(25):19637–46.
230. Liu Z, Leng EC, Gunasekaran K, Pentony M, Shen M, Howard M, et al. A novel antibody engineering strategy for making monovalent bispecific heterodimeric IgG antibodies by electrostatic steering mechanism. Journal of Biological Chemistry. 2015 Mar 20;290(12):7535–62.
231. Goulet DR, Orcutt SJ, Zwolak A, Rispens T, Labrijn AF, De Jon RN, et al. Kinetic mechanism of controlled Fab-arm exchange for the formation of bispecific immunoglobulin G1 antibodies. Journal of Biological Chemistry. 2018 Jan 12;293(2):651–61.
232. Labrijn AF, Meesters JI, De Goeij BECG, Van Den Bremer ETJ, Neijssen J, Van Kampen MD, et al. Efficient generation of stable bispecific IgG1 by controlled Fab-arm exchange. Proceedings of the National Academy of Sciences of the United States of America. 2013 Mar 26;110(13):5145–50.
233. Tustian AD, Endicott C, Adams B, Mattila J, Bak H. Development of purification processes for fully human bispecific antibodies based upon modification of protein

A binding avidity. https://doi.org/101080/19420862201611601 92. 2016 May 18;8(4):828–38.
234. Schirrmann T, Menzel C, Hust M, Prilop J, Jostock T, Dübel S. Oligomeric forms of single chain immunoglobulin (scIgG). mAbs. 2010 Jan;2(1):73.
235. Klein C, Schaefer W, Regula JT. The use of CrossMAb technology for the generation of bi- and multispecific antibodies. mAbs. 2016 Aug 17;8(6):1010.
236. Lewis SM, Wu X, Pustilnik A, Sereno A, Huang F, Rick HL, et al. Generation of bispecific IgG antibodies by structure-based design of an orthogonal Fab interface. Nature biotechnology. 2014 Feb;32(2):191–8.
237. Mazor Y, Oganesyan V, Yang C, Hansen A, Wang J, Liu H, et al. mAbs Improving target cell specificity using a novel monovalent bispecific IgG design Improving target cell specificity using a novel monovalent bispecific IgG design. 2015;
238. Zhao Q. Bispecific Antibodies for Autoimmune and Inflammatory Diseases: Clinical Progress to Date. BioDrugs. 2020 Apr 1;34(2):111–9.
239. Brinkmann U, Kontermann RE. Bispecific antibodies. Science. 2021 May 28;372(6545):916–7.
240. Ma J, Mo Y, Tang M, Shen J, Qi Y, Zhao W, et al. Bispecific Antibodies: From Research to Clinical Application. Frontiers in Immunology. 2021 May 5;12:1555.
241. Kantarjian H, Stein A, Gökbuget N, Fielding AK, Schuh AC, Ribera JM, et al. Blinatumomab versus Chemotherapy for Advanced Acute Lymphoblastic Leukemia. The New England journal of medicine. 2017 Mar 2;376(9):836–47.
242. Gökbuget N, Dombret H, Bonifacio M, Reichle A, Graux C, Faul C, et al. Blinatumomab for minimal residual disease in adults with B-cell precursor acute lymphoblastic leukemia. Blood. 2018 Apr 5;131(14):1522–31.
243. Bai L, Sun M, Xu A, Bai Y, Wu J, Shao G, et al. Phase 2 study of AK104 (PD-1/CTLA-4 bispecific antibody) plus lenvatinib as first-line treatment of unresectable hepatocellular carcinoma. https://doi.org/101200/JCO20213915_suppl4101. 2021 May 28;39(15_suppl):4101–4101.
244. Mestas J, Hughes CCW. Of mice and not men: differences between mouse and human immunology. Journal of immunology (Baltimore, Md : 1950). 2004 Mar 1;172(5):2731–8.
245. Labrijn AF, Meesters JI, Bunce M, Armstrong AA, Somani S, Nesspor TC, et al. Efficient Generation of Bispecific Murine Antibodies for Pre-Clinical Investigations in Syngeneic Rodent Models. Scientific Reports 2017 7:1. 2017 May 30;7(1):1–14.
246. Wang F, Tsai JC, Davis JH, Chau B, Dong J, West SM, et al. Design and characterization of mouse IgG1 and IgG2a bispecific antibodies for use in syngeneic models. mAbs. 2020 Jan 1;12(1).
247. Klein C, Schaefer W, Regula JT. The use of CrossMAb technology for the generation of bi- and multispecific antibodies. https://doi.org/101080/19420862201611974 57. 2016 Aug 17;8(6):1010–20.
248. Akkaya B. Modulation of the PD-1 pathway by inhibitory antibody superagonists. University of Oxford; 2012.
249. Paluch C. Manipulating immune checkpoint signalling pathways with antibodies. University of Oxford; 2019.
250. Huo J, Mikolajek H, Le Bas A, Clark JJ, Sharma P, Kipar A, et al. A potent SARS-CoV-2 neutralising nanobody shows therapeutic efficacy in the Syrian golden hamster model of COVID-19. Nature Communications 2021 12:1. 2021 Sep 22;12(1):1–18.

251. Lilienthal GM, Rahmöller J, Petry J, Bartsch YC, Leliavski A, Ehlers M. Potential of murine IgG1 and Human IgG4 to inhibit the classical complement and Fcγ receptor activation pathways. Frontiers in Immunology. 2018 May 9;9(MAY):1.
252. Bruhns P, Jönsson F. Mouse and human FcR effector functions. Immunological Reviews. 2015 Nov 1;268(1):25–51.
253. Ono M, Bolland S, Tempst P, Ravetch J V. Role of the inositol phosphatase SHIP in negative regulation of the immune system by the receptor FeγRIIB. Nature 1996 383:6597. 1996;383(6597):263–6.
254. Cragg MS, Amano H, Verbeek JS, Sjef Verbeek J, Hirose S, Nishimura H. The Complex Association of FcγRIIb With Autoimmune Susceptibility. The Complex Association of FcγRIIb With Autoimmune Susceptibility Front Immunol. 2019;10:2061.
255. Müller D, Karle A, Meißburger B, Höfig I, Stork R, Kontermann RE. Improved Pharmacokinetics of Recombinant Bispecific Antibody Molecules by Fusion to Human Serum Albumin *. Journal of Biological Chemistry. 2007 Apr 27;282(17):12650–60.
256. Clynes RA, Towers TL, Presta LG, Ravetch J V. Inhibitory Fc receptors modulate in vivo cytoxicity against tumor targets. Nature Medicine 2000 6:4. 2000 Apr;6(4):443–6.
257. Baudino L, Shinohara Y, Nimmerjahn F, Furukawa JI, Nakata M, Martínez-Soria E, et al. Crucial Role of Aspartic Acid at Position 265 in the CH2 Domain for Murine IgG2a and IgG2b Fc-Associated Effector Functions. The Journal of Immunology. 2008 Nov 1;181(9):6664–9.
258. Nimmerjahn F, Bruhns P, Horiuchi K, Ravetch J V. FcγRIV: A novel FcR with distinct IgG subclass specificity. Immunity. 2005 Jul 1;23(1):41–51.
259. Jin J, Hjerrild KA, Silk SE, Brown RE, Labbé GM, Marshall JM, et al. Accelerating the clinical development of protein-based vaccines for malaria by efficient purification using a four amino acid C-terminal 'C-tag.' International Journal for Parasitology. 2017 Jun;47(7):435–46.
260. Register AC, Tarighat SS, Lee HY. Molecular Sciences Bioassay Development for Bispecific Antibodies-Challenges and Opportunities. 2021;
261. Gassner C, Lipsmeier F, Metzger P, Beck H, Schnueriger A, Regula JT, et al. Development and validation of a novel SPR-based assay principle for bispecific molecules. Journal of Pharmaceutical and Biomedical Analysis. 2015 Jan 5;102:144–9.
262. Malyala P, Singh M. Endotoxin Limits in Formulations for Preclinical Research. Journal of Pharmaceutical Sciences. 2008 Jun 1;97(6):2041–4.
263. Copeland S, Shaw Warren H, Lowry SF, Galvano SE, Remick D. Acute Inflammatory Response to Endotoxin in Mice and Humans. Clinical and Diagnostic Laboratory Immunology. 2005 Jan;12(1):60.
264. Van Den Bremer ETJ, Labrijn AF, Van Den Boogaard R, Priem P, Scheffler K, Melis JPM, et al. Cysteine-SILAC Mass Spectrometry Enabling the Identification and Quantitation of Scrambled Interchain Disulfide Bonds: Preservation of Native Heavy-Light Chain Pairing in Bispecific IgGs Generated by Controlled Fab-arm Exchange. Analytical Chemistry. 2017 Oct 17;89(20):10873–82.
265. Taylor K, Howard CB, Jones ML, Sedliarou I, MacDiarmid J, Brahmbhatt H, et al. Nanocell targeting using engineered bispecific antibodies. mAbs. 2015 Jan 1;7(1):53.

266. Kurts C, Heath WR, Carbone FR, Allison J, Miller JFAF, Kosaka H, et al. Constitutive class I-restricted exogenous presentation of self antigens in vivo. Journal of Experimental Medicine. 1996 Sep 9;184(3):923–30.
267. Silver J, Zuo T, Chaudhary N, Kumari R, Tong P, Giguere S, et al. Stochasticity enables BCR-independent germinal center initiation and antibody affinity maturation. Journal of Experimental Medicine. 2018 Jan 1;215(1):77–90.
268. Dougan SK, Ogata S, Hu CCA, Grotenbreg GM, Guillen E, Jaenisch R, et al. IgG1 + ovalbumin-specific B-cell transnuclear mice show class switch recombination in rare allelically included B cells. Proceedings of the National Academy of Sciences of the United States of America. 2012;109(34):13739–44.
269. Xu JL, Davis MM. Diversity in the CDR3 region of V(H) is sufficient for most antibody specificities. Immunity. 2000 Jul 1;13(1):37–45.
270. Bruneau G, Anouassi A, Réhault-Godbert S, Canépa S, Blanc MR. Selection and characterization of recombinant dromedary antiovalbumin antibody fragments that do not cross-react with ovalbumin-related protein X: Use for immunoaffinity. Journal of Agricultural and Food Chemistry. 2012 Dec 12;60(49):12157–63.
271. Kurts C, Kosaka H, Carbone FR, Miller JFAP, Heath WR. Class I-restricted Cross-Presentation of Exogenous Self-Antigens Leads to Deletion of Autoreactive CD8 T Cells. Vol. 186, J. Exp. Med. 1997.
272. Hänninen A, Nurmela R, Maksimow M, Heino J, Jalkanen S, Kurts C. Islet β-cell-specific T cells can use different homing mechanisms to infiltrate and destroy pancreatic islets. American Journal of Pathology. 2007 Jan;170(1):240–50.
273. Martin-Orozco N, Wang YH, Yagita H, Dong C. Cutting Edge: Programed Death (PD) Ligand-1/PD-1 Interaction Is Required for CD8 + T Cell Tolerance to Tissue Antigens. The Journal of Immunology. 2006 Dec 15;177(12):8291–5.
274. Liu X, Alexiou M, Martin-Orozco N, Chung Y, Nurieva RI, Ma L, et al. Cutting Edge: A Critical Role of B and T Lymphocyte Attenuator in Peripheral T Cell Tolerance Induction. The Journal of Immunology. 2009 Apr 15;182(8):4516–20.
275. Friesen TJ, Ji Q, Fink PJ. Recent thymic emigrants are tolerized in the absence of inflammation. Journal of Experimental Medicine. 2016;213(6):913–20.
276. Behrens GMN, Li M, Davey GM, Allison J, Flavell RA, Carbone FR, et al. Helper Requirements for Generation of Effector CTL to Islet β Cell Antigens. The Journal of Immunology. 2004;172(9):5420–6.
277. Kurts C, Carbone FR, Barnden M, Blanas E, Allison J, Heath WR, et al. CD4+ T cell help impairs CD8+ T cell deletion induced by cross- presentation of self-antigens and favors autoimmunity. Journal of Experimental Medicine. 1997;186(12):2057–62.
278. Hogquist KA, Jameson SC, Heath WR, Howard JL, Bevan MJ, Carbone FR. T Cell Receptor Antagonist Peptides Induce Positive Selection. Cell. 1994;76:17–27.
279. Barnden MJ, Allison J, Heath WR, Carbone FR. Defective TCR expression in transgenic mice constructed using cDNA- based α- and β-chain genes under the control of heterologous regulatory elements. Immunology and Cell Biology. 1998;76(1):34–40.
280. Giwa AM, Ahmed R, Omidian Z, Majety N, Karakus KE, Omer SM, et al. Current understandings of the pathogenesis of type 1 diabetes: Genetics to environment. World Journal of Diabetes. 2020 Jan 1;11(1):13.
281. Berglund ED, Li CY, Poffenberger G, Ayala JE, Fueger PT, Willis SE, et al. Glucose Metabolism In Vivo in Four Commonly Used Inbred Mouse Strains. Diabetes. 2008 Jul;57(7):1790.

282. Kehry MR, Manorek G, Fisher J, Del Cid N, Rooks A, Altobell III L, et al. Discovery of a PD-1 Checkpoint Agonist Antibody for Autoimmune/Inflammatory Disease [Internet]. Festival of Biologics Conference. 2020 [cited 2022 Sep 6]. Available from: https://www.anaptysbio.com/wp-content/uploads/ANB030.FestivalofBiologics.030220presentation.final2_.pdf
283. Kehry M, Parmely S, Morse RP, Gold GN, Fisher J, Dahl ME, et al. PD-1 AGONIST AND METHOD OF USING SAME. EU; https://worldwide.espacenet.com/patent/search/family/071895175/publication/EP3980460A2?q=WO2020247648A2, 2020.
284. Moreno-Vicente J, Willoughby JE, Taylor MC, Booth SG, English VL, Williams EL, et al. Fc-null anti-PD-1 monoclonal antibodies deliver optimal checkpoint blockade in diverse immune environments. Journal for ImmunoTherapy of Cancer. 2022 Jan 1;10(1):e003735.
285. Selby MJ, Engelhardt JJ, Johnston RJ, Lu LS, Han M, Thudium K, et al. Preclinical development of ipilimumab and nivolumab combination immunotherapy: Mouse tumor models, In vitro functional studies, and cynomolgus macaque toxicology. PLoS ONE. 2016 Sep 1;11(9).
286. Mosser DM, Zhang X. Interleukin-10: new perspectives on an old cytokine. Immunological Reviews. 2008 Dec 1;226(1):205–18.
287. Moore KW, De Waal Malefyt R, Coffman RL, O'Garra A. Interleukin-10 and the Interleukin-10 Receptor. https://doi.org/101146/annurev.immunol191683. 2001 Apr 1;19:683–765.
288. Kumar S, Shukla R, Ranjan P, Kumar A. Interleukin-10: A Compelling Therapeutic Target in Patients With Irritable Bowel Syndrome. Vol. 39, Clinical Therapeutics. Elsevier; 2017. p. 632–43.
289. Josephson K, DiGiacomo R, Indelicato SR, Ayo AH, Nagabhushan TL, Parker MH, et al. Design and analysis of an engineered human interleukin-10 monomer. Journal of Biological Chemistry. 2000 May 5;275(18):13552–7.
290. Riley JK, Takeda K, Akira S, Schreiber RD. Interleukin-10 Receptor Signaling through the JAK-STAT Pathway. Journal of Biological Chemistry. 1999 Jun 4;274(23):16513–21.
291. Kjellev S, Lundsgaard D, Poulsen SS, Markholst H. Reconstitution of Scid mice with CD4+CD25− T cells leads to rapid colitis: An improved model for pharmacologic testing. International Immunopharmacology. 2006 Aug 1;6(8):1341–54.
292. Spencer SD, Di Marco F, Hooley J, Pitts-Meek S, Bauer M, Ryan AM, et al. The Orphan Receptor CRF2-4 Is an Essential Subunit of the Interleukin 10 Receptor. Journal of Experimental Medicine. 1998 Feb 16;187(4):571–8.
293. Liu C, Chu D, Kalantar-Zadeh K, George J, Young HA, Liu G. Cytokines: From Clinical Significance to Quantification. Advanced Science. 2021 Aug 1;8(15).
294. Rose S, Misharin A, Perlman H. A novel Ly6C/Ly6G-based strategy to analyze the mouse splenic myeloid compartment. Cytometry Part A : the journal of the International Society for Analytical Cytology. 2012 Apr;81(4):343.
295. Piazzon MC, Lutfalla G, Forlenza M. IL10, A Tale of an Evolutionarily Conserved Cytokine across Vertebrates. Clinical Review in Immunology. 2016;36(2):99–129.
296. Kim SC, Tonkonogy SL, Karrasch T, Jobin C, Balfour Sartor R. Dual-association of gnotobiotic IL-10-/- mice with 2 nonpathogenic commensal bacteria induces aggressive pancolitis. Inflammatory bowel diseases. 2007 Dec;13(12):1457–66.
297. Zigmond E, Bernshtein B, Friedlander G, Walker CR, Yona S, Kim KW, et al. Macrophage-Restricted Interleukin-10 Receptor Deficiency, but Not IL-10

Deficiency, Causes Severe Spontaneous Colitis. Immunity. 2014 May;40(5):720–33.
298. Saxton RA, Tsutsumi N, Su LL, Abhiraman GC, Mohan K, Henneberg LT, et al. Structure-based decoupling of the pro- And anti-inflammatory functions of interleukin-10. Science. 2021 Mar 19;371(6535).
299. Albring JC, Sandau MM, Rapaport AS, Edelson BT, Satpathy A, Mashayekhi M, et al. Targeting of B and T lymphocyte associated (BTLA) prevents graft-versus-host disease without global immunosuppression. The Journal of Experimental Medicine. 2010 Nov 11;207(12):2551.
300. Bruhns P. Properties of mouse and human IgG receptors and their contribution to disease models. Vol. 119, Blood. 2012. p. 5640–9.
301. Li F, Ravetch J V. Antitumor activities of agonistic anti-TNFR antibodies require differential FcγRIIB coengagement in vivo. Proceedings of the National Academy of Sciences of the United States of America. 2013 Nov 26;110(48):19501–6.
302. Li J, Yin Q, Wu H. Structural Basis of Signal Transduction in the TNF Receptor Superfamily. Advances in immunology. 2013;119:135.
303. Wajant H. Principles of antibody-mediated TNF receptor activation. Cell Death & Differentiation 2015 22:11. 2015 Aug 21;22(11):1727–41.
304. Medler J, Nelke J, Weisenberger D, Steinfatt T, Rothaug M, Berr S, et al. TNFRSF receptor-specific antibody fusion proteins with targeting controlled FcγR-independent agonistic activity. Cell Death & Disease 2019 10:3. 2019 Mar 4;10(3):1–13.
305. Dickopf S, Georges GJ, Brinkmann U. Format and geometries matter: Structure-based design defines the functionality of bispecific antibodies. Computational and Structural Biotechnology Journal. 2020 Jan 1;18:1221–7.
306. Ramos-Casals M, Brahmer JR, Callahan MK, Flores-Chávez A, Keegan N, Khamashta MA, et al. Immune-related adverse events of checkpoint inhibitors. Nature Reviews Disease Primers 2020 6:1. 2020 May 7;6(1):1–21.
307. Wei F, Zhong S, Ma Z, Kong H, Medvec A, Ahmed R, et al. Strength of PD-1 signaling differentially affects T-cell effector functions. Proceedings of the National Academy of Sciences of the United States of America. 2013 Jul 2;110(27):E2480–9.
308. Wang W, Wang EQ, Balthasar JP. Monoclonal Antibody Pharmacokinetics and Pharmacodynamics. Clinical Pharmacology & Therapeutics. 2008 Nov 1;84(5):548–58.
309. Hoffmann RM, Coumbe BGT, Josephs DH, Mele S, Ilieva KM, Cheung A, et al. Antibody structure and engineering considerations for the design and function of Antibody Drug Conjugates (ADCs). Oncoimmunology. 2018 Mar 4;7(3).
310. Opaliński Ł, Sokołowska-Wędzina A, Szczepara M, Zakrzewska M, Otlewski J. Antibody-induced dimerization of FGFR1 promotes receptor endocytosis independently of its kinase activity. Scientific Reports. 2017 Dec 1;7(1).
311. Cheng J, Liang M, Carvalho MF, Tigue N, Faggioni R, Roskos LK, et al. Molecular Mechanism of HER2 Rapid Internalization and Redirected Trafficking Induced by Anti-HER2 Biparatopic Antibody. Antibodies. 2020 Sep 1;9(3):1–21.
312. Dahl ME, Hare E, Luu K, Randazzo B, Lizzul P. Rosnilimab, a Novel PD-1 Agonist Monoclonal Antibody, Demonstrated Modulation of Peripheral T cell Activity and Reduction of Circulating PD-1 high Expressing CD4 and CD8 T cells in a Phase 1 Healthy Volunteer Clinical Trial. In: FOCIS. 2022.
313. Klarquist J, Janssen EM. The bm12 Inducible Model of Systemic Lupus Erythematosus (SLE) in C57BL/6 Mice. Journal of Visualized Experiments : JoVE. 2015 Nov 1;2015(105):53319.

314. Ahn E, Araki K, Hashimoto M, Li W, Riley JL, Cheung J, et al. Role of PD-1 during effector CD8 T cell differentiation. Proceedings of the National Academy of Sciences of the United States of America. 2018 May 1;115(18):4749–54.
315. Zotos D, Coquet JM, Zhang Y, Light A, D'Costa K, Kallies A, et al. IL-21 regulates germinal center B cell differentiation and proliferation through a B cell–intrinsic mechanism. The Journal of Experimental Medicine. 2010 Feb 2;207(2):365.
316. King IL, Mohrs M. IL-4-producing CD4+ T cells in reactive lymph nodes during helminth infection are T follicular helper cells. The Journal of experimental medicine. 2009 May 11;206(5):1001–7.
317. Sage PT, Francisco LM, Carman C V., Sharpe AH. The receptor PD-1 controls follicular regulatory T cells in the lymph nodes and blood. Nature Immunology 2012 14:2. 2012 Dec 16;14(2):152–61.
318. Granger SW, Rickert S. LIGHT–HVEM signaling and the regulation of T cell-mediated immunity. Cytokine & Growth Factor Reviews. 2003 Jun 1;14(3–4):289–96.
319. Šedý J, Balmert MO, Ware BC, Smith W, Nemčovičova I, Norris PS, et al. A herpesvirus entry mediator mutein with selective agonist action for the inhibitory receptor B and T lymphocyte attenuator. The Journal of biological chemistry. 2017 Dec 22;292(51):21060–70.
320. Yoon SI, Jones BC, Logsdon NJ, Harris BD, Deshpande A, Radaeva S, et al. Article Structure and Mechanism of Receptor Sharing by the IL-10R2 Common Chain. Structure/Folding and Design. 18:638–48.
321. Staerk J, Defour JP, Pecquet C, Leroy E, Antoine-Poirel H, Brett I, et al. Orientation-specific signalling by thrombopoietin receptor dimers. The EMBO Journal. 2011 Nov 2;30(21):4398–413.
322. Vivona S, Ramadass M, Kastelein R, Rokkam D, Lupardus P. WO2022032022A2 - IL10 RECEPTOR BINDING MOLECULES AND METHODS OF USE. WIPO; 2022.
323. Harris KE, Lorentsen KJ, Malik-Chaudhry HK, Loughlin K, Basappa HM, Hartstein S, et al. A bispecific antibody agonist of the IL-2 heterodimeric receptor preferentially promotes in vivo expansion of CD8 and NK cells. Scientific Reports 2021 11:1. 2021 May 19;11(1):1–15.